

Master Thesis
2010/12

Laurens J. F. Kee

Faculty of Geosciences
Department of Earth Sciences
Utrecht University, The Netherlands

Project commissioned by EBN
www.ebn.nl

Onshore Shale Gas Potential of the Lower Jurassic Altena Group in the West Netherlands Basin and Roer Valley Graben



Statement of originality of the MSc thesis

I declare that:

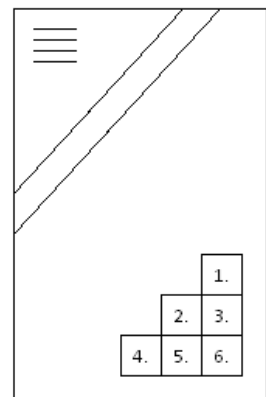
1. this is an original report, which is entirely my own work,
2. where I have made use of the ideas of other writers, I have acknowledged the source in all instances,
3. where I have used any diagram or visuals I have acknowledged the source in all instances,
4. this report has not and will not be submitted elsewhere for academic assessment in any other academic course.

Student data

Name : Laurens Joost Frederik Kee
Registration number : 3063593

Front-page Illustration Sources

1. 'Crinoids and Blastoids'; Acrylics on Illustration Board; Marshall's Art - <http://www.marshalls-art.com>
2. Utrecht University Logo – text reads “Sol Iustitiae Illustra Nos” (“May the Sun of Justice Enlighten Us”) – www.uu.nl
3. Grey shales; apparently a Barnett shale outcrop – photographer: unknown - <http://energytechstocks.com/wp/?p=570>
4. Gas flame – photographer unknown – <http://www.battelle.org/Environment/publications/EnvUpdates/Fall2001/article7.html>
5. Oil Rig at sunset – photographer: Nestor Galina – retrieved from: <http://www.bikeradar.com/mtb/news/article/riders-angered-by-plans-for-oil-well-on-surrey-hillside-20681>
6. EBN Logo – text reads ‘EBN – Best Access to Dutch Gas’ – www.ebn.nl



Onshore Shale Gas Potential of the Lower Jurassic Altena Group in the West Netherlands Basin and Roer Valley Graben

A thesis
by
Laurens Joost Frederik Kee
BSc

for attaining the degree of
Master of Science in the discipline of **Earth Sciences**

at Utrecht University,
Faculty of Geosciences,
Department of Earth Sciences,
The Netherlands

December, 2010

Board of Supervisors:

Utrecht University

Dr. Hans de Bresser

EBN

Drs. Sander Bouw

Dr. Maarten-Jan Brolsma

Independent

Dr. Jan de Jager

(Free University of Amsterdam (VU))

Vita

Laurens J. F. Kee was born at 30 January 1985 in the town of Nieuwegein, the Netherlands. After finishing preparatory schools, he started his education in Aerospace Engineering at Delft University of Technology. In 2005 however, he decided that an education in Earth Sciences was more in league with his general interests and began studying Earth Sciences at Utrecht University.

In the fifth and last year of Earth Sciences he applied for an internship at the dredging company Royal Boskalis Westminster nv and worked for them for 5 months ; both at the main office in the Netherlands and on site in Bahrain, middle East.

Following the successful completion of his internship in February, he started his graduation project at EBN in April after an earlier project was cancelled at the last moment. Due to this minor delay and the extensiveness of the project at EBN, he completed his thesis in December 2010.

Acknowledgements

I wish to thank my direct supervisors, Hans de Bresser (Utrecht University), Sander Bouw (EBN), Maarten-Jan Brolsma (EBN) and Jan de Jager (Free University Amsterdam (VU)) for their guidance and support during this project.

In addition, I wish to thank Frank van Bergen (TNO) for his help with acquiring data and making the maturity model available to me. Further thanks go to Daan den Hartog-Jager(NAM) and Jan Penninga (NAM) for providing me with the core samples.

Last but not least, I wish to thank my colleagues at EBN for their support, advice and hospitality during the duration of my research.

Abstract

Global demand for fossil fuels rises every day as the world population and its standard of living increase. For decades, the Netherlands have had the privilege to provide part of Western Europe with natural gas, contributing to the national economy with its resulting profit. In 2009, Dutch gas production was over 70 billion cubic metres (BCM), of which 37 BCM came from the Groningen field.

At the present day however, most conventional gas fields have already been located and put into production, and only few significant prospects remain. Even the giant Groningen field is nearing depletion. Consequently, the Netherlands will have to find new, unconventional, gas resources or face losing their economic role as gas producer. One such unconventional resource is shale gas, gas trapped in its shale source rock. Following the great success of the North American Barnett shale, oil companies worldwide have gained interest in this new, high-potential reservoir.

In the Netherlands, two onshore shale strata occur that have potential for shale gas: the Lower Jurassic Altona Group, including the Posidonia shale, and the Lower Namurian Geveik member. For the Geveik member, very few data are available. This makes defining its potential difficult. Therefore, this thesis focuses on the Lower Altona group of the West Netherlands Basin and Roer Valley Graben, comprising the Posidonia Shale, Aalburg and Sleen formation.

In this study, the experience from successful plays in other parts of the world is combined with regional log data to investigate the potential of each formation. Additionally, shale cores were pyrolysed for TOC content and kerogen, and analysed for bulk mineralogy and clay-content by Qemscan. Five Jurassic cores were also subjected to adsorption measurements, which are one of the first adsorption measurements ever performed for Dutch substrata.

From the various data sources, it appeared that on average the Posidonia formation is the formation with the highest potential for shale gas, despite its low maturity. Its substantial thickness, TOC content, wide-spread occurrence, and high gas shows make it a formation with good shale-gas prospects. The Aalburg and Sleen formation are found to be of less importance. This is mainly due to the low TOC content of both formations. However, significant gas shows in mainly the western part of the Netherlands suggest that these formations have more potential than TOC level suggests.

Areas with the highest shale-gas potential (so-called sweet spots) have been identified for each formation. Although an estimate of gas-in-place is made using all measured and analysed parameters, production potential does not only depend on whether or not the gas is physically in place, but also on factors such as technical feasibility, environmental impact, political stance toward fossil fuels, and economic conditions. This thesis however states that all three formations contain sweet spots that may be of economic importance. It is therefore recommended that the study of these spots is continued in order to assess their development. It is recommended that the focus of such a study should be in the region between the cities of Utrecht and Tilburg, where a major sweet spot for the organically-enriched Posidonia shale overlaps sweet spots for the Aalburg and Sleen formation.

Table of Contents

VITA.....	II
ACKNOWLEDGEMENTS	III
ABSTRACT.....	V
TABLE OF CONTENTS.....	VI
LIST OF FIGURES	X
LIST OF TABLES	XII
LIST OF EQUATIONS	XII
GLOSSARY.....	XIII
1. INTRODUCTION.....	1
1.1 General Introduction.....	1
1.1.1 Introduction to the Research.....	1
1.1.2 Objectives of the Study and Methods	3
1.1.3 Outline of this Thesis.....	4
1.2 History of Conventional Dutch Hydrocarbon Exploration	5
1.3 Introduction to Shale Gas	6
1.3.1 General Introduction.....	6
1.3.2 Depositional Environment.....	7
1.3.3 History of Shale-Gas Production Techniques	7
2. GEOLOGICAL SETTING	10
2.1 Present-day Situation.....	10
2.2 Sedimentary and Tectonic History.....	10
2.2.1 The Palaeozoic Era	10
2.2.2 The Mesozoic Era	14
2.2.3 The Cenozoic Era	15

2.3 Prospective Shale-Gas Formations in the Dutch Subsurface	16
2.3.1 <i>The Sleen Formation</i>	17
2.3.2 <i>The Aalburg Formation</i>	17
2.3.3 <i>The Posidonia Shale Formation</i>	17
3. KEY-PROPERTIES FOR PRODUCTIVE GAS-SHALES	18
3.1 Literature Study	18
3.1.1 <i>Gas-Shale Dimensions</i>	18
3.1.2 <i>Total Organic Carbon (TOC)</i>	18
3.1.3 <i>Kerogen Type</i>	19
3.1.4 <i>Maturity and Maximum Temperature</i>	21
3.1.5 <i>Porosity, Storage Capacity and GIIP</i>	22
3.1.6 <i>Clay-Mineral Content</i>	23
3.2 Case Studies	24
3.2.1 <i>The Mississippian Barnett Shale</i>	24
3.2.2 <i>The Lewis Shale</i>	25
3.3 Discussion and Conclusions concerning the Literature Study	27
4. LABORATORY METHODOLOGY AND DATA ACQUISITION TECHNIQUES.....	29
4.1 Core Analysis.....	29
4.1.1 <i>Rock Eval</i>	29
4.1.2 <i>Qemscan</i>	29
4.1.3 <i>Adsorption Isotherm</i>	30
4.2 Log Data, Parameter Modelling and Calculations.....	31
4.2.1 <i>Log Data</i>	31
4.2.2 <i>Parameter Modelling and Calculation</i>	32
4.3 Gas-Initially-In-Place Calculation	36
4.4 The Winterswijk Quarry	37
5. RESULTS.....	40
5.1 Lithological Classification	40
5.2 Formation Thickness	41
5.3 Kerogen Type	41

5.4 Maturity	42
5.4.1 Maturity from Basin Modelling.....	42
5.4.2 Maturity from Pyrolysis.....	43
5.5 Total Organic Carbon	44
5.5.1 Pyrolysis Results	44
5.5.2 TOC Modelling (Passey)	45
5.6 Gas Shows	45
5.7 Mineralogy	47
5.7 Methane Adsorption.....	47
6. DISCUSSION	49
6.1 Formation Thickness	49
6.1.1 Interpretation and Accuracy	49
6.1.2 Thickness Mapping.....	50
6.1.3 GIIP Calculation Input.....	50
6.2 Kerogen Type	50
6.3 Maturity	53
6.3.1 Interpretation and Accuracy	53
6.3.2 Maturity Mapping.....	55
6.4 Total Organic Carbon	56
6.4.1 Interpretation and Accuracy	56
6.4.2 TOC Mapping	58
6.5 Gas Shows	58
6.5.1 Interpretation and Accuracy	58
6.5.2 Gas Show Mapping	63
6.6 Clay-Mineral Content	64
6.7 Methane Adsorption.....	66
6.7.1 Interpretation and Accuracy	66
6.7.2 GIIP Input.....	68
6.8 Sweet Spot Determination.....	70
6.8.1 Posidonia Shale Formation Sweet Spots	70
6.8.2 Aalburg Formation Sweet Spots.....	71
6.8.3 Sleen Formation Sweet Spots.....	72
6.8.4 Final Shale-Gas Potential per Formation based on Sweet Spots	72

6.9 Gas-Initially-In-Place Estimate	76
6.9.1 Free Gas Content and Adsorbed Gas Content.....	76
6.9.2 GIIP Results.....	76
7. CONCLUSIONS.....	78
8. RECOMMENDATIONS.....	79
9. REFERENCES.....	79
Appendix A: ANALYSES OVERVIEW & PYROLYSIS RESULTS	A-I
Appendix B: MODELLED MATURITIES.....	A-II
Appendix C: MODELLED TOC LEVELS	A-IV
Appendix D: BULK MINERALOGY & HEAVY MINERALS.....	A-V
Appendix E: SORPTION MEASUREMENTS AND LANGMUIR FIT	A-VII
Appendix F1: INTERPRETED THICKNESS MAPS.....	A-IX
Appendix F2: INTERPRETED MATURITY MAPS.....	A-XII
Appendix F3: INTERPRETED TOC MAPS	A-XV
Appendix F4: INTERPRETED GAS SHOW MAPS	A-XIX
Appendix G: A3-FORMAT MATURITY MAPS	A-XXIII

List of Figures

Figure 1.1:	The oil window indicating temperature, pressure (depth) and vitrinite reflectivity ranges associated with particular hydrocarbon generation	1
Figure 1.2:	Schematic representation of conventional and unconventional hydrocarbon occurrences	3
Figure 1.3:	Map of the Dutch and neighbouring territories oil and gas fields	5
Figure 1.4:	Five depositional environments of Black Shales and their main characteristics	8
Figure 2.1:	Structural elements in the Dutch subsurface	11
Figure 2.2:	Lithostratigraphic column for the West Netherlands Basin	12
Figure 2.3:	The main tectonic features in the North Sea region and the position of the three cratons with respect to each other in the present-day geological setting of the Netherlands	13
Figure 2.4:	Worldwide stepwise modelling of post Pangaea break-up	15
Figure 2.5:	Timing and Basin-specific intensity of the four pulses of the Subhercynian event	16
Figure 3.1:	Maturation pathways of kerogen Type I – IV displayed in a van Krevelen diagram	20
Figure 3.2:	Distribution of the Barnett Shale in Texas	25
Figure 3.3:	Distribution of the Lewis Shale in the San Juan Basin	26
Figure 3.4:	Spider charts plotting R_o , GIP, TOC, Thickness, and relative quantity of adsorbed gas for the Mississippian Barnett Shale and Cretaceous Lewis shale	27
Figure 4.1:	Schematic representation of the adsorption measuring apparatus	31
Figure 4.2:	Correlation diagram between LOM and various other maturity indices	35
Figure 4.3:	R_o plotted against LOM	35
Figure 4.4:	Location of the Winterswijk quarry in the Netherlands and the quarry lay-out	37
Figure 4.5:	Photograph of the Winterswijk quarry	38
Figure 4.6:	Photograph of the Winterswijk quarry	39
Figure 5.1:	Histogram plotting Posidonia formation thickness distribution	41
Figure 5.2:	Histogram plotting Aalburg formation thickness distribution	41

Figure 5.3: Histogram plotting Sleen formation thickness distribution	41
Figure 5.4: Van Krevelen diagram with all samples plotted according to formation	42
Figure 5.5: Plot of several proposed correlations between T_{max} and R_0	43
Figure 5.6: Distribution histogram of maturity per formation	44
Figure 5.7: TOC levels sorted on formation	44
Figure 5.8: TOC profile vs. gas log for borehole WED-03	45
Figure 5.9: Part of the Gaag-05 gas log	46
Figure 5.10: Part of the Gaag-01 gas log	46
Figure 5.11: Average Quartz content per sample	47
Figure 5.12: resulting adsorption measurements per sample normalised to 100% TOC	48
Figure 6.1: Present-day TOC levels plotted against kerogen type	51
Figure 6.2: Krevelen diagram indicating the spread in data for two wells	51
Figure 6.3: Two core fragments clearly showing fossil-remains (bivalves) in the Aalburg formation	52
Figure 6.4: Modelled R_0 versus R_0 derived from measurements (TNO) or inferred from the van Krevelen diagram	55
Figure 6.5: Zoomed gas show map for the Gaag-area	59
Figure 6.6: Diagram plotting mud weight versus measured gas	60
Figure 6.7: Uninterpreted E-W seismic section of the Gaag-area in the western West Netherlands Basin	61
Figure 6.8: Interpreted E-W seismic section of the Gaag-area in the western West Netherlands Basin	62
Figure 6.9: TOC profiles and gas log for the GAG-01 and GAG-05 well	63
Figure 6.10: Histogram displaying the distribution of clay-mineral content per formation	65
Figure 6.11: Relative sorption capacity plotted against TOC content	67
Figure 6.12: Clay-mineral and mica content vs. relative adsorption capacity	67
Figure 6.13: Non-normalised adsorption measurements	69
Figure 6.14: Langmuir isotherms for each GIIP scenario	70

Figure 6.15: Sweet spot map for the Posidonia formation	73
Figure 6.16: Sweet spot map for the Aalburg formation	74
Figure 6.17: Sweet spot map for the Sleen formation	75

List of Tables

Table 1.1: Characteristics overview for each type of unconventional reservoir	2
Table 3.1: Comparison Overview of the Barnett Shale and the Lewis Shale	26
Table 5.1: R_0 to T_{max} conversion table	42
Table 6.1: Overview of mappable and non-mappable attributes	49
Table 6.2: TNO-measured R_0 averages and their standard deviations versus the modelled R_0	54
Table 6.3: Calculated average, standard deviation, and classification for the clay-mineral content of each well	66
Table 6.4: Important properties and their value range per scenario	76
Table 6.5: Overview of calculated GIIP estimated per sweet spot and scenario	77

List of Equations

Equation 3.1: Equation for calculating the production index from carbon fractions	19
Equation 3.2: Equation for calculating adsorbed gas per unit volume	22
Equation 4.1: Relation between T_{max} at location A and T_{max} at location B	33
Equation 4.2: Passey's equation for modelling TOC level from resistivity and sonic logs	34
Equation 4.3: Passey's equation for modelling TOC level from resistivity and porosity logs	34
Equation 4.4: Passey's equation for modelling TOC level from resistivity and density logs	34
Equation 4.5: Deduced relation between LOM and R_0	35
Equation 4.6: Equation for calculating free gas content per unit volume	36
Equation 4.7: Equation for calculating GIIP for a defined volume	37
Equation 5.1: Relation for T_{max} from R_0	43
Equation 5.2: Relation for R_0 from T_{max}	43

Glossary

- Absorption* : The permeating of a fluid into another fluid or solid.
- Adsorption* : The adhesion of fluid molecules to a surface.
- ATAL* : Abbreviation for the Aalburg formation. AT indicates it is part of the Altena Group.
- ATPO* : Abbreviation for the Posidonia formation. AT indicates it is part of the Altena Group.
- ATRT* : Abbreviation for the Sleen formation. AT indicates it is part of the Altena Group.
- BCM* : Billion Cubic Metres expanded gas. Term used to indicate gas quantities.
- Biogenic* : Term indicating hydrocarbons were generating by bacterial activity.
- Carboniferous* : A geological period lasting from ~360 – 299 Ma.
- Conventional Reservoir* : A reservoir in which buoyant forces keep hydrocarbons trapped below a sealing formation.
- Core* : Also called core sample; A cylindrical section of rock extracted from depth by a hollow drill. The process of extracting the core is called 'coring'.
- Cretaceous* : A geological period lasting from ~145 – 65 Ma.
- Formation* : A distinct lithostratigraphic unit, sufficient distinctive and continuous that it can be mapped.
- Gas Show* : Gas that is brought up with the circulating mud, originating from the drilled formation. It is detected at the surface by a gas chromatograph.
- GIIP* : 'Gas Initially In Place'; term used to indicate the initial gas content of a potential reservoir.
- Hydrocarbons* : Generic term for fossil fuels.
- Jurassic* : A geological period lasting from ~199 – 145 Ma.
- Kerogen* : The original substance of organic matter present in the source rock. Can generate hydrocarbons when sufficiently heated. Is subdivided in groups I – IV.
- Lamination* : A term used to indicate millimetre-scale layers of sediment. Common in shales.
- Lithology* : Macro-scale characteristics of rock, based on mineral content, grain size, texture and colour.

<i>Ma</i>	: Abbreviation of Mega Annum (Latin), meaning million years. Can be used both for indicating age or time interval.
<i>Maturity</i>	: Measure for indicating the ability of a source rock to generate oil or gas based on reservoir temperature (past or present).
<i>Mud weight</i>	: Specific density of the drilling mud used.
<i>Pyrolysis</i>	: Technique that analyses a sample by heating/burning it and measuring the generated products.
<i>Onshore</i>	: On-land or accessible from land by side-ways drilling (max. ~5 km from the coast).
<i>R₀</i>	: Vitrinite Reflectivity Index. Indicative for maturity.
<i>Reservoir</i>	: A lithological unit which is sufficient porous to store significant quantities of hydrocarbons
<i>Shale</i>	: Fine-grained sedimentary rock consisting of clay particles. Often shows lamination.
<i>Sorption capacity</i>	: The ability of a medium to absorb and/or adsorb fluids
<i>STP</i>	: Abbreviation of 'Standard (or Surface) Temperature & Pressure'. Usually 20° C and 1 bar (101325 Pa)
<i>Sweet Spot</i>	: Distinct area that has the most favourable properties for hydrocarbon potential
<i>Thermogenic</i>	: Term indicating hydrocarbons were generated by heating of the kerogen
<i>TOC</i>	: Total Organic Carbon; Term indicating the weight percentage of organic matter in a Lithology/source rock
<i>Unconventional Reservoir</i>	: Generic term for oil and gas reservoirs different from the conventional reservoir. The term is subject to definition changes as technique and the perception of resource characteristics change.

This glossary is partially derived from the Schlumberger Oilfield Glossary - <http://www.glossary.oilfield.slb.com/>

1. Introduction

1.1 General Introduction

1.1.1 Introduction to the Research

Traditionally, hydrocarbons have been extracted from what are now called “conventional reservoirs”. Such hydrocarbon occurrences are dependent on the presence of a source rock, a reservoir rock, a seal rock, and a structural or stratigraphic trap. The source rock contains the organic material and has to be buried deep enough for temperature to increase to a specific temperature corresponding to the oil window of the particular source rock (figure 1.1). When this temperature is reached, the source rock will start generating hydrocarbons from the organic material. These hydrocarbons migrate buoyantly upward where they can be trapped in a porous reservoir rock overlain by an impermeable seal rock that prevents further upward migration. The structural trap prevents lateral movement and effectively traps the hydrocarbons in a semi-confined space.

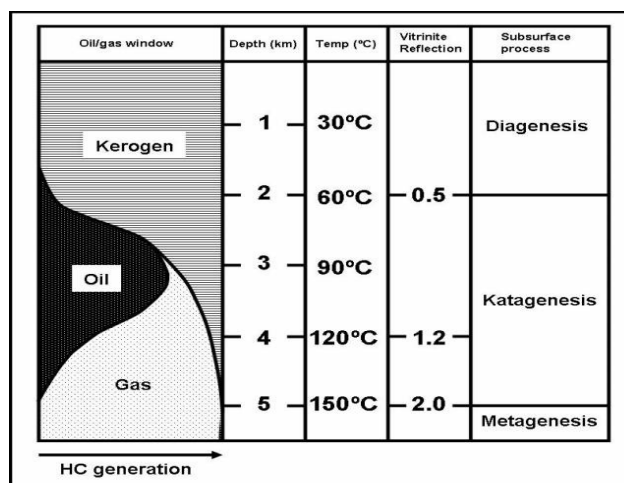


Figure 1.1: The oil window indicating temperature, pressure (depth) and vitrinite reflectivity ranges associated with particular hydrocarbon generation (Source: www.oilandgasgeology.com).

With world-wide commercial hydrocarbon exploration now going on for decades, most of the large hydrocarbon reservoirs appear to have been discovered and put into production. With increasing demand for energy and the world’s dependence on fossil fuels for its major energy supply, it is important to find new hydrocarbon deposits in order to ensure future energy supply.

Energie Beheer Nederland or EBN, a corporate governance with its roots in Dutch State Mines (DSM), has been fulfilling a role of participant and encourager of hydrocarbon exploration activities in the Netherlands for the last decades. EBN has participated in 125 joint ventures and this number is still rising. EBN recognises the impending depletion of the conventional hydrocarbon fields and the decreasing potential for finding new major conventional fields. Consequently, EBN’s role of participation and encouragement is now changing to a more active policy of exploration and research to find both the remaining conventional reserves and assessing the potential of unconventional reservoirs in the Dutch subsurface. Worldwide there are currently three main concepts for finding new hydrocarbon resources:

1. Recover hydrocarbons from greater depths or as of yet unmapped stratigraphic units
2. Recover hydrocarbons from reservoirs formerly inaccessible (e.g. due to ice, such as the Arctic)
3. Recover hydrocarbons from unconventional reservoirs

The first two concepts use the same methods for hydrocarbon exploration and exploitation as is used currently, although the reservoirs are commonly more risky, more difficult to reach, and more expensive to exploit. The third concept however uses a new method and concept of hydrocarbon trapping and reservoirs.

Unconventional reservoirs (or -hydrocarbons) are not just one unorthodox occurrence of gas or oil where one would not expect it. Rather, unconventional reservoirs are subdivided in six distinct groups as follow:

1. Shallow gas
2. Tight gas
3. Basin-centred gas
4. Coal Bed Methane
5. Aquifer Gas
6. Shale Gas

Shallow gas is the term used for gas shows in shallow sediments. This usually means conventionally trapped gas in unconsolidated sediments at a depth of 1000 metres below the seabed or less (Schroot & Schüttenhelm, 2003). Tight gas reservoirs refer to low-permeability conventionally trapped gas occurrences that produce mainly dry gas. In tight gas reservoirs, the gas flow is too low to produce economically on its own and thus requires stimulation, also called fraccing (the injection of fluids under high pressure to fracture the rock), to increase the permeability (Holditch, 2006). The third type of unconventional gas is a bit more difficult to define. Mohan et al. (2006) defined Basin-centred gas, or ‘deep gas’, as “an abnormally pressured, gas-saturated accumulation in low-permeability reservoirs lacking a down-dip water contact”. The next unconventional resource in the list, Coal-Bed Methane, is defined as methane absorbed to the surface of coal. Historically seen as a nuisance and threat to coal-miners, modern petroleum industries see it as a high-potential unconventional reservoir (Simpson, 2008). Aquifer gas is gas that is dissolved in formation water within the source rock. Although the amount of gas soluble in water at shallow depths is small, this amount rapidly increases with higher depths. It is believed that water within the source rock and along gas migration paths is first saturated with gas before free-gas migration can take place. Because of this, water-containing source rocks and aquifers through which gas has migrated at greater depths potentially possess high amounts of this aquifer gas (Nederlof, 1988). The last type on unconventional gas and the subject of this thesis, shale gas, is gas both derived and stored within a shale source rock. Since the shale reservoir has often very low permeability, stimulation is required to release the gas. Figure 1.2 depicts the various types of unconventional reservoirs as they occur in the field. The table below presents an overview of the differences between the various types of unconventional reservoirs (table 1.1).

Table 1.1: Characteristics overview for each type of unconventional reservoir (source: EBN)

	Conventional	Shallow Gas	Tight Gas	Shale Gas	Basin-centred Gas	Coalbed Methane
Rock	any (sst, lst)	Unconsolidated (sand)	any	shale	any	coal rich
Permeability	>1 mD	> 1 mD	<1 mD	<<1 mD	<1 mD	<10 mD
Trap Type	Buoyancy	Buoyancy	Buoyancy	Autotrap	Permeability Trap	Adsorption Trap

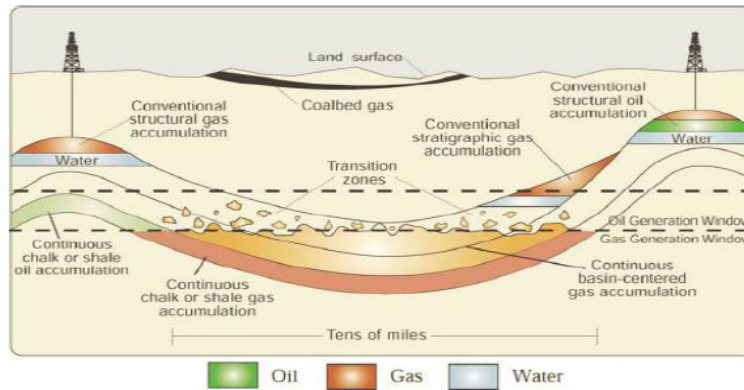


Figure 1.2: Schematic representation of conventional and unconventional hydrocarbon occurrences
(Source: Pollastro et al. 2003)

One might notice that these groups all refer only to the occurrence of natural gas while oil is omitted. Unconventional oil reservoirs however do occur. The reason why they are not mentioned in the list above is that the high viscosity of oil, in conjunction with the high degree of compactness of the unconventional reservoirs, makes it currently technically impossible to extract the oil from the rock economically. According to first estimates of potential unconventional gas-resources presented during the World Gas Conference (WGC) in October 2009, unconventional gas plays can add 60-250% to world reserves (Watson, 2009). Because of this high potential and following the success in the United States and Canada, research is carried out for other high-potential shale-gas occurrences in many other parts of the world.

This thesis, a direct result of EBN's policy to active research, will give an assessment of the potential for shale gas in the Lower Jurassic (black) shale formations (Altena Group) for the onshore West Netherlands Basin and Roer Valley Graben. Producibility of this shale gas and occurrences of other kinds of unconventional gas are beyond the scope of this thesis.

1.1.2 Objectives of the Study and Methods

The objectives of this study are:

1. To compile a set of geological constraints that a potential formation must meet in order to have shale-gas potential
2. To determine which properties are the most critical in predicting the potential of possible shale-gas plays
3. To locate regions within the Dutch onshore West Netherlands Basin and Roer Valley Graben that have the highest shale-gas potential (sweet spots)
4. To give an estimate of the expected gas-initially-in-place (GIIP)

These objectives are addressed in several steps. Firstly, a literature study is performed from which essential reservoir properties are derived, based on field experience and laboratory results attained by varying authors. The next step is collecting all necessary data required for an assessment of the region under consideration. Part of this information, such as formation occurrences and borehole logs, are already available in a raw form from TNO and the NAM. Other information, such as methane adsorption curves, is constructed from core samples specifically for this project. The third step is to appraise the Lower Jurassic shale formations using the specifications determined from the literature study and to locate the regions with the highest potential in terms of economic gas shale occurrence. Additionally, the validity of all key-properties and their usefulness in predicting shale gas potential is discussed. The fourth and last step is to make a calculated estimate of the Gas Initially In-Place (GIIP) in these high-potential regions.

1.1.3 Outline of this Thesis

Following this general introduction to the research, the rest of the first chapter is used to give the reader some more introductory background information about hydrocarbon exploration in the Netherlands, the basic theory behind shale gas and black shales, and the history of shale-gas specific exploitation techniques. Following this chapter, chapter 2 presents the present day geologic situation and a summarised sedimentological and tectonic history of the southern Netherlands. Additionally, the three formations focussed on in this thesis, the Lower Jurassic Posidonia Shale formation, Aalburg formation, and Sleen formation, are shortly described based on literature.

The third chapter deals with the literature study of already existing shale gas plays in the world and the properties that made these plays so successful. Each property is shortly introduced and discussed and the chapter ends with two cases studies of productive yet very different North American shale-gas plays. The fourth chapter presents the methodology applied during this study to retrieve data and samples required to compile results on which this thesis is based. These results are presented in chapter 5 and discussed and interpreted in chapter 6. All conclusions resulting from chapter 6 are summarised in chapter 7. In order to improve readability of this thesis, data tables and maps have been placed in the appendix section as much as possible.

1.2 History of Conventional Dutch Hydrocarbon Exploration

Dutch hydrocarbon exploration began as early as 1923 when the first natural oil in the Dutch subsurface was found near the German border in the town of Corle. Although the deposit was very small, with only 240 litres of oil extracted from Zechstein anhydrites and Carboniferous sandstones, it was the start of hydrocarbon exploration as it exists today. Fifteen years later, in 1938, a second indication of Dutch hydrocarbon deposits was found when a well drilled by the predecessor of Shell International, the Bataafse Petroleum Maatschappij, accidentally encountered oil stains during a demonstration near The Hague. Five years later, during the German occupation of the Netherlands in the Second World War, the first commercially viable oilfield was found at a depth of approximately 800 metres in Lower Cretaceous sandstones near the town of Schoonebeek (de Jager & Geluk, 2007).

The first commercial gas field was discovered 10 years later in 1948 near Coevorden. Commercially viable as they were, all these discoveries were no-where as important as the discovery of the Groningen gas field in 1959. Although initially not completely appreciated for its size, its discovery triggered a rush of exploration and development events in the whole North-Sea region as soon as its massive size was uncovered leading to the exploration of many more large gas fields in the Permian Rotliegend sandstone underlying large parts of the North Sea basin (Breunese & Rispens, 1996; de Jager & Geluk, 2007). Figure 1.3 presents a map of present-day oil (green) and gas (red) field in Dutch- and neighbouring territories.

In the North Sea basin, most of the gas fields are charged by the Westphalian coal-measures. Gas generated from these source rocks then migrates into the Rotliegend sandstone-reservoir which is overlain by the Zechstein formation, consisting of predominantly halite and anhydrite, which act as a seal. Oil reservoirs are predominantly charged from the Posidonia Shale of Jurassic age. Recent studies however suggest that, based on biphenyl source-rock markers, both the Posidonia and Westphalian source rocks produced oil, and that locally Westphalian charge may be mistaken for Posidonian oil charge (de Jager et al.; 1996).

Although the gigantic Groningen gas field, harbouring ca. 2700 billion cubic metres of recoverable gas, is by far the largest gas field of Western Europe and ranked ninth in the list of largest gas fields of the world, it was decided by the Dutch government that still more exploration activities for smaller fields should occur. By edict of the small-fields policy (Dutch: 'kleine velden beleid'), these smaller fields were allowed to produce at maximum capacity while the Groningen field was used to provide extra production capacity as a swing producer during periods of higher gas-consumption, like winter-seasons.

At present, the Groningen gas field is approximately for two-thirds depleted. The decrease in reservoir pressure associated with the state of depletion makes it increasingly difficult for the Groningen gas field to fulfil its role of swing producer. Three underground gas-storage facilities have therefore been constructed to provide additional supply in case the Groningen field proves unable to fulfil this role, and more are under construction.

Since the discovery of the first commercial field, over 1500 exploration and appraisal wells have been drilled in the Dutch subsurface, resulting in the discovery of hundreds of additional oil- and gas fields. Aided by 2-dimensional and 3-dimensional seismic surveys, drilling now occurs far more accurate and with a higher success rate than in the past (Breunese & Rispens, 1996). However, annual estimates for undiscovered reserves decrease with each passing year and in the not-too

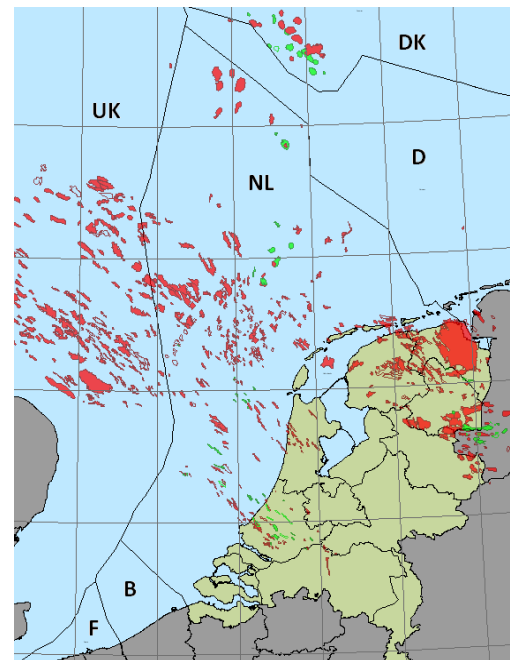


Figure 1.3: Map of the Dutch and neighbouring territories oil (green) and gas (red) fields (source: EBN)

distant future, Dutch peak-oil from conventional reserves has been reached, even though current redevelopment of the Schoonebeek field will delay this with a few years. Therefore it is important that other, unconventional, methods and possibilities are being evaluated and applied so that energy-demand can be met in the future as well.

1.3 Introduction to Shale Gas

1.3.1 General Introduction

Of the 6 types of unconventional gas resources mentioned in section 1.1, shale gas is often regarded as an unconventional resource with one of the largest potentials in terms of quantities of recoverable natural gas, while having a relatively good chance to be economically viable and developable as well. In the United States, multiple shale gas fields are already in production and more are currently being developed (Stevens & Kuuskraa, 2009).

Shales are the world's most common sedimentary rock. Most shales however are not suited to generate hydrocarbons since they lack sufficient quantities of organic matter (so-called 'grey shales'). Additionally, the high degree of compaction found in shales minimises the pore space and therefore renders grey shales unable to store large quantities of natural gas (Lewis et al., 2004). The rarer *black shales* however, shales rich in organic matter and therefore very dark in colour, are able to generate hydrocarbon and can, under certain conditions, store some amount of natural gas as well, provided that they also fulfil some other requirements (e.g.: maturity and type of kerogen).

Conventional plays for natural gas consist of a mature source rock that generates hydrocarbons which migrate upwards to an overlying reservoir rock. Gas-shales do not follow this process. Rather than migrating upwards, the oil and/or natural gas formed in the shale becomes, at least partially, trapped in its inner structure due to the low porosity and permeability of the shale (auto-trapping). In this way, the gas-shale no longer exclusively acts as a source rock but as a reservoir and seal rock as well, forming a self-sourced reservoir (Zhao et al.; 2007). The potential of shale gas is enormous. Organic-rich black shales cover large parts of many continents and shallow seas and, when subject to the right conditions, may have generated gas over vast areas.

Gas-shales have two principle ways for storage of natural gas (Jarvie, 2007):

1. adsorption to the organic matrix (chemical) or absorption in the organic matrix (physical)
2. as free gas in fractures and pore spaces

The pores and fractures are formed either by tectonic or diagenetic processes or by decomposition of organic matter (Jarvie et al.; 2007).

These two methods of gas storage indicate that the amount of organic material present in the gas-shale is not only important for the amount of hydrocarbons that can be generated, but also positively affects the gas-shale's ability to store the natural gas. Moreover, a higher amount of organic material also means a higher amount of decomposition in the shale, generating more pore space and again positively affecting the shale's storage ability. A simulation published by Jarvie et al. (2007) concerning the storage capacity of a shale-gas play from the United States, the so-called Barnett Shale, indicates that under sub-ideal conditions the storage capacity of gas-shales should generally be sufficient to store significant amounts of the gas generated in a high-mature source rock. Gas shales are generally oil-prone source rocks that will generate oil at lower maturities. When maturity increases, oil that has not yet escaped from the source rock is thermally cracked into wet gas (gas with abundant hydrocarbon chains larger than that of methane) and, at even higher maturities, eventually into dry gas (gas consisting of mainly methane).

1.3.2 *Depositional Environment*

Black shales are typically deposited in low-energy environments under anoxic and high-nutrient conditions, such as deep stagnant lakes or seas. Present-day examples of regions where black shales are deposited are the Black Sea and Baltic Sea. In general, five main depositional environments for black shales can be distinguished (Arthur & Sageman, 1994):

1. Deep enclosed basins with a positive water balance
2. Deep borderland-basins with an O₂-minimum zone
3. Regions of coastal upwelling on western continental slopes
4. Shallow stratified basins
5. Coastal or intertidal zones

For the organic matter in potential black shales to survive it is essential that oxygen is in short supply. Some environments, such as the deep enclosed basin (e.g.: the Black Sea) contain stagnant water with an anoxic lower water-column. In these regions organic matter, for example dead organisms or organic debris carried in by rivers, can be slowly deposited without the risk of oxidation before burial is completed. In general, black shales deposited under these conditions have medium-high organic matter content and relatively low hydrogen content. Other environments, such as places of upwelling, simply generate such high quantities of organic matter that oxygen cannot be supplied quickly enough to decompose it all before it is buried under siliclastic sediment and more organic material. These regions often have very high contents of organic matter as well as high relative hydrogen content. Regions in coastal settings, such as intertidal zones, mainly rely on the rapid burial of the organic matter to prevent oxidation. This last group often comprises patchy, discontinuous layers dominated by terrestrial components which are therefore relatively low in hydrogen content (Arthur & Sageman, 1994; Murphy et al., 2000).

Because of the reducing environment created by the organic material, elements such as Uranium will be extracted from the seawater and be incorporated in the black shale. The result of this is relatively high levels of radioactivity compared to other, non-reducing sedimentary rocks, resulting in the term 'hot shale' and a characteristic high gamma ray signal (Finch et al.; 1982).

After deposition, the organic-rich mud must be buried where enhanced pressure and temperature will stimulate compaction and diagenesis processes, reforming the mud to finely laminated black shale. Figure 1.4 depicts the five depositional environments for black shales together with some of their key properties.

1.3.3 *History of Shale-Gas Production Techniques*

With an unconventional gas play comes an unconventional way of extracting the hydrocarbons from the reservoir. Although shale gas is often presented as a type of giant sub-surface gas bubble in which one would only have to stick a tube to suck all the natural gas out, much like the case for a conventional play, the reality is somewhat more complicated.

The first shale-gas play that came into production was the Barnett shale, starting production in 1981, located in the northern part of Texas, United States. Originally, the Barnett shale was exploited by drilling vertical wells only. Since the gas-shale is so tightly-packed, the reservoir had to be stimulated by fracturing. For this fracturing a combination of foam, sand and nitrogen was injected. Only four years later, the foam was replaced by cross-linked gel in combination with clay stabilisers and fluid-loss additives to increase production (Martineau, 2007; Pollastro, 2007).

The first major innovation in shale-gas exploitation techniques came with the introduction of water fracturing in 1997, 16 years after initial production began. The use of sandy water over foams or gels increased fracturing (and flow) rates by 25-75%, reduced cost by 50-60%, and made the use of clay-stabilisers and surfactants superfluous. These new techniques allowed older wells initially fractured with gel to be refractured, increasing production rates and recoverable reserves (Martineau, 2007).

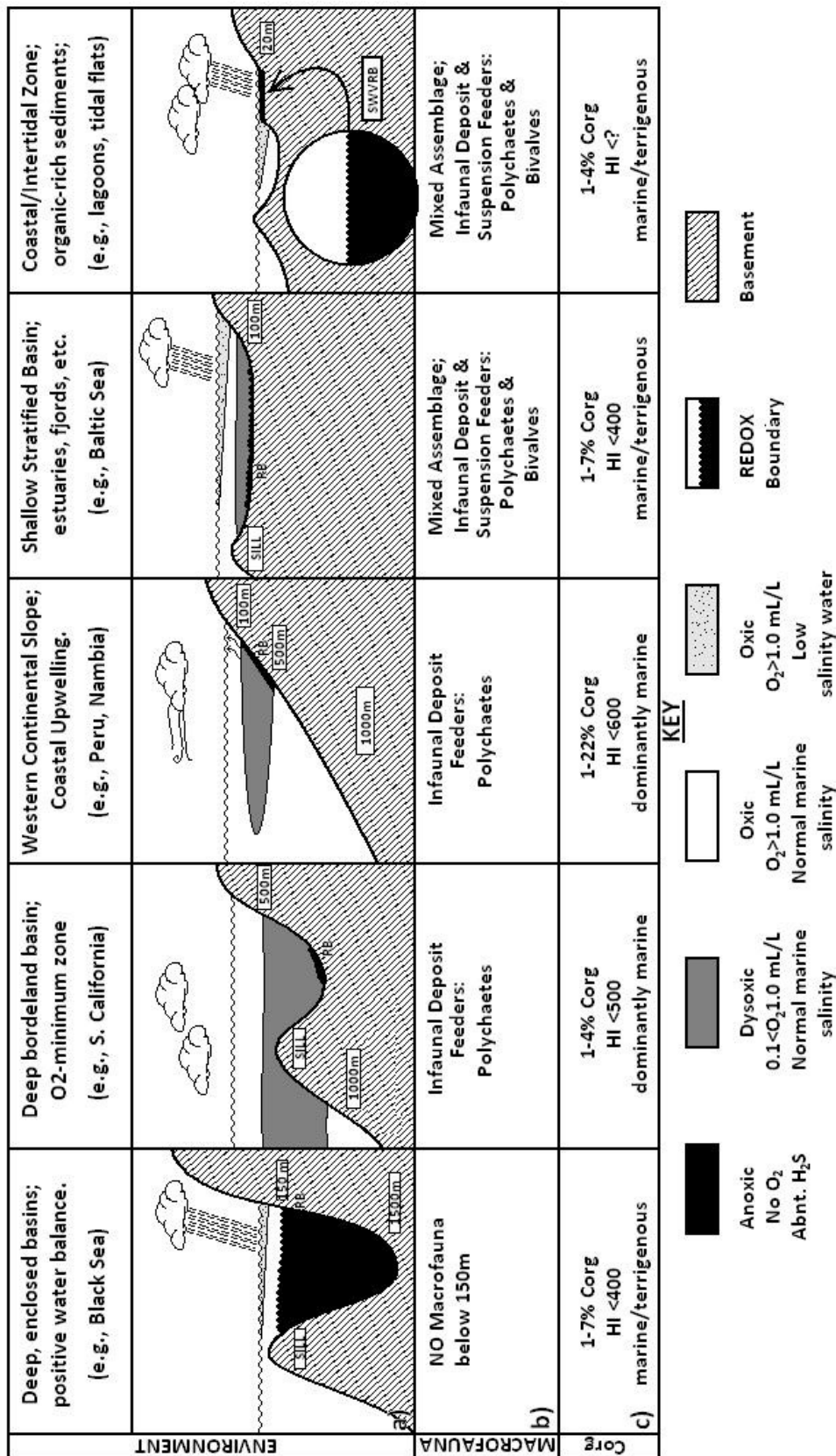


Figure 1.4: Five depositional environments of Black Shales and their main characteristics
 a) Idealised basin setting depicting water-mass distribution, redox-boundary and prevalent climate; b) predominate macro-fauna found for oxygen-deficient regions; c) organic matter characteristics
 The original image and detailed explanation of the models were published by Arthur & Sageman, 2004.

The second major innovation came with the concept of horizontal drilling. Rather than many vertical wells, a single well with horizontal side-tracks could cover lengths of 300-1200 metres. These side-tracks were then injected with water to fracture a large area in the shale to produce gas from. The horizontal drilling, first applied in 2003, furthermore reduced the risk of fracturing overlying or underlying formations which potentially contained unwanted by-products such as water, which would have to be disposed of if produced. The latest concept for shale-gas production is the 'simo-frac' in which two wells are drilled 150-300 metres apart after which both wells are fractured simultaneously (Martineau, 2007).

From the experience and development of exploiting gas shales in the past, Martineau (2007) described a number of pitfalls that should be identified and avoided as much as possible to reduce the risk associated with shale-gas exploitation.

1. *Major and minor faults and karsts* – Faults were initially thought to enhance production since the porosity and migration rates would be higher. It was later found however that, since stimulations techniques are used, the presence of pre-fracturing micro-faults hardly influenced migration rates while large faults are often associated with lower gas content and possibly hydrocarbon degeneration by bacteria (Stevens & Kuuskraa, 2009)
2. *Thickness variation* – Interbedded formations or members with a different lithological composition can both decrease the estimate of recoverable gas, and obstruct gas recovery from wells.
3. *Variation or pinch-out of fracture barriers* – Fracture barriers, e.g. underlying or overlying formations that are more resistant to fracturing and thus prevent the unwanted fracturing of surrounding (e.g.: water-carrying) lithologies, can laterally change in lithological properties, making them less effective in resisting fracturing, or can even disappear completely.
4. *Changes in maturation* – A sudden change in maturation can change the nature and composition of the hydrocarbons that are being extracted from the source rock. This in turn changes the amount of recoverable resources and production rate.
5. *Urban developments and city ordinances* – Not all locations are available for drilling due to urban developments and city ordinances. This is especially true for highly urbanised regions.

According to Martineau, most of these pitfalls can be overcome by 3-D seismic evaluations and careful planning.

2. Geological Setting

2.1 Present-day Situation

The Netherlands, both onshore and offshore, has been subjected to many periods of sedimentary deposition and erosion, basin subsidence and basin inversions during its geological past. The region of the Netherlands has known shallow coastal areas, salt deserts, deep anoxic seas and vast coal swamps. These events and climatic settings all left their mark on the Dutch subsurface, resulting in more than 10 kilometres of predominantly siliclastic sediments overlying the metamorphic basement. This sedimentary package is, opposed to what one would expect from the flat monotonous surface of the Netherlands today, locally heavily faulted and varied (de Jager, 2007). The Dutch geologic history has led to the formation of a multitude of highs and lows in the area such as the Dutch Central Graben, London-Brabant Massif, Broad Fourteens Basin, West-Netherlands Basin and Roer Valley Graben. For this thesis, the latter two structures are of interest.

The West Netherlands Basin and Roer Valley Graben are two elongated structures more or less in line with each other. There is no clear boundary between the basins. The orientation of the basins is roughly NW-SE (figure 2.1) and covers a large part of the southern Netherlands. The basins combined are roughly 65 kilometres wide and 300 kilometres long. Surrounding the two basins are the Peel Block, Maas-Bommel High and Rhenish Massif in the east, the London-Brabant Massif in the South, the Central-Netherlands Basin, Zandvoort Ridge, IJmuiden High and Broad-Fourteens Basin to the North and the Winterton High to the west.

Main stratigraphic units in the West Netherlands Basin and Roer Valley Graben are the Cenozoic Upper and Lower North Sea group (shale and sand), Cretaceous Chalk Group (carbonate) and Rijnland Group (marl, shale and sand), Jurassic Altena Group ((grey/black) shale with some carbonate and sand), Triassic Upper Germanic Trias Group and Carboniferous Limburg Group. In contrast to basins located more to the north, the Permian Zechstein salt is completely absent in the Roer Valley Graben and West Netherlands Basin. Instead, a major unconformity is in place (Saalian unconformity) (van Balen et al., 2000). For the West-Netherlands Basin and Roer Valley Graben, the sediment is 5 kilometres thick on average and is generally much more faulted than other basins or highs (Duin et al., 2006). Figure 2.2 presents a lithostratigraphic column of the West Netherlands Basin.

Especially the western part of the West Netherlands Basin (both onshore and offshore) has been of great interest to the petroleum industry due to oil and gas occurrences derived from Jurassic (oil) and Carboniferous (natural gas) source rocks. Because successful production of gas-shales requires the drilling of many wells that will only supply gas for a short time, this technique is too expensive for offshore projects. As a result, the offshore area of the West Netherlands Basin is not a part of the studied area save for a small near-shore strip that can be accessed from land-based rigs.

2.2 Sedimentary and Tectonic History

2.2.1 *The Palaeozoic Era*

The Dutch basement underlying the Roer Valley Graben and West Netherlands basins consists of two separate provinces. In the north the basement is part of the Caledonian basement, while the south consists of Gondwana-derived Avalonia. The West Netherlands Basin and Roer Valley Graben are located by approximation on the contact zone between these two parts.

The Early Palaeozoic era in the current Dutch region was dominated by the convergence of three main land masses: Laurentia, Baltica and Gondwana. These landmasses collided resulting in the formation of the supercontinent Pangaea during the Ordovician and Silurian, a process that would last at least until the early Jurassic. The process began in the Ordovician when a fragment of

Gondwana, Avalonia, drifted northwards toward the converging cratons of Laurentia and Baltica, resulting in an almost simultaneous collision of the three, giving rise to the Laurussian landmass. The collision zone between these cratons is the Caledonian fold belt (de Jager, 2007, Lyngsie et al., 2006). Figure 2.3 indicates these three cratons and their current respective position.

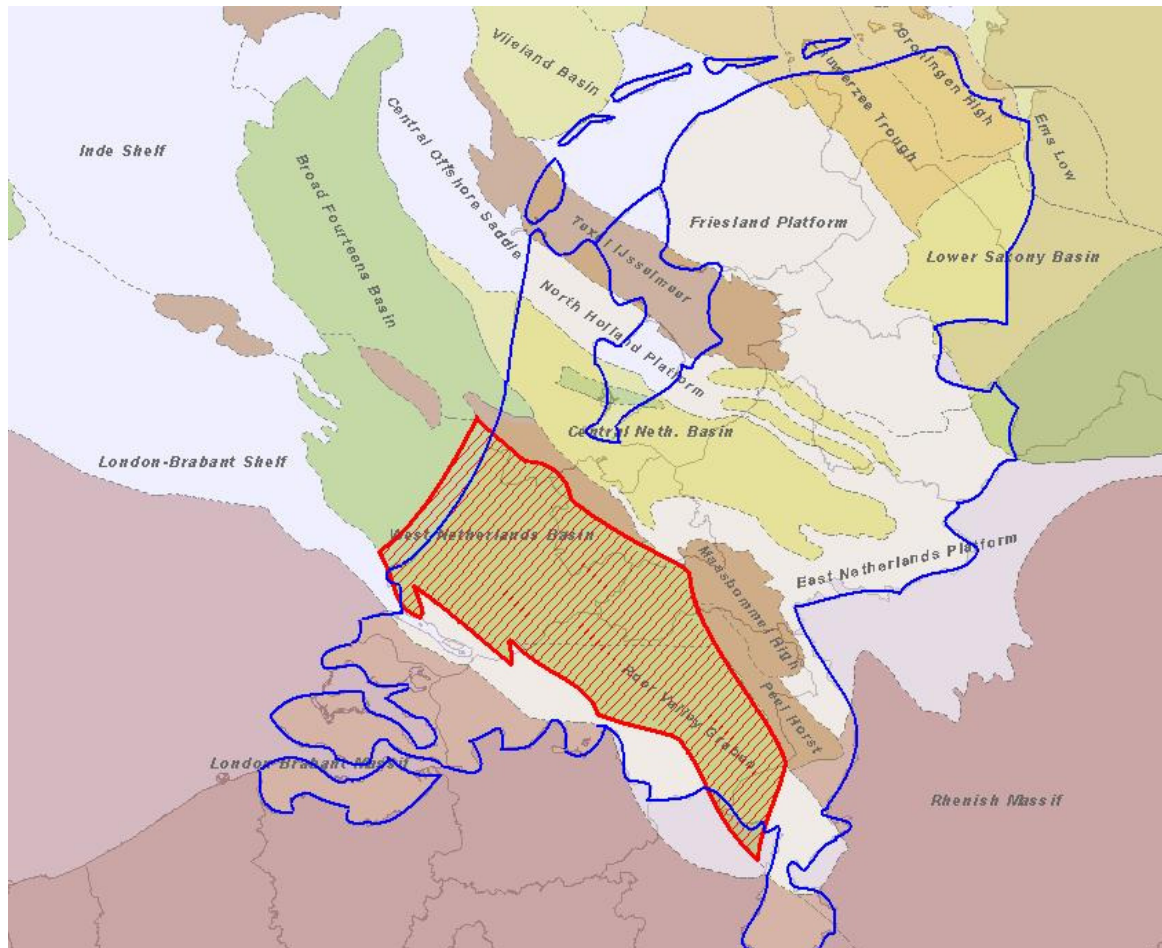


Figure 2.1: Structural elements in the Dutch subsurface. Present-day continental borders and coastline are indicated in blue. The red shaded area is the area studied for this thesis (including the coastal 'near-shore' strip).
Source: EBN

In the Netherlands, the oldest encountered sediments are of Silurian age, drilled at the northern end of the London-Brabant Massif. Due to the great depth at which these lie however, many wells in the Netherlands have not reached these sediments, nor are they well imaged by seismic reflection. As a result little is known about their exact composition and lateral variation. All knowledge about the structural and depositional environment of the Netherlands during the Early- to Middle Palaeozoic era is therefore derived from regional data (de Jager, 2007).

The nature and rate of sedimentation during the Palaeozoic era is difficult to assess. From regional data it is known that the Cambrian period comprised sedimentation of shales, sandstones and quartzites in both Denmark and eastern England. This suggests similar depositions in the region of the Netherlands. Following the Cambrian, the Ordovician is marked by the deposition of thick marine shales, again derived from England, suggesting regional sea level rise. From marine mudstones followed by sandstones and conglomerates of younger, Silurian, age, it appears that the sea level at this point was falling again, allowing coarser sediment to be deposited (Sorgenfrei, 1969).

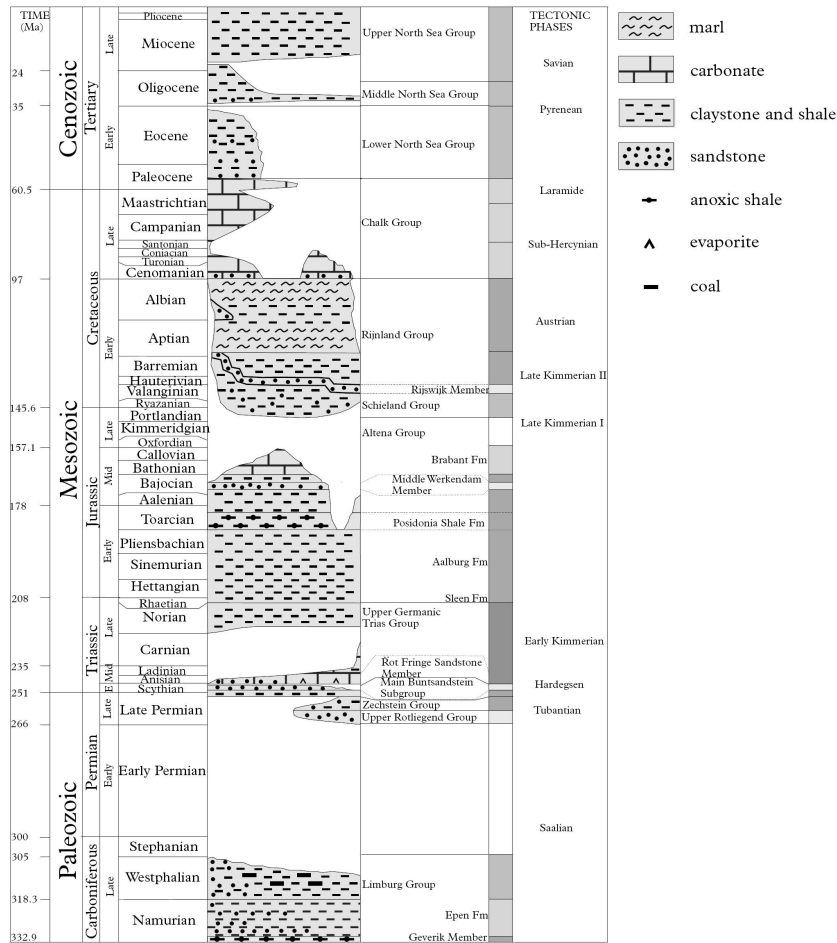


Figure 2.2: Lithostratigraphic column for the West Netherlands Basin. (Source: van Balen et al., 2000)

Following the Caledonian Orogeny, Gondwana and Laurussia began to converge during the Devonian eventually colliding with each other and resulting in the Variscan orogenic event, which lasted from early Carboniferous (Namurian & Westphalian) to late Permian, and completed the assembly of Pangaea. During this orogeny, which was similar in scale to the present-day Himalayan orogeny, the Dutch basement was strongly influenced by the formation of major fault systems (de Jager, 2007; Duin, 2006). From the fact that these fault systems, enclosing amongst others the present-day West Netherlands Basin and Roer Valley Graben, cannot be traced past Carboniferous sediment it appears that the formation of the two basins was staged in this period. This possibility is enhanced by the fact that successions of Carboniferous sediment with varying thickness are located within these future basins. Full development of the basins however would not occur until during the Jurassic period (Geluk et al., 1994).

Based on the English and Danish lithostratigraphies of the Palaeozoic era it is inferred that the Devonian period was marked by a dry desert environment, as indicated by the occurrences of oxidised red sand deposits derived from the arid *Old Red Continent*. Gradually, this red sandstone is replaced with sands, clay and limestone (reefs) indicating a relative sea level rise and the formation of a shallow sea (de Jager, 2007; Sorgenfrei, 1969; Lyngsie, 2006). The existence of this sea continues in the Dutch area during the early (Namurian) Carboniferous as derived from the deposition of thick limestone successions in conjunction with black shales. This late deposit, of which the well-known Geverik member is part, suggests that at least for a time anoxic conditions prevailed in the local marine environment during the Early Carboniferous.

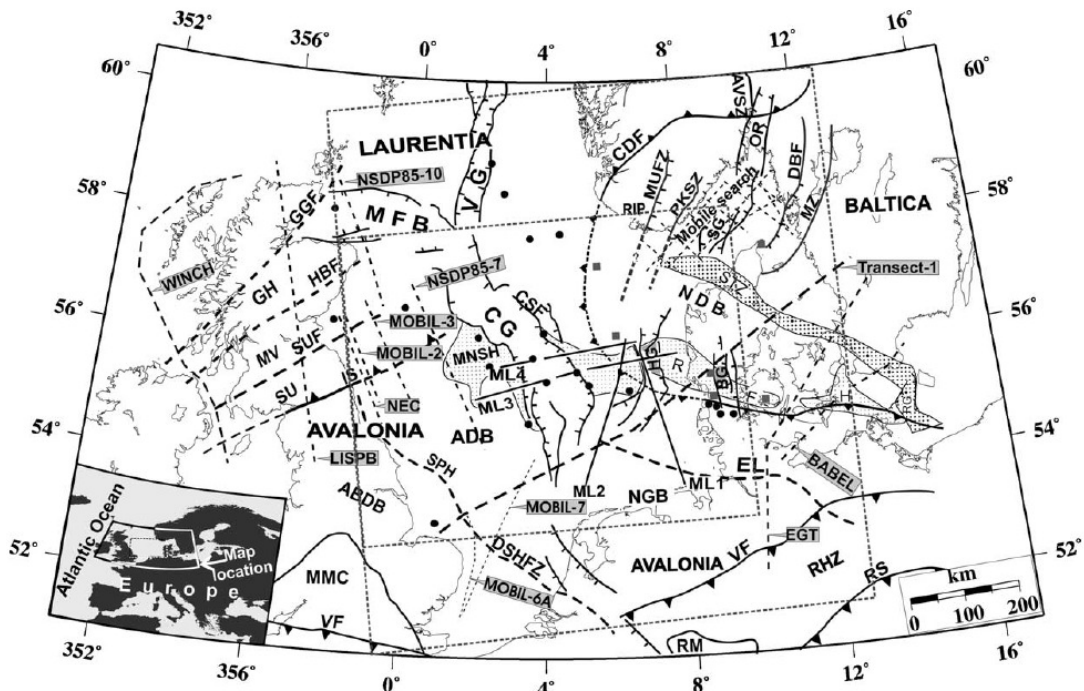


Figure 2.3: The main tectonic features in the North Sea region and the position of the three cratons with respect to each other in the present-day geological setting of the Netherlands. (Source: Lyngsje et al.; 2006)

The Variscan orogeny was initiated by large-scale uplift in the region resulting in the Dutch area to become landlocked. There is however no evidence of deformation that suggests that compression induced by this orogeny reached as far north as the Netherlands (de Jager et al., 2007). The marine conditions of the Early Carboniferous period were steadily replaced by progressively coastal conditions, eventually converting the area to a moist, swampy environment during the Westphalian. The resulting massive swamp-forests gave rise to highly increased deposition of organic material and plant debris, that was later on buried and compacted to form coal seams from which much of the present-day conventional gas (such as the Slochteren gas field) is derived.

At the end of the Variscan orogeny, during the Late Carboniferous to Early Permian, large-scale wrench faulting and consecutive crustal thinning and thermal uplift took place. The crustal thinning is thought to have been caused by magmatic activity, evidenced by volcanic deposits and associated sedimentary rocks in Lower-Permian Rotliegend deposits. This so-called Saalian event resulted in reactivation of the NW-SE trending fault system and inversion of the basins (Lyngsje et al., 2006; de Jager et al., 2007). To the north of the Variscan orogeny, amongst others in the region of the future Roer Valley Graben, deformation was limited to block-faulting and tilting, partly along strike-slip faults (Geluk et al., 1994). Based on the stratigraphic column of the West Netherlands Basin, this inversion induced wide-spread erosion of Stephanian and Westphalian sediments (Saalian unconformity) (Geluk et al., 1994; de Jager, 2007).

During the Early Permian the southern part of the Netherlands experienced limited subsidence. While the northern part was covered by a repeatedly refilling shallow salt lake, resulting in the deposition of thick Zechstein salt deposits, the southern area mostly acted as a fault-bounded platform over which sediments were transported from the progressively degrading Variscan Mountains. It was during the late phase of the Permian period that sedimentation in the area of the West Netherlands Basin and Roer Valley Graben was resumed, resulting in the deposition of coarse clastics of the Upper Rotliegend group (Geluk et al., 1994; van Balen et al., 2000; de Jager et al., 2003, 2007; Duin et al., 2006). Lithological successions found in this group for the area comprise fluvial and aeolian sandstones, claystones, siltstones and finally carbonate deposits (van Balen et al., 2000).

2.2.2 *The Mesozoic Era*

The Permian-Triassic boundary is characterised by a mass-extinction event that heralded the end of the Permian period. The first major-scale tectonic event that occurred was the break-up of Pangaea. This event, the early Kimmerian tectonic phase, initiated far to the north in the Arctic-North Atlantic and slowly propagated southwards carving the shape of future continents. Continued thermal subsidence of the southern Netherlands during the end of the Permian and Jurassic period resulted in the deposition of thick deposits of fine-grained clastics that are part of the Buntsandstein formation (Michon et al., 2003; de Jager, 2007). During Middle Triassic times the eastern rift-branch of the extensional event had reached the southern North Sea. Extensional rates in this branch however had been greatly reduced. The western branch on the other hand continued extension southwards, resulting in the opening of the Atlantic Ocean and continental break-up (de Jager, 2007). The area of the West Netherlands Basin and Roer Valley Graben formed a large-scale half-graben bound to the north by a major fault zone, resulting in uplift of the northern part of the area and consecutive erosion of the Buntsandstein formation (van Balen et al., 2000). As a result, a major intra-Triassic hiatus characterises the stratigraphy of the West Netherlands Basin and Roer Valley Graben (Geluk et al., 1994; van Balen et al., 2000). Extension of the western Atlantic rift zone continued in the Late Triassic and Early Jurassic, resulting in North America drifting further away from Europe. In the mean time, rifting between Africa and Europe had begun in the Mediterranean area. Crustal separation here opened the Tethys Ocean and caused the European continent to drift northwards to higher latitudes (de Jager, 2007).

The Late Triassic and Early Jurassic saw reduced tectonic activity for the area of the West Netherlands Basin and Roer Valley Graben. A wide epicontinental sea formed following regional subsidence, providing the sedimentary environment for the deposition of very thick deposits of shales, relatively rich in organic material, of the Altena Formation (de Jager, 2007). On top of that, black shales of the Posidonia Formation were deposited (van Balen et al., 2000). As a result of regional thermal uplift, deposition of Middle Jurassic sediments came to a halt outside the deep basins, resulting in a stratigraphic hiatus (van Balen et al., 2000; de Jager, 2007).

During the Middle and Late Jurassic, crustal separation both in the Atlantic and Mediterranean area resulted in increased rifting in the North Sea. The southern part of the Netherlands experienced rifting along a NW-SE structural trend which marked finally the actual development of the West Netherlands Basin and Roer Valley Graben. This tectonic event is named the late Kimmerian event, as a successor of the event that occurred during the Triassic period. Rifting continued into the Early Cretaceous resulting in thick accumulations of Cretaceous sandstones and shales of the Schieland Group in the West Netherlands Basin and Roer Valley Graben. This rifting was accompanied by igneous activity in both basins, indicating deep crustal fracturing and resulting volcanism, which may have had a local impact on maturity. Radiometric dating has determined that the two main occurrences of volcanic rock found in the south-eastern West Netherlands Basin are by approximation of 133 and 150 Ma, respectively (van Balen et al., 2000).

Near the end of the Cretaceous era, Africa-Arabia separated from South-America and began to rotate around the Iberian Peninsula and converge with the Eurasian continent, closing the Tethys Ocean. In Europe this tectonic event led to the gradual development of the Alpine Orogeny and is aptly named the Alpine tectonic event (de Jager, 2007). Figure 2.4 below presents the tectonic drift of continents during the last part of the Mesozoic and entire Cenozoic era including both the opening of the Atlantic Ocean and the Alpine Orogeny, amongst others. The maps are based on the work of Scotese (1998) for the PALEOMAP Project of the University of Texas at Arlington.

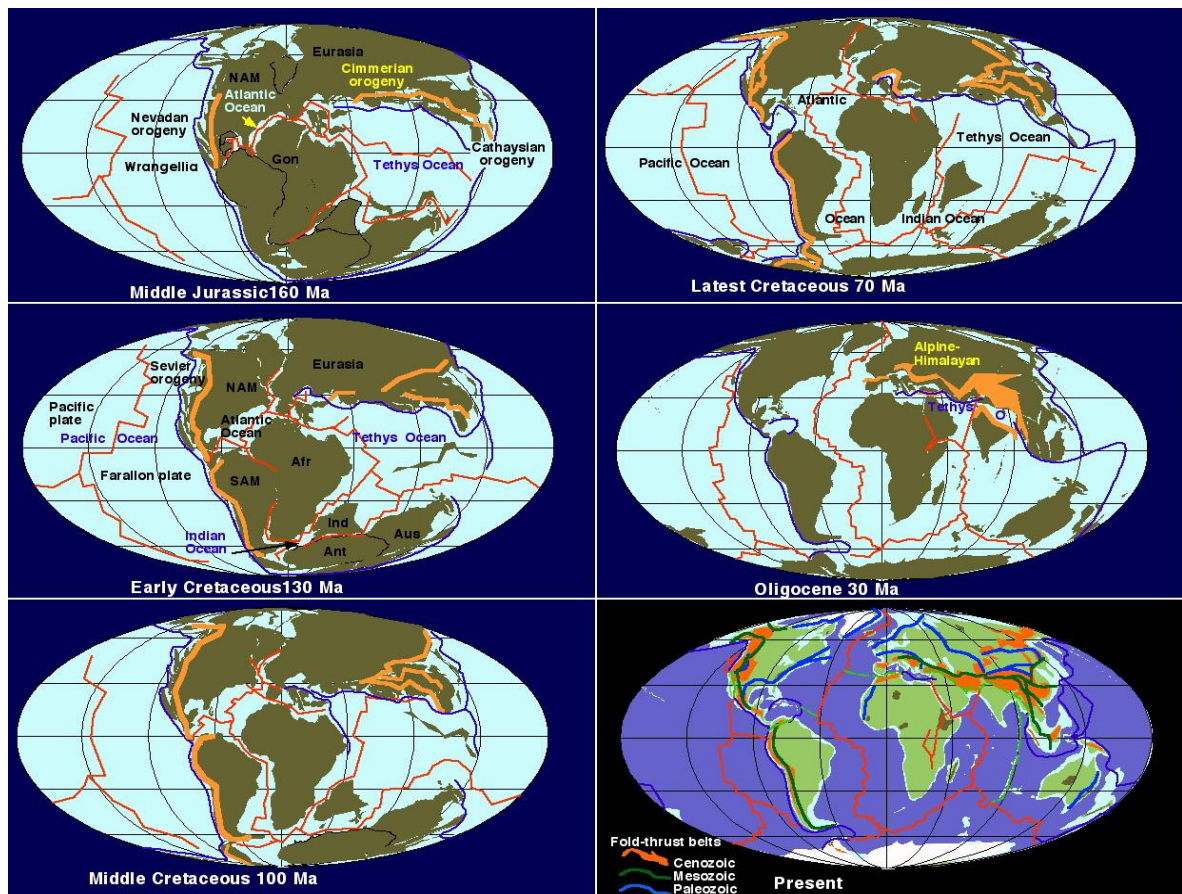


Figure 2.4: Worldwide stepwise modelling of post Pangaea break-up, opening of the Atlantic Ocean, closing of the Tethys Ocean and the related Alpine orogeny, and continental drift toward the present-day situation. (Source: Scotese, 1998; adapted by Northern Arizona University)

During the Late Cretaceous and Early Palaeocene, compressive forces originating from the Alpine orogenic system led to inversion of the Mesozoic extensional basins, among others the West Netherlands Basin and Roer Valley Graben. This tectonic event, the Subhercynian phase, caused erosion of early deposits of the Cretaceous Chalk Group (Geluk et al., 1994; van Balen et al., 2000 Duin et al.; 2006; de Jager, 2007). The event is believed to have occurred in two or three distinct pulses, depending on the basin, which continued far into the Cenozoic era (Michon et al., 2003; de Jager; 2007). These three pulses are designated, from oldest to youngest, as the Subhercynian pulse, the Laramide pulse and the Pyrenean pulse. A fourth pulse, the Savian pulse, can be distinguished in some basins but is of minor importance for the West Netherlands Basin and absent in the Roer Valley Graben (Duin, 2006; de Jager, 2007). The presence of Maastrichtian and Tertiary sediments indicate that no other major inversion events have taken place in the Roer Valley Graben after the Subhercynian phase. The Laramide and younger tectonic pulses did however occur in the Central- and West Netherlands Basin, locally eroding sediments down to the Triassic (de Jager, 2003).

Figure 2.5 presents the timing of the pulses associated with the Subhercynian event and their relative intensity on the various basins.

2.2.3 The Cenozoic Era

During the Cenozoic Era, tectonic events related to the Subhercynian event continued as indicated by figure 2.5. While the Roer Valley Graben experienced a time of tectonic quiescence, the West Netherlands Basin remained active until the Early Miocene period. Although the Subhercynian and Laramide pulse in the West Netherlands Basin resulted in reverse reactivation of pre-existing faults, the Pyrenean pulse was marked only by broad basin uplift (de Jager, 2003). In the Roer Valley Graben, Palaeocene calcaranite deposits followed by continental sands and clays that increase in

thickness toward the centre of the basin testify of an episode of downwarping in the area (Geluk et al., 1994). Steady subsidence and sedimentation followed during the Palaeocene and Eocene, shortly interrupted by a local hiatus, until subsidence strongly increased in the Oligocene resulting in the deposition of the Veldhoven Formation. In the last part of the Cenozoic, sedimentation in the Roer Valley Graben became more restricted. The total thickness of Tertiary sediments in the Roer Valley Graben amounts to 2000 metres (Geluk et al., 1994, de Jager, 2003, 2007).

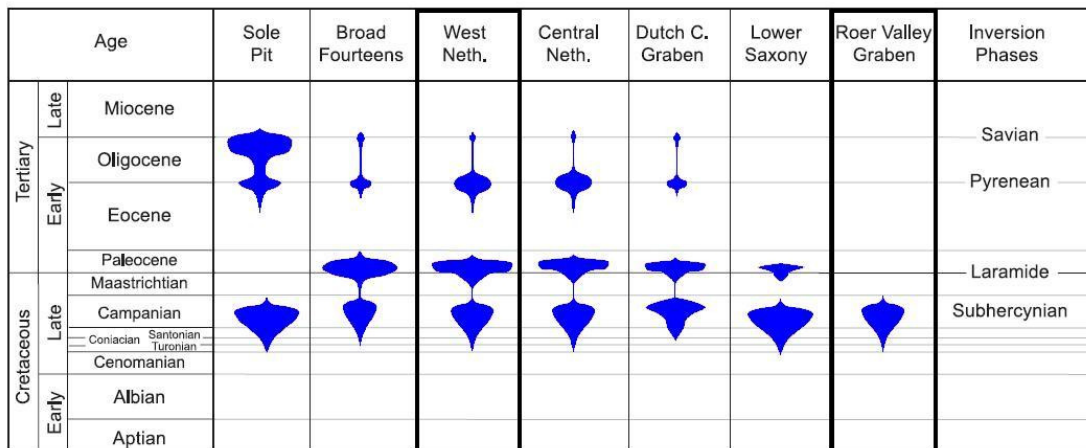


Figure 2.5: Timing and Basin-specific intensity of the four pulses of the Subhercynian event (Source: de Jager, 2007)

The West Netherlands Basin has a much thinner veneer of Tertiary sediments, locally not exceeding 500 metres (de Jager, 2003). These much thinner deposits are the result of the longer-lasting tectonic activity in the West Netherlands Basin. For example, while Palaeocene sediments were deposited in the West Netherlands Basin post-dating the Laramide pulse, these were again eroded during the Eocene-Oligocene pulse, indicating new uplift in the area. Subsidence, and thus sedimentation, accelerated however in the Neogene, when the area was tectonically quiet (van Balen et al., 2000; de Jager, 2007).

Recent seismic activity along the bounding faults indicates that tectonic activity has not completely stopped in the area of the Netherlands. Currently, most of the area of the Netherlands continues to subside, possibly in response to the build up of a compressional stress field with a NNW-SSE orientation. The southern part of the onshore Netherlands however rises due to uplift of the Rhenish Massif (de Jager, 2007).

2.3 Prospective Shale-Gas Formations in the Dutch Subsurface

This thesis focuses on the shale-gas potential of the Lower Jurassic Sleen, Aalburg and Posidonia formation. These formations are shortly described below based on literature. Beside the three Jurassic formations, two other formations present in the West Netherlands Basin and Roer Valley Graben may be of interest with respect to shale gas. These formations are the Upper Cretaceous Plenus Marl and the Carboniferous Geverik member. The Plenus Marl however is found to be very thin (less than 10 metres in general), immature and not sampled. Due to this, this formation has quickly been dismissed as potential shale-gas play. Concerning the Geverik member, the great depth at which this formation is located causes it to be hardly penetrated by the drill. A result of this is that very few data are available on this formation and that, without additional data, an accurate assessment of this formation is not possible at the present time. Both these formations will not be treated further in this thesis.

2.3.1 The Sleen Formation

The Sleen formation is the oldest formation of the Altena Group: a thick sedimentary succession of argillaceous sediment that ranges within the region of the Netherlands (both onshore and offshore) from a few metres up to over 1500 metres in thickness. The sediments of the Altena Group are of Early Jurassic age and consist of pelitic and marine lithofacies (Pienkowski et al.; 2008)

The lithofacies of the Sleen formation itself consists of very-fine grained shales from the Rhaetian period, and are therefore technically of Late Triassic age. The shales incorporate abundant lacustrine and marine fossils and were deposited during a marine transgressive event after sedimentation had long been restricted to continental deposition during the Triassic period (Herngreen et al., 2003; van Leverink & van Bergen, 2008). The Sleen formation is identified from wire line logs since it emits relatively high levels of gamma radiation and has low acoustic values. The boundary with the overlying Aalburg formation however is not always as clear from the logs and is often distinguished by examination of cuttings. The shales of the Sleen formation are more brownish in colour than the Aalburg shales (van Leverink & van Bergen, 2008). The average thickness of the Sleen formation is approximately 30 metres although absolute thicknesses range from 1 to 80 metres. In deep basins, such as the West Netherlands Basin, formation-depths in excess of 5 kilometres are known to occur (Muntendam-Bos et al., 2009). The Sleen formation is considered a source rock but little is known about its potential for generating and storing hydrocarbons (Clark-Lowes et al., 1987).

2.3.2 The Aalburg Formation

The Aalburg formation is the second-oldest formation of the Jurassic Altena Group and was deposited during the Hettangian to Pliensbachian stages of the Lower Jurassic. The depositional environment was a shallow to relatively-deep neritic, open-marine environment (van Leverink & van Bergen, 2008). The formation consists of a uniform succession of dark grey- to black claystones that are locally sandy or silty (Herngreen, 2003; van Leverink & van Bergen, 2008). In the formation, abundant pyritised fossil remains of molluscs and ammonites can be found. Towards the southern boundary of the West Netherlands Basin and Roer Valley Graben an increasing number of thin interbedded beds of limestone are found (Herngreen, 2003). The Aalburg formation lies conformably on top of the Sleen formation and is overlain by the Posidonia Shale. The prospectivity of the Aalburg is greatly enhanced by its great thickness, averaging around 250 metres but locally reaching in excess of 1000 metres. On wire line logs, the Aalburg formation is characterised by relatively low gamma-ray emissions and acoustic values and high resistivity (de Schiffart, 1983).

The organic-rich sections of the Aalburg shale are mainly located in the basal sections. Geochemical analyses performed by TNO indicate that TOC levels can reach values of up to several percent (van Leverink & van Bergen, 2008). In the deepest sections of the Dutch basins, the top of the Aalburg formation can reach depths of up to 3800 metres. As a result of this burial depth, the Aalburg is generally mature enough to generate hydrocarbons (de Jager et al., 1996).

2.3.3 The Posidonia Shale Formation

The Posidonia Shale formation is probably the best-known member of the Jurassic Altena group. The formation is thought to have charged several small oil fields in the Netherlands and is usually described as an organic-rich black shale. Total Organic Content levels can reach values of up to 10% with a kerogen of type II (HI ~800) and is by far the richest source rock formation of the three. The thickness is usually around the 20 to 30 metres in thickness. The formation occurs onshore predominantly in the West Netherlands Basin and Roer Valley Graben. A smaller occurrence is found more to the north in the Lower Saxony Basin.

Being the shallowest of the three formations of the Lower Altena group, the Posidonia formation is the least mature. Only in the deepest regions of the basins is the Posidonia shale mature enough to generate gas thermogenically (Herber & de Jager, 2010). In seismic sections the Posidonia formation is easily recognised since it acts as a clear reflector due to this organic richness. On well logs the formation is easily recognised as well due to its high emission of gamma radiation (hot shale).

3. Key-properties for Productive Gas-Shales

3.1 Literature Study

This section describes and discusses the apparent key-properties for shale-gas plays required to have economic potential. These properties are derived from already existing shale gas plays in the world, predominantly in the United States. According to studies of these existing plays, the most important properties of such plays are dimension, maturity, Total Organic Carbon content (TOC), kerogen type, porosity, and clay-mineral content (Robison, 1997; Lewis et al.; 2004; Bowker, 2007; Pollastro et al.; 2007; Jarvie et al.; 2007; Hill et al.; 2007; Zhao et al.; 2007; Zdanavičiūtė & Lazauskiene, 2009). Rock-mechanical properties, such as tensile- and compressive strength, Young's modulus and shear modulus are predominantly important for production-evaluations of economic gas deposits, and therefore beyond the scope of this thesis.

3.1.1 Gas-Shale Dimensions

The thickness and continuity of gas-shale occurrences are probably the more obvious requirements for a gas-shale play. A small-scale, non-continuous (e.g. patchy) gas-shale distribution makes correct mapping of its presence in the subsurface extremely difficult and leads to uncertainty in determining its presence at a certain location. Small patches of shale are also likely to contain only small amounts of hydrocarbons. In addition, horizontal production wells in small-scale shale patches are likely to fracture surrounding lithologies as well, risking encounters with unwanted side-products, such as water. Concerning the thickness of the shale, it is difficult to assign a standard minimum. Pollastro et al. (2007) reported that a gas-shale should be at least 33 to 66 metres (100-200 ft) thick to render sufficient natural gas for it to be profitable to drill while Bowker (2007) reported a 10 metre thick part of the Barnett shale that was prolific. Generally said, a minimum thickness of 20 to 30 metres should be applied to gas-shales to avoid the greatest risks, with thicknesses greater than 50 metres being the most favourable (Pollastro et al., 2007; Stevens and Kuuskraa, 2009)

3.1.2 Total Organic Carbon (TOC)

The amount of organic matter present in the source rock is generally considered to be an important property for classifying the generative potential, Production Index (PI), of that rock. In general, the higher the amount of organic carbon in the sample, the more hydrocarbons can potentially be generated from the source rock.

TOC levels are usually measured by pyrolysis. Prior to pyrolysis, silicate and carbonate should be removed by solving the sample in hydrochloric acid (Zdanavičiūtė & Lazauskiene; 2009; Robison, 1997). When measuring TOC levels it must be understood that these are the current levels of TOC rather than the original TOC levels. Hydrocarbons that were already generated, most notably gas, will likely have escaped during sample preparations, if not already migrated to other formations during the geologic past. Measured TOC levels therefore only tell something about the source rock's current potential to generate gas, not about how much gas had been generated in the past. TOC levels can also be estimated by using borehole logs (e.g.: resistivity and sonic logs) (Passey et al., 1990). This estimation of TOC however can be disturbed by the presence of free gas and larger pores.

Organic carbon can play a major role in gas storage, a subject treated in section 3.1.5. From studies of other gas-shale plays, it is derived that a TOC level of 2.5-5% is generally considered to be a minimum requirement for prospective plays (Bowker, 2007; Stevens & Kuuskraa, 2009).

The total organic content can be subdivided in three main groups (Jarvie et al., 2007; Muscio & Horsfield, 1996):

- I. Organic carbon retained in hydrocarbons (C_{HC} or S_1)
- II. Organic carbon that potentially could be converted to hydrocarbons, also called *convertible-, reactive- or labile carbon* (C_C or S_2)
- III. Carbonaceous organic residue that has no potential of generating hydrocarbons since it is lacking sufficient hydrogen, called *inert- or dead- or residual organic carbon* (C_R or S_3)

Initially, an immature source rock will have a high percentage of convertible carbon (C_C) and a low percentage of retained carbon (C_{HC}). As the source rock matures, more hydrocarbons will be generated by the conversion of convertible carbon to retained carbon, until at one point, all convertible carbon is converted (Jarvie et al., 2007; Muscio & Horsfield, 1996). The percentage of residual carbon remains stable unless there is an influx (or drain).

The Production Index (PI) can be calculated once the retained, reactive carbon and dead carbon have been quantified using equation 3.1 below.

$$PI = \frac{C_{HC}}{C_{HC} + C_C} \quad (3.1)$$

The production index gives the ratio of hydrocarbons that have already been generated versus the amount of hydrocarbons that ultimately can be generated. A high Production Index thus indicates that the majority of the organic matter in the source rock has already been converted to hydrocarbons (and possibly migrated out) and that mainly the residual phase remains (Espitalié, 1986).

The organic matter in source rocks can be used for another purpose as well. By evaluating the C_1/C_2 (methane/ethane) ratio plotted against the ^{13}C isotope value, the gas can be traced back to the respective source rock from which it was derived (de Jager et al., 1996).

3.1.3 Kerogen Type

The kerogen type present in a source rock depends on the type of biogenic molecules from which the kerogen is formed. Diagenetic transformations and maturation processes have some influence on the resulting kerogen composition as well (Rondeel, 2001). Kerogens are subdivided into four groups, all covering a specific range of kerogen composition. These groups are represented in a van Krevelen diagram, displayed in figure 3.1. A van Krevelen diagram plots either the pyrolysis parameters Hydrogen Index (HI) versus the Oxygen Index (OI) or the atomic ratio H/C versus O/C, depending on the data available. Although the atomic ratios are often assumed to be more accurate in determining the kerogen type of organic matter, the two sets of axes can be easily correlated with each other (Baskin, 1997). The diagram in figure 3.1 displays both these sets of axes.

In general, the higher the kerogen number, the more aromatic structures can be found in the organic matter. Aromatic structures are characterised by low hydrogen content and high oxygen content and they are more prone to generate natural gas than liquid hydrocarbons (Muscio et al., 1994). The following is a short description of each kerogen type based on Rondeel (2001).

Type I – Type I kerogen is generally of lacustrine origin, derived from algae whose organic debris has sunk to the bottom and was buried. Type I kerogen is relatively rare since anoxic lakes have never been very common and because lakes are relatively small in terms of surface area. The main organic component in type I kerogen is alginite. This kerogen has great potential for the generation of liquid hydrocarbons and can be found in shale lithologies.

Type II – Type II kerogen is derived from more than one source generally, these sources being marine algae, spores, pollen, leaf waxes, dinoflagellate cysts, and fossil resin. Type II kerogens are predominantly of marine origin, all being composed of lipids which are deposited under reducing conditions. This type of kerogen generally has a high potential for generating liquid hydrocarbons and gas. Most gas-shales have type II kerogen as their main organic constituent. The dominant organic component in type II kerogen is exinite, although cutinite, resinite and liptinite macerals are common too, depending on the main origin for organic matter. Some type II kerogens contain high amounts of sulphur, giving them the sub classification Type II-S.

Type III – Type III kerogen is mainly of terrestrial origin consisting of wood and other plant material (cellulose) and lack the waxy components found in type II kerogen. Type III kerogen is often found in coals. The main component of type III kerogen is vitrinite, which is used for maturity determination, a technique that originated from the period of intensive coal exploration and exploitation. Type III kerogens are less capable of generating hydrocarbons due to their high amount of aromatic structures and low hydrogen content and generally only produce gas. Under special conditions however, type III kerogens are known to be able to produce some oil (de Jager et al., 1996).

Type IV – Type IV kerogen (also called residue kerogen) consists mostly of reworked organic debris and oxidised material. The hydrogen content of type IV kerogen is very low while the oxygen content is very high. The dominant atomic structure is aromatic and the main component is inertinite. Type IV kerogen is considered to have no significant hydrocarbon-generative capabilities.

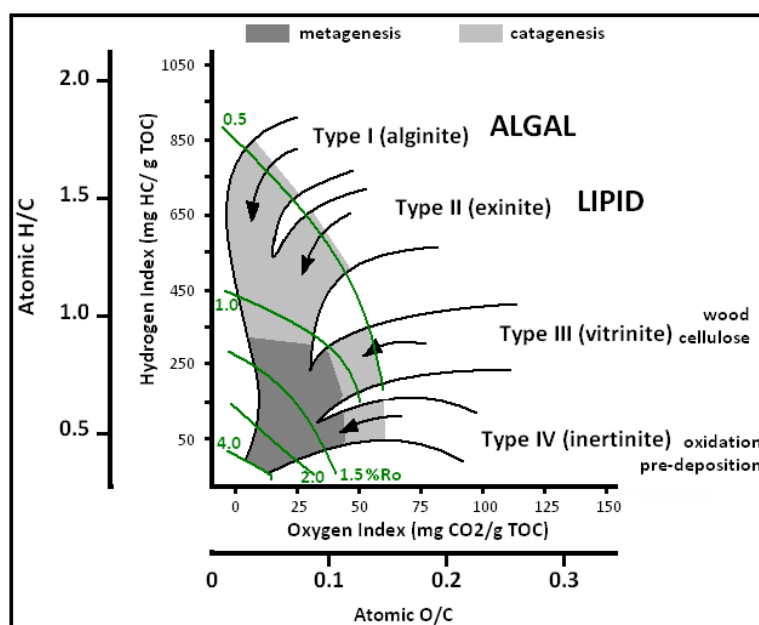


Figure 3.1: Maturation pathways of kerogen Type I – IV displayed in a van Krevelen diagram; the pathway is traced by changes in atomic H/C & O/C ratios. Shaded areas indicate differences between diagenesis (blank), catagenesis (light grey) and metagenesis (dark grey). The green lines indicate regions of equivalent vitrinite reflectivity. (Source: Re-imaged after Rondeel (2001))

A common unit for HI is the mass of hydrocarbon generated per mass of organic matter (mg HC / g TOC) while OI is defined as mass of carbon-dioxide versus mass of organic matter (mg CO₂ / g TOC). Present-day values for the hydrogen index are, at high maturities, not representative for the original kerogen type. As can be seen from figure 3.1, HI changes with maturity, which changes over time. It can be used however to define the amount of hydrocarbons that can still be generated (Jarvie et al., 2007).

3.1.4 Maturity and Maximum Temperature

Maturity is one of the most important criteria for hydrocarbon generation. If the maturity is not high enough, no thermogenic hydrocarbons will be found. In the case of shale gas, as figure 1.1 already illustrates, high quantities of natural gas start being generated thermogenically around temperatures of around 100 degrees Celsius. In the case of a standard geotherm these temperatures are reached at depths of over 3000 metres. However, in the case of active and fast basin inversion or for areas with volcanic or hydrothermal activity, these depths may be much shallower for the duration the enhanced geothermal conditions continue (Pollastro et al., 2007).

The maturity of source rocks is generally determined optically by assessing the reflectivity of vitrinite macerals and converting this to mean vitrinite reflectivity (R_o). For large-scale gas production a mean vitrinite reflectivity of $R_o > 1.1\%$ is generally assumed to be required. At the temperature range indicative for this reflectivity the source rock is heated enough for the oil that was generated earlier at lower temperatures to be broken down into smaller hydrocarbon chains by the process of cracking. Above maturity levels of $R_o > 1.4\%$ the gas generation really speeds up generating large quantities of gas in a relatively short time (Pollastro et al., 2007; Jarvie et al., 2007; Hill 2007; Pollastro, 2007; Stevens & Kuuskra, 2009; Zdanavičiūtė & Lazauskiene, 2009). Vitrinite reflectivity is only one of many other parameters used to define source rock maturity, but it is the most widely used. Measuring vitrinite reflectivity requires the presence of terrestrial organic matter in the source rock since only plant debris contains vitrinite. For non-terrestrial source rocks or for circumstances wherein measuring the vitrinite reflectivity is not possible, the inferred R_o value can be approximated using the maturity-equivalent regions in a van Krevelen diagram, featuring approximated maturity areas for type I, II and III kerogen. These areas were also observed in figure 3.1 on the previous page.

Although still highly valued and proven on a multitude of occasions, maturity is not an unfailing asset for finding hydrocarbons since examples exist of immature source rocks that still generated high quantities of hydrocarbons. In addition, a major difficulty with vitrinite reflectivity in black shales is that vitrinite is derived from terrestrial plant material and therefore mainly absent in marine black shales.

Recent results however might render maturity of source rocks less important while exploring for potent source rocks than is generally appreciated. On various occasions an immature gas-shale source rock was found to contain high concentrations of indigenous natural gas. In the Netherlands an example of such a feat is found in an immature part of the Posidonia shale at the Ottoland-01 well. A perhaps better documented example of this occurrence is found for the Bakken Shale (Willingstone Basin, U.S.A./Canada). The maturity of the shale was locally found to be $R_o < 0.7\%$ but still contained indigenous gas. Moreover, in regions where $0.7\% < R_o < 1.1\%$, the amounts of natural gas were found to be significantly reduced. The authors (Muscio et al., 1994) could at the time not determine the exact cause for the occurrence of natural gas in an immature source rock, but suggested an enhanced aromatic nature of the Bakken shale kerogen, specific biological precursor material derived from bacteria (biogenic gas), and enhanced adsorption capabilities (concerning the gas-gap at medium maturity) as possibilities for their observations.

Low-temperature gas generation

A recent study (Mango & Jarvie, 2009) reported laboratory-proven generation of large quantities of natural gas at temperatures as low as 50°C , which would indicate a maturity of $R_o \sim 0.3\%$. Laboratory experiments performed by these authors indicate that, under anoxic conditions, marine black shales are capable of generating significant quantities of natural gas by a catalytic reaction, most likely with low-valent transition metals. Although the authors could not completely exclude the possibility of biogenic gas generation, the characteristics of the generated gas made it unlikely that bacterial activity was involved. These findings may have major consequences for the potential of black shale-derived hydrocarbons, of which shale-gas is a good example.

Type II kerogen is preferred for both regular hydrocarbon generation and low-temperature gas generation (Zdanavičiūtė & Lazauskiene, 2009; Muscio et al., 1994; Lewis et al., 2004)

3.1.5 Porosity, Storage Capacity and GIIP

The ability of shale to store natural gas is another property that is often indicated to be of high importance for gas-shales. Since, for an unconventional shale-gas play, the source rock is no longer solely the source of the hydrocarbons from where hydrocarbons emerge but the reservoir as well, porosity has become a property worth considering. Porosity of the source rock is used both for storage of free gas and, if the pores are interconnected prior to or after fracking, for gas migration and transport within the shale. Existing gas-shale plays indicate that a porosity percentage of 6-12% minimum (Stevens & Kuuskraa, 2009) is generally assumed to be a requirement for an economically prospective gas-shale.

Porosity alone, however, is not the full equation for gas storage. It is true that a shale-rock with a higher porosity generally can hold more free gas, but gas in a shale is not only stored as free gas. A gas-shale applies three concepts for storing gas (Jarvie et al., 2007)

1. Free gas in pores and cracks
2. Adsorbed gas on the surface of the organic matrix
3. Absorbed gas within the organic matrix

These last two options only use porosity to a certain extent. Adsorbed natural gas of course needs a surface to accumulate onto but does not need large pores. Instead, micro porosity (<1 μm) is sufficient for this purpose. Dense micro porosity causes a larger total pore-space surface than macro-pores do, creating more potential surface-storage space for gas adsorption. Natural gas which is absorbed in the organic matrix has no immediate need for pore space since it is contained within the matrix itself. Lewis et al. (2004) documented that the amount of adsorbed gas in a gas-shale can vary from 20 to 85% of the total, depending on reservoir pressure; a huge range that allows grave errors in estimates of the GIIP if only free gas is considered.

In a gas-rich source rock, equilibrium exists between the amount of adsorbed gas and free gas. This equilibrium, depending on reservoir pressure, temperature and TOC levels can be described by a Langmuir isotherm (Langmuir, 1918). This isotherm indicates that at higher reservoir pressure, the balance between free gas and adsorbed gas shifts in favour of adsorbed gas, with less free gas present in the rock. This, however, also indicates that during pressure release from the source rock, for example due to gas production at a well, the equilibrium will shift back towards free gas and the adsorbed gas will be released, adding more hydrocarbons to the GIIP then would be estimated by measuring the free gas only. For the construction of a Langmuir curve, adsorption measurements have to be taken from a core sample. It is generally assumed that for a given lithology and basin, only one isotherm is required to describe the adsorbed amount of gas for a specific field or sub-basin (Lewis et al., 2004). The isotherm, which is described by equation 3.2, can then be corrected for local temperature and TOC levels to estimate gas adsorption at other localities.

$$gC_{ads} = \frac{V_l p}{(p + P_l)} \quad (3.2)$$

where,

gC_{ads}	=	adsorbed gas content	[m ³ /ton]
p	=	reservoir pressure	[Pa]
V_l	=	Langmuir volume	[m ³ /ton]
P_l	=	Langmuir pressure	[Pa]

The Langmuir volume defines the maximum amount of gas that can be adsorbed by the source rock. The Langmuir pressure is the pressure at which 50% of the adsorption capacity of the source rock is reached.

It must be noted that the main weakness of the Langmuir isotherm-derived adsorbed gas calculation is that it calculates the amount of gas that *could* be adsorbed by the source rock rather than the amount of gas that *has* been adsorbed at a specific temperature and pressure. Factors such as moisture content and gas saturation decrease the actual amount that is adsorbed, resulting in an overestimation of the GIIP in the source rock.

The free gas and adsorbed gas combined yield an estimate of the total gas initially in place (GIIP) for the gas-shale. Chemically absorbed gas is released much more slowly since it is incorporated in the matrix and therefore does not add significant numbers to the GIIP estimate.

It was stated by Shtepani et al. (2010) that the total initial gas content of a formation can be determined by determining its three components. These components are *lost gas* -the gas liberated during retrieval of a sample from the well prior to emplacement inside a canister-, *desorbed gas* -the measured gas released from the shale inside the canister-, and *residual gas* -the gas that remains adsorbed even at atmospheric pressure-, and adding these together. Residual gas and sorbed gas can be measured in the laboratory. Lost gas however cannot be directly measured and is determined by extrapolating early desorption rates to 'time zero' using an appropriate mathematical relation.

3.1.6 Clay-Mineral Content

The mineralogy of the clay is important for more than one reason. Clay minerals in gas-shales influence the properties and potential of the shale in the following ways.

Gas storage – Clay minerals do not appear to adsorb natural gas on their surfaces. This has been proven for the American Barnett-shale play (Bowker, 2007). If the inability of clay minerals to adsorb gas is a common occurrence in gas shales it indicates that, regarding gas storage, clay minerals are 'lost space'. They do take up space in the shale but cannot be used for storage, thus decreasing the maximum storage capability of the shale.

Gas generation – In the study of Mango and Jarvie (2009) it was indicated that for marine shales of kerogen type II, low valent transition metals are the most likely cause for catalytic gas generation at temperatures as low as 50° C. Hill et al. (2007) already suggested that gas-generation in low-mature shales might be influenced by the presence of clay-minerals. These clay-minerals are the most likely source for in-situ low-valent transition metals and are thus directly influencing the production of hydrocarbons, especially at low temperatures.

Gas production – From studies of the Barnett shale and others, it became apparent that productive gas-shales in general have far lower clay-mineral contents than most shales (Lewis et al., 2007; Bowker, 2007; Jarvie et al., 2007). Explorationists were recommended to look especially for shales that contain less than 50% clay minerals (Bowker, 2007), although less than one-third is possibly even better (Loucks & Ruppel, 2007). The reason for this requirement is that shales with a high amount of clay minerals are more ductile and therefore less sensitive to stimulation (fracking of the reservoir). Even if a gas-shale is capable of generating, retaining and storing high amounts of hydrocarbons, these can only be retrieved if the gas is able to freely move to the production well (Jarvie et al., 2007). The brittleness of a shale is related to its mineralogy and, although shale by particle size and name, clay minerals may not dominate.

3.2 Case Studies

Although one could assume from the previous section that all shale-gas plays are more or less the same, significant differences exist between them. To illustrate this, the next two sections contain case studies of two major North American productive shale-gas reservoirs: The Barnett Shale play, Texas, and the Lewis Shale play from New Mexico/Colorado.

3.2.1 *The Mississippian Barnett Shale*

For many geologists involved in unconventional gas-shales, the Mississippian Barnett Shale, located in the state of Texas, U.S.A., is the textbook example of an economically producing shale-gas reservoir and indicative for the possible potential of shale-gas in the world. The Barnett shale covers a large area, is mature and organic-rich, responds well to stimulation processes, and is under- and overlain by fracture-resistant impermeable limestones that avoid contamination of the gas field by water or other fluids of surrounding formations. Although production of the Barnett shale began in the early 1980's, only since the beginning of the last decade have production rates really increased and have technological innovations uncovered the real potential of this play (Martineau, 2007). The Newark East Field, the largest producing field of the Barnett Shale in Texas, had a total of 6203 wells completed in 2006. These produced approximately 56 MMsm³ (Million standard cubic meters) of natural gas per day (2.0 bcf/d) to a total of 65 BCM (Billion standard cubic meters) of natural gas in 2006 (2.3 tcf). The majority of this gas was produced in the preceding last eight years (Martineau, 2007). Recently, the U.S. Geological Survey estimated for two Barnett shale gas assessment-units (within the Fort Worth basin) a total mean volume of about 736 BCM (26 tcf) of undiscovered gas that could technically be recovered from the area (Pollastro et al., 2007).

The Barnett shale is located in the Bend arch - Fort Worth Basin in north-central Texas; an asymmetric, wedge-shaped basin containing over 3500 metres of sedimentary deposits. The mean thickness of the Barnett shale is 75 to 200 metres (Stevens & Kuuskraa, 2009). The structure formed as a foreland basin in front of the advancing Ouachita thrust belt in the Late-Mississippian to Early-Pennsylvanian (Carboniferous) episode of plate convergence over the North-American craton (Hill et al., 2007; Pollastro et al., 2007). Deposition of the Barnett Shale formation occurred most likely in a deep-water continental slope-to-basin setting below storm-wave base and the oxygen minimum zone, in a long and narrow foreland basin that was poorly connected to the open ocean, resulting in a water-column stratification (Loucks & Ruppel; 2007). The Barnett shale is presently buried to depths of around 1800-2200 metres although initial burial may have been higher. The formation consists of black to brown organic shale, dark fossiliferous shale, dolomite Rhomb shale, dolomitic shale, concretionary carbonite and phosphorite, although the first two are the dominant lithofacies. Some however choose to define the lithology of the Barnett shale more as a mixture of laminated siliceous mudstone and laminated argillaceous- or fossiliferous lime -mudstone or -packstone (Loucks & Ruppel; 2007).

The TOC values vary between 3% and 13% with an average of about 4-5% (Pollastro et al., 2007; Hickey & Henk, 2007; Loucks & Ruppel; 2007; Jarvie et al; 2007). The kerogen type is defined as type II marine oil-prone kerogen, based on an average original hydrogen index (HI_o) of 475 mg HC/g TOC for immature outcrop samples (Jarvie et al.; 2007). The major portion of the outline of the Newark East field encompasses gas-mature Barnett shale ($R_o > 1.0$) (Zhao et al.; 2007). In general, successful non-associated gas production in the Barnett Shale occurs for areas where the shale is organic-rich and within the thermal gas generation window ($R_o \geq 1.1\%$) (Pollastro et al.; 2007).

The Barnett shale in the Fort Worth basin is known for varying rates of production depending on location. The main producing field in the basin, the Newark East field or 'core', has two regions where gas production rates are significantly higher than at other locations. The exact reason for the great difference in gas flow rates is still largely unknown although it is speculated that it is related to either a better gas-transition mechanism in the shale or simply due to the fact that more gas is in place there (Bowker, 2007). The formation is overpressured at 11.8 kPa/m (0.52 psi/ft). The cause for

this relatively high pressure is not entirely understood but it is thought that it is either due to the overpressure resulting from continuing gas generation to the present day, or due to past-time overpressures caused by burial.

The Barnett shale responds well to stimulation. This is the result of the low clay-mineral content of the shale (generally <50%) resulting in a higher silica content and thus a more brittle rock-mechanical behaviour (Bowker, 2007). The best producing wells come with a quartz content of 45% and a clay-mineral content of only 27% (Jarvie et al.; 2007). Although the Barnett shale is an acknowledged deep-horizon shale success, doubts remained whether or not this play was a one-of-a kind geological occurrence, similar to the San Juan fairway coalbed methane play, New Mexico, which is still not matched in terms of producibility and gas rate. It was not until several breakthroughs in shale gas at other localities that these doubt were finally quenched (Stevens & Kuuskraa; 2009).

It is recommended that explorationists who wish to find new gas deposits in either the Barnett shale or other shale plays do not look for sections that are already extensively fractured, but rather look for sections that *can* be fractured since the Barnett shale is the best example of a play that has no fractures but is still of great economic importance (Bowker, 2007). Because the Barnett shale is over- and underlain by the Marble Falls Limestone and Chappel Limestone respectively, which are both much more resistant to fracturing, the Barnett shale is shielded from water-bearing permeable layers that surround it. This too enhances the prospectivity of the Barnett shale since these 'fracture-shields' reduce the chance that water will seep into the producing well, causing production of water. Produced water will have to be disposed at a cost and will possibly reduce flow rates; both are unfavourable for the production process (Bowker, 2007; Hill et al.; 2007). In general, it is believed that the Barnett shale is so successful because it has (1) a favourable combination of high diffusion rates, (2) a very high gas concentration, and (3) high ability to be fractured (Bowker, 2007).

Figure 3.2 displays the distribution of the Barnett Shale in the state of Texas.

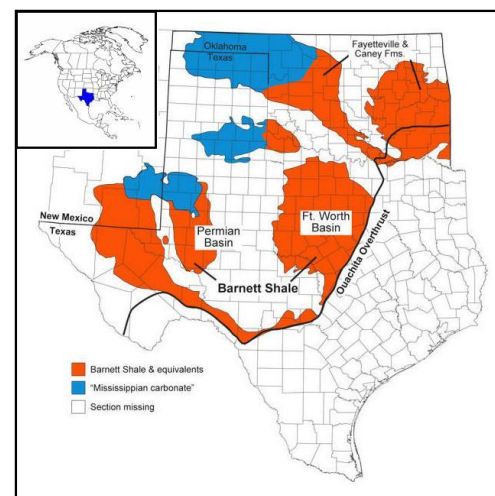


Figure 3.2: Distribution of the Barnett Shale in Texas (Source: USGS)

3.2.2 The Lewis Shale

The Lewis Shale is the youngest play on the North American continent, consisting of Upper Cretaceous sediments. Commercial development of the play began in the late 90's in the San Juan Basin, located in the Rocky Mountains in the states of Colorado and New Mexico. It is the largest source of natural gas in that area. Prior to production, 16 wells were already drilled in the San Juan basin for exploration purposes during the period 1950's to 1990's. Although the wells were aimed for deeper formations, making the Lewis Shale not specifically a target for hydrocarbon exploration, the shale was penetrated and extensive healed natural fractures were found. However, the Lewis shale, like all gas-shales, still has to be stimulated for production. The main producing company of the Lewis shale is Burlington Resources, which have drilled over 6500 wells in the basin, approximately one-third of the total (Campbell et al. 2000). The Lewis play is interesting because it has a very high thickness and thermal maturity and a low TOC content (Curtis, 2002). The formation has been deposited in a lower shore-face to distal offshore setting. Lithofacies in the shale include quartz-rich mudstone, sandy siltstones, shales, and a smaller percentage of sandstone (Dube et al., 2000; Curtin, 2002). The beds of the Lewis shale contain a wide variety of fossils, especially many species of ammonites (Cobban et al., 1974).

Exploitation of the Lewis shale originally started as a secondary completion zone in new wells or a recompletion zone in existing wellbores. At the beginning, production in the San Juan basin was mainly aimed for naturally fractured, low permeability, Cretaceous sandstones and for the Fruitland

coal. It was however discovered during drilling for deeper formations that flow rates in the Lewis Shale were far higher and production was consequently rerouted to this formation (Dube et al.; 2000).

The Lewis shale is generally thick, having a thickness ranging between 300 and 500 metres. It currently lies at depths of 1000-2000 metres after having been uplifted in the Miocene. The shale is slightly overpressured at 4.6 to 5.7 kPa/m (0.2-0.25 psi/ft). The thermal maturity for the Lewis shale is very high; vitrinite reflectance values in excess of 1.6% R_o are common. The amount of organic material on the other hand is quite low. Most of the formation does not contain more than 2% TOC.

Measurements have indicated that the Lewis shale contains approximately 0.4-1.3 m³/ton natural gas. This value is far lower than that for most other producing gas shales. The Barnett shale for example contains in general over 8.5m³/ton gas. Its flow rates are somewhat on the low side as well, at 2800-5600 m³/day of natural gas per well. This is generally lower than the Barnett shale, which produces at 2800-28000 m³/day per well, but the production rates are still increasing. Estimates of the reserves mean volume of technically recoverable gas of the Lewis shale indicate that the play may contain 0.2-11.3 BCM of gas (Curtis, 2002; Bustin, 2005). Figure 3.3 displays a map depicting the occurrence of the Lewis Shale in the San Juan Basin.

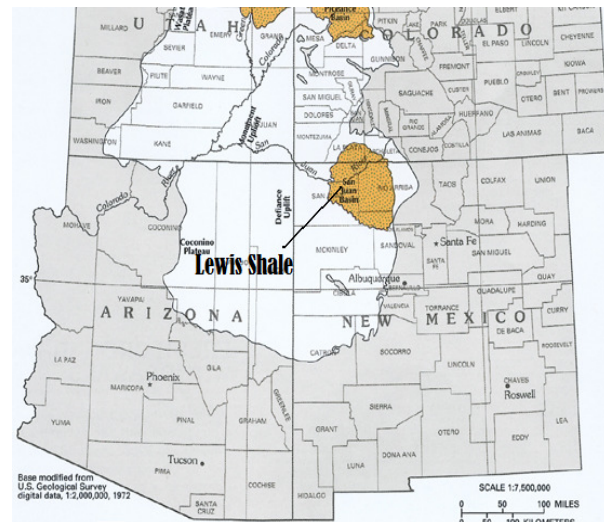


Figure 3.3: Distribution of the Lewis Shale in the San Juan Basin, New Mexico/Colorado. Source: USGS

Figure 3.4 and table 3.1 below compare the important properties of both plays. From the spider chart it can be seen that they are almost each other's opposites in terms of GIIP, TOC, thickness and quantity of absorbed gas. Clearly, although their properties differ quite a lot, both satisfy the set of reservoir requirements. The only factor that does not meet minimum requirements is the TOC level for the Lewis shale. However, both shales are still capable of providing a commercial natural gas flow. The Lewis shale may not be such a near-perfect play as its Mississippian counterpart but it is still good enough to be of significant importance both with respect to profits and energy deliverance. Clearly, shale gas plays are very variable in terms of properties, yet can still be profitable.

Table 3.1: Comparison Overview of the Barnett Shale and the Lewis Shale

	Barnett Shale	Lewis Shale
No. of Wells	6200+ (2006)	18000+
Production per well per day	2800-28000 m ³ /well/day	2800-5600 m ³ /well/day
GIIP	736 BCM	0.2-11.3 BCM
Formation Thickness	75-200m	300-500m
Formation Depth	1800-2200m	1000-2000
TOC Content	3-13% (av. 4-5%)	~2%
Kerogen Type	type II	type II?
Maturity	$R_o \geq 1.0$	$R_o \geq 1.5-1.6$
Overpressure	0.52 psi/ft	0.25psi/ft
Clay-Mineral Content	<50%	No Data

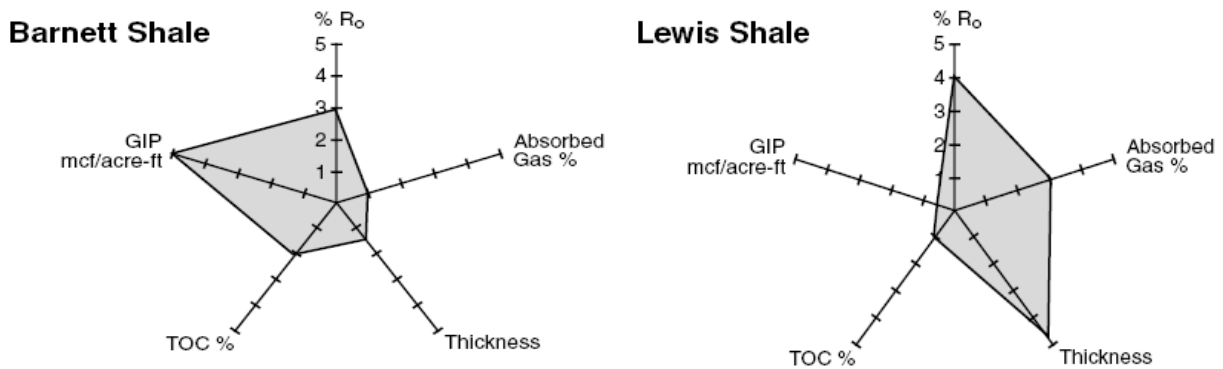


Figure 3.4: Spider chart plotting R_o , GIP, TOC, Thickness, and relative quantity of adsorbed gas for the Mississippian Barnett Shale and Cretaceous Lewis shale. Note that both shales are somewhat the opposite of the other.
Source: Curtis, 2002

3.3 Discussion and Conclusions concerning the Literature Study

The preceding section has summarised the literature opinions with regard to essential properties required for determining the potential of shale-gas plays. These properties were mainly derived by comparing two sets of data, denominated as ‘set A’ and ‘set B’ for easier reference purposes.

- A. Set A comprises the measured properties as found for existing economic shale-gas plays. Although most source rock properties vary over a wide range of possibilities, the minimum value was often taken as an approximate lower boundary for an economic play.
- B. Set B comprises experience built-up for conventional plays. Since the start of petroleum production geologists have studied and documented properties of source rocks, reservoir rocks and seals and the knowledge acquired by these studies are implemented for gas-shale potential as well.

It can be argued however that both these data sets are flawed. When using dataset **A**, there is always the chance that another, yet unexplored, play will possess strikingly different properties that are much more extreme than the reference set while still possessing a high economic potential. By defining a certain range of properties as ‘average’ or ‘minimum’, this unexplored, potentially economic play could be discarded for lack of estimated economic potential because it does not fulfil the defined requirements, even though it is actually the reference data set that is incomplete. An example of such an *extreme* situation would be a play that was never heated beyond 60° C but generated its gas by a catalytic reaction. Another example was seen during the case studies, where the Lewis shale was found to have generally less than 2% TOC. Although some thin beds of TOC-enriched shales occur, these are generally too thin to be of major importance.

Regarding dataset **B**, this data set might have been working well for conventional plays, but shale-gas is not a conventional play. Conventional plays have a clear differentiation between source, reservoir and seal, and as long as the reservoir contains hydrocarbons and the seal is intact there is not that much interest in the source rock. For gas-shales however this differentiation does no longer exist. All three dominant aspects of a conventional play are combined to a single self-sourced reservoir. A result of this is that properties that were formerly separated are now interacting with each other, e.g. porosity and TOC content.

For conventional plays porosity is the only factor for storing hydrocarbons. TOC content on the other hand is only indicative for the petroleum index and related to trap and seal-emplacment as to ascertain that not all hydrocarbons had been formed prior to the seal and trap development; this

would result in an empty reservoir. This clear differentiation leads to a minimum requirement for porosity and TOC value for a conventional prospective play.

In the gas-shale play however, these distinct attributes have been replaced by interacting attributes between the two properties. With the organic material being capable of storing hydrocarbons as well, by means of adsorption and microporosity, pores in the source rock are no longer the only means of storage. In addition, porosity space is increased by the conversion of organic material into hydrocarbons. Since the seal and reservoir are both contained within the source rock the high present-day TOC level is no longer required to ascertain that the reservoir will not be empty due to a previously missing reservoir, trap or seal.

Unconventional shale-gas plays are *not* equal to conventional plays and should thus not be treated as such. The old concepts for conventional plays should be re-evaluated for their use and priority. In the mean time, another method has to be developed for assessing the potential of gas-shales.

A possible attribute for assessing the potential of gas-shales are gas shows. Gas shows are measured whilst drilling and are a first source of information for the occurrence/presence of gas in the penetrated sequence. For areas such as the Netherlands, where many wells have penetrated overlying (shale-) formations, these records may well be the most accurate method for a first assessment. This concept is backed by a recent study of Shtepani et al. (2010) who argue that for gas shales the dominant key-parameters are gas content and storage capacity. Just as was argued above, it is speculated that as long as the source rock can store sufficient gas and as long as gas shows indicate a high gas content it does no longer matter whether or not the rock has high maturity or a favourable burial history; at least gas is there so the only parameters that matters are the GIIP, the desorption factor and the method how to get the gas out. Gas shows may, however, not be considered the most trustworthy of measured properties, but that is mainly due to gas show experience for conventional plays, where porous reservoirs were choked by intra-formational mud injection. Either way, one can argue that as long as sufficient gas shows are found, the shale gas may be deemed prospective. If no gas shows are found, one can use the other attributes (TOC, maturity etc.) to estimate the likeliness that the shale is gas-bearing after all.

4. Laboratory Methodology and Data Acquisition Techniques

The focus of attention of oil companies operating in the Netherlands has always predominantly been with the reservoir- and seal rock properties rather than with those of the source rock. Although source rocks are occasionally sampled and analysed, the test results are generally not made available to the public. As a consequence of this, little available data exists for the Jurassic source rocks. Therefore, new data has been generated for this study from cores taken by NAM from the Lower Jurassic formations. With new data it will be possible to draw more accurate conclusions with regard to the gas potential of Jurassic shales in the southern Netherlands. In addition, Langmuir methane-adsorption isotherms are constructed. Beside these new data, the existing data (well logs) are used as well.

4.1 Core Analysis

In total, 295 samples have been taken from cores from 16 different boreholes, covering four formations. These formations are the Aalburg Formation (188 samples, 14 boreholes), the Sleen Formation (9 samples, 1 borehole), and the Posidonia Shale Formation (98 samples, 5 boreholes). A fourth formation, the Jurassic *Werkendam Formation* was accidentally sampled as well (28 samples, 1 borehole) but these cores are not analysed. Not all relevant core samples are processed due to budget limitations. A selection of 94 core samples (93 unique units and 1 reference unit) were sent to Fugro Robertson Ltd. laboratories for pyrolysis (Rock Eval) and mineralogy analysis (Qemscan). In addition, 5 of these 94 samples have also been sent to RWTH Aachen for adsorption isotherm construction. A complete list for the core samples indicating the analysis performed on each sample is included in Appendix A.

4.1.1 Rock Eval

Rock Eval is a pyrolysis analysis tool used for the determination of TOC, C_{HC} , C_c , and C_R . The tool has been developed in 1978 by the Institut Francais du Petrole and was successfully applied in the field for the first time in the same year (Clements et al., 1979). The latest version of the technique, Rock Eval 6, is widely used in the petroleum industry.

Rock Eval analyses the rock by heating the sample in an open pyrolysis system under non-isothermal conditions (Behar et al.; 2001). Hydrocarbons that are formed and released during the heating process are registered by a detector called the *Flame Ionization Detector* or *FID*. These measurements result in peaks for the carbon retained in hydrocarbons (S_1 or C_{HC}) and convertible carbon (S_2 or C_c). After all hydrocarbons have been formed and released, the remaining rock is combusted at 850° C. The CO and CO₂ that are released during this combustion are measured to determine the residual carbon (S_3 or C_R) (Behar et al.; 2001).

4.1.2 Qemscan®

Qemscan® (originally marketed as 'QEM-SEM' or 'Quantitative Evaluation of Minerals by Scanning Electron Microscopy') is a relatively new analysing technique developed by the Australia-based *Commonwealth Scientific and Industrial Research Organisation* (CSIRO) and was made available for commercial use in 1998. The following description of the system's operations is based on information provided by CSIRO, Intellection®, and Fugro Robertson Ltd., as well as a publication by French et al. (2008).

The Qemscan system utilises scanning electron microscopy and is equipped with 4 energy-dispersive X-ray spectrometers for quick mineralogy mapping with variable resolution depending on

the contractor's needs. The output of the analyses typically contains data on mineralogy, grain size, sorting, pore space and micro-fractures and their preferred orientation. The system works differently from other SEM-systems in that a full X-ray spectrum is acquired at each measuring point of a rectangular grid superimposed on the particle. This spectrum, consisting of both backscattered electron- and dispersive energy- X-ray signals, is used to discriminate between grains of different mineral types or phases of which representative samples are used for mineralogical determination. The point-wise line-scanning of the system along the lines of the rectangular grid provides a broad dataset of different mineral grains and their shape, allowing not only the determination of mineral type and abundance but also the grade of sorting and porosity.

The Qemscan analysis was chosen over the traditional XRD analysis for this thesis because it provides a much larger data set with respect to the sample's properties and is better suited for samples enriched in (clay-) minerals since XRD cannot differentiate between separate clay-minerals. Another major advantage of the Qemscan system over traditional XRD analysis is that, in addition to bulk mineralogical and elemental information of the sample, the rock texture is understood as well.

Concerning the core samples, the same 94 samples that were selected for pyrolysis are also analysed with Qemscan. One of these 94 samples is a duplicate to determine the accuracy and consistency of the system. The analysis has been performed by Fugro Robertson Ltd. based in the United Kingdom; one of the first oil industry-related laboratories to purchase the Qemscan system. The main purpose of the Qemscan technique for this specific thesis is to acquire additional data with respect to (macro-) porosity (>3 μm) and clay-mineral content.

4.1.3 Adsorption Isotherm

As was already described in section 3.1.5, the adsorption of methane on organic material is important for making a more accurate estimate of the amount of natural gas present in a shale. Adsorption is described by an adsorption isotherm, which plots the amount of adsorbed gas against the reservoir pressure.

Although it is argued by some that a single isotherm is sufficient for a basin, six samples were selected to construct an adsorption isotherm. The isotherms are constructed by the geosciences department of RWTH Aachen University.

In order to construct an adsorption isotherm, first the sample has to be ground or milled to a smaller grain size. Depending on the time available, the grain size can range from micron to millimetres/bulk scale. The smaller the grain size is, the faster the isotherm can be constructed. However, smaller grains will improve permeability of the shale beyond original quality, which causes a possible overestimation of the maximum amount of gas the source rock can adsorb. The next step is placing the sample in a pressure chamber, heating the chamber to the desired temperature, and adding helium up to a certain pressure. Since the adsorption capacity for shale- and clay fragments for helium is insignificant, this can be used to determine the amount of free space within the sample-container by measuring the added volume. Once the free volume is known the helium is flushed from the pressure chamber and methane is added. This methane first enters a sub-station of known volume where the pressure can be measured. Following this step, the volume is allowed to enter the pressure chamber with the sample. Using Boyle's Law ($P_1V_1 = P_2V_2$) and knowing the pressure and volume of the sub-station and the volume of the pressure chamber, it is possible to calculate the expected pressure for the pressure chamber, taking into account a compressibility factor Z for methane. The measured pressure however will be lower due to enhanced accommodation space resulting from methane adsorption. Using the ideal gas law ($PV = nRT$), the pressure-difference can be converted to a volume difference which yields the volume of adsorbed gas at the measured pressure and temperature; performing these measurements for increasing pressures while keeping the temperature constant yields the adsorption isotherm from which the Langmuir constants can be derived. Figure 4.1 presents a schematic representation of the apparatus set-up. For the construction of an adsorption isotherm, the most important factors are the temperature, pressure range, moisture content, and grain size. Inaccuracies or deviations in these factors will result in reduced accuracy of the isotherm.

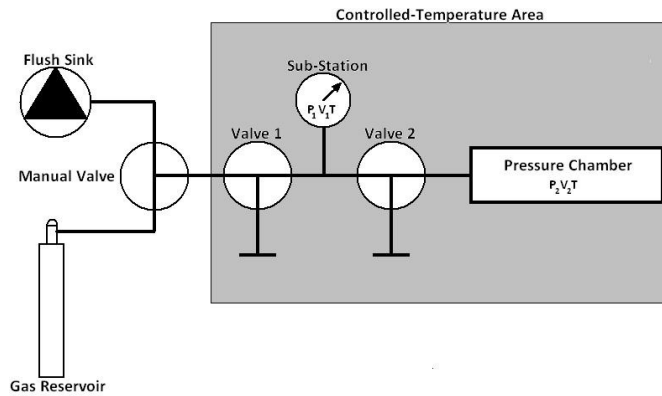


Figure 4.1: Schematic representation of the adsorption apparatus. The grey area is kept at a constant temperature.

4.2 Log Data, Parameter Modelling and Calculations

When drilling new boreholes it is common practice to compile a data set of measurements along the entire well-track. The resulting well logs are often publically available via the Dutch Oil and Gas portal (www.nlog.nl). Data for the selected wells for this thesis was collected from this portal and used for both qualitative inspections of the various wells, as for quantitative calculations of new parameters. Although a broad spectrum of log-types exists for Dutch wells, not all of these logs are useful or required for the research. The focus with respect to the logs lies with those that describe the geological rock- or hydrocarbon properties.

4.2.1 Log Data

The most important logs used for this research where logs for the gamma ray intensity, electrical resistivity, travel time for sonic pulses (both P and S waves), density, deflected neutrons, and gas logging.

Gamma Ray

The gamma ray intensity log measures the intensity of natural γ -radiation along the borehole using a Geiger-Müller probe. Gamma ray intensity is especially useful for locating hot shales that have been enriched in radioactive elements (e.g. Uranium, Potassium and Thorium). Low gamma radiation usually indicates sandy sedimentary rocks. The cause for hot shales to be radioactively enriched is due to the reducing conditions that prevail in black shales and which are induced by the presence of organic carbon. A high gamma-ray measurement is therefore indicative for organic-rich shales (Lüning et al.; 1999).

Electrical Resistivity

A resistivity log measures the electrical resistance of the surrounding lithology by sending an electrical current into the rock-material and measuring the electrical signal some distance away from this source. There are several variations of the resistivity log, all of which have a different measuring distance from the borehole. Shallow resistivity measures the resistivity close to the borehole and may therefore be affected by mechanical disruption of the surrounding lithology or injection of drilling mud into the formation. Deep resistivity consequently takes its measurements furthest from the borehole (by lateral drilling) and is least affected by the drilling sequence.

The resistivity of a formation may indicate the presence of water, oil, and gas. Low resistivity often indicates water-filled pores and thus relatively high amounts of formation water, high resistivity might indicate oil- or gas occurrences. In general, resistivity is the most important tool for estimates of hydrocarbon saturation (Archie, 1941).

Sonic Transit Time

Sonic travel times are measured as an alternative or substitute to conventional seismic sections. Travel times are measured using an acoustic sonde, which is lowered into the borehole. The transit time yields data concerning the lithology and porosity, assuming that it only changes when either the lithological facies or porosity changes. Sonic travel times can be converted to a measure of porosity using one of the relationships available (Dvorking & Nur, 1998). Depending on the degree of fracturing induced in the surrounding rock by the drilling and borehole geometry, sonic velocity readings may deviate from actual propagation velocities for the material under consideration. For sonic logging, both P-wave and S-wave acoustics can be used.

Neutron Deflection

Neutron deflections are measured by lowering a radioactive source into the well. The measurements are used to give an indication of formation porosity. During neutron logging, the source will emit neutrons at a high velocity into the formation and collide with the nuclei of atoms belonging to the formation material. Depending on the mass of the nuclei the neutron will slow down. The neutron is slowed most when it collides with nuclei of similar mass (e.g. hydrogen). The decrease in travel speed causes the neutron to move erratically through the formation until it is eventually absorbed by a nucleus. When it is absorbed by hydrogen- or chlorine nuclei, the newly formed isotope will rapidly decay and emit gamma rays. These gamma rays are measured by the detector and neutron porosity can be calculated using the formation's hydrogen index. In general, the higher the amount of hydrogen the faster the neutrons are slowed down and are thus absorbed closer to the source, resulting in less radiation reaching the detector. Low radiation detections are indicative for high formation porosity, assuming the pores are filled with water. Gas- or air-filled pores are generally not detected by older detectors (Myers, 2007).

Continuous Mud Gas Logging

Gas in a shale formation is released by fracturing of the rock by the drill bit and allowed to travel upwards along the borehole with the circulated drill mud. At the opening of the borehole a gas chromatograph measures the amount and composition of the gas. Since it takes a certain time for the gas to travel from the drill bit to the surface, an uncertainty factor is introduced in the gas log when determining its source. Gas chromatography presents data on the availability and flow-rate of natural gas in a formation. When drilling mud with a diesel-oil additive is used, gas readings will be artificially enhanced and are no longer representative for the formation's gas content in an absolute sense. In general, mud logging is a useful tool for qualitative appraisal of gas occurrence and composition but cannot be used for conversion to gas concentrations in the drilled rocks (Erzinger et al., 2006).

4.2.2 Parameter Modelling and Calculation

Using the data available, new data can be generated by calculations. TOC content and maturity are two of those attributes that can be calculated using mathematical relations. Although there is always a certain range of error when calculating this kind of data instead of measuring it, calibration and the use of reasonable assumptions can still make these relations a valuable asset to the study.

Maturity Determination for Core Samples

Maturity is often expressed in terms of vitrinite reflectivity since it was developed to measure relative maturity of vitrinite-rich coals of type III kerogen. Other types of kerogen however do not contain abundant quantities of vitrinite making it difficult to measure their maturity. Nonetheless, the vitrinite-system is still commonly used. Resultantly, various methods or relations have been proposed for the determination of vitrinite-reflectivity equivalents for non-vitrinite bearing kerogen. One easy method for doing this is by means of an altered van Krevelen diagram in which vitrinite maturity equivalents have been plotted. Such an altered diagram was already displayed in figure 3.1. The HI and OI of a sample are used in the diagram, and the maturity equivalents give an estimate of

the vitrinite reflectivity-equivalent. Although indicative for relative maturity, this method is not very accurate in absolute sense.

Maturity Modelling and Extrapolation

The maturity of the Posidonia formation was mapped and modelled by TNO (van Bergen et al., 2010) for the West Netherlands Basin and Roer Valley Graben. Unfortunately, at the moment of the analyses, the final high-resolution version was not yet available. Consequently, a low resolution model is used due to the lack of alternative. This low-resolution model has a resolution of 6km²/pixel and is therefore not very accurate. The model accuracy has therefore been taken into account while interpreting the modelled results. Both versions of the model are only compiled for the Posidonia formations. Since, however, not only the Posidonia formation but also the Aalburg and Sleen formation are under consideration in this thesis, a mathematical relation is constructed to empirically extrapolate the modelled maturity of the Posidonia formation to attain maturity maps for all Lower-Jurassic shale formations.

Using several studies of the relation between vitrinite reflectivity and the maximum temperature of the reservoir T_{max} , a correlation table is created and used to derive two empirical equations: one to calculate T_{max} from R_o , and one to calculate R_o from T_{max} (see section 5.4.1). Since for all wells the top- and bottom depth of the lower Jurassic formation are known, it is possible to define the difference in depth, Δd , between the centre-point of one formation and another. With this difference in depth, it is possible to calculate the increase in T_{max} by using equation 4.1.

$$T_{max\ B} = T_{max\ A} + (0.03 * \Delta d) \quad (4.1)$$

where,

$T_{max\ B}$	=	maximum reservoir temperature of formation B (at centre-point)	[°C]
$T_{max\ A}$	=	maximum reservoir temperature of formation A (at centre-point)	[°C]
Δd	=	dept-difference between centre points of formation A and B	[m]

The value 0.03 represents a standard geotherm for the Dutch subsurface and is given in degrees per metre (°C / m). Since no erosion is assumed to have taken place between the time of deposition of the Sleen formation and the time of deposition of the Posidonia formation this geotherm is a qualified approximation of the internal geotherm. Once the maximum temperature for the new formation is calculated, this temperature can be converted to a value for maturity again to give an approximation of the maturity at that depth.

TOC Calculation from Well-logs

A model for TOC calculation from resistivity and sonic logs was proposed by Passey et al. (1990) and has since become the standard approach for calculation of organic richness along the well track. Their method, called the $\Delta \log R$ technique, is stated to be innovative with respect to other techniques in the way that it is more accurate, does not require calibration from cuttings, is applicable to all rock types, and is not affected by the presence of minerals. The technique calculates the TOC content using the following equation (equation 4.2):

$$TOC = \left(\log_{10} \left(\frac{R}{R_{baseline}} \right) + 0.02 \left(\frac{\Delta t}{\Delta t_{baseline}} \right) \right) \times 10^{(2.297 - 0.1688 LOM)} \quad (4.2)$$

where,

TOC	=	Calculated Organic Carbon	[Wt%]
R	=	Resistivity	[Ω/m]
R _{baseline}	=	Resistivity at baseline	[Ω/m]
Δt	=	Sonic Transit Time	[μsec/ft or μsec/m]
Δt _{baseline}	=	Sonic Transit Time at baseline	[μsec/ft or μsec/m]
LOM	=	Level of Organic Metamorphism / maturity	[-]

The baseline values are defined at a depth range where the mirrored sonic log directly overlies and follows the logarithmic resistivity log and are assumed to represent 0% TOC. Since the TOC calculation is seated entirely on the base line selection, it should be selected with care.

If for a borehole no sonic log is available, two alternative calculations are proposed, using either the neutron log or density log, which are given by equation 4.3 and 4.4 below.

$$TOC = \left(\log_{10} \left(\frac{R}{R_{baseline}} \right) + 4.0 \left(\frac{\phi N}{\phi N_{baseline}} \right) \right) \times 10^{(2.297 - 0.1688 LOM)} \quad (4.3)$$

where,

φN	=	fractional porosity	[vol%]
φN _{baseline}	=	fractional porosity at baseline	[vol%]

$$TOC = \left(\log_{10} \left(\frac{R}{R_{baseline}} \right) - 2.50 \left(\frac{\rho_b}{\rho_{baseline}} \right) \right) \times 10^{(2.297 - 0.1688 LOM)} \quad (4.4)$$

where,

ρ _b	=	rock density	[g/cm ³]
ρ _{baseline}	=	rock density at baseline	[g/cm ³]

The level of organic metamorphism (LOM) required for the calculation was defined by Hood et al. (1975) as a standardised, easy-to-use index for maturity meant to replace all other maturity indices. Figure 4.2 presents the correlation diagram between LOM and other maturity indices as published in 1975.

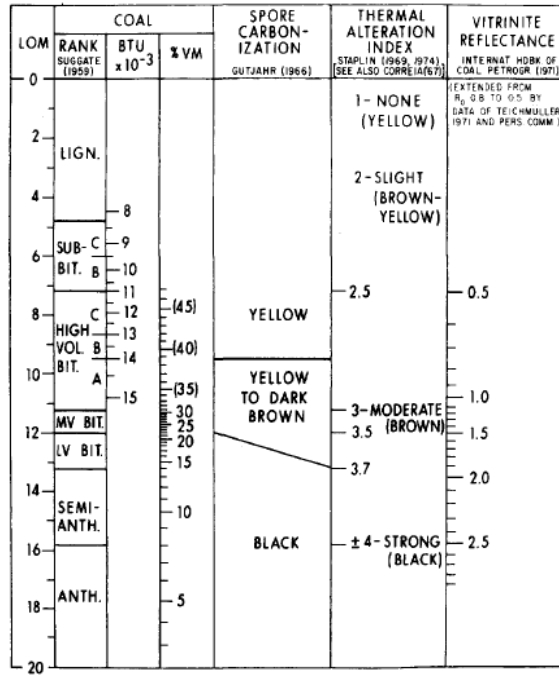


Figure 4.2: Correlation diagram between LOM and various other maturity indices. (Hood et al., 1975)

When the R_0 and corresponding LOM values are extracted from the diagram and plotted against each other (figure 4.3) the resulting general relation can be quite accurately approximated by the polynomial:

$$LOM = -1.4504(R_0)^4 + 10.832(R_0)^3 - 28.267(R_0)^2 + 33.476(R_0) - 3.7319 \quad (4.5)$$

Using the method for maturity modelling explained in the previous sub-section, R_0 -equivalents can be calculated for every depth interval, resulting in a continuous LOM-depth profile.

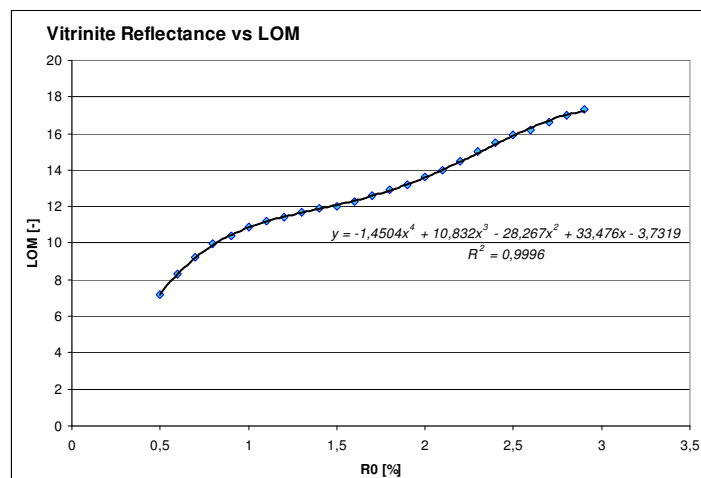


Figure 4.3: R_0 plotted against LOM. The mathematical relation between the two is approximated with relative high accuracy by a polynomial function.

If the LOM value is calculated incorrectly for a locality, the calculated TOC value there will be in error. The relative TOC levels will however still be useful (Passey et al., 1990).

Black shales almost always contain some amount of measurable ‘back ground’ organic material. A study performed by Tissot and Welte in 1984 indicates that worldwide the TOC level in shales lies between 0.2 and 1.6 wt.% with most of these shale exceeding levels of 0.8 wt.%. The baselining method however essentially designates the region used to define the baseline qualifies as being devoid of TOC. To compensate for this a constant of 0.8 wt% TOC is added to the calculate TOC-profile.

For this thesis, most of the wells for which a resistivity log existed also had a sonic log. Some wells did not have a sonic log but had a neutron of porosity log instead. The older wells unfortunately often only had a Spontaneous Potential (SP) log available which cannot be used for TOC calculations.

4.3 Gas-Initially-In-Place Calculation

As was already mentioned in section 3.1.5, an estimate of the initial gas content (GIIP) of a field or formation is made by combining two occurrences: free gas and adsorbed gas. As was also mentioned in this section, the adsorbed gas content is determined by using a Langmuir adsorption isotherm for methane. This isotherm has to be fitted to measurement-data using equation 3.2, which is redisplayed below.

$$gC_{ads} = V_l p / (p + P_l) \quad (3.2^{bis})$$

where,

gC_{ads}	=	adsorbed gas content	$[m^3/m^3]$
P	=	reservoir pressure	$[Pa]$
V_l	=	Langmuir volume	$[m^3/m^3]$
P_l	=	Langmuir pressure	$[Pa]$

The relevant reservoir pressure for a field is estimated assuming hydrostatic equilibrium. The reservoir pressure then equals the interstitial fluid density ($\sim 1000 \text{ kg/m}^3$) times the average reservoir depth times the gravitational acceleration. Depending on the unit-format of the measurements, the adsorbed gas content may have to be multiplied with an expansion factor to determine the exact adsorbed volume at standard (surface) pressure and temperature conditions ($T_{STP} = 15^\circ \text{ C}$; $P_{STP} = 1 \text{ bar}$).

The free gas content per cubic metre can be approximated by an equation as well, which is given below (equation 4.6).

$$gC_{free} = \bar{\phi} * S_g * f_x \quad (4.6)$$

where,

gC_{free}	=	free gas content	$[m^3/m^3]$
$\bar{\phi}$	=	average porosity of the reservoir	$[m^3/m^3]$
S_g	=	gas saturation of the reservoir	$[-]$
f_x	=	expansion factor to STP conditions	$[-]$

Now that both equations yield the gas content per standard cubic metre (scm), the total gas content for this unit is determined by simply adding the two components together. If, instead of cubic metre, the gas content is requested for an entire field (or other three-dimensional entity), initial gas content is estimated by:

$$GIIP = (gc_{free(STP)} + gc_{ads(STP)}) * A * d \quad (4.7)$$

where,

$GIIP$	=	estimated Gas Initially In Place for the field	$[m^3]$
A	=	surface area of the field	$[m^2]$
d	=	(average) thickness of the field or gas-bearing strata	$[m]$

4.4 The Winterswijk Quarry

By far the majority of the Dutch onshore area is covered in Quaternary and Tertiary sediments, with the Jurassic formations either eroded during the Hercynian inversion events or covered under up to 4 kilometres of sediment. Only in the most eastern and southern regions of the country do older stratigraphic outcrops sporadically exist. Although there are no Posidonia- or Aalburg outcrops, the Sleen formation outcrops in a limestone quarry near the town of Winterswijk, close to the German border (Herngreen et al., 2005). This occurrence provides an outstanding opportunity to investigate the shale formation in-situ rather than from core samples that have been stored for up to 50 years since extraction from their respective borehole.

The Sleen formation outcrop is located at the slope of quarry IV (figure 4.4).

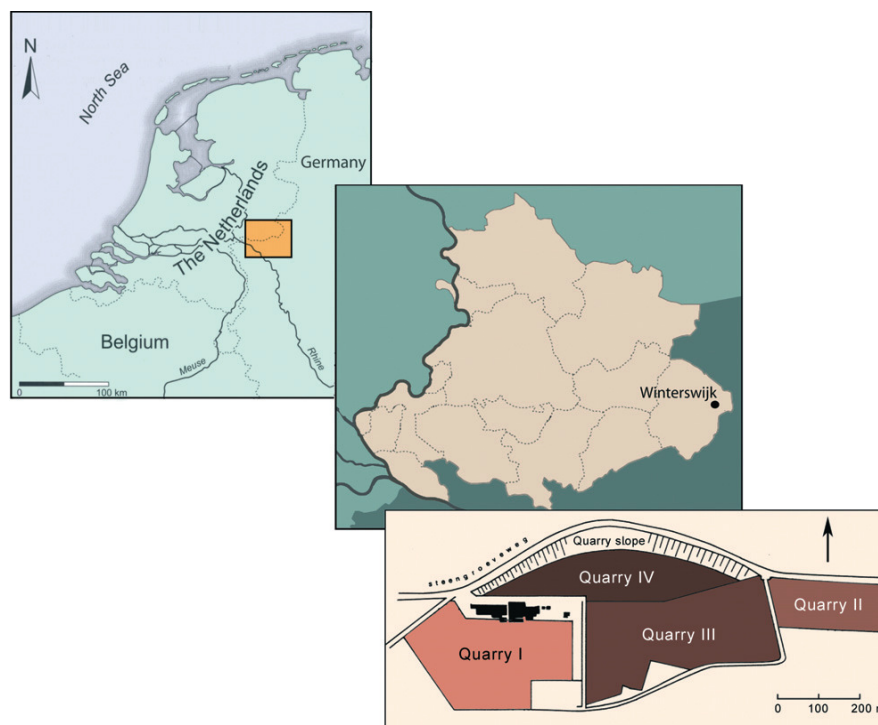


Figure 4.4: Location of the Winterswijk quarry in the Netherlands and the quarry lay-out. The Sleen formation outcrop is located in the near-surface area of the northern quarry slope of quarry IV. (Herngreen et al., 2005)

The Sleen formation occurs within the quarry as a sub-horizontal dark-brown to black band of approximately 2-3 metres thick that is easily distinguished from the grey-whitish limestone of the quarry's main target, the Muschelkalk formation, which underlies the Jurassic shale. The Sleen formation is overlain by a 4 metres thick veneer of Tertiary sediment of Oligocene age (Herngreen et al., 2005), indicating a major time hiatus due to uplift and erosion or non-deposition. Apart from low maturity, it is unknown what influence this uplift has had on the Sleen formation. Due to the impermeability of the shale, meteoric water collected by the Tertiary sediment is unable to seep deeper into the ground and streams from the outcrop creating pools of water. Whenever this water comes into contact with pyrite accumulations, which are quite common in the shale, the iron is oxidised creating rusty-brown stains. The shale formation is thin-bedded at sub-millimetre scale and has a clear and well-developed bedding plane with a sub-horizontal orientation. The shale consists of fine clay fragments and does not appear to contain any sand. Pyrite crystals of up to a few centimetres occur especially in the lower bands of the formation and have a reasonably well-developed cubic crystal structure. Wherever a fresh sample was retrieved, no obvious sulphurous smell was registered. Figures 4.5 and 4.6 display photographs of the shale formation in the Winterswijk quarry. From the Winterswijk quarry, two additional samples were acquired that will also be analysed for mineralogical properties and organic content using the Qemscan and Rock-Eval methods. Additionally, a sample of this outcropping formation will be used for Langmuir Isotherm construction to assess the variability of this isotherm with major changes in depth.

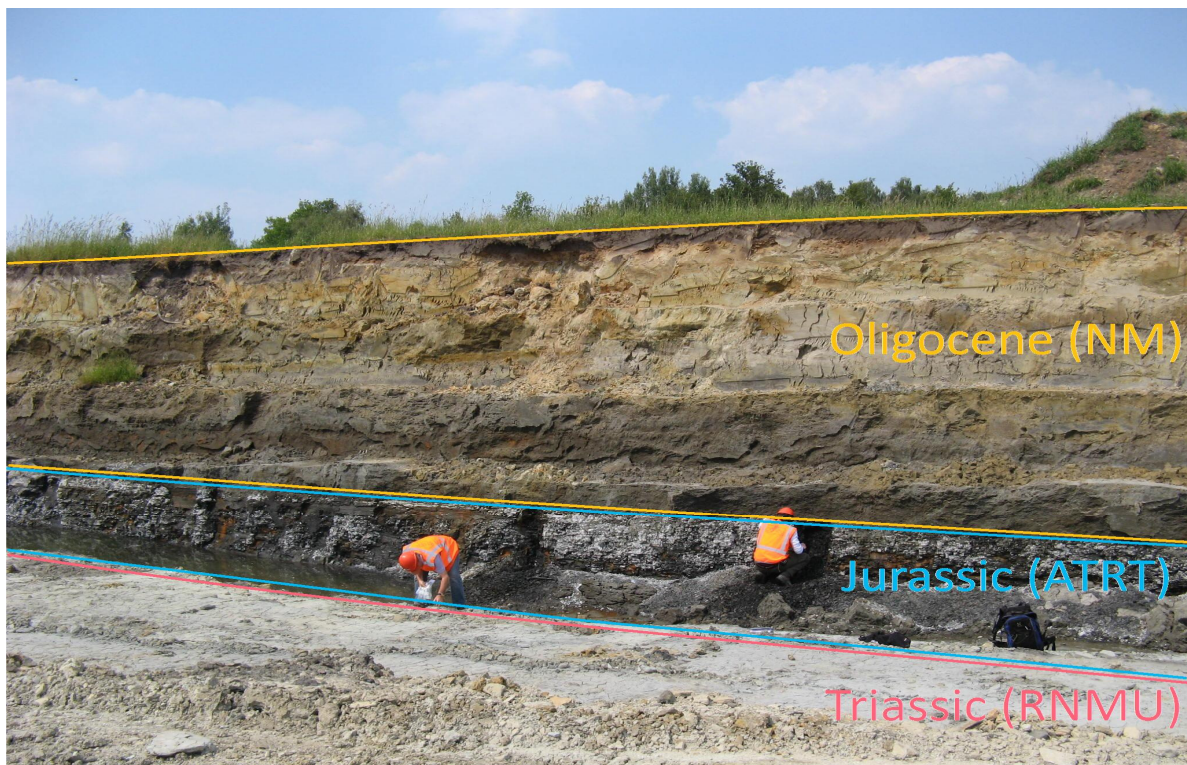


Figure 4.5: Photograph taken in NNW direction depicting the Sleen formation (ATRT) outcrop in the Winterswijk quarry. On top is the Oligocene Middle North-Sea Group sediment. Below the Sleen formation is the Triassic Muschelkalk situated.



Figure 4.6: A freshly dug ditch in the Sleen formation clearly showing the grey/blackish shale. The rusty stains are the result from pyrite oxidation. The pen in the photograph is used as scale-reference and is approximately 20 centimetres long.

5. Results

5.1 Lithological Classification

The cores provided by the NAM provided an opportunity to examine the lithology of the Lower Jurassic formations more closely. Based on purely physical observation the cores were sorted into 7 distinct lithological groups. A short description of each group follows.

Group 1 – Homogenous claystone

The main distinguishing factor for this group is the apparent lack of lamination or otherwise internal structure. Sometimes micro-lamination (sub-millimetre size) can be seen on the exterior of the core samples but this lamination is completely indistinguishable on a fresh surface. Colour ranges from light- to dark grey or nearly black. Samples from this group may contain small amounts of pyrite, fossil fragments (bivalve fragments), or mica's. Quartz is not found. The grain size falls in the range of 62.5-88 μm . The core samples of this group are generally highly resistant to impact before fracturing, probably due to the lack of a preferred fracture surface.

Group 2 – Claystone with well-developed micro-lamination

In contrast to group 1, members of group 2 have well developed lamination at millimetre scale. Within this group a subdivision can be made between those samples containing abundant fossil remains and those that do not. Samples without fossil remnants are generally much darker (near black) on fresh surfaces than their fossil-rich counterparts and can contain well-developed pyrite crystals ranging in size from sub-millimetre to centimetre scale. Fossil-types in this group cover bivalve shell-fragments and gastropods. The grain size ranges from 62.5 to 125 μm . Group 2 specimens are less resilient to impact than members of group 1. In general, members of group 2 appear to be the most enriched in organic material.

Group 3 – Claystone with well-developed macro-lamination

This group is essentially similar to group 2 except for the fact that the lamination in members of this group is far coarser than for those of group 2. Lamination occurs on millimetre to sub-centimetre scale with the average distance between neighbouring lamination-planes ranging around 8 millimetres. Other properties are similar to group 2: gastropod and bivalve fragments; 62.5-88 μm grain size; small pyrite crystals; no quartz and locally small amounts of mica's. Group 3 samples are however much more resistant to impact than group 2 members.

Group 4 – Mica-Rich claystone

The main differentiating factor for members of group 4 core samples is the very high abundance of micro-scale mica crystals. As a result of this the surface of samples belonging to this group appears to be glittering in the light. In essence, high mica concentrations are the only requirement for this group allowing cores with very varying properties (e.g. lamination) in this group. Most of the samples from group 4 however demonstrate very little lamination and little fossil remains, placing members of group 4 in general closest to members of group 1. The generally light grey claystones of this group have an average grain size of 88-125 μm . Pyrite was not found in samples belonging to this group. Some specimen however did contain minor amounts of quartz. The resistance to impact is average compared to specimen of other groups.

Group 5 – Claystone affected by contact-metamorphism

Group 5 is actually more like a side group instead of one of the dominant lithologies derived from the core samples. The group exists of claystones that were located in close proximity of a felsic dike or sill, which was also cored. The samples belonging to this group are very dark to nearly black in

appearance. The grain size is 62.5-88 μm . All specimens of this group displayed quartz-filled veins intersecting the sample. No pyrite or fossils and only little micas were found. The specimens had a millimetre-scale lamination of 3-4 millimetres on average. Due to the extreme condition by which samples of this group form, it is not commonly found in wells.

Group 6 – Siltstone

The members of this group were found to be composed of material of such coarse texture (125-177 62.5-88 μm) that the nomenclature ‘claystone’ does not apply anymore. Although derived from a small minority among the core samples, they were found to contain neither pyrite nor micas. The specimen did generally contain quartz however. Bivalve fragments were present in some specimens.

There does not seem to be a distinct correlation between lithological groups and formations.

5.2 Formation Thickness

The thickness for the three Jurassic formations is derived from the stratigraphic log of each borehole. It is however observed (by the occurrence of repetitive lithological sequences along the well track and from seismic imagery) that in many instances the thickness of one or more formations is altered by tectonics. Because these altered stratigraphies do not represent the regional thickness of the area, wells indicating the presence of faults are discarded. The resulting (true vertical) formation-thickness distribution for the Posidonia, Aalburg and Sleen formations are displayed in histograms in figures 5.1 to 5.3, respectively. The criteria for determining top and base of some of the formations have not always been the same. Within the context of this project it has not been attempted to rectify this, and it is accepted that this generates scatter in the data. The thickness of the Posidonia Formation, for example, is probably more constant than the data suggests.

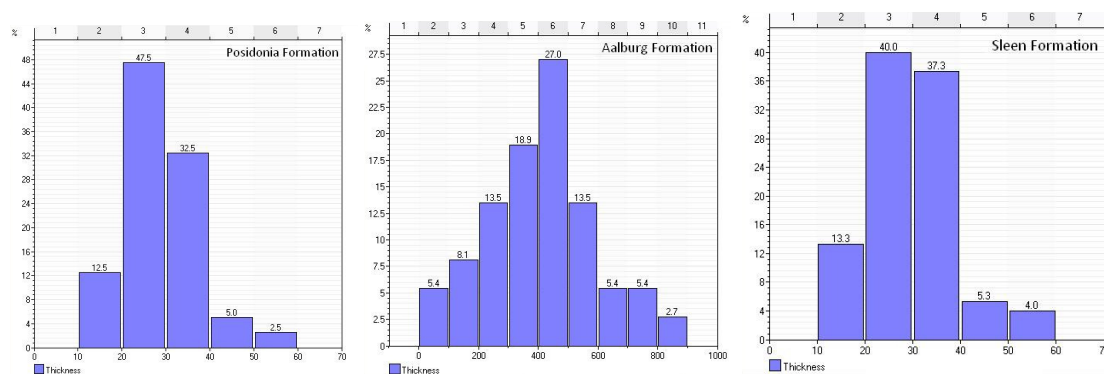


Figure 5.1, 5.2 and 5.3: Histograms plotting the thickness per formation. Notice the scale change for the Aalburg formation with respect to the other two formations. Thicknesses are true vertical.

5.3 Kerogen Type

The type of kerogen per sample was determined by plotting the oxygen- and hydrogen indices in a van Krevelen diagram, of which the result is shown in figure 5.4.

It is seen that the Posidonia formation plots mainly between kerogen types I and II. Some of the Posidonia cores however, as well as all the Sleen cores and the majority of the Aalburg cores, plot in the inertinite (type IV) and vitrinite part (type III) of the van Krevelen diagram. This suggests that the sampled sections of the Sleen and Aalburg formation are not good source rocks. Some sample record extremely high OI values, beyond the plotting boundary of 150 mg CO₂ / g TOC. The HI value of these samples is generally still low.

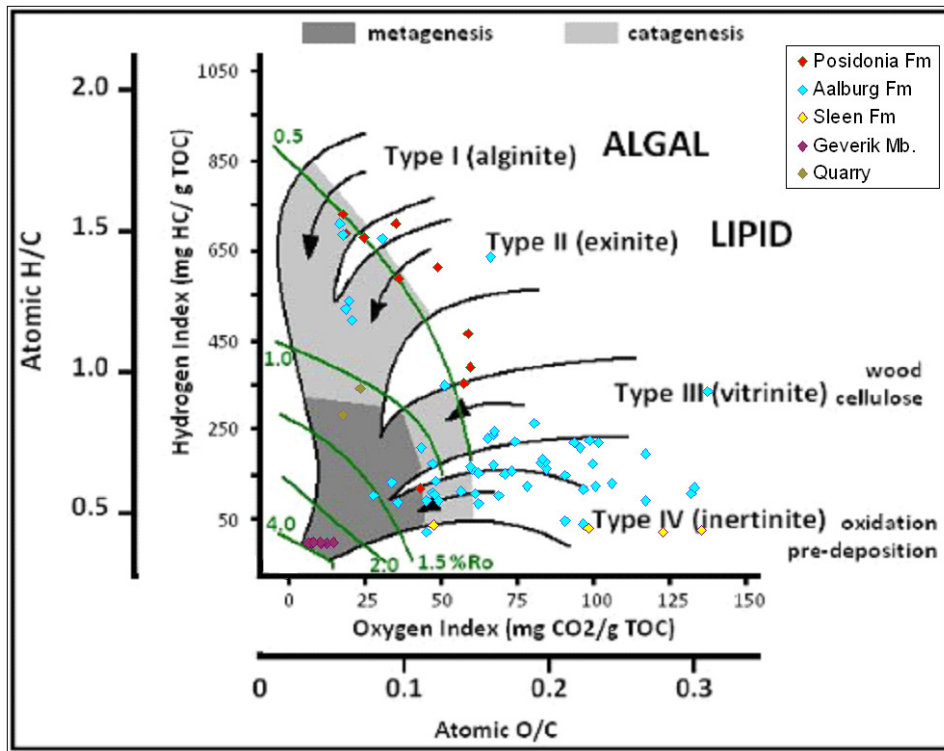


Figure 5.4: Van Krevelen diagram with all samples plotted according to formation.

5.4 Maturity

5.4.1 Maturity from Basin Modelling

The maturity of the Posidonia formation for each borehole is derived from the TNO model. For those wells where the Posidonia formation is not interpreted but the Werkendam formation is present, a standard thickness of 30 metres above the Aalburg formation top is reserved for the Posidonia. For the conversion from maturity, expressed as vitrinite reflectivity (R_o), to local maximum reservoir temperature, several relations are examined. These relations, established by DeMaison and Moore (1980), Hood et al. (1975), and Kantsler (1978) respectively, are numerically displayed in table 5.1 and plotted in figure 5.5.

Table 5.1: R_o to T_{max} conversion table

R_o %	DeMaison, 5-20 Ma T_{max} (Celsius)	DeMaison, 20-75 Ma T_{max} (Celsius)	DeMaison, 75+ Ma T_{max} (Celsius)	Kantsler T_{max} (Celsius)	Hood T_{max} (Celsius)
0.3	65	55	50		
0.5	93	80	65	60	41
0.6					49
0.7				80	61
0.8	150	110	93		75
1.0	165	120	110	115	107
1.3				130	129
1.4	190	150	135		
1.5					137
1.9				160	153
2.0	205	175	150		158
2.5				175	184
4.0	230	205	175		

When plotted in a R_0 vs. T_{max} diagram, the correlation of Kantsler was deemed most plausible for the reservoir based on the long burial time (longer than 75 My) and best correlation with the rule-of-thumb for maturities ($R_0 = 0.5\%$ corresponds roughly to a reservoir temperature of 60°C).

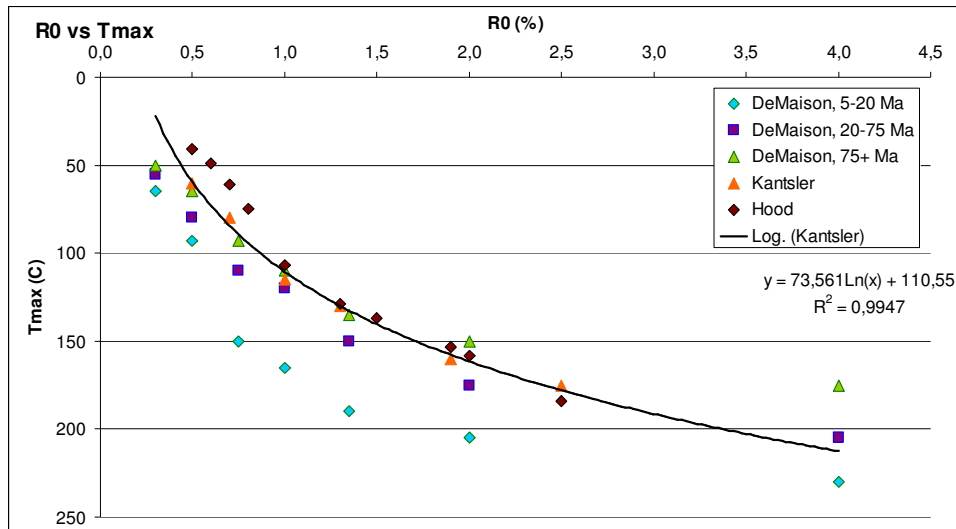


Figure 5.5: Plot of several proposed correlations between T_{max} and R_0 . The correlation by Kantsler (1978) was deemed best fit and a relation was derived, given by the logarithmic function on the right.

The R_0 - T_{max} measurements established by Kantsler are approximated by a natural logarithm (equation 5.1). Likewise, R_0 can be calculated from T_{max} using the inverted form of this logarithm, yielding equation 5.2.

$$T_{max} = 73.561\text{Ln}(R_0) + 110.55 \quad (5.1)$$

$$R_0 = e^{\frac{(T_{max}-110.55)}{73.561}} \quad (5.2)$$

These two relations, combined with equation 4.1 yield a method to extrapolate the modelled maturity to other depths and formations along each borehole. The resulting extrapolated maturities are presented in appendix B. From the distribution histogram of the modelled maturities per formation displayed in figure 5.6 it is seen that most wells plot in the range $R_0 = 0.6$ - 1.0% .

5.4.2 Maturity from Pyrolysis

Besides maturity from the basin model, an approximation of the sample maturity can be derived from a van Krevelen diagram as well using the result of the pyrolysis. The green lines crossing the diagram (figure 5.4) divide the diagram in areas of approximated maturity in terms of vitrinite reflectivity. These areas however are only useful for kerogen types I, II and III. When the maturity is appreciated it is seen that the Posidonia formation is quite immature, plotting around R_0 -equivalents of around 0.5% . The type I-III kerogen samples of the Aalburg are generally slightly more mature at value or $R_0=0.6$ - 0.8% . Since the Sleen formation plots entirely in the inertinite range its maturity cannot be determined.

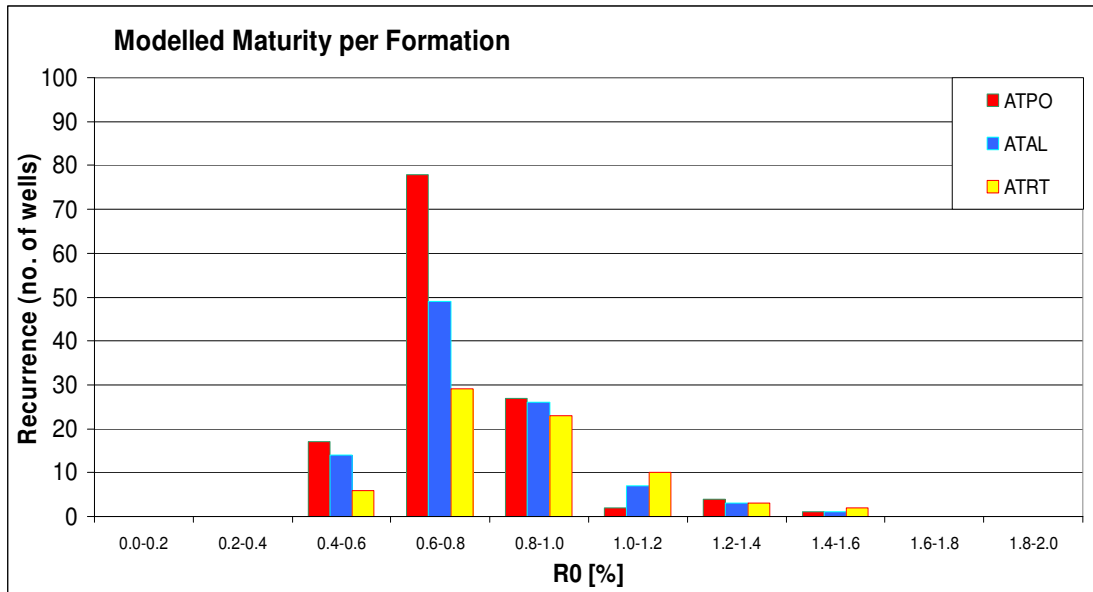


Figure 5.6: Distribution histogram of maturity per formation

5.5 Total Organic Carbon

5.5.1 Pyrolysis Results

TOC levels resulting from the pyrolysis show a relatively large spread. The majority of the samples do not have TOC levels above 2%, mostly from the Aalburg and Sleen formation, but some others have greatly elevated TOC levels, with a maximum value of over 12.7% for a sample belonging to the Aalburg formation. From figure 5.7, which plots TOC levels against formation, it can be seen that, in general the Posidonia formation appears the most enriched formation in terms of organic material. The average TOC level for this formation is around the 6%. The Sleen formation on the other hand is the least enriched formation. TOC levels here average around 0.5%. The Aalburg and Posidonia formation show a large variability. Values range from 0.04% to 12.7% and from 2.27% to 12.1%, respectively. The majority of the Aalburg formation contains very low amounts of organic matter, with an average of ~1%.

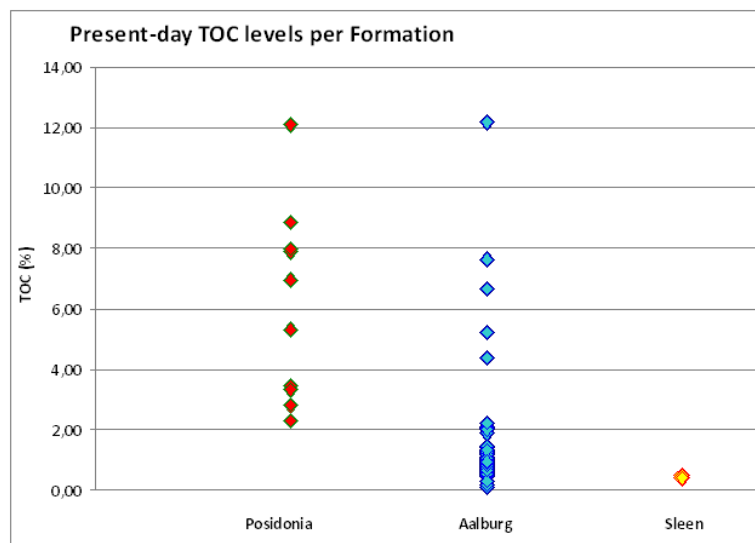


Figure 5.7: TOC levels sorted on formation

5.5.2 TOC Modelling (Passey)

TOC profiles have been calculated for all 39 wells for which the required well logs were available. Depending on the variability and resolution of the resistivity and sonic log (in some cases the neutron log) the profiles depict a relatively smooth curve or an erratic graph. The correlation with gas logs varies as well: most, but not all, profiles, like the WED-03 TOC profile, correspond relatively well with the gas log of that well (figure 5.8). For each formation and borehole an average TOC and its standard deviation is calculated. These averages are the values used for TOC mapping. The Aalburg formation is subdivided in an Upper Aalburg (ATAL1) and Lower Aalburg (ATAL2) formation because of its thickness and variability in TOC levels between the lower and upper part of this formation, as was observed in some instances. The Lower Aalburg formation is commonly between 60 and 100 metres in thickness. The precise boundary between the two parts is somewhat arbitrary but is situated just above the sudden change in relative TOC levels observed in many wells (figure 5.8).

The table listing the TOC averages and standard deviations can be found in appendix C. It is seen that on average, the Posidonia formation is by far the most enriched in organic carbon. Values for this formation range from 1.2% up to 12.9%, averaging around 5.1% with a standard deviation of 1.9%. Overall, the two parts of the Aalburg formation both have average TOC quantities of 1.2%, which is far lower than the Posidonia formation. The standard deviation is 1.0%. Locally however, differences may exist between the average TOC value of the Upper Aalburg and that of the Lower Aalburg formation. TOC levels in excess of 3% average TOC however are rare.

The Sleen formation is the least enriched in organic carbon, averaging around 0.9% with a standard deviation of 0.8%. Average values for this formation rarely exceed 1.5%.

A remarkable observation is that some wells that were seen to have high gas readings (such as GAG-05; locally +200k ppm CH₄ in the lower Aalburg and Sleen formation) but have low modelled TOC levels and standard deviations for that sector (1.4% and 0.6%, respectively). These are hardly different from neighbouring boreholes with low or absent gas readings (such as GAG-01; <1k ppm CH₄ over its entire length with an average TOC of 1.5% and a standard deviation of 1.6%, respectively). When plotting average values with respect to their location on a map, there does not appear to be a clear relation between location and TOC level.

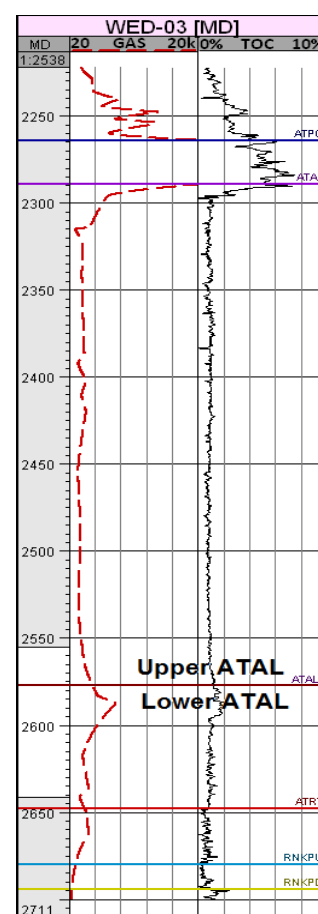


Figure 5.8: TOC profile vs. gas log for borehole WED-03. (MD = Measured Depth)

5.6 Gas Shows

More than fifty wells that penetrated the Jurassic strata in the West-Netherlands Basin and Roer Valley Graben had gas logs available. Gas shows from these logs were digitalised and sorted in four categories: low gas content (0 – 8000 ppm total gas); marginal gas content (8000 – 10.000 ppm total gas); high gas content (10.000 – 40.000 ppm total gas) and very high gas content (40.000+ ppm total gas). Although gas shows of only 10.000 ppm total gas (1%) are generally already considered quite high, gas shows in excess of 100.000 ppm total gas (10.0%) were found locally. It was observed that for the Aalburg and Sleen formation the highest gas shows were generally found in the western part of the West-Netherlands Basin, south of the city of The Hague. The Posidonia formation on the other hand has its highest shows in the central part of the West-Netherlands Basin, in the region between the cities of Utrecht and Tilburg. For the Roer Valley Graben, hardly any gas logs were available. The highest gas show was found for the Gaag-05-well, located in the most south-western part of the

West-Netherlands Basin. For this well a gas show in excess of 60.000 ppm (6%) has been measured over a length of 130 metres (along hole, but sub-vertical) in the lower Aalburg and Sleen formation, with peaks of up to 235.000 ppm total gas (23.5%) (figure 5.9).

However, although the Gaag-05 gas shows indicate massive gas shows, a well close by, the Gaag-01 well, indicates hardly any gas shows at all. The gas shows that are visible are, at least partly, due to degassing of the 20% Diesel-oil mud used for drilling. The Gaag-01 gas log is presented in figure 5.10. The observations, possible explanations, and conclusions are further discussed in section 6.5.

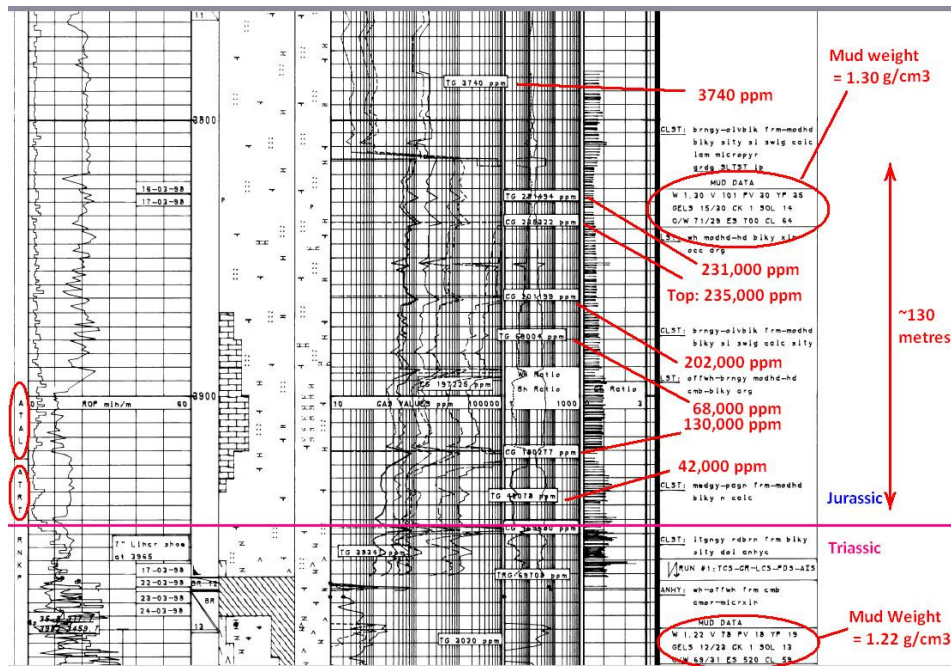


Figure 5.9: Part of the Gaag-05 gas log indicating very high gas shows over an along-hole length of approximately 130 metres. Also note the relatively low gas show in the underlying Triassic Keuper formation.

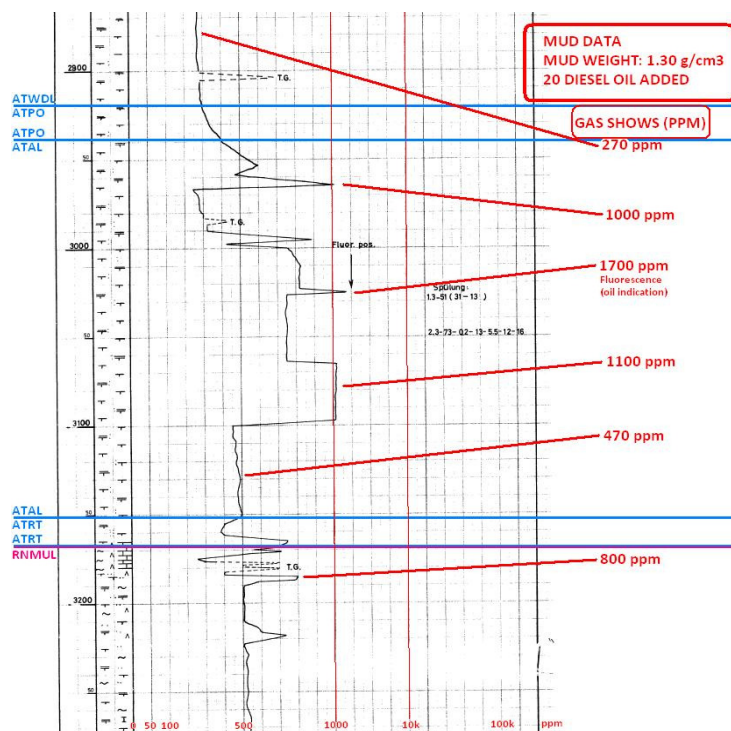


Figure 5.10: Part of the gas log for well Gaag-01. Gas shows measured here are significantly lower than those measured at the neighbouring Gaag-05 well.

5.7 Mineralogy

The Qemscan analysis provided bulk-mineralogical data of the core samples. This data is used to evaluate the clay-mineral content of each sample. Since evaluating clay-minerals is part of the interpretation, the clay-contents are not displayed here. The table with bulk-mineralogy is given in appendix D. In general, most samples appear to contain little quartz (figure 5.11) and high amount of clay-minerals. The implication of this observation is discussed in section 6.6.

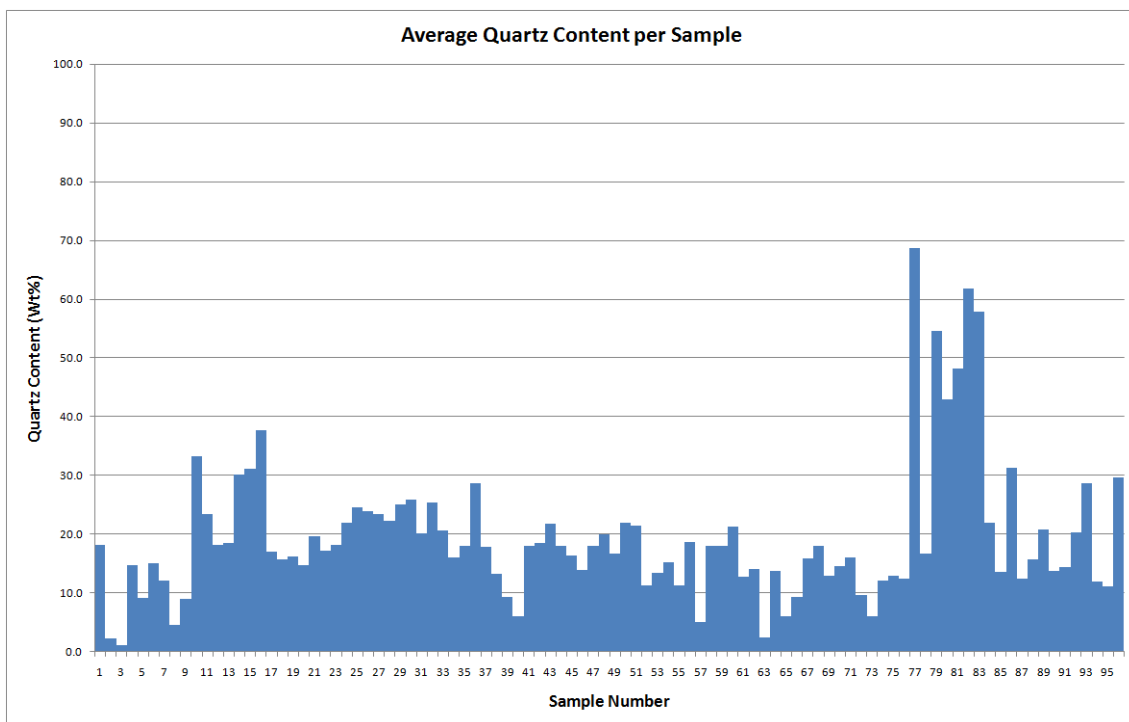


Figure 5.11: Average Quartz content per sample

5.8 Methane Adsorption

The resulting adsorption measurements for the five Jurassic core-samples sent to RWTH Aachen are displayed in figure 5.12. Note that the adsorption measurements are given as millimole CH_4 gas adsorbed per gram material and normalised to 100% TOC. As can be seen, quite large variations occur between the normalised adsorption capacities of the various samples. Sample 74, derived from the Sleen formation of the 'The Hague-02' well, appears to yield the best sorption capacity after normalisation with a maximum of 14 millimole methane per gram pure TOC. Sample 31 (Aalburg formation and also from well 'The Hague-02') and sample 86 (Posidonia formation; Loon-op-Zand-01 well) on the other hand have the lowest adsorption capacity of less than 2 millimole methane per gram TOC.

It must be noted here that sample 74 has the lowest measured TOC content (measured per sample by RWTH) at 0.82% while sample 31 and sample 86 have the highest TOC content of the five samples, at 5.04% and 10.49% respectively.

In general it is assumed that only organic carbon adsorbs methane in shales. As a result, samples with a high TOC level are expected to have better adsorption capacities. Since this is not reflected in the resulting adsorption measurements, RWTH Aachen decided to re-run the analysis on some samples in a slightly different setting, as to verify that the curves displayed below were the actual

adsorption curves. The result of these extra analyses did not vary significantly from the original ones and thus it must be assumed that these measurements reflect the true adsorption capacity of each sample.

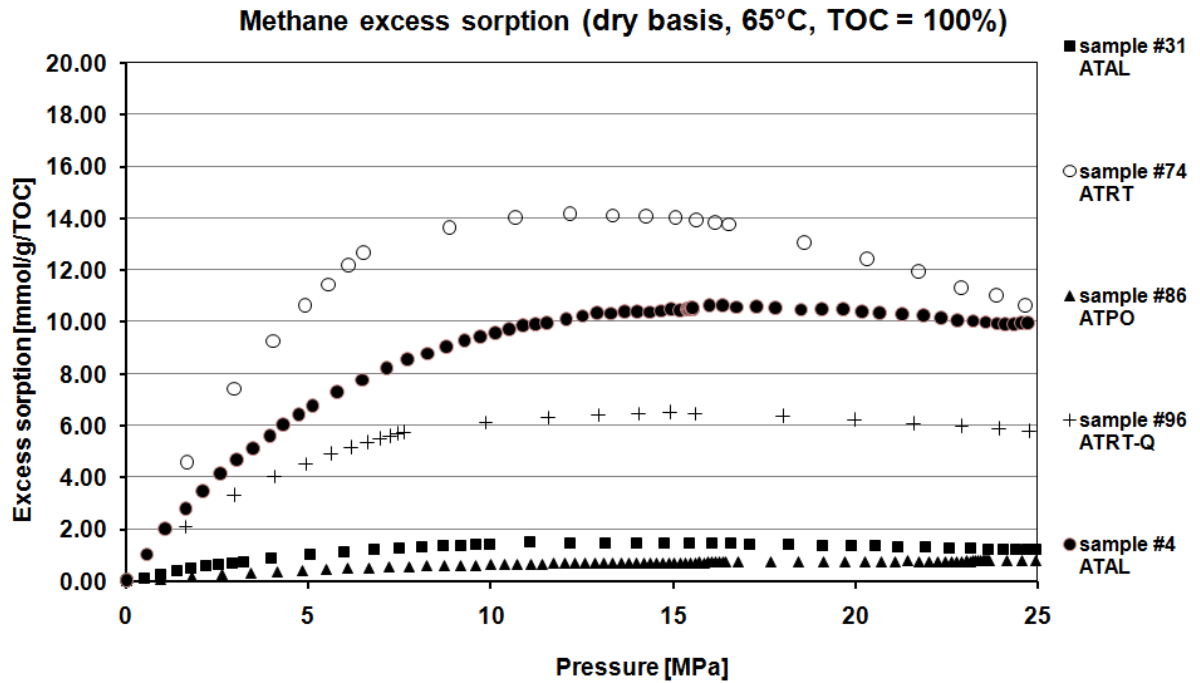


Figure 5.12: The resulting adsorption measurements per sample normalised to 100% TOC. The respective formation is given in the legend. ATRT-Q represents the Sleen formation sample retrieved from the Winterswijk Quarry.

6. Discussion

This section covers both the interpretation and conclusions that come forth from the results section, as well as the sources for error and inaccuracies of the methods. Per attribute, first the advantages and disadvantages and overall accuracy of the applied technique are treated, as well as interpretations of important observations. For mappable attributes, a second section treats the mapping technique, map accuracy and any interpretations that arise from the map.

Note however that not all attributes are fit for mapping. Some attributes just vary too much with depth for the same well to be able to choose a representative mean value, while other attributes simply have too few data points to be able to interpolate the attribute throughout the basin. Table 6.1 presents an overview of mappable and non-mappable attributes.

Table 6.1: Overview of mappable and non-mappable attributes

Mappable	Non-Mappable	Reason if non-mappable
Thickness	Kerogen Type	Too variable, too few data points
Maturity TOC Gas Show		
	Clay-Mineral Content	Too variable, too few data points
	Porosity	Too few data points
	Langmuir Isotherms	Too few data points

For those attributes that are mappable, attributes are extrapolated to cover larger parts of the basin if possible.

6.1 Formation Thickness

6.1.1 Interpretation and Accuracy

Although some discussion still exists of exact minimum requirements for thickness, as seen in section 3.1.1, it was concluded that generally a formation should at least be 20 metres (true vertical) in thickness to have a potential for economic viable shale-gas deposits, although 30 metres or more was preferred. Thicknesses of 50 metres and more were indicated to be most favourable. These ranges can be presented as a thickness classification as follows:

- 0-20 metres thick : Poor
- 20-30 metres thick : Marginal
- 30-50 metres thick : Good
- 50+ metres thick : Excellent

This classification is deemed reasonable since a formation much thinner than the minimum value of 20 metres probably does not contain enough gas to make drilling profitable. In addition, fracturing is likely to fracture surrounding formations as well, which is undesired.

When the distribution histogram of section 5.2 is examined with the classification for thickness in mind, it is seen that all three formations classify for the greater majority as marginal- to excellent. As expected, the large thickness of the Aalburg formation ranks it as 'excellent' for all data points. Although the Posidonia and Sleen formations are less massive with respect to thickness they too score relatively well in the classification, ranging from marginal to excellent for 87.5% and 86.6% of the Posidonia and Sleen wells, respectively. It can thus be safely assumed that all three formations are sufficiently thick to be prospective in terms of formation dimensions.

6.1.2 Thickness Mapping

Technically speaking, data maps belong to the result section. However, since the maps depend on classifications, these classes first have to be established and discussed before they can be implemented in the maps.

The thickness map is constructed from all wells for which a reliable stratigraphy was present. Although most wells give the stratigraphic intervals as along-hole depth measurements, this can be easily corrected for in various programs (e.g. Petrel (by Schlumberger)) with the aid of a well-deviation log to yield true vertical thickness. The map in appendix F1 displays this corrected thickness.

For the Aalburg formation the map shows little that was not expected. All data points indicate excellent stratigraphic thicknesses so the Aalburg formation is mapped as '(Assumed) Good' throughout the basin. It is possible that at the edges of the basin the formation becomes gradually thinner but without data points there and due to a lack of clear seismic reflectors for this formation this is difficult to verify.

The Posidonia formation is somewhat more irregular. Thicknesses of classes 'marginal' and 'good' are distributed without apparent structural trend. This is partly due to the fact that the Posidonia averages around 30 metres in thickness while 30 metres is also a class boundary. Thicknesses slightly over or slightly under the 30 metres therefore plot as different classes resulting in a seemingly erratic thickness distribution. Locally, 'excellent' or 'poor' Posidonia thicknesses are plotted. These however are assumed to be local features, possibly the result of inconsistent picking of top and base of the formation. As a result, the entire basin is interpreted to be of marginal-to-good thickness wherever undisturbed by tectonics. Again, the thickness may decrease toward the edges of the basin.

The Sleen formation is somewhat more interesting. Thickness distributions throughout the basin for the Sleen formation suggest that the edges of the basin are thinnest, with the thickness gradually increasing toward the centre of the basin. Since the Sleen formation has hardly been subjected to erosion and the current extensive fracturing of the basin was not present at the time, this is not an unlikely scenario. The interpolated map shows this trend of increasing thickness toward the centre of the basin. For all maps, the data points are plotted as well for reference purposes.

6.1.3 GIIP Calculation Input

The GIIP calculation requires an input of thickness of a region in order to be able to estimate gas content. Thickness however can be misleading: a formation that is hundreds of metres thick may have a gas bearing interval of only several metres. Consequently, instead of the total formation thickness, the gas bearing thickness is derived from gas logs. If these logs are unavailable, an estimate of (possible) gas bearing interval is made based on gas logs of nearby wells. The specific scenario defines the minimum gas show required.

6.2 Kerogen Type

Kerogen Type vs. Pyrolysis TOC

From the results section it is known that two sources for TOC levels are used in this study: the TOC levels resulting from the pyrolysis and the TOC levels resulting from logs using the equation of Passey et al. (1990). In section 5.3 the oxygen and hydrogen indices were plotted against each other in a van Krevelen diagram. What is seen in this diagram is that, according to the pyrolysis results the entire Sleen formation, most of the Aalburg formation, and some of the Posidonia formation appears to consist of type III or type IV kerogen due to high OI and low HI values, respectively. This is in apparent contradiction with the assumption that all three formations are potential source rocks and therefore needs some further examination.

When the present-day TOC levels resulting from the pyrolysis are plotted per kerogen type (figure 6.1) it is seen that those samples plotting for kerogen type I or II are generally richer in organic

matter than the samples plotting for type III or IV. So, not only is the organic matter present in the sample chemically largely inert, there is also far less of it. The abundance of apparent type IV (and type III) kerogen in formations where type II (and perhaps locally type I) kerogen is expected can be explained by several theories, following next.

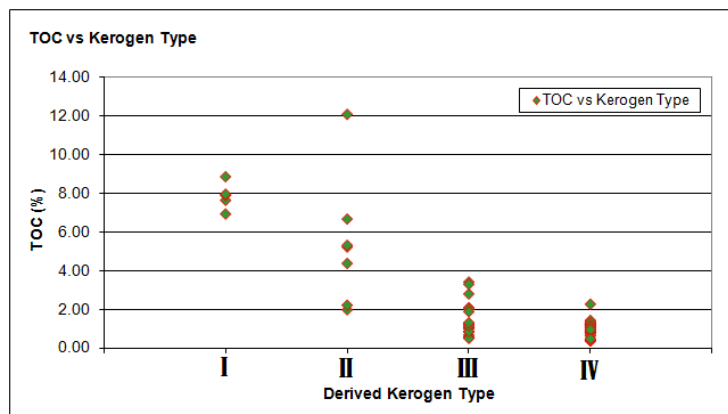


Figure 6.1: Present-day TOC plotted against kerogen type

Out-of-hole Bacterial Activity

The first explanation is a non-geological cause for the low HI and high OI values observed. Some of the cores have been lying in storage for over 50 years in normal atmospheric, oxygen rich conditions. It is possible that bacteria have infiltrated the cores and oxidised the reactive carbon and available hydrocarbons, thus decreasing the TOC level and H/C ratio (and thus HI) and leaving only the inert carbon. However, if this was true one would expect to observe two things. The first thing is that all samples coming from the same core should display similar degrees of oxidation and thus plot in similar parts of the Krevelen diagram. The second observation should be that the older cores plot as more oxidised than the younger cores. Unfortunately, all cores are from around the 1950's and 60's, so between cores little difference due to age would be expected. However, between samples from the same core a major difference *is* observed. For example, within the LOZ-01 well (Loon-op-Zand-01) HI values range from 20 up to 700 mg HC / g TOC. Within the same well the OI values range from 18 to 502 mg CO₂ / g TOC and TOC levels range from <1% up to 12+%. The same variation is seen in other cores, such as the Rijswijk-01 well (figure 6.2). Because of these intra-core variations, out-of-hole bacterial activity is an unlikely cause of the observations.

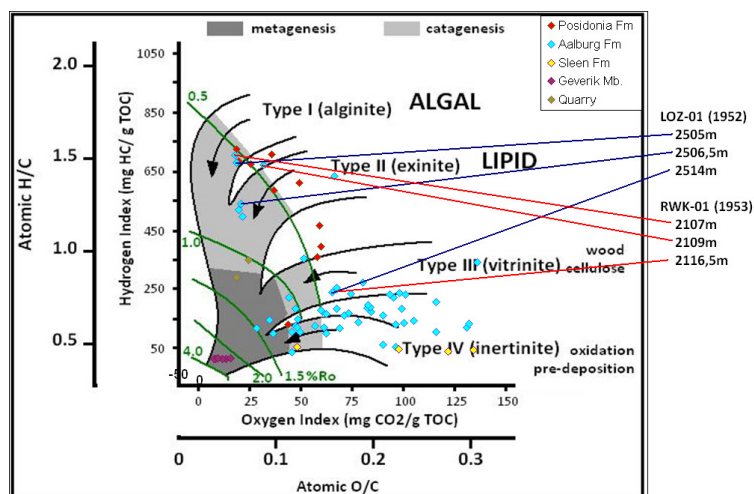


Figure 6.2: Krevelen diagram indicating the spread in data for two wells

Non-Organic Carbon Contamination

A second possible explanation is that there is a mineral present in the samples which contains high amounts of carbon but low amounts of hydrogen and which is combusted at high (>500° C) temperatures. From the bulk mineralogy provided by Qemscan the most likely mineral that could cause this behaviour is calcite. The bulk mineralogy indicates that some samples contain high degrees of calcite while others contain hardly any. However, again there appears to be no direct relation between TOC, HI and OI values and the presence of calcite. To illustrate this, a sample of LOZ-01 is again high-lighted. This sample (#86, see appendix A) consists according to the bulk mineralogy for the greater part of calcite (see appendix D). The pyrolysis results for this same sample however indicate high HI and TOC levels (684 mg HC / g TOC and 7.91% respectively) while having a low OI value (19 mg CO₂ / g TOC). Additionally, calcite is removed from the sample by acid treatment prior to pyrolysis. Moreover, it was already observed that type IV sample have very low TOC levels, which is not what one would expect if carbon was added by combustion of minerals. Due to this paradox, addition of carbon by mineral combustion is not a logical explanation either.

Oxic Deposition and Pre-burial Decomposition

The third explanation is that the shale was deposited in an oxic environment. As a result of an oxic environment, any organic material that is deposited would be oxidised, leaving only an inert carbon-residue. The result would be shale with low TOC levels, relatively low HI values, and a relatively high OI value, since all carbon that is available would be burned rather than converted to hydrocarbons due to lack of hydrogen. This is exactly what is observed and therefore the most likely cause for the presence of inertinite in the shales. This interpretation is reinforced by the observation of fossils and burrows in the cores (figure 6.3).

The fact that all samples plotting as type III or IV kerogen are deposited in an oxic depositional environment means that all the stratigraphic layers from which these samples are derived are poor source rocks and, due to low TOC content, are unable to adsorb large quantities of gas. Although the cores are only a few metres in length while the formations are tens to hundreds to metres thick, the observations made on the cores can be extrapolated to the entire formation with the aid of TOC profiles.



Figure 6.3: Two core fragments clearly showing fossil-remains (bivalves) in the Aalborg formation

As became apparent from figure 6.1, for all formations it seems that high TOC (>2%) is representative for type I or II kerogen while low TOC (<2%) represents (at least partially) inert kerogen and thus poor source rocks. When the TOC profile constructed from the sonic and resistivity logs is evaluated, one could make an estimate of kerogen type for those sections for which no cores are available. Even if the TOC profile is only appreciated qualitatively (since the absolute values may not be very accurate) one notes that in general the entire Aalburg and Sleen formation are of expected poor kerogen type. Within the Aalburg and Sleen profiles, small sections of enhanced TOC levels and thus (assumedly) better kerogen types exist, possibly representing actual short-term anoxic depositional environments. These 'TOC-spikes' however are generally too thin to be of real potential

When summarising the observations, one could say that, save some samples, the Posidonia formation generally plots well into the type I to type II region and is a valid source rock. The Sleen formation plots completely in the inertinite region and is, from a Kerogen-type point of view, unqualified as a source rock. The Aalburg formation, in general, appears to be a poor source rock as well, although there are distinct intervals of better potential. This leads to the following classification per formation for kerogen type.

Formation	Classification	Notes
Posidonia Fm	Good	Mainly type I or II
Aalburg Fm	Poor	Mainly type IV; locally type I or II
Sleen FM	Poor	Mainly type IV

Kerogen type is deemed unmappable with the currently available data, both due to the large variations of kerogen type within formations and due to the low amount of data points (only 13 wells).

6.3 Maturity

6.3.1 Interpretation and Accuracy

The modelled maturities given in section 5.3 indicate that, in accordance with expectations and applied technique, the Posidonia formation – the youngest and shallowest of the three – is generally the least mature formation while the lowermost Sleen formation is most mature. Since the maturities within a formation differ greatly due to different depths of the formation, an average value is not given since it is not meaningful.

Although the modelled maturities for the Posidonia formation and the extrapolated maturities for the Aalburg and Sleen formations are indicative for relative maturity, they are neither very accurate nor are they absolute values. This is due to several causes discussed below.

Low Resolution of the Model

The maturity of the Posidonia formation per well is derived from an intersection between wells and an ArcGIS raster-grid. This grid is an interpolation of vitrinite reflectivity measurements at some specified wells and has a very coarse resolution of 6 km² per pixel. This coarse resolution implies that if the maturity is extracted from two different wells located within a single grid-block, they will both be assigned the same Posidonia maturity, even though the depth of the fault block targeted by each well may be very different. While this technique may be fairly accurate for continuous, sub-horizontal formations and vertical wells, it is not accurate for the faulted and inverted West Netherlands Basin, where an offset between separate fault blocks can reach up to several hundred metres. For those situations, at least one of the wells will be assigned a maturity that is unrepresentative for the local formation

Maturity Extrapolation Technique

The method applied for extrapolating the maturity from the Posidonia formation to the Aalburg and Sleen formation is empirical and based on some assumptions and simplifications. To begin with, it is assumed that, no tectonic disturbance has occurred within the Lower Altona group, and that therefore the original (and standard) geotherm from top Posidonia to bottom Sleen applies. This seems a reasonable assumption, as there are no unconformities or hiatuses known to occur in this section. The relation between reservoir temperature and vitrinite reflectivity is based on a mathematical approximation of the results of selected literature but it must be noted that several other studies show significant deviations.

A more important source for inaccuracy, at least for the Aalburg formation, is the fact that per formation a single maturity is calculated for each well. This maturity is calculated for a thickness midpoint. While this is of less significance for the relatively thin Sleen and Posidonia formation, it may cause a rather large over- or underestimation of maturity for the top and bottom of thick Aalburg sequences. If, for example, the Aalburg formation is locally 600 metres thick, as is the case for approximately 15% of the wells according to section 5.4, the 300 metres difference between mid and bottom of the section may represent a maturity difference of up to 0.15%; a value that, at average maturities of the Aalburg formation, can make the difference between entering the gas-window or not.

Modelled Maturity versus Sample Data

Maturity in terms of vitrinite reflectivity is determined by means of a microscope. This method has not been applied to the core samples available for the Altona Group; instead an approximation of vitrinite reflectivity was derived from the van Krevelen diagram. There are however some R_0 -measurements, performed by TNO, for cuttings from various wells (table 6.2). The Krevelen-inferred maturities can be combined with the cutting maturities to establish a reference framework to plot the modelled maturities against; this can be used to determine the correlation between modelled maturities and measured/inferred maturities. The resulting plot is given in figure 6.4.

As can be seen, in general the low-resolution model appears to overestimate the maturity-trend with respect to the measurements. Due to the poor regional coverage from the measurements however the model is currently the best method available for mapping and assessing the maturity in the basin. Correlation of the model with the measured and derived maturities is unlikely to make the model provably more accurate since neither the cuttings nor the van Krevelen diagram yield very accurate maturities either. The TNO cutting-maturities are average values and have very large standard deviations; the Krevelen-maturities are only an approximation. Since the model can neither be easily improved nor any alternatives exist, the model will remain to be used in this study. It's up to the reader's discretion to note that modelled maturities give relative maturities, not absolute maturities.

Table 6.2: TNO-measured R_0 averages and their standard deviations versus the modelled R_0

TNO	Formation	Modelled R_0	Measured R_0	Standard Deviation
EVD-1	ATAL	0,9	0,4	0,9
GAG-1	ATPO	0,9	0,6	0,1
GAG-1	ATAL	1,0	0,5	0,0
GAG-1	ATRT	1,3	0,7	0,7
HST-1	ATPO	0,6	0,5	0,9
HST-1	ATAL	0,7	0,6	0,9
HVB-1	ATAL	0,6	0,9	0,4
HVB-1	ATAL	0,56	1,22	0,3
HVB-1	ATAL	0,56	1,50	0,4
HVB-1	ATAL	0,6	0,9	0,3
JUT-1	ATAL	0,6	0,6	0,1
JUT-1	ATRT	0,6	0,6	0,9
WAS-23	ATAL	1,3	0,5	0,1
WAS-23	ATAL	1,3	0,6	0,1
WOB-1	ATAL	0,7	0,7	0,8
WOB-1	ATPO	0,6	0,6	0,1

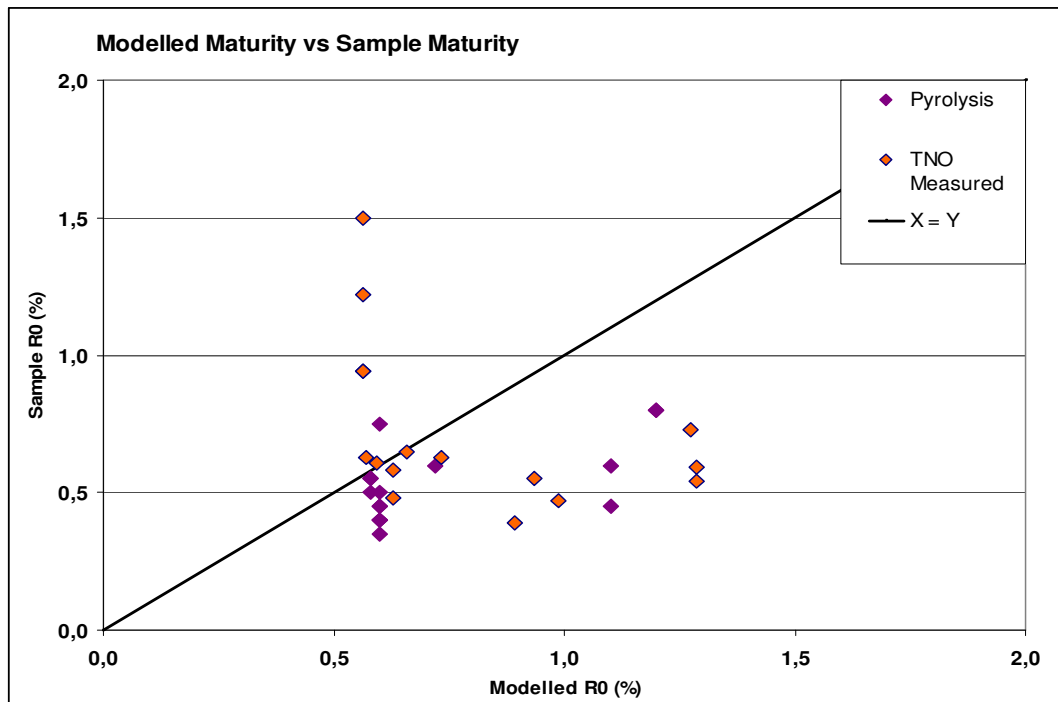


Figure 6.4: Modelled R_0 versus R_0 derived from measurements (TNO) or inferred from the van Krevelen diagram. In general the model appears to overestimate the maturity although the opposite occurs as well.

Thermogenic gas generation requires maturities above 1.0% R_0 in order to generate sufficient gas to have economic potential (section 3.1.4). At $R_0 > 1.2$, gas generation is increasing significantly. Taking into account the potential high degree of error for the modelled maturities with respect to the deeper lying sections of the formation, a marginal class is introduced of 0.8-1.0%, where gas may be generated depending on actual maturities. Consequently, the following classification is applied:

$R_0 = 0.0-0.8\%$	Poor
$R_0 = 0.8-1.0\%$	Marginal
$R_0 = 1.0-1.2\%$	Good
$R_0 = 1.2+\%$	Excellent

With this classification, it is seen that only 20% of the Posidonia well plot as 'marginal' and that only 6% of the Posidonia wells plot as 'good' or 'excellent'. The Aalburg formation is somewhat better. Of this formation, 26% plots as 'marginal' and 11% as good or excellent. The Sleen formation is of course most mature with 31% of the wells plotting as 'marginal' and 20% as 'good' or 'excellent'. It must be noted however that, apart from lower gas generation rates, a lower maturity also means that because less oil in the oil-prone shale is converted to gas, also less pore space is opened up, which decreases the storage capacity of the shale. This too is a reason to favour high maturity areas beside the actual gas generation rates.

6.3.2 Maturity Mapping

The maturity maps for the Sleen, Aalburg and Posidonia formation constructed for this thesis are all derived from an (interpolated) coarse-gridded maturity map of the Posidonia formation. As a result data points may not always plot expected maturities for their location. To compensate this, the structural map and base-depth map have been used in conjunction with the maturity data points to construct maturity maps that respect both depth and tectonic environment in the West Netherlands Basin and Roer Valley Graben by following depth patterns and fault blocks. The resulting maps show that the region between The Hague and Rotterdam is generally the most mature, with

maturities exceeding $R_0 = 1.0\%$ for all three formations. The areas of marginal and good maturity increase with increasing depth of the formation resulting in the Sleen formation having the most mature regions. The Roer Valley Graben is represented by only few wells but based on the base depth of the Altena Group interpretations have been made for this basin. From this interpretation it appears that the centre of the Roer Valley Graben is potentially sufficiently mature to have local gas potential. The maturity maps can be found in appendix F2. All interpolations have been done manually by defining areas of similar maturities and formations, instead of by statistical interpolation. This is because statistical interpolation cannot account for the presence of faults and depth variations and the current data coverage and used grid resolution. Instead of blunt extrapolation of present-day data with statistics, careful observation and interpretation using geologic understanding of the present-day basin and its history will result in a better product.

6.4 Total Organic Carbon

6.4.1 Interpretation and Accuracy

The pyrolysis TOC values are varying greatly within a single well, which is most likely the result of changing depositional environments (as was discussed in section 6.2). Although it is assumed that the pyrolysis technique is accurate, some samples that have been retested yielded sometimes significant different results; presumably due to oversensitivity of the detector. According to the respective laboratory, other samples did not suffer from this detector sensitivity and should thus reflect the true TOC content of each sample.

For the modelled TOC, TOC profiles constructed from (most often) sonic and resistivity well logs have proved to be a valuable tool for modelling organic carbon content for wells without core data. The profiles are empirically calculated and their accuracy depends on several factors. Firstly, the resolution and back-ground noise of the logs is of great importance. Where some resistivity, sonic, or other logs show relatively smooth curves with small and gradual variations from one interval to the other, other logs suffer from severe background-noise or other sources of disturbance resulting in erratic logs with many extremities: something that is also reflected in the standard deviation of calculated TOC averages. This, however, is something that is, although not desired, not unexpected either; empirical derivations are always dependent on the resolution of their source data. Although of possible great influence when examining well-sections in detail, for the overall TOC averages the extremes are assumed to be of minor importance seen from the great amount of depth-intervals used for the calculations of average TOC. In addition, the relative trend of the TOC profile is still clearly observed when examined visually, thus sections with a relatively higher TOC level are still easily distinguished.

It was, from examination of the logs, initially thought that the Lower Aalburg formation was typically richer in TOC than the Upper Aalburg Formation. Average TOC levels for these parts however show little difference and on re-examination it was noted that the TOC difference, where present, is generally too small to have a significant influence on the overall TOC level.

The accuracy of the TOC-averages is illustrated by their standard deviation. Standard deviations similar or greater than the calculated average are not uncommon, indicating that 33% of the section used for the TOC-average is either zero or more than twice as high than the average. Because of these large deviations, the calculated average value may not be very meaningful, especially not for the case of the hundreds of metres thick Aalburg formation. Subdividing the Aalburg formation in intervals will probably not result in a major improvement as high TOC peaks could not be correlated.

A second source for error comes from the calculation of the LOM value. The LOM value is derived from the vitrinite reflectivity by an observed mathematical relation between the two. Although this relation is quite precise, the values for vitrinite reflectivity may not be. These values are derived from a modelled maturity in a tectonically much disrupted basin based on point-data. The vitrinite input is

thus dependent on the accuracy of the model. As seen in section 6.3, this accuracy is quite low for the model used.

An additional problem with the coarse grid of the model is that wells with a graphical starting point within the same grid section are assigned the same maturity although their target depth (and thus real maturity) may be very different. The effect of LOM on calculated TOC levels around 1.0% can be as large as plus or minus 0.4% per addition or subtraction of 1 LOM, which roughly corresponds to 0.1% R_0 . Since the change in TOC (Δ TOC) due to LOM variation is dependent on the difference between the sonic/resistivity log value, and thus directly related to the TOC level itself, the value of Δ TOC increases with increasing TOC. For TOC levels around 2.0% for example, single-unit variation of LOM results in a Δ TOC \sim 0.8%. This is a major weakness in the TOC profiling method and one should keep this weakness in mind when selecting high-potential shale-gas regions based on modelled carbon-content. Calibration of the profiles with TOC values resulting from pyrolysis was not possible since the wells for which the profiles could be constructed were different from those for which cores were available. The only exception here was for well DON-01 (Dongen-01). The erratic nature of the logs used for this well however, and as a result the erratic nature of the TOC profile itself, makes calibration very difficult and is unlikely to result in any improvements with respect to the absolute accuracy and plausibility of the TOC profile for this well. If the pyrolysis results and TOC profiles are compared more generally however, it is seen that the calculated average for the pyrolysis results per formation is generally slightly higher than the conjugating average of the profiles. The average of pyrolysis TOC for the Aalborg formation for example is 1.43% while the conjugating profile average is 1.25%. For the Posidonia formation this difference is 6.09% against 5.11%. For the Sleen formation the situation is reversed: 0.40% against 0.94%, although this may be due to the small amount of Sleen cores (5 cores, 1 well) or the addition of a standard TOC background level of 0.8%.

A third and final source for inaccuracy is the addition of a global back-ground TOC average for black shales of 0.8% TOC. This average comes from different source rocks worldwide and does not take into account the respective history of the source rock for which the TOC is modelled. It is not unlikely, for example, that a TOC-rich source rock such as the Posidonia shale has a much higher back-ground TOC value than the assumed 0.8%, while the TOC-poor regions of the Aalborg formation, which are probably deposited under oxic reducing conditions, have a much lower (if any at all) back-ground TOC level. Even so, the result in terms of TOC levels will probably not vary too much on absolute level. Even with the added 0.8% TOC the Posidonia is still well enough enriched to have potential while the Aalborg is still mainly marginal to unprospective even with the possible overestimation of the back-ground levels.

From the literature study the following classification for TOC arose:

- TOC = 0-2% Poor
- TOC = 2-3% Marginal
- TOC = 3-5% Good
- TOC = 5+% Excellent

With this classification, and generalising the formations, they can be graded as follows:

Formation	Classification	Notes
Posidonia Fm	Good	High TOC levels, generally >5.0%
Aalborg Fm	Poor	Generally low TOC levels (<2.0%)
Sleen Fm	Poor	Generally low TOC levels (<2.0%)

Note however that, unlike commonly assumed, a low TOC level does not automatically mean that the play has no potential. The best example for this was brought forth in the case study of the Lewis Shale. This shale has generally a TOC level of less than 2% (poor) but is still highly viable from economic perspective (Curtis, 2002).

6.4.2 TOC Mapping

For the mapping of TOC both the pyrolysis results and the model averages are used. Note however that two different symbols are used for easy recognition of the data source (Appendix F3).

For the Posidonia TOC map an additional symbol is used (circle with question mark). This is done because for these wells the Posidonia formation was not interpreted in the stratigraphic column. The averages calculated for these locations are therefore not necessarily from the Posidonia formation (this formation could have been faulted out or eroded). These averages are therefore considered to be less important than those averages for which the Posidonia formation was interpreted in the lithostratigraphic column. The Posidonia TOC map shows that almost all Posidonia TOC averages indicate high TOC levels for this formation (exceeding 5%).

Those few data points that do not indicate excellent TOC levels are, all-save-one, inferred values and appear not to be representative for the Posidonia formation after all. On average, the Posidonia seems to be very rich in organic material wherever present. As a result, the Posidonia formation is interpreted to be of good to excellent TOC class throughout the basin.

The Aalburg formation is mapped twice, once for the Upper Aalburg formation and once for the Lower Aalburg formation. Since the pyrolysis results are only representative for the Upper Aalburg formation they are not plotted in the map for the Lower Aalburg. The resulting maps however are almost identical. By far the majority of TOC values are classified as poor for both sections. Those data points that are of marginal, good or excellent class are almost all inaccurate. Some data points are pyrolysis averages derived from few samples, others are modelled values that suffer from incorrect TOC-modelling due to insufficient compaction (shallow wells). As a result, for both the Lower and Upper Aalburg formation it is assumed that the entire formation is generally poor in TOC. The same goes for the Sleen formation, for which all data points indicate less than 2.0% TOC.

6.5 Gas Shows

6.5.1 Interpretation and Accuracy

Gas shale potential is often derived from attributes such as TOC content, maturity, or the presence of natural fractures. Almost all of these attributes however have examples of shale gas plays that do not meet the attribute-requirements. The Lewis shale is far too poor in TOC, the Bakken shale is immature, and the Barnett shale does not possess a network of natural fractures. Yet all of them have been found to be economic important resources. Because of these exceptions, the validity of some attributes when assessing the potential of a play becomes doubtful. So, if maturity or TOC level cannot accurately describe the potential of a play, then what attribute can?

One of the most promising distinctive attributes is perhaps the gas show; after all, if gas is measured it is certain to be there, even though the exact quantity cannot be determined. However, gas shows are not easily extrapolated to other areas. Gas generation alone depends on many factors of tectonic and sedimentary nature. In addition, drilling process may enhance or quench gas shows. Seen that the other attributes however are inaccurate in determining the potential of a gas shale, gas shows are, although unproven, a valuable asset for estimates of potential.

Gas shows often vary significantly in lateral directions. As a result, combinations of very high and very low gas measurements may be seen close together. If one is to extrapolate gas shows to other areas as to estimate the potential there, the factors on which gas shows depend must first be understood.

The most remarkable of observations in gas shows is found near the town of 'de Gaag' (figure 6.5). Measurements performed on one of the wells drilled here, Gaag-05, displays very high gas shows up to 235.000 ppm total gas; the highest reading found anywhere in the two basins. Another well however, Gaag-01, having its starting position only tens of metres away Gaag-05, displays hardly any gas shows for the Lower Jurassic formations; moreover, the gas shows that *can* be seen in the well's gas log are at least partly due to the addition (and vaporisation) of 20% diesel oil to the drilling mud.

An obvious question to ask here is: “How is it possible that the same formation shows such large variability in gas shows on such a small interval?”

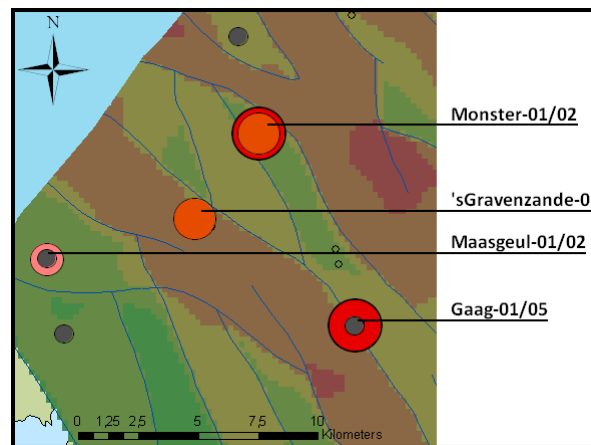


Figure 6.5: Zoomed map of the Gaag area. Grey circles represent low gas readings, larger, red circles represent higher gas readings.

This question is attempted to be answered by considering the following explanations:

1. Detection Error
2. Interpretation Error
3. Geological Variability
4. Gas Escape

Detection Error

This explanation assumes that the gas in Gaag-01 is locally present but is not detected while drilling. A first explanation for a detection error would be a wrongly installed or defect gas chromatograph. Although this is certainly the easiest explanation and not necessarily impossible (on various occasions such an error was noted somewhere halfway a gas log) it is unlikely that problems occur at so many instances and left unnoticed (>10% of the locations show significant variability). Although drilling will perhaps not be stopped for a broken chromatograph, one may assume that a note will be made in the log explaining the situation and warning others not to use the gas log. No such notes were found.

Another possibility belonging to the detection error category is the suppression of gas in Gaag-01 due to a high mud weight or mud injection into the formation. If the density of the used drilling mud is very high, the gas may be unable to make its way through to the surface and no or hardly any gas readings will be measured at the well. This however is not a likely explanation either. High gas shows have been measured at very high mud weights of up to 1.45 g/cm^3 (e.g.: well Molenaarsgraaf 2 (MOL-02)). In the case of the two Gaag wells the highest used density for the mud is 1.31 g/cm^3 for both wells. In addition, if we cross-plot the gas shows for all wells analysed versus the mud weight used, no correlation is found between mud weight and gas show (figure 6.6). Mud injection is not very likely either seen that shales are very impermeable. Neither a problem with the chromatograph nor a high mud weight is therefore likely to explain the difference in the gas shows.

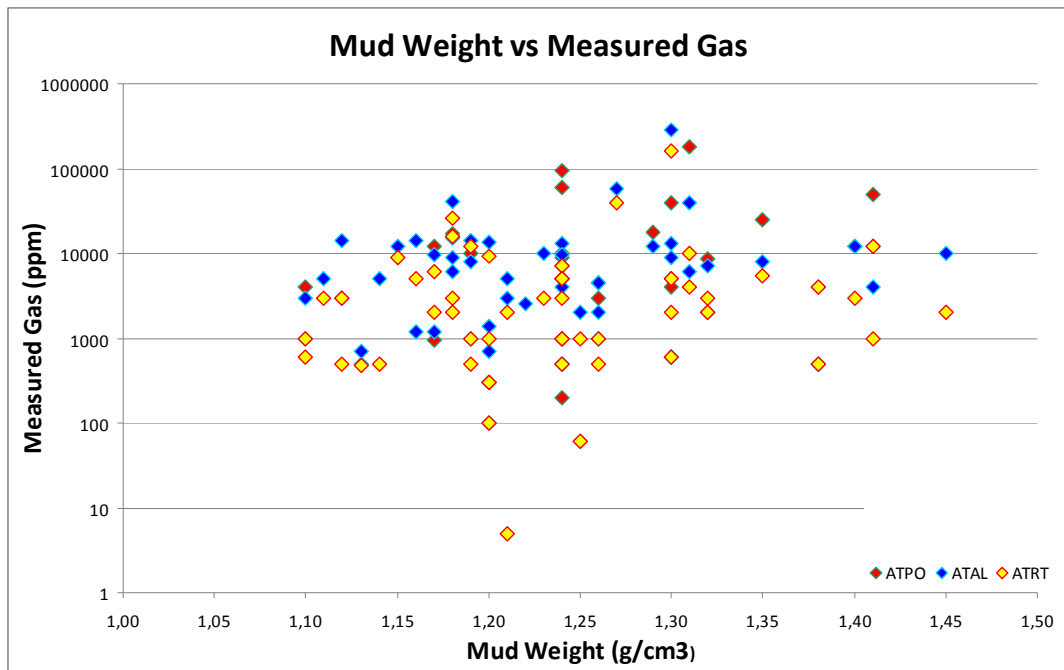


Figure 6.6: Diagram plotting mud weight versus measured gas. No clear relation is distinguished between them.

Interpretation Error

An 'interpretation error' can be interpreted in various ways; what is meant in this context however is that the extreme gas shows found in the Gaag-05 well are falsely interpreted as being indigenous while they are actually not. For example, the gas found in the lower Aalburg formation and Sleen formation could be Carboniferous in origin, having migrated from greater depths to the bottom of the shales. Via a network of fractures the gas could then migrate upwards into the shale until, at some point, the fracture network ends and the gas is trapped, not unlike a conventional reservoir. An observation supporting this hypothesis is that, as seen in figure 5.9 the lower part of the shale is enriched in natural gas while the shallower parts of the Aalburg formation show far less spectacular gas shows.

However, if such a Carboniferous charge existed, one would expect that the underlying Keuper formation contains some gas as well. Instead, the gas shows in Gaag-05 completely disappear going from Sleen to Keuper. If a Carboniferous charge occurred here, at least some elevation in gas show should be visible in underlying formations, including the Keuper formation. Although the West Netherlands Basin is severely fractured and a fault network cannot be completely discarded without taking and examining core samples from that area, it is not the most likely solution either. The only fault recorded during the drilling is a major fault located 400 metres higher in the Werkendam formation. In addition, the large vertical interval in which the gas occurs (approximately 130 metres) is too large to be likely to be fracture-sourced. Unfortunately, the only way to confirm that the gas in the Gaag-05 well is indigenous to the Jurassic shales or not, is by taking a sample of the gas and plotting its C_1/C_2 ratio against the ^{13}C isotope value and comparing this to similar plots of known gas sources as described by de Jager et al. (1996). Without this, a final answer cannot be deduced and it can only be assumed that the gas is indigenous.

Geological Variability or Gas Escape

If the cause for the observations made at, amongst others, Gaag-01 and Gaag-05 is neither a technical error nor an interpretation error, the observed difference in gas yield is really there and is the result of geological factors. The most likely circumstances that can explain such an intraformational variability are following:

1. *Gas Escape* – gas was generated at both wells but escaped from the area of well Gaag-01 in a later stage.
2. *TOC Variability* – gas was not generated at Gaag-01 due to inhomogeneous distribution of organic matter, with insufficient organic matter content at the Gaag-01 well.
3. *Maturity Variability* – the sections at Gaag-01 and Gaag-05 have a different level of thermal maturity allowing gas generation at one location but not at the other.

For all three possibilities the Gaag-01 well and Gaag-05 well must penetrate different sections of the Jurassic shale with very different properties, respectively. The most likely method of achieving this situation is if the two wells have targeted different fault blocks. When examining the well deviation for each well, it can already be seen that their trajectory is quite different. The Gaag-01 well is sub-vertical while the Gaag-05 track displays a relatively sharp curvature. The best method for testing the hypothesis that these wells are penetrating different blocks is by interpreting the seismic section for this area.

Figure 6.7 shows the uninterpreted E-W section for the lower Jurassic formation. The next figure, figure 6.8, shows an interpreted version of the same section.

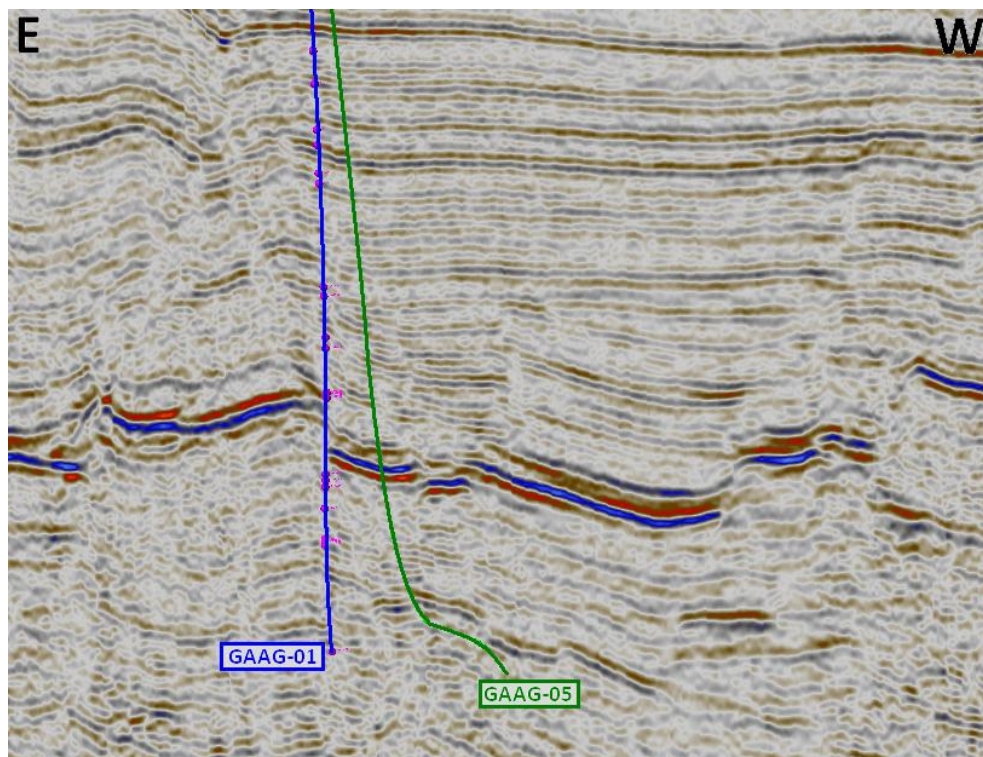


Figure 6.7: Uninterpreted E-W seismic section of the Gaag-area in the western West Netherlands Basin

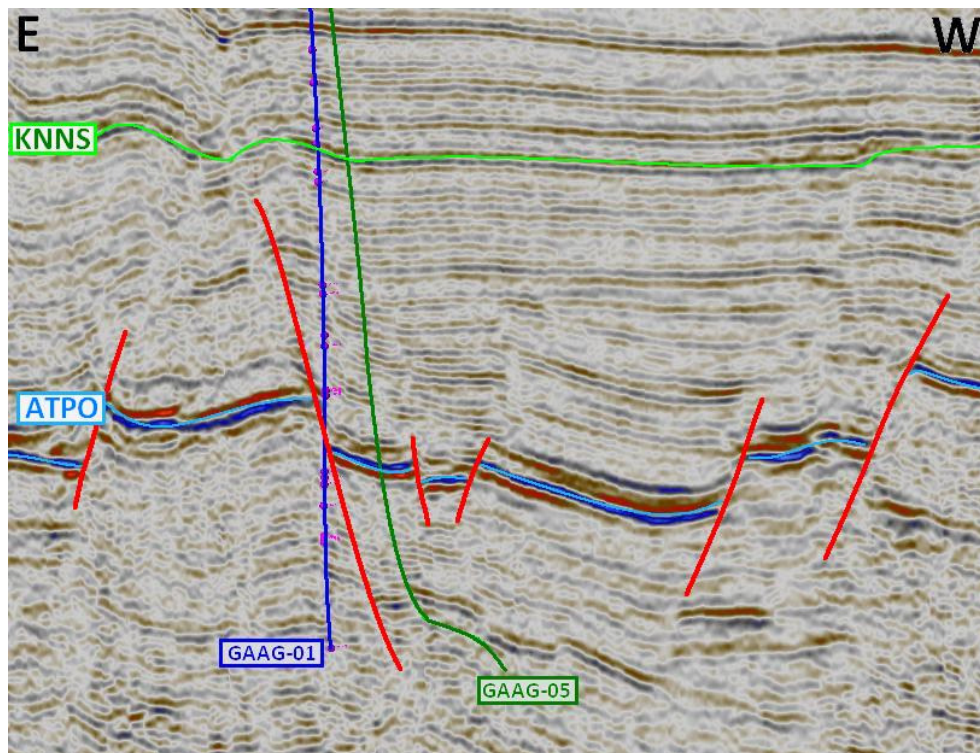


Figure 6.8: Interpreted version of the same section. The target for the two wells are Permian (Gaag-01) and Triassic (Gaag-05) conventional reservoir rocks, respectively.
 Reflectors: ATPO = Jurassic Posidonia Formation; KNNS = Cretaceous Vlieland Sandstone Formation

As can be seen from the interpreted section, Gaag-05 and Gaag-01 indeed appear to penetrate different fault blocks, with the Gaag-05 well penetrating the hanging wall-block of the large-scale fault on the left, and the Gaag-01 well penetrating the Jurassic in the foot wall-block of this fault.

This is an important observation since with it the plausibility of any of the above mentioned possibilities increases. The first possibility, gas escape, could be explained by the close proximity of the fault to the Gaag-01 well trace. The bright red-blue reflector represents the Posidonia Formation, implying that the Aalburg formation is located directly below it, very close to the fault. Motion along this fault after gas generation in the Aalburg formation may have induced the formation of secondary fractures, resulting in loss of gas from the formation. The chance however that an impermeable shale filled with gas is completely drained by the formation of secondary fractures, derived from a main fault, to the extent that hardly any gas remains is very unlikely.

In a way, gas drainage of the formation by secondary fractures can be compared with the production method of fracking. Although fracking is a useful method of producing from impermeable reservoirs, it fails to extract all gas; there will always, even at high-density fracking, remain an unproducable remnant of gas. One may assume that industrial high-fracture density stimulation of specific layers is more efficient than fracture density as it occurs in nature. As such, even more gas should remain in naturally fractured formations. Since no gas pockets are seen in the gas log and the overall gas content of the well is extremely low it is unlikely that tectonic fracturing-induced gas escape is the cause for the low gas shows in the Gaag-01 well.

The second possible explanation is that the fault block penetrated by the Gaag-01 well contains far less organic matter than the Gaag-05 well due to differences in depositional environment. The most accurate method for testing this hypothesis would be by retrieving core samples from the lower Aalburg formation of the two wells and pyrolysing them. Unfortunately however, cores are unavailable for either well. Luckily, both wells do have resistivity and sonic logs available allowing TOC modelling for the Aalburg formation using the method of Passey et al. (1990). The resulting TOC profiles are displayed in figure 6.9.

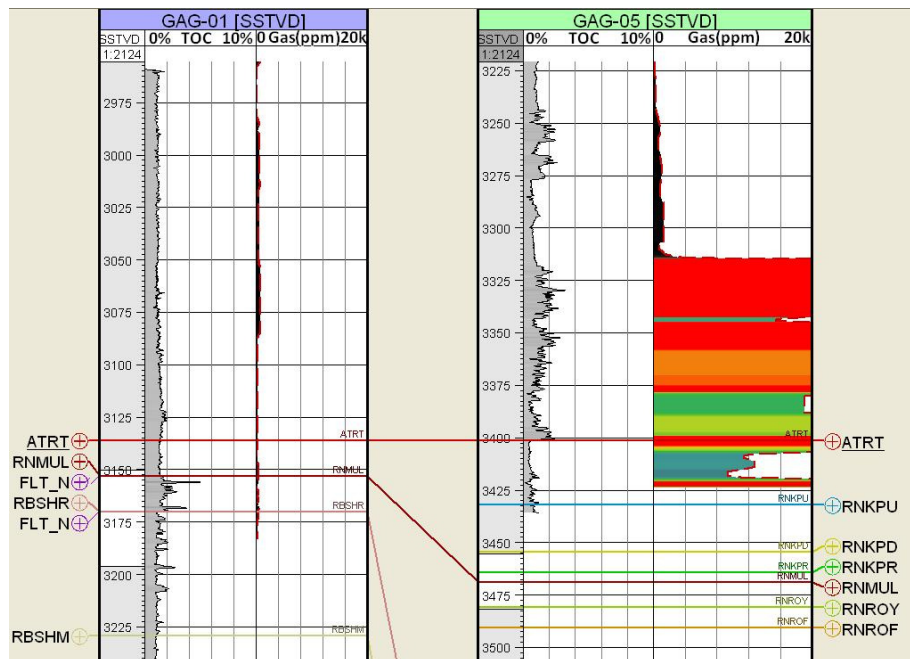


Figure 6.9: TOC profiles and gas log for the GAG-01 and GAG-05 well. Note the relative low TOC values and the significant difference in gas shows. Depth is given as true vertical depth. Note also the difference in depth (True-Vertical) between the two wells.

The model states that TOC levels for both wells are not very high. The Gaag-05 well may perhaps show some enhancement in TOC levels with respect to Gaag-01, but it still averages around 1.5% (versus ~2.2% for Gaag-05); neither is extremely high. The difference in TOC between the two wells is therefore unlikely to be responsible for the great difference in gas.

The third hypothesis is that of variability in maturity. In the present-day situation observed from the seismic profile in figure 6.8, it is seen that the Aalburg formation is at greater depth in the Gaag-05 well than it is in the Gaag-01 well. Keeping in mind that the West Netherlands Basin has undergone several phases of inversion it is plausible that the Gaag-05 section of the Aalburg has reached even greater depths prior to the inversion events and has therefore been at higher temperatures than the Gaag-01 well. The modelled maturities presented in the results section are of no use for this problem since the resolution of the model is too coarse to model maturities for different wells lying so close together. Again, the best method for testing this hypothesis is by means of core samples, which are not available. Another method would be by performing a study of the depositional history of the West Netherlands Basin and back-stripping the sedimentary successions. This however is beyond the scope of this thesis. It seems however one of the more likely explanations for the observations made. It is certain that the West Netherlands Basin has been inverted and the lower Aalburg formation in the Gaag-05 well is even at the present already located more than 250 metres deeper than for the Gaag-01 well (3401 m TVD and 3135 m TVD respectively). At these depths a difference of 250 metres represents already a difference of approximately $R_0 = 0.1\%$ so at even greater depth-variations, which are very likely to have occurred in the past, this will become a significant factor in gas generation potential.

Since gas shows appear to be a very important attribute in determining a play's potential, additional study of the dependence of gas shows on other attributes is strongly recommended. Due to time constraints however, this is currently beyond the scope of this thesis.

6.5.2 Gas Show Mapping

Due to the dependence of gas shows on a wide variety of factors (e.g.: maturity, TOC, kerogen, tectonics), it is extremely difficult to make a good extrapolation of gas shows; even more so in a basin disrupted by tectonics to such high degree as the West Netherlands Basin. As a result, only

regions close to (and on the same fault block as) those wells with high gas readings can be assumed with some accuracy to have high gas shows as well. The gas show maps therefore show large areas marked as 'unknown' since it simply cannot be said what the gas show will be in these areas. As was already seen, gas shows may change significantly from fault block to fault block for no apparent reason. The maps (which can be found in appendix F4) are therefore only one of many possible interpretations based on the gas shows found in mud logs.

For the Posidonia formation, high gas readings are predominantly found in the immature region between Utrecht and Tilburg. Another area with high gas readings is found in the vicinity of the cities of Spijkensisse and Reedijk. Other localities for which mud logs are available do not show spectacular gas shows. Without a sample of the gas, it cannot be said whether the gas here is indigenous and whether it has been generated thermogenically or biogenically.

The Aalburg Formation's main area of interest with respect to gas shows is the area roughly from the town of Monster to the town of Barendrecht. Beside this area, two other areas exist with high gas shows: the region between Boskoop and Valkenburg, and the region between Waalwijk and Brakel; neither of these areas however have gas-shows as high as the former. Areas with expected significant gas shows are situated in the deepest part of the West Netherlands Basin and the deepest part of the Roer Valley Graben due to their expected high level of maturity. Without data points however, it cannot be verified whether or not the assumed potential for these areas is correct.

Of the three formations, the Sleen formation is probably the formation with the least gas shows. Only two small regions in the studied area exist that appear to have at least some potential, one being near the towns of de Gaag and Monster, the other being near the towns of Barendrecht and Oud Beijerland. The region between The Hague and Rotterdam has a suspected potential, similar to the area for the Aalburg formation. Again however, this potential cannot be verified without additional data points.

6.6 Clay-Mineral Content

Section 5.7 presented the bulk-mineralogical data resulting from the Qemscan analysis. The major use of this data for the gas-shale project is the evaluation of clay-mineral content in the shales. Shales rich in clay-minerals are more ductile and therefore far less sensitive to stimulation. As was stated in section 3.1.6, a prospective gas-shale should have clay-mineral concentrations below 50 vol%, with <30 vol% being even more desirable (Bowker, 2007; Loucks & Ruppel, 2007). However, one would not discard a very promising play because it has slightly over 50% clay-minerals, so a margin-class is introduced of 50-60 vol%. Resultantly, the following classification applies:

>60	vol% clay-minerals:	Poor
50-60	vol% clay-minerals:	Marginal
30-50	vol% clay-minerals:	Good
<30	vol% clay-minerals:	Excellent

The definition of clay-mineral is however not very clear. There does exist a 'Clay-Group', with primary constituents being minerals such as Illite, Smectite and Kaolinite. However, many other minerals are only occasionally considered a part of the Clay group, when specific properties are considered.

For this study, clay-minerals are defined as all those minerals that have a negative influence on stimulation due to their ductility. With this definition, the following two groups are established:

Clay Minerals – All those bulk-minerals with a high ductility and thus a negative impact of stimulation sensitivity. This includes the original clay-group (Illite, Smectite, Kaolinite) but also the mica group (Muscovite, Biotite, Chlorite, Phlogopite, Glauconite).

Non-Clay Minerals – Those minerals that have no affiliation with clay at any level. Their members constitute silicates (Quartz, Feldspar & Plagioclase), Carbonates (Calcite, Dolomite, Ankerite & Siderite), Sulfides (Pyrite); Sulphates (Anhydrite, Gypsum and Barite), heavy minerals and trace minerals.

By adding the constituents of each group together, the clay-mineral content per sample can be calculated, which can be plotted in a histogram displayed below (figure 6.10).

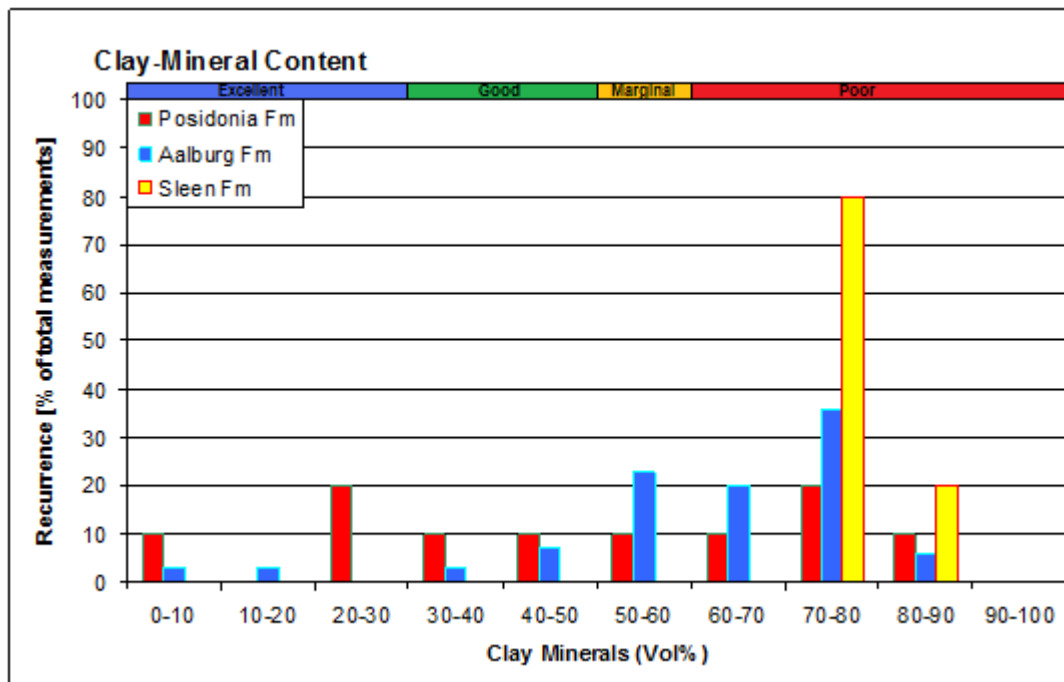


Figure 6.10: Histogram displaying the distribution of clay-mineral content per formation

What can be seen in this histogram is that the Sleen formation plots entirely above the 70 vol% interval, rewarding it a 'poor' classification. The Aalburg formation is distributed over a broader range, but 61% of the samples still contain clay-mineral contents classifying as poor. An additional 23% classifies as marginal, meaning that only 16% of the samples are classified as good (10%) or excellent (6%). The Posidonia formation shows a more even distribution and is on average the most prospective formation of the three with respect to clay-mineral content. Only 40% of the Posidonia samples classify as poor and 10% as marginal, implying that the other 50% is classified as good (20%) or excellent (30%).

Just as for other properties derived from core samples, the low amount of core samples for the Posidonia and Sleen formation reduces the accuracy of interpretations based on these cores. Especially for the Sleen formation, for which all cores are from the same well, the representativeness of the cores can be questioned. For the Aalburg formation, the fact that almost all samples have been taken from the upper half of the formation restrict interpretations derived from these samples generally to the upper half.

For the Posidonia and Sleen formation, only few samples are available. All of these samples come from only two wells. Mapping and interpolating clay-mineral content for these formations is therefore impossible. The Aalburg formation has a better coverage but hardly enough to base any lateral relations upon. In addition, when the well-averages are calculated, it can be seen that all save two wells plot as marginal/poor. When considering the two wells that classify as good: one of them

has a standard deviation that allows its average to plot anywhere from excellent to poor; the other well is derived from a single sample.

Due to the low data coverage and high error range, mapping clay-mineral content is neither practical nor accurate. Instead, a calculated average and resulting classification is likely to pose a better representation than inferred maps based on few data.

Table 6.3 below presents the calculated average for each well in addition to its classification. Per formation the average is also calculated. With this formation-average, the Posidonia formation receives a Good/Marginal classification since, although averaging slightly below 50 vol%, its standard deviation is too high to classify as 'good' over the whole. The opposite goes for the Aalburg formation, which therefore plots as poor/marginal. The Sleen formation is classified as poor with respect to clay-mineral content.

Table 6.3: Calculated average, standard deviation, and classification for the clay-mineral content of each well. In addition, the formation average and its standard deviation are displayed.

Well Name	Formation	Average Clay-Mineral Content (Vol%)	Standard Deviation of Average (Vol%)	Classification
Loon-op-Zand-01	Posidonia Fm	27,0	23,7	Excellent
Andel-02	Posidonia Fm	56,8	24,9	Marginal
AVERAGE	Posidonia Fm	47,9	27,3	Good/Marginal
Andel-02	Aalburg Fm	44,9	39,1	Good
Asten-01	Aalburg Fm	62,8	20,4	Poor
Bleskensgraaf-02	Aalburg Fm	72,8	12,8	Poor
Berkeel-02	Aalburg Fm	54,5	19,5	Marginal
Dongen-01	Aalburg Fm	60,6	1,4	Poor
Den Haag-02	Aalburg Fm	53,0	4,2	Marginal
Haarlemmermeer-01	Aalburg Fm	66,1	19,5	Poor
Haastrecht-01	Aalburg Fm	34,9	0,0	Good
Loon-op-Zand-01	Aalburg Fm	64,4	19,1	Poor
Moerkapelle-04	Aalburg Fm	77,1	3,6	Poor
Rijswijk-01	Aalburg Fm	61,0	26,6	Poor
Spijkenisse-01	Aalburg Fm	61,1	22,2	Poor
Wassenaar-23	Aalburg Fm	73,4	3,6	Poor
AVERAGE	Aalburg Fm	62,1	17,4	Poor/Marginal
Den Haag-02	Sleen Fm	77,0	7,5	Poor
QUARRY-1	Sleen Fm	81,2	3,2	Poor
AVERAGE	Sleen Fm	78,2	6,6	Poor

6.7 Methane Adsorption

6.7.1 Interpretation and Accuracy

Section 5.8 presented the resulting adsorption measurements for the 5 Jurassic samples. It was noted that the two samples with the highest measured TOC content were also the two samples with the lowest measured adsorption capacity.

A fragment of sample #31 (ATAL; HAG-02) that was sent to RWTH Aachen was measured by this institute to have a TOC content of 5.0%. The other sample, #86 (ATPO, LOZ-01) was measured to have a TOC content of 10.5%. According to general theory, organic carbon is assumed to be the only significant adsorbing medium in a lithology and as such, samples with a high TOC content should be capable of adsorbing larger quantities of gas than samples with low TOC contents. From the measurements however, the opposite appears to be true for this situation. When TOC content is plotted against sorption capacity it is seen that those samples with the lowest TOC content are the best adsorbing media and vice versa (figure 6.11). Especially the TOC measurements performed by Fugro clearly show the anti-correlation trend of decreasing sorption capacity with increasing TOC content for every sample. Since it is difficult to assign a single value to an adsorption isotherm due to the variability in shape and maximum-sorption pressure, the plots below are relative to each other.

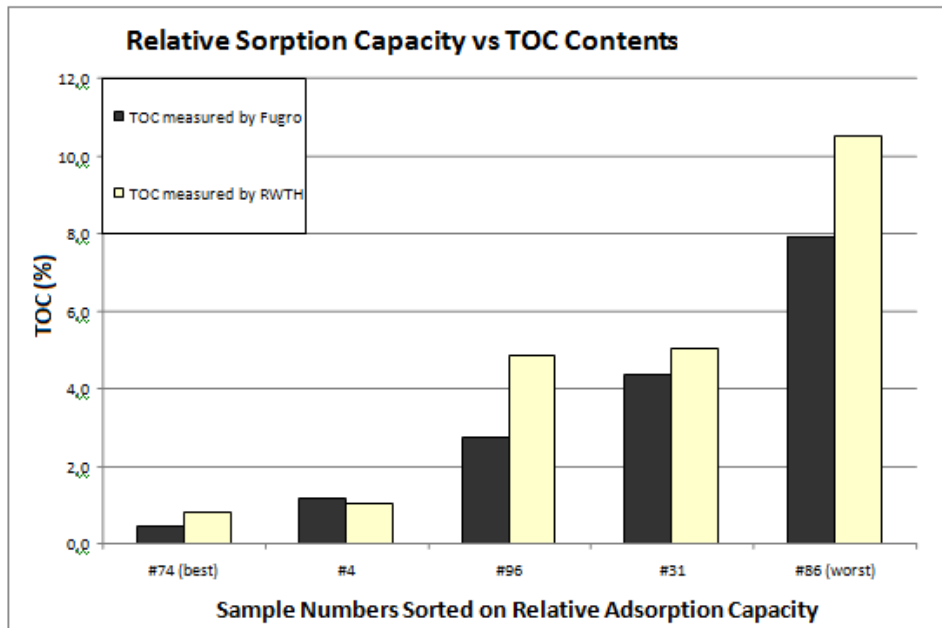


Figure 6.11: Relative sorption capacity plotted against TOC content

Clearly, these measurements are not in agreement with the theory that (only) TOC adsorbs methane. So could it be that another mineral is also adsorbing methane for these samples?

Apart from organic carbon, clay-minerals and micas are also sometimes named as having the potential to store methane gas. If that is the case for these samples, this should be visible in a similar plot as figure 6.11 above, but now plotting respective mica and clay-mineral content against the relative adsorption capacities (figure 6.12).

From this plot it is derived that clay-minerals are fairly unlikely to be responsible for the unexpected adsorption results. Although sample 86 and 31 do contain the least clay-minerals of all, a clear trend of increased adsorption capacity and increased clay-mineral content is not observed. Additionally, the capacity of gas adsorption in gas shales has been studied for American shale-gas plays and it was found that clay-minerals are not capable of acting as an adsorbing agent (Bowker, 2007). Mica content on the other hand does seem to correlate to a higher degree with relative adsorption content, with the highest mica content (~5%) belonging to sample 74 and the worst (~0.1%) belonging to #86.

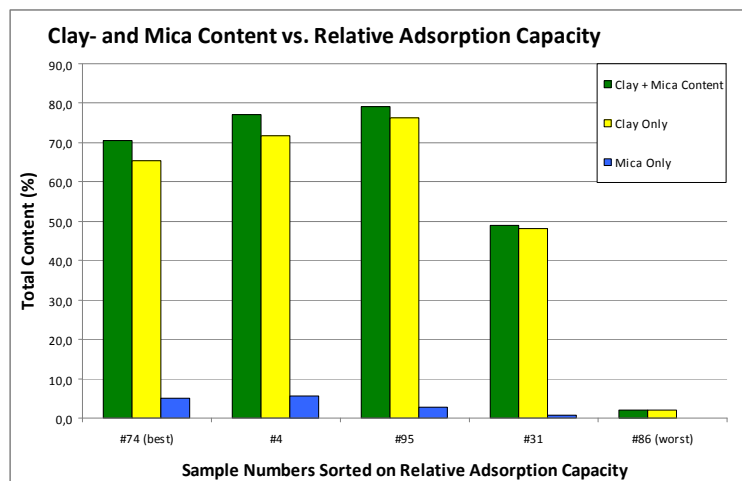


Figure 6.12: Clay-mineral and Mica content vs. relative Adsorption Capacity

In the original study of Irving Langmuir (1918) it can be read that “(...) *at room temperature the adsorption [of several gasses] by mica and glass was negligible, certainly not over one percent of the surface being covered by a single layer of molecules. At 183° and at 118° C, relatively large amounts of gas were adsorbed, except in case of hydrogen.*”

So, according to Langmuir’s experiments, adsorption of methane by micas is possible although it is dependent of temperature. Unfortunately, the temperatures at which the Jurassic shales were analysed for sorption are, at 65° C, somewhat in the middle of Langmuir’s reference temperatures. It is therefore assumed that at 65° some gas is adsorbed by micas, although not as much as would be possible at even higher temperatures. Even so this would partially explain the observations.

The sorption department of RWTH Aachen stated that an anti-correlation with TOC content and apparent correlation with mica content for gas adsorption was observed occasionally, but that a definite explanation for this observation had not yet been found. It was also pointed out that non-normalised capacities of 0.3 mmol/g sample, as found for sample 96, are extremely high for shales. Sorption capacities such as these cannot be accounted for by TOC alone and it is therefore likely that other minerals such as micas are responsible for the increased sorption capacity.

If this is true, it means that correcting isotherms for their TOC content does not give a representative normalised adsorption capacity. Although micas are a suspected secondary sorption agent, it is unknown whether, and to what extent, this mineral group may adsorb gas. There is simply too little data and knowledge available at this time, even at the laboratory of RWTH Aachen, to explain or normalise the measured sorption capacities and to transfer them to specific formations. As such, only the non-normalised isotherms remain to be useable. It is either using these, more or less representative, non-normalised isotherms, or picking global averages for shale adsorption, derived from formations that may be very different in composition from the Dutch Jurassic shales. Since the latter option does not exclude the presence of other, non-organic sorption agents, it would only incur an even higher imprecision since now also the shale composition itself is no longer representative. Because of this, the original, non-normalised isotherms are used for GIIP calculations instead. These non-normalised measurements are plotted in figure 6.13.

6.7.2 GIIP Input

Isotherm Selection per Scenario

Following the inconsistency of section 6.7.1, the normalised isotherms are found to be unrepresentative due to sorption enhancement by another, unknown, sorption agent. Resultantly, three non-normalised isotherms have been selected that plot within the region of expected sorption capacities for shales to represent a worst, medium and best case scenario for all formations. Since the measurements cannot be corrected for TOC content, the three separate formations will use the same isotherm per specific scenario. Assigning the best isotherm to the formation with the highest TOC as to compensate for the inability to correct for true TOC levels is not logical since the influence of mica on sorption capacity would then be completely neglected.

Consequently, the non-normalised measurements for sample 74 are chosen to represent the best-case scenario, measurements for sample 31 will present the medium case scenario, and measurements for sample 86 will represent the worst case scenario.

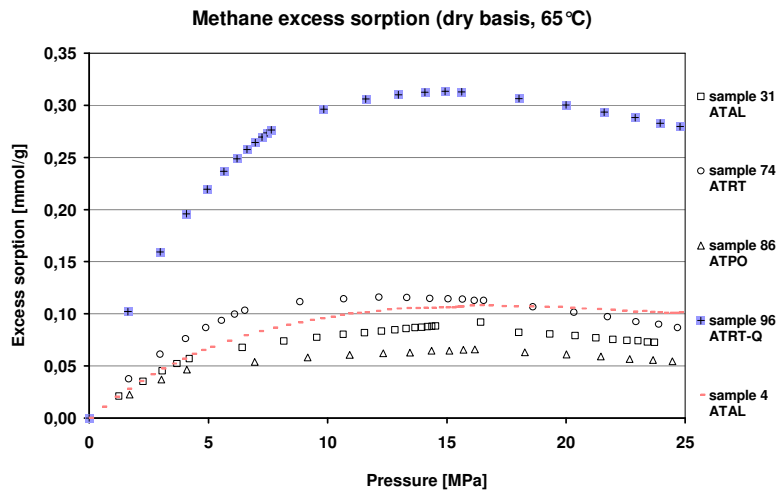


Figure 6.13: Non-normalised adsorption measurements (mmol/g)

Molar Volume and Shale Density

Since the results are given in quantities of moles per unit sample weight, assumptions have to be made for the molar volume of the gas and the specific density of the shale-material. The bulk-density can be estimated from density logs and is found to average around 2625 kg/m^3 .

The molar volume is calculated using the adapted ideal gas law $V=(nRT/P)$, which calculates the molar volume of n -moles of gas with gas constant R at temperature T and pressure P . The temperature and pressure are taken as standard surface temperature and pressure ($P = 0.101 \text{ MPa}$; $T = 15^\circ \text{ C}$). The molar volume then becomes $0.0236 \text{ m}^3/\text{mole}$.

Langmuir Fits

Now that representative adsorption measurements have been selected, a Langmuir isotherm can be constructed for each scenario. Since the Langmuir fit is unable to make such sharp turns as found in the measurements without gravely overestimating the maximum adsorption capacity at greater depths, the fit is chosen to be less accurate in the low-pressure zone resulting in a better estimate of the maximum adsorption capacity. However, all adsorption measurements show some degree of decrease in adsorption capacity at high pressures. This is a result of the assumption used in the measurements that the void volume of the test-chamber remains constant. Evidently however, this assumed volume decreases by adsorption. This is partly corrected for by gas-density increase, which is not taken into account for the pure Langmuir equation. As a result, the pure Langmuir equation somewhat overestimates the gas adsorption at high pressures, although the exact amount of overestimation cannot be determined without correcting for void-volume and density increase. The exact fits with respect to the data are found in appendix E. The Langmuir isotherms themselves are plotted for each formation and scenario in figure 6.14.

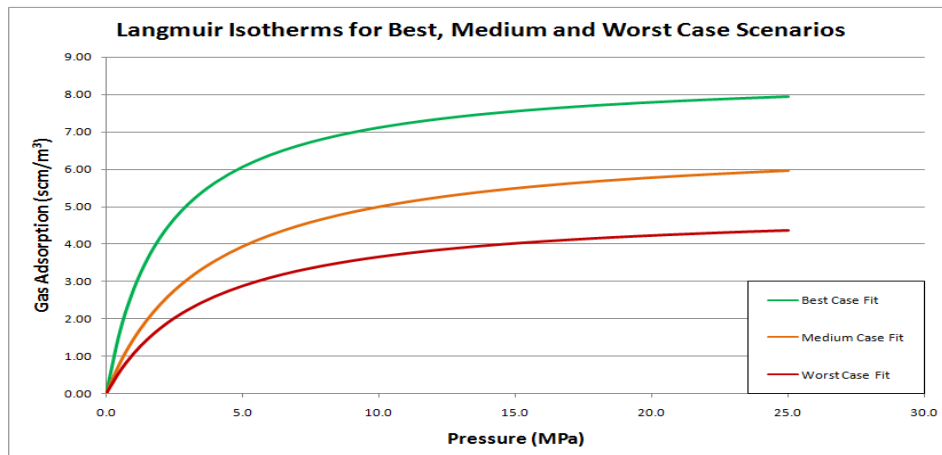


Figure 6.14: Langmuir isotherms for each GIIP scenario

6.8 Sweet Spot Determination

Based on the four mappable attributes discussed in the previous sections (thickness, maturity, average TOC level, and gas shows), sweet spots can be distinguished. Sweet spots are those areas that, according to the classifications used, possess the most favourable properties of the region. Because classifications are derived by interpretation, other interpretations of the data will lead to different shapes of the sweet spots.

The sweet spots are manually picked by overlying all attribute maps. By doing so, favourable areas for each attribute will locally overlap favourable areas for other attributes. The more of these areas overlap with each other, the higher the potential for shale gas becomes. In addition to identifying sweet spots, each spot also receives a confidence level. A higher confidence level indicates that there is a high chance that the attributes are interpolated correctly. A lower confidence level indicates that there is a high chance that the attributes are interpolated incorrectly, for example due to a large data spread, lack of correlation with the local geology, or due to conflicting or fluctuating measurements. Due to the existence of shale gas plays with either low maturity (Bakken Shale) or low TOC levels (Lewis Shale), these two attributes were considered of less importance than gas shows and thickness. In general, areas with measured attributes (completely filled) were given more significance here than inferred attributes (shaded).

Of the four mappable attributes, only thickness is considered critical for the potential of an area. If the measured, or inferred, areas indicate a poor thickness this area is rendered insignificant. Gas show is a very important attribute too, but is not considered to be a so-called 'show stopper' since it is poorly understood. Maturity and TOC content are not show stoppers either, since for both attributes examples exist of viable shale-gas plays where these attributes were lower than generally deemed necessary.

Per formation, each sweet spot is indicated on the map. Completely filled areas indicate that the sweet spot is based on measured data, while shaded areas indicate inferred sweet spots. Larger versions (A3) of the sweet spot maps can be found in appendix G. Radar charts indicate the basic properties (TOC content, maturity, thickness, surface area, and average gas measurement) for each sweet spot. The red pentagrams give an indicative area outside which the sweet-spot properties are most favourable.

6.8.1 Posidonia Shale Formation Sweet Spots

The Posidonia formation can be seen to have four sweet spot areas; two measured and two inferred (figure 6.15). Each area is given a zone-name derived from proximal urban areas/cities. As was discussed in the previous sections, the thickness and the TOC content for the Posidonia formation were considered to be sufficient throughout the basin based on measurements. The

maturity and gas shows however are more unevenly distributed. As a result, Posidonia sweet spots will be mainly based on these two attributes.

When comparing the maturity and gas show maps, it is seen that for the Posidonia formation most significant gas shows are found in thermogenically immature regions. In the regions of marginal maturity however, gas shows are generally low. For the mature regions no gas shows are available. As was discussed in section 3.1.4, gas that is generated by bacterial activity (biogenic gas) or catalytic reactions is also found in very immature regions. Regions of marginal maturity however are devoid of gas in those situations, since bacteria cannot survive at these temperatures, and catalytic reactions do not take place (Mango & Jarvie, 2009). This makes it possible that the gas found in the immature regions is in fact catalytic- or biogenic gas, and maturity becomes a less important factor here. The two measured sweet spots are therefore defined by the gas show measurements in these areas.

Since no gas logs are available for those few wells that do penetrate the deeper parts of the basins, it is difficult to determine whether sufficient gas will be available there. Based however on the fact that TOC levels are high for the Posidonia, and maturity is expected to be sufficient in at least the deepest regions of the basins, two sweet spots for thermogenic gas have been inferred: one in the deepest part of the West Netherlands Basin, and one in the deepest part of the Roer Valley Graben. The inferred sweet spot in the Roer Valley Graben is currently of interest to Cuadrilla Resources Ltd, who plans of drilling appraisal wells for the Posidonia and Aalburg formation (and possibly even deeper) near the town of Boxtel. Since no other wells have been drilled in that area before, it can only be speculated on how much gas they will find in place.

6.8.2 Aalburg Formation Sweet Spots

The Aalburg formation has, with six sweet spots, more sweet spots than the Posidonia formation despite its overall low TOC content. The sweet spots for the Aalburg formation are however smaller and their level of confidence is locally somewhat lower. The thickness of the Aalburg formation is not expected to be a problem anywhere in the basin and is therefore not a factor for sweet spots. The TOC content likewise, is considered to be insufficient at all locations. Since TOC has proven not to be an unfailing criterion in estimate of potential, and is therefore not considered a critical factor for potential, sweet spots are still defined for this formation. These areas however do have a higher risk than those sweet spots with sufficient TOC levels.

Resultantly, all sweet spots in figure 6.16 have low expected TOC levels and high expected thicknesses. Since no significant difference is observed for TOC content between the Lower Aalburg formation and the Upper Aalburg Formation, the sweet spots will be similar and only one map is constructed for this formation.

The most important sweet spots, those with the highest (qualitative) level of confidence, are the sweet spots named 'Zone Monster' and 'Zone Tilburg'. Zone monster envelops the Gaag-05 well and generally has very high gas shows. The maturity appears to be quite high there as well, especially in the lower parts of the basin, where the high gas shows are found. Following the observation with the Gaag-01 well, care should be taken when drilling in the shallower fault blocks since these are assumed to be without high gas content. The other high-confidence zone, Zone Tilburg, a small elongated sweet spot, follows a stratigraphic low (fault block) for which high gas shows were found as well. The maturity here however is expected to be somewhat less than for the Monster zone, although still sufficient for gas generation (especially in the lower sections of the Aalburg formation).

The only other measured sweet spot, Zone Spijkenisse, has gas shows that are greatly variable, which makes it difficult to assess its overall potential. Moreover, maturity is not very high either (<1.0% R_0). As a result, this sweet spot is assigned a medium level of confidence.

The three remaining sweet spots are all inferred sweet spots since no gas shows are available for them. These areas are Zone Delft, in the deepest part of the West Netherlands Basin, and Zone Oisterwijk and Zone Veghel in the Roer Valley Graben. These regions are expected to contain thermogenic gas based on their relatively high maturity but an appraisal well will be required to assess the true potential of these regions.

6.8.3 Sleen Formation Sweet Spots

For the Sleen formation, three sweet spots have been determined (figure 6.17). As for the Aalburg formation, the TOC levels of the Sleen formation are expected to be low throughout the basin. The thickness of the Sleen formation is generally thick enough except for a small strip around the edges of the basin. The resulting sweet spots are mostly the result of maturity and gas-show analyses.

The area with the highest confidence level is Zone Naaldwijk. This region is similar to Zone Monster for the Aalburg formation since the Sleen formation too displays high gas shows in this area. Due to the relatively great depth of the respective fault block, the zone is mature enough for the gas to be of thermogenic origin. The second sweet spot area, Zone Gorinchem, is found at the boundary between the West Netherlands Basin and Roer Valley Graben. Although some significant gas shows occur, there are only few measurements taken in this area. This combined with the relative low maturity causes this area to be of low confidence. The third and final sweet spot is located in the deepest part of the West Netherlands Basin. Since no gas logs are available here, the sweet spot is inferred rather than measured.

Based on sweet spot locations, the region between Utrecht and Tilburg seems an interesting location for further gas shale assessments. Drilling here at a carefully selected location means that not only the high-potential Posidonia shale can be further investigated, but that at the same time sweet spots for the Aalburg and Sleen formation can be assessed with little extra effort.

Additionally, the Gaag-05/Monster fault block should be investigated further. The fact that two wells show very high gas shows over the same interval suggest that the entire fault block may have this quality, and the potential for such a large gas reserve can validate the cost for drilling an appraisal well.

6.8.4 Final Shale-Gas Potential per Formation based on Sweet Spots

In general, the Posidonia formation appears to have the most favourable attributes and the highest potential for an economic shale-gas play. Given the low data coverage in the high-mature regions and the high gas readings in immature regions of the two basins however, makes it difficult to assess the potential of thermogenic gas and the origin of (assumed) biogenic or catalytic gas. However, it is still the formation that has the highest estimated chance of bearing economic quantities of natural gas.

The Aalburg formation is generally not very favourable in terms of attributes. The formation may be very thick in general, but if the majority of it consists of dead carbon or otherwise unprospective material the effective thickness is only a fraction of the total. Following conventional guidelines, the entire formation would be discarded based on the low average TOC level. Those small pockets within the Aalburg that actually do contain sufficient organic carbon are generally far too thin to be of significant influence. However, there are locations where the gas measurements in the drilling mud are extremely high. Thick stratigraphic sections such as found for the Gaag-05 well are not something that should be discarded too lightly. Compiling a cost overview and assessing the technical (and social-environmental) feasibility of producing in this region is the least that should be done before a decision is made concerning developing or discarding this field.

The Sleen formation is generally the least favourable and is assumed to have the least potential of the three formations. Except for the region of the Gaag-05 well, no regions of exceptional potential are found.

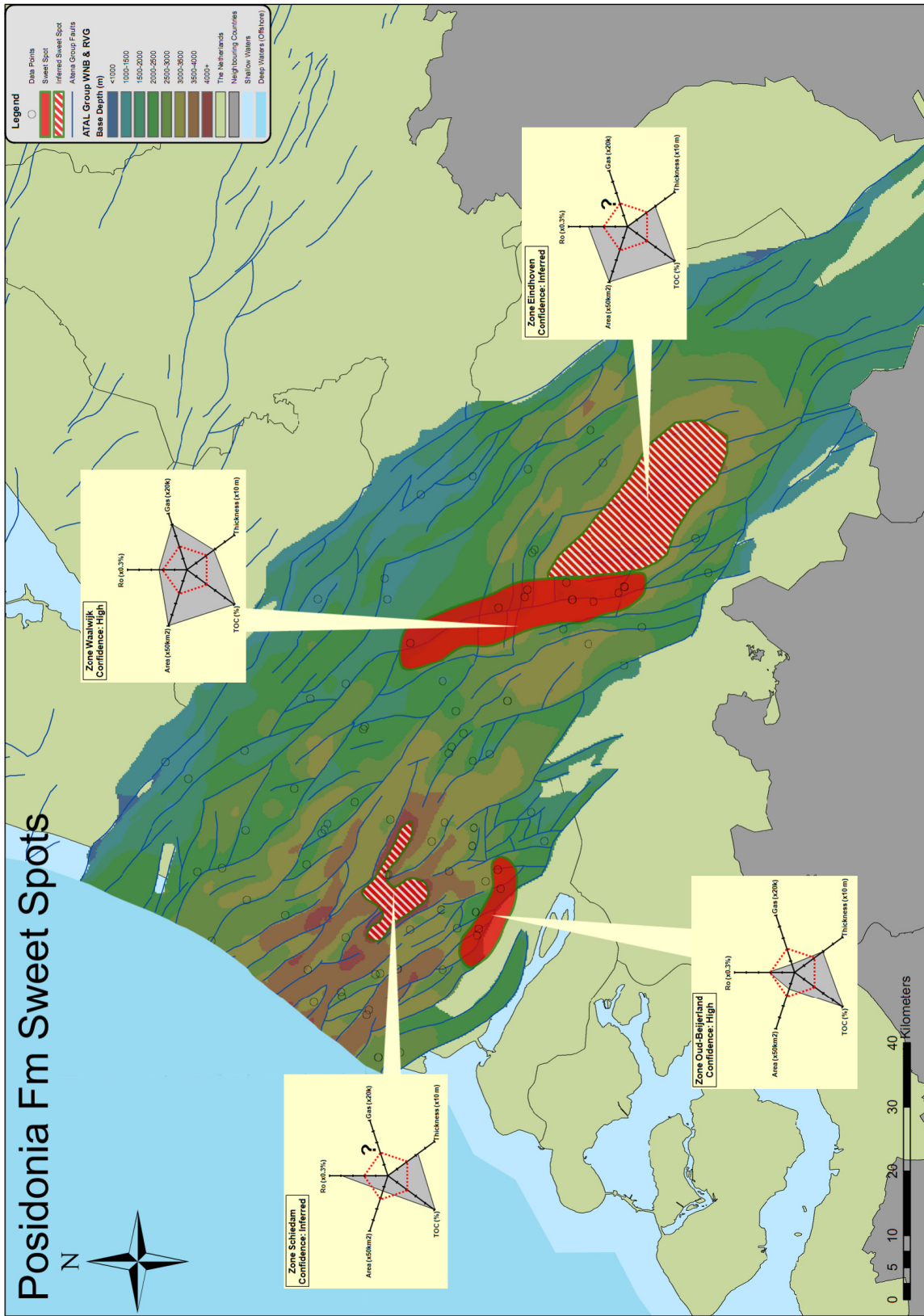


Figure 6.15: Sweet Spot map for the Posidonia formation. For more information refer to the legend in the top-right corner of the map. A question mark in the spider diagram indicates that no information is available for the respective attribute.

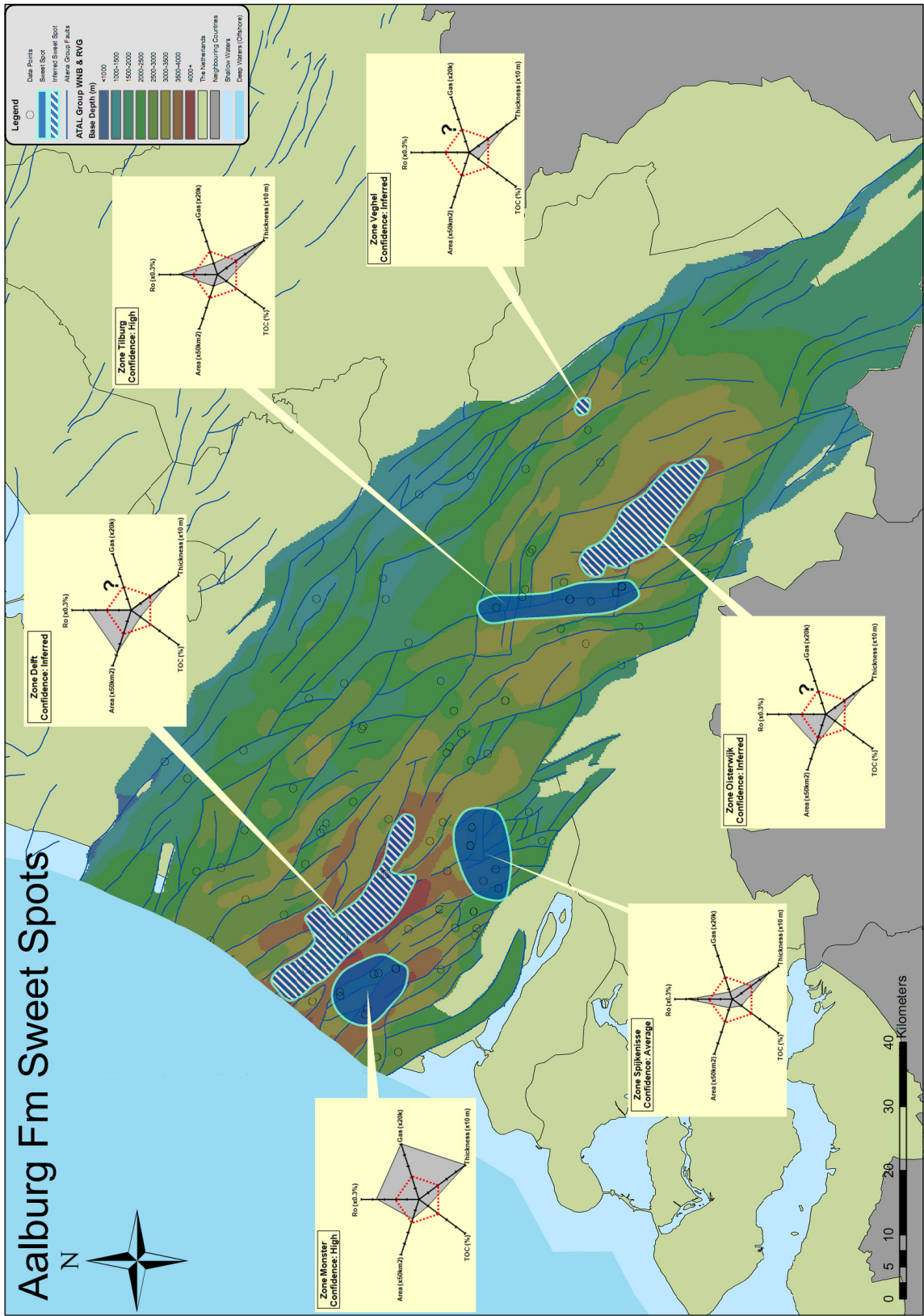


Figure 6.16: Sweet Spot map for the Aalburg formation.

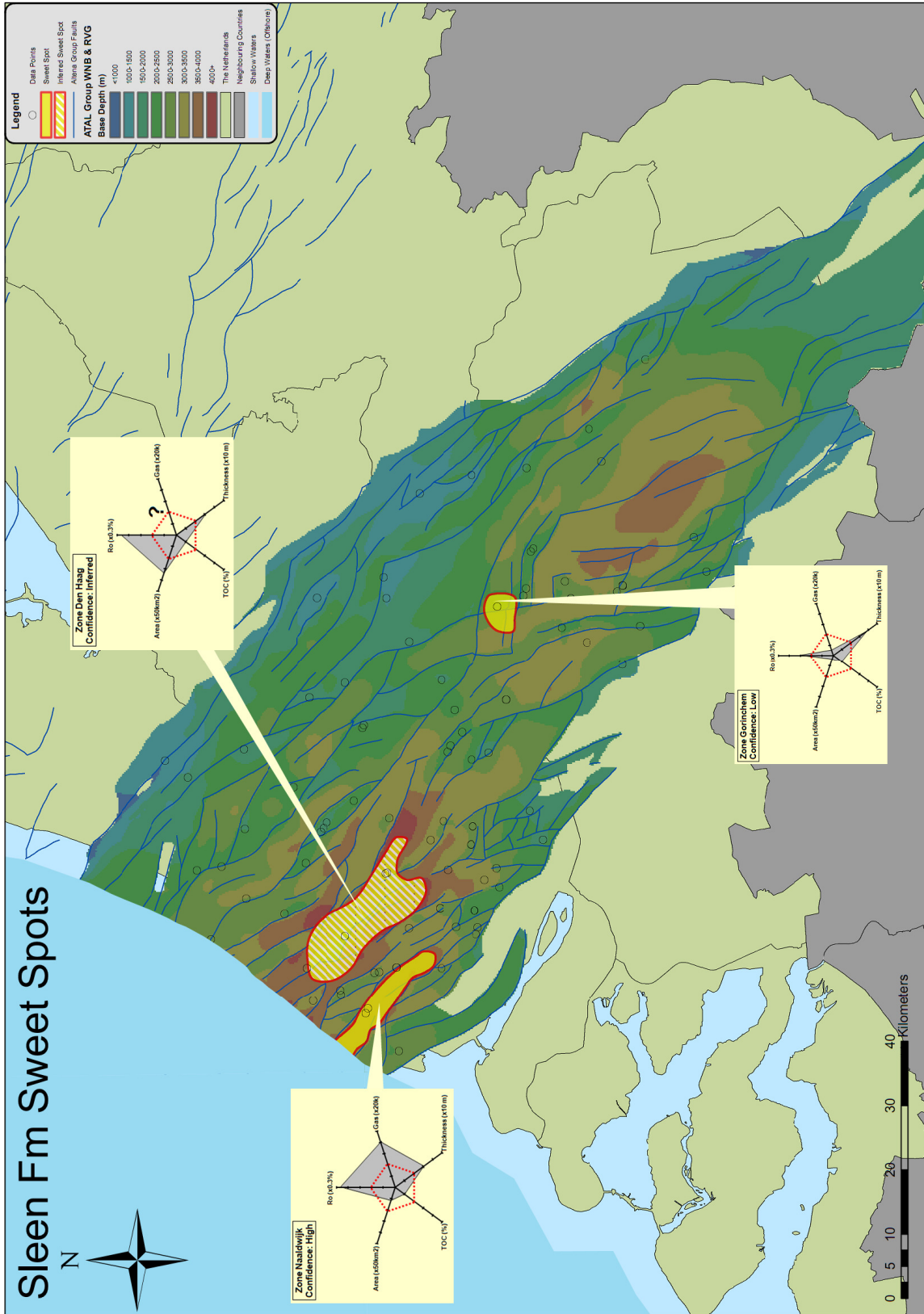


Figure 6.17: Sweet Spot map for the Sleen formation.

6.9 Gas-Initially-In-Place Estimate

Using the equations for free gas (equation 4.6) and adsorbed gas content (equation 3.2), an estimate can be made of the total initial gas content (GIIP) for a specified area.

6.9.1 Free Gas Content and Adsorbed Gas Content

Free Gas Content

To calculate the free gas content of an area for the three specified scenarios, assumptions have to be made with respect to porosity and gas saturation. In addition, the expansion factor of the gas has to be calculated.

The porosity is not measured and is therefore not known. However, using a mass balance calculation and the matrix-densities provided by Fugro for the 95 samples, the porosity can be approximated.

The matrix-density of the shale-samples was found to average around 2757 kg/m³. As reported in section 6.7.2, an average bulk-density of ~2625 kg/m³ was derived from logs. Gas saturations have never been measured for the Jurassic shales and can only be estimated. For the medium case (average) scenario an gas saturation of 50% is assumed. Using a (compressed) gas density of ~200 kg/m³ (at 30 MPa and 90° C) it is found by mass balance of the three components that the porosity is approximately 6%.

The calculated porosity will be used for the medium-case scenario. The best- and worst-case scenarios will use values of 9% and 3%, respectively. Gas saturation varies as well, ranging from 20% (worst case) to 80% (best case).

The last factor is the gas-expansion factor. This factor is calculated by EBN for an average gas found in the West Netherlands Basin, consisting of 89% methane, 6% ethane, 2% propane, 0.6% carbon dioxide, 1.1% nitrogen and 1.3% other constituents. The expansion factor is depth and temperature dependent and is therefore different per sweet spot. The expansion factor is constant for each scenario.

Adsorbed Gas Content

Most of the requirements for calculating adsorbed gas content were already discussed in section 6.7.2. With the Langmuir volume (V_L) and Langmuir Pressure (P_L) determined from the measurement plots and the reservoir pressure calculated assuming hydrostatic equilibrium (with a fluid density of 1.0 g/cm³) all elements are available for the calculation of adsorbed gas content.

In order to present a better overview of properties, table 6.4 presents all properties used in the GIIP calculation and indicates whether or not the property changes with changing scenario.

Table 6.4: Important properties and their value range per scenario.

Property	Scenario-dependent?	Best Case	Medium Case	Worst Case	Units
Bulk-Density	No	2650	2650	2650	kg/m ³
Surface Area	No	Area-Specific	Area-Specific	Area-Specific	m ²
Mean Reservoir Depth	No	Area-Specific	Area-Specific	Area-Specific	m
Gas-Bearing Interval	Yes	Area-Specific; Thickest Interval	Area-Specific; Average Interval	Area-Specific; Thinnest Interval	m
Porosity	Yes	9	6	3	%
Gas Saturation	Yes	80	50	20	%
Expansion Factor	No	Depth/Area Specific	Depth/Area Specific	Depth/Area Specific	-
Langmuir Volume	Yes	8,6	6,9	5,0	scm/m ³
Langmuir Pressure	Yes	2,1	3,7	3,7	MPa

6.9.2 GIIP results

Table 6.5 presents the calculated GIIP per km² and per total sweet spot area for each specific scenario. Additionally, the percentage of the GIIP that is expected to have been adsorbed is given.

As can be seen, the calculated estimates, both per field or per square kilometre, are sometimes quite significant. It must be remembered however that these number have been calculated using many assumptions and are not actual unrisksed gas contents per reservoir. For a more definite answer of extractable gas per region, a consecutive study has to be performed that investigates reservoir properties (such as porosity and gas saturation) as well as producibility (e.g. sensitivity to fracking).

Table 6.5: Overview of calculated GIIP estimated per sweet spot and scenario. BCM stand for billion-cubic-metres; STP for Standard (Surface) pressure & temperature (~1 bar and 15° C)

BEST CASE							
Field Name	Formation	Confidence	GIIP per Sweet Spot (STP) BCM	GIIP per km2 (STP) BCM	Percentage of GIIP Adsorbed %	Surface Area (km2)	(Gas Bearing) Interval (m)
Zone Oud-Beijerland	ATPO	High	71,6	1,0	32,8	75	40
Zone Waalwijk	ATPO	High	355,5	0,7	39,7	475	40
Zone Schiedam	ATPO	Inferred	77,9	1,1	29,2	70	40
Zone Eindhoven	ATPO	Inferred	332,4	1,1	30,0	310	40
Zone Monster	ATAL	High	358,6	4,0	30,2	90	150
Zone Spijkenisse	ATAL	Medium	245,8	2,3	33,3	105	100
Zone Tilburg	ATAL	High	208,6	6,0	33,9	35	260
Zone Delft	ATAL	Inferred	260,8	1,4	29,5	190	50
Zone Oisterwijk	ATAL	Inferred	189,2	1,4	29,8	140	50
Zone Veghel	ATAL	Inferred	6,7	1,3	30,0	5	50
Zone Naaldwijk	ATRT	High	67,1	1,1	29,1	60	40
Zone Gorinchem	ATRT	Low	63,1	1,6	30,4	40	60
Zone Den Haag	ATRT	Inferred	192,3	1,1	28,8	170	40
Total GIIP:			2429,8				

MEDIUM CASE							
Field Name	Formation	Confidence	GIIP per Sweet Spot (STP) BCM	GIIP per km2 (STP) BCM	Percentage of GIIP Adsorbed %	Surface Area (km2)	(Gas Bearing) Interval (m)
Zone Oud-Beijerland	ATPO	High	28,2	0,4	46,7	75	30
Zone Waalwijk	ATPO	High	143,3	0,3	53,2	475	30
Zone Schiedam	ATPO	Inferred	30,3	0,4	43,0	70	30
Zone Eindhoven	ATPO	Inferred	129,5	0,4	43,9	310	30
Zone Monster	ATAL	High	124,3	1,4	44,1	90	100
Zone Spijkenisse	ATAL	Medium	51,7	0,5	47,2	105	40
Zone Tilburg	ATAL	High	59,2	1,7	47,7	35	140
Zone Delft	ATAL	Inferred	108,2	0,6	43,3	190	40
Zone Oisterwijk	ATAL	Inferred	78,6	0,6	43,7	140	40
Zone Veghel	ATAL	Inferred	2,8	0,6	43,9	5	40
Zone Naaldwijk	ATRT	High	26,1	0,4	42,9	60	30
Zone Gorinchem	ATRT	Low	21,9	0,5	44,3	40	40
Zone Den Haag	ATRT	Inferred	74,6	0,4	42,7	170	30
Total GIIP:			878,6				

WORST CASE							
Field Name	Formation	Confidence	GIIP per Sweet Spot (STP) BCM	GIIP per km2 (STP) BCM	Percentage of GIIP Adsorbed %	Surface Area (km2)	(Gas Bearing) Interval (m)
Zone Oud-Beijerland	ATPO	High	8,4	0,1	76,2	75	20
Zone Waalwijk	ATPO	High	46,1	0,1	80,6	475	20
Zone Schiedam	ATPO	Inferred	8,6	0,1	73,4	70	20
Zone Eindhoven	ATPO	Inferred	37,3	0,1	74,0	310	20
Zone Monster	ATAL	High	26,9	0,3	74,2	90	50
Zone Spijkenisse	ATAL	Medium	11,6	0,1	76,5	105	20
Zone Tilburg	ATAL	High	7,7	0,2	76,9	35	40
Zone Delft	ATAL	Inferred	23,2	0,1	73,6	190	20
Zone Oisterwijk	ATAL	Inferred	17,0	0,1	73,9	140	20
Zone Veghel	ATAL	Inferred	0,6	0,1	74,0	5	20
Zone Naaldwijk	ATRT	High	7,4	0,1	73,3	60	20
Zone Gorinchem	ATRT	Low	4,8	0,1	74,4	40	20
Zone Den Haag	ATRT	Inferred	21,2	0,1	73,1	170	20
Total GIIP:			220,8				

Note again that these values are rough estimates of unrisksed gas content. According to Herber & de Jager (2010), a commercial cut-off volume is 0.3 BCM/km² producible gas, assuming 3 wells per square kilometre. According to Gault and Stotts (2007), average shale gas recovery factors in the United States currently range between 10-20%. Whether this means that above-mentioned sweet spots can or cannot be economically produced is beyond the scope of the thesis. The values above are too coarse and too generalised to be used for these kinds of evaluations at this moment. An in-depth study of high-potential sweet spots is recommended.

7. Conclusions

- The properties that are generally used to assess the potential of a shale gas play are not absolutes and indicative at best. Multiple profitable plays exist that do not fit all requirements specified and plays should therefore not be discarded based solely on them.
- Formation thickness is generally good for all three formations although care should be taken along the basin-edge. Thickness appears to be the only real 'show-stopper' for shale-gas potential due to the uncertainty of other attributes.
- TOC is favourable for the Posidonia formation but generally not for Aalburg and Sleen formations, although small enriched intervals in the Aalburg formation occur. Seen from the Lewis shale however, a low TOC content does not necessarily implicate low potential for shale-gas.
- Maturity is generally favourable for gas generation for large parts of the Aalburg and Sleen formations. Maturity of the Posidonia formation is generally low. However, as also seen in other shale-gas plays, immature regions are sometimes observed to have significant gas shows, possibly due to biogenic or catalytic gas generation.
- Gas shows are potentially a good indicator for shale gas potential. Such shows are however found to be extremely difficult to predict. A better insight in the dependence of gas shows of other attributes would increase the usefulness of gas shows.
- The Sleen formation and most of the Aalburg formation do not appear to be black shales. Instead, the organic material has been decomposed during deposition, resulting in predominantly inert carbon contained in these formations. Some intervals of the Aalburg formation and most of the Posidonia formation consist of high potential type I/II kerogen however.
- Clay content is generally high. All formations are marginal at best with respect to clay-mineral classification.
- Based on four mappable attributes, a total of 7 measured and 5 inferred high-potential areas (sweet spots) have been located for the three Jurassic formations.
- The Posidonia formation appears to be the formation with the greatest shale gas potential for the Lower Jurassic, even in immature regions. Especially the area between the cities of Tilburg and Utrecht is of great interest. For the Aalburg and Sleen formation, only an area in the west of the onshore basin, near the towns of de Gaag and Monster, is of particular interest.
- Sorption measurements on Jurassic core samples have led to the first sorption isotherms available for the Dutch substrate. Due to an unaccounted sorption agent however, they cannot be normalised yet.
- An indicative GIIP calculation indicates that some of the areas designated as sweet spots may have significant shale-gas potential. Depending on the scenario and assumptions used, estimated GIIP/km² can range from several million to several billion standard cubic metres per square kilometre.

8. Recommendations

During this study, a lot of new information has surfaced regarding not only the properties and potential of the Lower Jurassic shales, but also with respect to general attribute behaviour. Recommendations for future work in this field of Earth Sciences can therefore be split in two sections.

1. Concerning the Jurassic formations themselves, the Rock-Eval and Qemscan analyses provided new insights. Often, the Lower Altona Group is assumed to be a more or less homogeneous package of black or grey shales. The Qemscan images however suggest a highly heterogeneous lithology with greatly varying TOC contents. A new study into the lithological and (micro)palaeontological variations, and their relation to TOC can provide a better insight in the depositional environment of the Jurassic shales in the Netherlands and how this environment is reflected in present-day TOC content.

A second recommendation for future work on the Jurassic formations comes directly from this thesis' conclusions. Firstly, all the inferred sweet spots should be studied in greater detail to better understand their potential for shale-gas. It may be necessary that appraisal wells are drilled in these regions to collect more data on attributes such as lithology, TOC and gas composition. Secondly, the measured sweet spots will have to be studied for their productive potential, rock-mechanical properties, and the effect of production activities on the environment. EBN has already planned these follow-up studies and is momentarily planning the first follow-up part regarding the production phase of such an endeavour.

Additionally, gas samples of immature source rocks should be taken as to ascertain that the gas is indeed indigenous, or that it has migrated from Carboniferous source rocks.

2. Outside of the Jurassic shale formations, two other studies should be considered as well. The first of these is to investigate the cause for gas show variations in vertical and lateral sense in the West Netherlands Basin and Roer Valley Graben and attempting to find a relation between a set of local attributes and the local gas shows. With such a relation, gas shows could be estimated for unmapped regions, which should greatly improve the level of confidence of potential assessments for inferred sweet spots. A second recommendation concerns the influence of mica or clay-minerals on adsorption isotherms. Not only a cause and correction/normalisation method should be investigated, but also the potential advantage or disadvantage this causes to the potential of shale-gas plays

9. References

Archie, G.E.; 1941; The Electrical Resistivity Log as an Aid in Determining Some Reservoir Characteristics; Petroleum Technology; January Issue; 54-62

Arthur, M.A.; Sageman, B.B.; 1994; Marine black shales: Depositional mechanisms and environments of ancient deposits; Annual Reviews – Earth & Planetary Sciences 22; 499-551

Van Balen, R.T. van; Bergen, F. van; Leeuw, C. de; Pagnier, H.; Simmelink, H.; Wees, J.D. van; Verweij, J.M.; 2000; Modelling the hydrocarbon generation and migration in the West Netherlands Basin, the Netherlands; Netherlands Journal of Geosciences 79; 29-44

Baskin, D.K.; 1997; Atomic H/C Ratio of Kerogen as an estimate of Thermal Maturity and Organic Matter Conversion; AAPG Bulletin 81; no. 9; 1437-1450

Behar, F.; Beaumont, V.; Penteado, H.L. De B.; 2001; Rock-Eval 6 Technology: performances and developments; Oil & Gas Science and Technology 56; no. 2; 111-134

Van Bergen, F.; Zijp, M.; Veld, H.; Verreussel, R.; Nelskamp, R.; 2010; Looking for sweetspots in shale gas, making good use of existing data - the example of the Netherlands; Poster presentation at AAPG Hedberg Research Conference "Critical assessment of shale gas resource plays"; Austin, Texas, U.S.A.

Bowker, K.A.; 2007; Barnett shale gas production, Fort Worth Basin: Issues and discussion; AAPG Bulletin 91; 523-533

Breunese, J.N.; Rispen, F.B.; 1996; Natural gas in the Netherlands: exploration and development in historic and future perspective; IN: Geology of gas and oil under the Netherlands; Rondeel, H.E.; Batjes, D.A.J.; Nieuwenhuijs, H. (editors); Kluwer Academic Publisher; 19-30

Burnham, A.K.; 1989; On the validity of the pristane formation index; Geochimica Cosmochimica Acta 53; 1693-1697

Bustin, R.M.; 2005; Gas shale tapped for big pay; AAPG Bulletin

Campbell, J.H.; Stephens, D.R.; 1976; Kinetic studies of gas evolution during pyrolysis of subbituminous coal; American Chemical Society 21; issue 7; 94-105

Campbell, S.M.; Fairchild, N.R.; Arnold, D.L.; 2000; Liquid CO₂ and sand stimulations in the Lewis Shale, San Juan Basin, New Mexico: A case study; SPE Rocky Mountain Regional Meeting Proceedings

Cobban, W.A.; Landis, E.R.; Dane, C.H.; 1974; Age relations of upper part of Lewis Shale on east side of San Juan basin, New Mexico; New Mexico Geological Society Guidebook; 279-282

Clark-Lowes, D.D.; Kuzemko, N.C.J.; Scott, D.A.; 1987; Structure and Petroleum prospectivity of the Dutch Central Graben and neighbouring platform areas. IN: Petroleum Geology of North West Europe; Brooks, J. & Glennie, K.W. (editors); Graham and Trotman (London); 337-356

Clements, D.M.; Demaison, G.J.; Daly, A.R.; 1979; Well site geochemistry by programmed pyrolysis; Offshore Technological Conference 11th Annual 1979

Curtis, J.B.; 2002; Fractured shale-gas systems; AAPG Bulletin 86, no. 11; 1921-1938

DeMaison, G.F.; Moore, G.T.; 1980; Anoxic environments and source bed genesis; AAPG Bulletin 64; 1179-1209

Dube, H.G.; Christiansen, G.E.; Frantz Jr., J.H.; Fairchild, N.R.; Olszewski, A.J.; Sawyer, W.K.; Williamson, J.R.; 2000; The Lewis Shale, San Juan Basin: What we know now; SPE Annual Technical Conference and Exhibition 1-4; 24p

Duin, E.J.T.; Doornenbal, J.C.; Rijkers, R.H.B.; Verbeek, J.W.; Wong, Th. E.; 2006; Subsurface structure of the Netherlands – results of recent onshore and offshore mapping; Netherlands Journal of Geosciences 85-4; 245-276

Dvorkin, J.; Nur, A.; 1998; Time-average equation revisited; Geophysics 63; 460-464
Erzinger, J.; Wiersberg, T.; Zimmer, M.; 2006; Real-time mud gas logging and sampling during drilling; Geofluids 6; 225-233

Espitalié, J.; Madec, M.; Tissot, B.; Mennig, J.J.; Leplat, P.; 1977; Source rock characterisation method for petroleum exploration; Proceedings of the 9th Offshore Technology Conference 3; 439-444

Espitalié, J.; 1986; Use of Tmax as a maturation index for different types of organic matter – Comparison with vitrinite reflectance; IN: Thermal modelling in sedimentary basins; Jean Burrus (editor); Institut français de pétrole, Centre Nationale de la recherche scientifique (France)

Finch, W.I.; Wright, R.A.; Adler, H.H.; 1982; Age, Sedimentary Environments, and Other Aspects of Sandstone and Related Host Rocks for Uranium Deposits – A Discussion; IAEA Uranium Geology Working Group on Sedimentary Basins and Sandstone-type Uranium Deposits 1978-1982; International Atomic Energy Agency, Vienna

French, D.; Ward, C.R.; Butcher, A.; 2008; QEMSCAN for characterisation of coal and coal utilisation by-products; Australian Coal Association Research Program; <http://www.acarp.com.au>

Gault, B.; Stotts, G.; 2007; Improve shale gas production forecasts; Energy and Petroleum Magazine; <http://www.epmag.com/archives/features/306.htm>

Geluk, M.C.; Duin, E.J.Th.; Duser, M.; Rijkers, R.H.B.; Berg, M.W. van den; Rooijen, P. van; 1994; Stratigraphy and tectonics of the Roer Valley Graben; Geologie en Mijnbouw 73; 129-141

Herber, R.; de Jager, J.; 2010; Oil and Gas in the Netherlands – Is there a future?; Netherlands Journal of Geosciences 89; 119-135

Herngreen, G.F.W.; van Konijnenburg – van Cittert, J.H.A.; Oosterink, H.W.; 2005; New geological data (Middle Triassic, Rhaetian-Liassic and Oligocene) of the Winterswijk quarry, the eastern Netherlands; Netherlands Journal of Geosciences 84; no. 4; 409-413

Herngreen, G.F.W.; Kouwe, W.F.P.; Wong, Th. E.; 2003; The Jurassic of the Netherlands; Geological Survey of Denmark and Greenland Bulletin 1; 217-229

Hickey, J.J.; Henk, B.; 2007; Lithofacies summary of the Mississippian Barnett Shale, Mitchell 2 T.P. Sims well, Wise County; Texas; AAPG Bulletin 91-4; 437-443

Hill, R.J.; Jarvie, D.M.; Zumberge, J.; Henry, M.; Pollastro, R.M.; 2007; Oil and gas geochemistry and petroleum systems of the Fort Worth Basin; AAPG Bulletin 91-4; 445-473

Hill, R.J.; Zhang, E.; Katz, B.J.; Tang, Y.; 2007; Modeling of gas generation from the Barnett Shale, Fort Worth Basin, Texas; AAPG Bulletin 91-4; 501-521

Holditch, S.A.; 2006; Tight Gas Sands; Journal of Petroleum Technology; June Issue

Hood, A.; Gutjahr, C.C.M.; Heacock, R.L.; 1975; Organic Metamorphism and the generation of petroleum; AAPG Bulletin 59-6; 986-996

De Jager, J.; Doyle, M.A.; Grantham, P.J.; Mabillard, J.E.; 1996; Hydrocarbon habitat of the West Netherlands Basin; In: Geology of gas and oil under the Netherlands; Rondeel et al. (editors); 191-209

De Jager, J.; 2003; Inverted basins in the Netherlands, similarities and differences; Netherlands Journal of Geosciences 82-4; 355-366

De Jager, J.; 2007; Geological Development; In: Geology of the Netherlands; Th.E. Wong, D.A.J. Batjes & J. de Jager (editors); Royal Academy of Arts and Sciences; 5-26

De Jager, J.; Geluk, M.C.; 2007; Petroleum Geology; In: Geology of the Netherlands; Th.E. Wong, D.A. J. Batjes & J. de Jager (editors); Royal Academy of Arts and Sciences; 241-264

Jarvie, D.M.; Hill, R.J.; Ruble, T.E.; Pollastro, R.M.; 2007; Unconventional shale-gas systems: The Mississippian Barnett Shale of north-central Texas as one model for thermogenic shale gas assessment; AAPG Bulletin 91; 475-499

Kantsler, A.J.; Smith, G.C.; Cook, A.C.; 1978; Lateral and vertical rank variation – implications for hydrocarbon exploration; Australian Petroleum Production and Exploration Association 18; 143-156

Langmuir, I.; 1918; The adsorption of gases on plane surfaces of glass, mica and platinum; Journal of the American Geochemical Society 40; 1361-1403

Van Leverink, D.J.; Bergen, F. van; 2008; Influence of Early Jurassic tectonics on present day source rock distribution; TNO internal study

Lewis, R.; Ingraham, D.; Percy, M.; Williamson, J.; Sawyer, W.; Frantz, J.; 2004; New Evaluation Techniques for Gas Shale Reservoirs; Schlumberger Reservoir Symposium 2004

Loucks, R.G.; Ruppel, S.C.; 2007; Mississippian Barnett Shale: Lithofacies and depositional setting of a deep-water shale-gas succession in the Fort Worth Basin, Texas; AAPG Bulletin 91, no. 4; 579-601

Lüning, S.; Craig, J.; Loydell, D.K.; Štorch, P.; Fitches, B.; 1999; Lower Silurian 'hot shales' in North Africa and Arabia: regional distribution and depositional model; Earth Sciences Review 49; 121-200

Lyngsie, S.B.; Thybo, H.; Rasmussen, T.M.; 2006; Regional geological and tectonic structures of the North Sea area from potential field modelling; Tectonophysics 413; 147-170

Mango, F.D.; Jarvie, D.M.; 2009; Low-temperature gas from marine shales; Geochemical Transactions 10; issue 3

Martineau, D.F.; 2007; History of the Newark East field and the Barnett shale gas reservoir; AAPG Bulletin 91; 399-403

Michon, L.; Balen, R.T. van; Merle, O.; Pagnier, H.; 2003; The Cenozoic evolution of the Roer Valley Rift System integrated at a European scale; Tectonophysics 367; 101-126

Mohan, R.; Sharma, R.; Baral, J.; 2006; Deep Gas exploration in Cambay Basin, India – A Case Study; 6th International Conference & Exposition of Petroleum Geophysics “Kolkata 2006”

Muntendam-Bos, A.G.; Wassing, B.B.T.; Heege, J.H. ter; Bergen, F. van; Schavemaker, Y.A.; Gessel, S.F.; Jong, M.L.; Nelskamp, S.; Thienen-Visser, K.; Guasti, E.; Belt, F.J.G. van den; Marges, V.C.; Abbink, O.A.; 2009; Inventory non-conventional gas; TNO-NiTG (TNO-034-UT-2009-00774/B); confidential internal report

Murphy, A.E.; Sageman, B.B.; Hollander, D.J.; Lyons, T.W.; Brett, C.E.; 2000; Black shale deposition and faunal overturn in the Devonian Appalachian basin: Clastic starvation, seasonal water-column mixing, and efficient biolimiting nutrient recycling; *Paleoceanography* 15; no. 3 280-291

Muscio, G.P.A.; Horsfield, B.; Welte, D.H.; 1994; Occurrence of thermogenic gas in the immature zone – implications from the Bakken in-source reservoir system; *Advances in Organic Geochemistry* 22; 461-476

Muscio, G.P.A.; Horsfield, B.; 1996; Neoformation of Inert Carbon during the Natural Maturation of a Marine Source Rock: Bakken Shale, Williston Basin; *Energy & Fuels* 10; 10-18

Myers, G.; Nuclear Logging, Chapter 3D, Reservoir Engineering and Petrophysics Volume V; IN: E. Holstein (editor); *Petroleum Engineering Handbook*

Nederlof, M.H.; 1988; The scope for natural gas supplies from unconventional sources; *Annual Reviews of Energy* 13; 95-117

Passey, Q.R.; Creany, S; Kulla, J.B.; Moretti, F.J.; Stroud, J.D.; 1990; A Practical Model for Organic Richness from Porosity and Resistivity Logs; *AAPG Bulletin* 74; no. 12; 1777-1794

Pelet, R.; 1985; Evaluation quantitative des produits formes lors de l'évolution géochimique de la matière organique; *Revue Institut Français de Pétrolé* 40; no. 5; 551-562

Peters, K.E.; Cassa, M.R.; 1994; IN: The petroleum system - from source to trap (Magoon, L.B. & Dow, W.G. (editors); *AAPG Memoir* 60

Peters, K.E.; Walters, C.C.; Moldowan, J.M.; 2006; Biomarkers and isotopes in the environment and human history; IN: *The Biomarkers Guide*; Cambridge University Press; 471

Pienkowski, G.; Schudack, M.E. et al.; 2008; Jurassic; IN: *The Geology of Central Europe – Volume 2: The Mesozoic and Cenozoic*; T. McCan (editor); The Geological Society; 823-923

Pollastro, R.M.; 2007; Total petroleum system assessment of undiscovered resources in the giant Barnett shale continuous (unconventional) gas accumulation, Fort Worth Basin, Texas; *AAPG Bulletin* 91; 551-578

Pollastro, R.M.; Jarvie, D.M.; Hill, R.J.; Adams, C.W.; 2007; Geological framework of the Mississippian Barnett Shale, Barnett-Paleozoic total Petroleum system, Bend arch-Fort Worth Basin, Texas; *AAPG Bulletin* 91-4; 405-436

Rondeel, H.E.; 2001; Hydrocarbon – Tekst voor grondstoffen en het Systeem Aarde; Reader; Vrije Universiteit Amsterdam

Schiffart, S. de; 1983; The electric log markers of the Aalburg Shale (Hettangian-Pliensbachian); Unpublished (NAM Internal Stratigraphical Notes no. 4)

Schroot, B.M.; Schüttenhelm, R.T.E.; 2003; Expressions of shallow gas in the Netherlands North Sea; Netherlands Journal of Geosciences 82; 91-105

Scotese, R.C.; 1998; PALEOMAP Project – Plate tectonic development of the continents and oceans for the last 750 million years;
<http://www.scotese.com/earth.htm> & <http://jan.ucc.nau.edu/~rcb7/1storder.html>

Shtepani, E.; Noll, L.A.; Elrod, L.W.; Jacobs, P.M.; 2010; A new regression-based method for accurate measurement of coal and shale gas content; SPE Reservoir Evaluation & Engineering

Simpson, D.; 2008; Chapter 14 – Coal Bed Methane; IN: Gas well deliquification 2nd edition; J. Lea et al. (editors); Gulf Publishing; 405-422

Sorgenfrei, T.; 1969; Geological Perspectives of the North Sea Area; Bulletin of the Geological Society of Denmark 19; 160-196

Stevens, S.H.; Kuuskraa, 2009; V.A.; Special Report: Gas-Shale – Seven plays dominate North America activity; Oil & Gas Journal 107; issue 36

Watson, N.J.; 2009; Unconventional gas could add 60-250% to global reserves; Petroleum Economist; October Issue

Tissot, B.P.; Welte, D.H.; 1984; Petroleum formation and occurrence; New York Springer-Verlag; 699

Wood, C.J.; Shephard-Thom, E.R.; Harris, C.S.; 1996; Ch. 4: Stratigraphy and regional geology; IN: Engineering Geology of the Channel Tunnel; C.S. Harris, M.B. Hart, P.M. Varley, C.D. Warren (editors); Thomas Telford Services Ltd.

Zdnavičiūte, O.; Lazauskiene, J.; 2009; Organic Matter of Early Silurian succession – the potential source of unconventional gas in the Baltic Basin (Lithuania); BALTICA 22; no. 2; 89-99

Zhao, H.; Givens, N.B.; Curtis, B.; 2007; Thermal maturity of the Barnett Shale determined from well-log analysis; AAPG Bulletin 91; no. 4; 535-549

Appendix A: Analyses Overview & Pyrolysis Results

Sample	Well Name	Formation	Sample Depth (ft/D)	Sorption Measurement	Pyrolysis	Qemscan	TOC	S1 (mg/g)	S2 (mg/g)	S3 (mg/g)	T max	HI	OI	PI	OI CO	TPI
#1	ANDEL-02	ATAL	1687.0	No	Yes	Yes	0.67	0.46	2.25	0.91	435	336	136	0.17	59	0.17
#2	ANDEL-02	ATAL	1688.3	No	Yes	Yes	0.42	0.03	0.15	3.96	487	35	954	0.17	1631	0.18
#3	ASTEN-01	ATAL	1608.0	No	Yes	Yes	0.58	0.30	1.33	0.96	437	229	164	0.18	65	0.19
#4	ASTEN-01	ATAL	1609.0	Yes	Yes	Yes	1.15	0.31	1.33	0.65	437	116	57	0.19	31	0.19
#5	BLESKENGRAAF-02	ATAL	1570.0	No	Yes	Yes	0.61	0.23	1.55	1.29	432	252	210	0.13	27	0.13
#6	BLESKENGRAAF-02	ATAL	1571.5	No	Yes	Yes	0.44	0.14	1.12	1.25	432	254	284	0.11	25	0.11
#7	BLESKENGRAAF-02	ATAL	1573.0	No	Yes	Yes	0.07	0.11	0.31	0.92	418	458	1355	0.26	254	0.26
#8	BLESKENGRAAF-02	ATAL	1574.5	No	Yes	Yes	0.74	0.14	0.9	1.86	433	121	251	0.13	19	0.14
#9	BLESKENGRAAF-02	ATAL	1576.0	No	Yes	Yes	1.12	0.22	1.25	1.46	432	111	131	0.15	19	0.15
#10	BERKEL-02	ATAL	3107.3	No	Yes	Yes	0.19	0.14	0.45	0.48	440	234	255	0.24	20	0.24
#11	BERKEL-02	ATAL	3108.5	No	Yes	Yes	0.83	0.25	1.46	0.39	445	176	47	0.15	14	0.15
#12	BERKEL-02	ATAL	3110.0	No	Yes	Yes	0.87	0.2	1.52	0.59	444	175	67	0.12	20	0.11
#13	BERKEL-02	ATAL	3111.5	No	Yes	Yes	0.54	0.23	0.94	1.19	442	176	223	0.20	59	0.20
#14	BERKEL-02	ATAL	3113.0	No	Yes	Yes	1.07	0.16	1.15	0.3	444	108	28	0.12	7	0.12
#15	BERKEL-02	ATAL	3114.5	No	Yes	Yes	0.53	0.18	0.95	0.44	442	179	82	0.16	23	0.16
#16	BERKEL-02	ATAL	3116.0	No	Yes	Yes	0.50	0.22	1.07	0.48	443	213	95	0.17	16	0.17
#17	DONGEN-01	ATAL	1523.0	No	Yes	Yes	2.09	0.46	5.58	1.67	425	267	80	0.08	20	0.08
#18	DONGEN-01	ATAL	1524.0	No	Yes	Yes	1.19	0.29	1.15	1.38	431	96	116	0.20	15	0.20
#19	DONGEN-01	ATAL	1525.5	No	Yes	Yes	0.67	0.1	0.35	1.37	424	52	206	0.22	37	0.23
#20	DONGEN-01	ATAL	1527.0	No	Yes	Yes	1.32	0.14	0.58	1.27	426	44	96	0.19	20	0.19
#21	DONGEN-01	ATAL	1533.0	No	Yes	Yes	2.02	0.55	4.57	1.5	427	226	74	0.11	18	0.11
#22	DONGEN-01	ATAL	1534.5	No	Yes	Yes	1.21	0.2	1.45	1.17	431	120	96	0.12	16	0.12
#23	DONGEN-01	ATAL	1536.0	No	Yes	Yes	1.38	0.33	1.86	1.45	433	135	105	0.15	21	0.15
#24	DEN HAAG-02	ATAL	2452.5	No	Yes	Yes	1.24	0.2	1.41	0.58	436	114	47	0.12	17	0.12
#25	DEN HAAG-02	ATAL	2453.5	No	Yes	Yes	1.26	0.21	1.73	0.43	438	137	34	0.11	12	0.11
#26	DEN HAAG-02	ATAL	2454.5	No	Yes	Yes	1.33	0.21	1.48	0.82	437	111	61	0.12	9	0.13
#27	DEN HAAG-02	ATAL	2455.5	No	Yes	Yes	1.27	0.22	1.77	0.61	437	139	48	0.11	11	0.11
#28	DEN HAAG-02	ATAL	2456.5	No	Yes	Yes	1.21	0.2	1.16	0.55	435	96	45	0.15	8	0.15
#29	DEN HAAG-02	ATAL	2457.5	No	Yes	Yes	1.24	0.22	1.18	0.61	437	95	49	0.16	13	0.15
#30	DEN HAAG-02	ATAL	2458.5	No	Yes	Yes	1.23	0.22	1.11	0.45	436	91	36	0.17	12	0.17
#31	DEN HAAG-02	ATAL	2609.0	Yes	Yes	Yes	4.38	2.04	21.61	0.92	428	493	21	0.09	8	0.09
#32	DEN HAAG-02	ATAL	2610.0	No	Yes	Yes	5.23	2.26	27.05	1.01	430	518	19	0.08	7	0.08
#33	HAARLEMMERMEER-01	ATAL	1118.5	No	Yes	Yes	0.80	0.18	0.42	0.72	429	52	90	0.30	15	0.30
#34	HAARLEMMERMEER-01	ATAL	1121.5	No	Yes	Yes	1.88	0.88	6.56	0.95	438	349	51	0.12	11	0.12
#35	HAASRECHT-01	ATAL	2087.5	No	Yes	Yes	0.64	0.34	0.8	0.85	442	124	132	0.30	19	0.30
#36	LOON OP ZAND-01	ATAL	2505.0	No	Yes	Yes	12.17	4.51	82.91	2.24	421	681	18	0.05	11	0.05
#37	LOON OP ZAND-01	ATAL	2506.5	No	Yes	Yes	6.68	1.6	35.86	1.37	425	537	20	0.04	9	0.04
#38	LOON OP ZAND-01	ATAL	2508.0	No	Yes	Yes	1.98	1.45	12.56	1.32	432	633	66	0.10	23	0.10
#39	LOON OP ZAND-01	ATAL	2509.5	No	Yes	Yes	0.46	0.37	1.55	2.3	439	339	502	0.19	34	0.19
#40	LOON OP ZAND-01	ATAL	2511.0	No	Yes	Yes	0.45	0.15	0.48	1.45	435	108	321	0.24	32	0.24
#41	LOON OP ZAND-01	ATAL	2512.5	No	Yes	Yes	1.11	0.23	2.22	1.29	437	199	116	0.09	21	0.09
#42	LOON OP ZAND-01	ATAL	2514.0	No	Yes	Yes	1.02	0.28	2.36	0.66	439	232	65	0.11	26	0.11
#43	LOON OP ZAND-01	ATAL	2515.5	No	Yes	Yes	1.06	0.17	1.76	0.64	441	165	60	0.09	13	0.09
#44	LOON OP ZAND-01	ATAL	2517.0	No	Yes	Yes	1.02	0.26	2.31	1.04	438	225	101	0.10	26	0.10
#45	LOON OP ZAND-01	ATAL	2518.5	No	Yes	Yes	1.02	0.24	2.29	0.95	439	224	93	0.09	20	0.09
#46	LOON OP ZAND-01	ATAL	2520.0	No	Yes	Yes	0.85	0.26	1.84	1.32	438	218	156	0.12	29	0.13
#47	LOON OP ZAND-01	ATAL	2522.5	No	Yes	Yes	0.85	0.33	1.93	0.83	438	229	98	0.15	27	0.15
#48	LOON OP ZAND-01	ATAL	2524.0	No	Yes	Yes	0.77	0.24	1.24	0.56	442	160	73	0.16	12	0.16
#49	LOON OP ZAND-01	ATAL	2525.5	No	Yes	Yes	0.79	0.33	1.31	0.67	441	166	84	0.20	23	0.20
#50	LOON OP ZAND-01	ATAL	2530.5	No	Yes	Yes	0.87	0.28	1.36	0.54	440	157	62	0.17	24	0.17
#51	LOON OP ZAND-01	ATAL	2580.0	No	Yes	Yes	0.93	0.09	0.24	0.42	433	26	45	0.27	21	0.27
#52	MOERKAPELLE-04	ATAL	1720.0	No	Yes	Yes	0.74	0.16	1.13	0.66	434	153	90	0.12	13	0.12
#53	MOERKAPELLE-04	ATAL	1721.5	No	Yes	Yes	1.26	0.21	1.93	0.89	435	153	71	0.10	13	0.10
#54	MOERKAPELLE-04	ATAL	1723.0	No	Yes	Yes	1.43	0.28	2.42	0.85	435	169	59	0.10	15	0.10
#55	MOERKAPELLE-04	ATAL	1724.5	No	Yes	Yes	1.29	0.29	2.33	1.08	434	181	84	0.11	19	0.11
#56	RIJSWIJK-01	ATAL	2107.0	No	Yes	Yes	7.65	2.45	54.05	1.31	424	707	17	0.04	10	0.04
#57	RIJSWIJK-01	ATAL	2109.0	No	Yes	Yes	2.22	1.22	14.94	0.69	425	673	31	0.08	9	0.08
#58	RIJSWIJK-01	ATAL	2115.0	No	Yes	Yes	0.81	1.19	2.6	1.77	419	321	219	0.31	347	0.31
#59	RIJSWIJK-01	ATAL	2116.5	No	Yes	Yes	1.24	0.28	3.01	0.83	334	243	67	0.09	26	0.09
#60	RIJSWIJK-01	ATAL	2118.0	No	Yes	Yes	1.16	0.24	2.88	0.78	439	248	67	0.08	37	0.08
#61	RIJSWIJK-01	ATAL	2119.5	No	Yes	Yes	1.15	0.3	2.16	0.95	437	188	83	0.12	29	0.12
#62	RIJSWIJK-01	ATAL	2121.0	No	Yes	Yes	0.97	0.2	1.64	1.5	438	169	155	0.11	26	0.11
#63	RIJSWIJK-01	ATAL	2123.0	No	Yes	Yes	0.53	0.2	0.7	3.15	432	132	594	0.22	353	0.22
#64	SPIJKENISSE-01	ATAL	2234.0	No	Yes	Yes	1.06	0.36	1.87	1.05	433	176	99	0.16	23	0.16
#65	SPIJKENISSE-01	ATAL	2235.5	No	Yes	Yes	0.31	0.11	0.4	0.91	432	129	294	0.22	45	0.22
#66	SPIJKENISSE-01	ATAL	2236.5	No	Yes	Yes	0.63	0.08	0.56	0.39	430	89	62	0.13	34	0.12
#67	WASSENAAR-23	ATAL	2032.0	No	Yes	Yes	0.86	0.08	0.95	0.41	436	110	48	0.08	23	0.08
#68	WASSENAAR-23	ATAL	2087.0	No	Yes	Yes	0.79	0.56	0.85	1.93	429	108	244	0.40	87	0.40
#69	WASSENAAR-23	ATAL	2088.5	No	Yes	Yes	1.31	0.17	2.8	0.57	437	214	44	0.06	61	20.00
#70	WASSENAAR-23	ATAL	2090.0	No	Yes	Yes	0.89	0.09	0.96	0.61	435	108	69	0.09	29	0.09
#71	WASSENAAR-23	ATAL	2091.5	No	Yes	Yes	0.95	0.1	1.21	0.74	437	127	78	0.08	37	0.08
#72	DEN HAAG-02	ATRT	2656.0	No	Yes	Yes	0.38	0.03	0.12	0.51	413	32	134	0.20	23	0.18
#73	DEN HAAG-02	ATRT	2657.0	No	Yes	Yes	0.37	0.02	0.1	0.45	442	27	122	0.17	77	0.16
#74	DEN HAAG-02	ATRT	2658.0	Yes	Yes	Yes	0.45	0.04	0.17	0.70	443	38	156	0.19	74	0.20
#75	DEN HAAG-02	ATRT	2659.0	No	Yes	Yes	0.40	0.03	0.17	0.19	437	43	48	0.15	84	0.17
#76	DEN HAAG-02	ATRT	2660.0	No	Yes	Yes	0.39	0.03	0.14	0.38	439	36	97	0.18	48	0.16
#78	WINTERSWIJK-01	Geverik	4235.0	No	Yes	Yes	4.72	0.1	0.11	0.61	345	2	13	0.48	1	0.46
#79	WINTERSWIJK-01	Geverik	4236.0	No	Yes	Yes	4.78	0.08	0.07	0.53	345	1	11	0.53	1	0.55
#80	WINTERSWIJK-01	Geverik	4237.0	No	Yes	Yes	5.13	0.14	0.15	0.56	312	3	11	0.48	1	0.47
#81	WINTERSWIJK-01	Geverik	4238.0	Yes	Yes	Yes	7.47	0.18	0.11	0.58	325	1	8	0.62	1	0.62
#82	WINTERSWIJK-01	Geverik	4239.0	No	Yes	Yes	6.10	0.08	0.08	0.42	348	1	7	0.50	1	0.50
#83	WINTERSWIJK-01	Geverik	4240.0	No	Yes	Yes	4.26	0.19	0.2	0.64	382	5	15	0.49	5	0.49
#84	WINTERSWIJK-01	Geverik	4241.0	No	Yes	Yes	5.30	0.21	0.2	0.46	315	4	9	0.51	2	0.52
#85	LOON OP ZAND-01	ATPO	2483.0	No	Yes	Yes	6.94	2.1	46.8	1.74	427	674	25	0.04	11	0.04
#86	LOON OP ZAND-01	ATPO	2491.0	Yes	Yes	Yes	7.91	4.4	54.1	1.52	426	684	19	0.08	8	0.08
#87	LOON OP ZAND-01	ATPO	2499.0	No	Yes	Yes	8.87	3.27								

Appendix B: Modelled Maturities

WELLNAME	ATPO Depth	ATPO Maturity	ATPO Tmax	ATPO LOM	ATAL Maturity	ATAL Tmax	ATAL LOM	ATRT Maturity	ATRT Tmax	ATRT LOM	Geothermal flux
ANDEL-02	1629.5	0.60	73	8.3	0.61	74	8.4				0.03
ANDEL-02	1703.5	0.60	73	8.3	0.62	76	8.5				0.03
ANDEL-06	1996.25	0.60	73	8.3	0.68	82	9.0	0.76	91	9.7	0.03
AARLANDERVEEN-01	1453	0.62	75	8.5	0.66	80	8.9	0.70	84	9.2	0.03
ASTEN-01	1575							0.27	13	3.4	0.03
BOEIKOP-01	848	0.67	81	9.0	0.72	86	9.4				0.03
BROEKZIJDE-01	1870.5	0.56	68	7.9	0.59	72	8.2	0.62	76	8.6	0.03
BLESKENSGRAAF-01	1490	0.70	84	9.2	0.74	89	9.5				0.03
BLESKENSGRAAF-02		0.81	95	10.0							0.03
BRAKEL-01	1828	0.79	93	9.8	0.85	98	10.2	0.91	104	10.5	0.03
BERKEL-01-S1	2985	1.51	141	12.1							0.03
BERKEL-02	3070	1.31	131	11.7	1.41	136	11.9				0.03
BARENDRECHT-01	2407	0.69	83	9.1	0.77	91	9.7				0.03
BARENDRECHT-02-S1		0.69	83	9.1							0.03
BARENDRECHT-02-S2		0.69	83	9.1							0.03
BARENDRECHT ZIEDEWIJ-01	2265	0.64	78	8.7	0.68	82	9.0	0.72	87	9.4	0.03
BARENDRECHT ZIEDEWIJ-02-S2		0.64	78	8.7							0.03
BARENDRECHT ZIEDEWIJ-02-S3		0.64	78	8.7							0.03
BARENDRECHT ZIEDEWIJ-04	2187	0.64	78	8.7	0.68	83	9.1	0.73	87	9.4	0.03
BOSKOOP-01	1423.5	0.72	86	9.4	0.80	94	9.9				0.03
BOTLEK-01	2360	0.62	76	8.6	0.64	78	8.7	0.66	80	8.9	0.03
BUURMALSEN-01	882	0.55	67	7.8	0.58	71	8.2	0.62	75	8.5	0.03
CAPELLE-01	2457	1.23	126	11.5	1.36	133	11.8	1.50	140	12.1	0.03
DONGEN-01	1468	0.42	47	6.1	0.45	52	6.5				0.03
DORDRECHT-01	3103	0.51	61	7.3	0.58	70	8.1	0.66	80	8.9	0.03
EVERDINGEN-01	999	0.79	94	9.9	0.81	95	10.0	0.82	96	10.0	0.03
GAAG-01	2929.05	0.94	106	10.6	0.98	109	10.8	1.03	113	11.0	0.03
GAAG-02-S1		0.94	106	10.6							0.03
GAAG-03	3310	0.94	106	10.6	0.97	108	10.7	1.00	111	10.9	0.03
GAAG-04	3570	0.94	106	10.6	1.01	111	10.9	1.10	118	11.2	0.03
GAAG-05	3299	0.94	106	10.6	1.07	115	11.1	1.22	125	11.5	0.03
GEWANDE-01	1599	0.62	76	8.5	0.64	78	8.7	0.66	80	8.9	0.03
GEWANDE-01	1865	0.62	76	8.5	0.66	80	8.9				0.03
GEWANDE-01-S1		0.62	76	8.5							0.03
GEWANDE-01-S1		0.62	76	8.5							0.03
DEN HAAG-02	2350	1.13	120	11.3	1.21	124	11.5	1.28	129	11.6	0.03
HUIBEVEN-01	1828	0.50	59	7.2	0.50	60	7.2	0.51	61	7.3	0.03
HAARLEMMERMEER-01	1043	0.68	82	9.1	0.73	87	9.4				0.03
HERPT-01	1747	0.78	93	9.8							0.03
HAASTRECHT-01	1411	0.63	76	8.6	0.73	88	9.5	0.86	99	10.2	0.03
HAASTRECHT-02	1354.5	0.63	76	8.6	0.71	85	9.3	0.80	94	9.9	0.03
HAASTRECHT-02-S1	1416	0.63	76	8.6	0.67	81	8.9	0.71	86	9.3	0.03
HEESWIJK-01	1976	0.45	52	6.5	0.48	56	6.9	0.51	60	7.3	0.03
HILVARENBEEK-01	1744.5	0.52	63	7.5	0.56	68	7.9	0.60	73	8.4	0.03
IJSSELMONDE-64	2613	0.90	102	10.4	0.96	107	10.7				0.03
IJSSELMONDE-64-S1	2835	0.90	102	10.4	0.96	108	10.7				0.03
IJSSELMONDE-64-S2	2850	0.90	102	10.4	1.01	111	10.9	1.12	119	11.3	0.03
JUTPHAAS-01	900	0.55	67	7.8	0.57	69	8.0	0.59	72	8.2	0.03
KELDONK-01	1605	0.64	78	8.7	0.66	80	8.9	0.68	82	9.0	0.03
KIJKDUIN-ZEE-02-S1	2629.25	1.05	114	11.0	1.14	120	11.3	1.25	127	11.6	0.03
KERKWIJK-01	1807	0.53	63	7.5	0.58	70	8.1	0.63	77	8.6	0.03
DE LIER-02-S1		0.82	96	10.0							0.03
DE LIER-45	2535	0.82	96	10.0	0.88	101	10.4	0.94	106	10.6	0.03
LOON OP ZAND-01	2484.5	0.58	71	8.1	0.60	72	8.3	0.73	87	9.4	0.03
LOON OP ZAND-01	2484.5	0.58	71	8.1	0.66	80	8.9	0.73	87	9.4	0.03
MOERKAPELLE-01	1162.5	0.71	85	9.3	0.73	87	9.4				0.03
MOERKAPELLE-01	1280	0.71	85	9.3	0.76	90	9.6				0.03
MOERKAPELLE-04	1675.75	0.89	102	10.4	0.94	106	10.6				0.03
MOERKAPELLE-04	1682.25	0.89	102	10.4	0.94	106	10.6				0.03
MOERKAPELLE-10	1201.5	0.71	85	9.3	0.76	90	9.7				0.03
MOERKAPELLE-14	1223.5	0.67	81	9.0	0.77	91	9.7	0.90	102	10.4	0.03
MOLENAARSGRAAF-02-S2	1808.5	0.68	82	9.1	0.78	92	9.8	0.90	103	10.4	0.03
MONSTER-02	2241	0.87	100	10.3	0.95	107	10.7	1.03	113	11.0	0.03
MONSTER-02-S1		0.87	100	10.3							0.03

WELLNAME	ATPO Depth	ATPO Maturity	ATPO Tmax	ATPO LOM	ATAL Maturity	ATAL Tmax	ATAL LOM	ATRT Maturity	ATRT Tmax	ATRT LOM	Geothermal flux
MONSTER-03	2332	0.72	86	9.3	0.78	92	9.8	0.85	99	10.2	0.03
MEERKERK-01	1355.75	0.68	82	9.0	0.74	88	9.5	0.81	95	10.0	0.03
MAASGEUL-01	3173	0.72	86	9.3	0.78	92	9.8	0.85	98	10.2	0.03
MAASGEUL-02	3210	0.72	86	9.3	0.81	95	10.0	0.91	104	10.5	0.03
MAASVLAKTE-01	2445	0.62	75	8.5	0.63	77	8.6	0.64	78	8.8	0.03
MAASVLAKTE-01-S1		0.62	75	8.5							0.03
MAASVLAKTE-01-S2		0.62	75	8.5							0.03
NEDERWEERT-01	1588							0.23	1	2.5	0.03
NOORDWIJK-02	1440	0.78	92	9.8	0.81	95	10.0	1.09	117	11.1	0.03
NOORDWIJK-02	1971	0.78	92	9.8	0.83	97	10.1	0.88	101	10.3	0.03
OUD ALBLAS-01	1341	0.60	73	8.4	0.68	82	9.0	0.76	90	9.6	0.03
OUD BEYERLAND-01	2648.75	0.74	89	9.5	0.79	93	9.9				0.03
OUD BEIJERLAND ZUID-01	2005	0.56	68	7.9	0.58	70	8.1	0.59	72	8.2	0.03
OEGSTGEEST-01	1921	0.82	96	10.0	0.88	101	10.3				0.03
OTTOLAND-01	1724.5	0.65	79	8.8	0.73	87	9.4	0.81	95	10.0	0.03
OTTOLAND-01-S1	1727	0.65	79	8.8	0.73	87	9.4	0.82	96	10.1	0.03
PAPEKOP-01	1339.25	0.70	85	9.2	0.77	91	9.7	0.85	98	10.2	0.03
PERNIS WEST-01	2623	0.76	90	9.7	0.80	94	9.9	0.84	97	10.1	0.03
PERNIS WEST-02-S1 (HOR)		0.76	90	9.7							0.03
PERNIS WEST-03-S2		0.76	90	9.7							0.03
PERNIS WEST-04	2734	0.76	90	9.7	0.79	93	9.8	0.81	95	10.0	0.03
PERNIS WEST-05	2539	0.76	90	9.7	0.80	94	9.9	0.85	98	10.2	0.03
REEDIJK-01	2401	0.67	81	8.9	0.70	84	9.2	0.73	87	9.4	0.03
RIDDERKERK-32-S-3	2629	0.80	94	9.9	0.88	101	10.3	0.96	108	10.7	0.03
ROTTERDAM SCHULPWEG-01	2659	0.98	109	10.8	1.05	114	11.0	1.11	119	11.2	0.03
RIJSWIJK-01	2094.25	0.99	110	10.8	1.09	117	11.1	1.19	123	11.4	0.03
ROZENBURG-01	2631	0.65	79	8.8	0.68	82	9.1	0.71	86	9.3	0.03
S-GRAVENZANDE-01-S1		0.96	108	10.7							0.03
S-GRAVENZANDE-03-S1		0.96	108	10.7							0.03
'S-GRAVENZANDE-04	5534	0.96	108	10.7	1.20	124	11.4	1.50	140	12.1	0.03
SINT-MICHELSENGESTEL-01	2028.5	0.49	58	7.1	0.57	69	8.0	0.66	80	8.9	0.03
SPRANG CAPELLE-01	2267	0.63	77	8.7	0.65	78	8.8	0.66	80	8.9	0.03
SPRANG-01	2649.25	0.85	98	10.2	0.86	99	10.3				0.03
SPRANG-01-S2		0.85	98	10.2							0.03
SPIJKENISSE-01	2128	0.63	77	8.7	0.69	83	9.1	0.74	89	9.5	0.03
SPIJKENISSE OOST-01	2359	0.62	76	8.5	0.67	81	8.9				0.03
SPIJKENISSE OOST-01-S1		0.62	76	8.5							0.03
SPIJKENISSE OOST-02	2873	0.62	76	8.5	0.65	79	8.8	0.68	82	9.1	0.03
SPIJKENISSE OOST-02-S1		0.62	76	8.5							0.03
SPIJKENISSE WEST-01	2364.75	0.62	76	8.6	0.67	81	9.0	0.71	85	9.3	0.03
SCHIPHOL-01	677	0.62	76	8.5	0.75	89	9.6	0.90	103	10.5	0.03
SCHIPHOL-01-S1		0.62	76	8.5							0.03
STRIJEN-01	1748	0.45	52	6.5	0.45	52	6.6	0.46	53	6.6	0.03
STRIJEN WEST-01	2063	0.46	53	6.7	0.48	57	7.0	0.51	61	7.3	0.03
VALKENBURG-01	2130	0.88	102	10.4	0.96	108	10.7	1.04	114	11.0	0.03
VLAARDINGEN NOORD-01-S1		0.82	96	10.0							0.03
VARIK-01	1007	0.59	72	8.2	0.61	74	8.4	0.63	77	8.6	0.03
WIJK-AALBURG-01	1636	0.60	73	8.3	0.72	86	9.3	0.85	99	10.2	0.03
WIJK-AALBURG-01-S1		0.60	73	8.3							0.03
WASPIK-01	2537	0.84	97	10.1	0.89	102	10.4				0.03
WASSENAAR-23	1995.5	1.20	124	11.5	1.29	129	11.6				0.03
WASSENAAR-23-S2		1.20	124	11.5							0.03
WASSENAAR-ZEE-01	2141	0.89	102	10.4	0.95	107	10.7				0.03
WERKENDAM-01	2216.5	0.75	89	9.6	0.80	94	9.9				0.03
WERKENDAM-02	2216.5	0.75	89	9.6	0.85	98	10.2	0.96	107	10.7	0.03
WERKENDAM-03	2276.75	0.75	89	9.6	0.81	95	10.0	0.88	101	10.3	0.03
WIJNGAARDEN-01		0.69	83	9.1							0.03
WILLESKOP-01	1085.5	0.56	68	7.9	0.64	78	8.8	0.74	88	9.5	0.03
WOUBRUGGE-01	1290.5	0.63	77	8.6	0.65	79	8.8				0.03
WOUBRUGGE-01-S1		0.63	77	8.6							0.03
WAALWIJK-01	2688.5	0.61	74	8.4	0.69	83	9.2	0.78	93	9.8	0.03
WAALWIJK NOORD-01-S2		0.78	93	9.8							0.03
WAALWIJK NOORD-02-S4	2918	0.78	93	9.8	0.86	99	10.2	0.94	106	10.6	0.03
WAALWIJK-NOORD-03	2455.25	0.78	93	9.8	0.91	104	10.5	1.07	115	11.1	0.03
WAALWIJK SOUTH-01-S1	2600.5	0.65	79	8.8	0.71	85	9.3	0.76	91	9.7	0.03
WAALWIJK SOUTH-02	3664	0.65	79	8.8	0.74	88	9.5				0.03
ZOETERMEER-02	1682	0.69	83	9.1							0.03

Appendix C: Modelled TOC levels

Well Code	ATPO TOC Average	ATPO st. Deviation	Upper ATAL TOC Average	Upper ATAL st. Deviation	Lower ATAL TOC Average	Lower ATAL st. Deviation	ATRT TOC Average	ATRT st. Deviation
ARV-01	1.50	1.14	0.73	0.55	0.54	0.96	0.14	0.32
BRT-01			0.97	0.36				
BSKP-01	5.84	1.11	0.96	0.51	0.57	0.47	0.30	0.28
BUM-01			2.14	1.55	0.57	0.61		
DON-01			3.39	4.28				
EVD-01	2.27	1.94			0.86	0.86	1.29	0.72
GAG-01			1.16	0.19	1.53	0.15	1.57	0.59
GAG-05			0.95	0.30	1.41	0.55	0.60	0.20
HST-02	6.81	1.61	0.44	0.64				
HSW-01	1.57	1.15	0.86	5.06	3.37	9.04	1.15	1.76
HVB-01	9.13	1.86	0.84	0.84	1.83	1.37	1.12	0.72
JUT-01	3.65	1.64	0.70	0.99	0.82	1.00	1.00	1.37
KDZ-02-S1	1.16	0.57	0.90	0.26	0.95	0.38	0.78	0.48
KWK-01			1.51	0.80	2.36	1.24	2.00	1.32
LIR-45	1.95	1.34	0.81	0.23	1.04	0.57	0.62	0.69
MKP-14	3.43	1.02	0.99	0.78	0.90	0.96		
MOL-02-S2	5.74	1.15	1.15	1.26	1.62	2.31		
MON-02			1.66	2.24	0.81	0.29		
MON-02-S1	2.22	1.00	0.78	0.77	0.91	0.38		
MRK-01	7.32	1.36	1.52	0.87	0.97	0.43	0.87	0.50
MSG-01			1.37	0.83				
MSV-01					1.28	0.95	0.63	0.44
MSV-01-S2					0.84	0.94	0.95	2.33
NWK-02			1.17	0.16	0.95	0.30	0.96	0.27
OTL-01	4.89	2.02						
PKP-01	12.90	9.35	1.38	1.55	0.77	0.52	1.36	2.12
PRW-01	2.74	3.44	1.20	0.67	1.93	0.72	1.23	0.55
RZB-01	4.21	2.18	1.16	0.67	1.68	0.96	1.19	0.93
SPG-01-S2	5.34	3.63	1.52	0.44	1.70	0.61	1.12	0.30
SPKO-01-S1			0.95	0.52	1.59	0.85	1.03	0.48
STW-01			0.60	0.85			0.48	0.75
WAA-01	7.65	1.57	1.30	0.55	0.84	0.63	0.30	0.34
WED-02	5.38	0.90	1.19	0.58	1.37	0.64	1.14	0.80
WED-03	5.24	0.89	0.94	0.61	1.08	0.30	0.64	0.24
WLK-01	11.36	1.57	2.97	1.04	1.64	0.74	1.09	0.75
WOB-01	8.38	2.95	1.96	2.26				
WOB-01-S1	3.10	1.06	1.24	0.64	0.63	0.40	0.84	0.49
WWN-01-S2			0.90	0.22				
WWN-03	4.02	1.08	0.75	0.22				
Averages	5.11	1.90	1.23	0.98	1.25	1.00	0.94	0.76

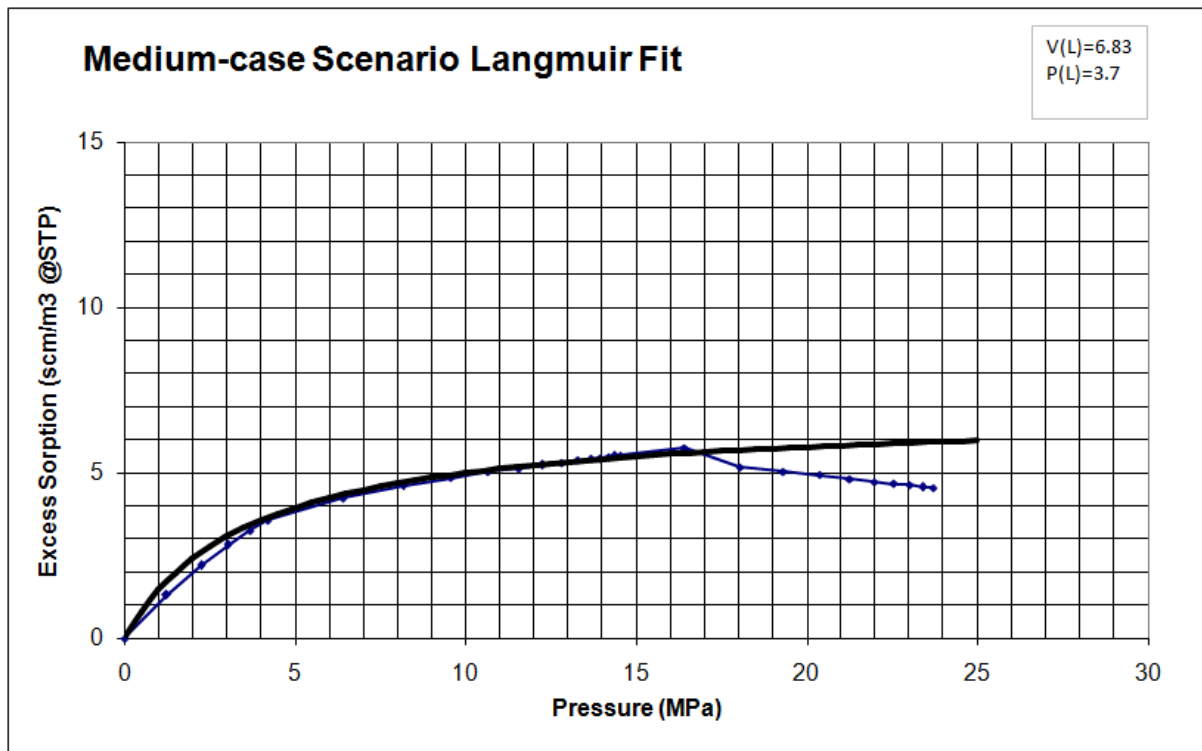
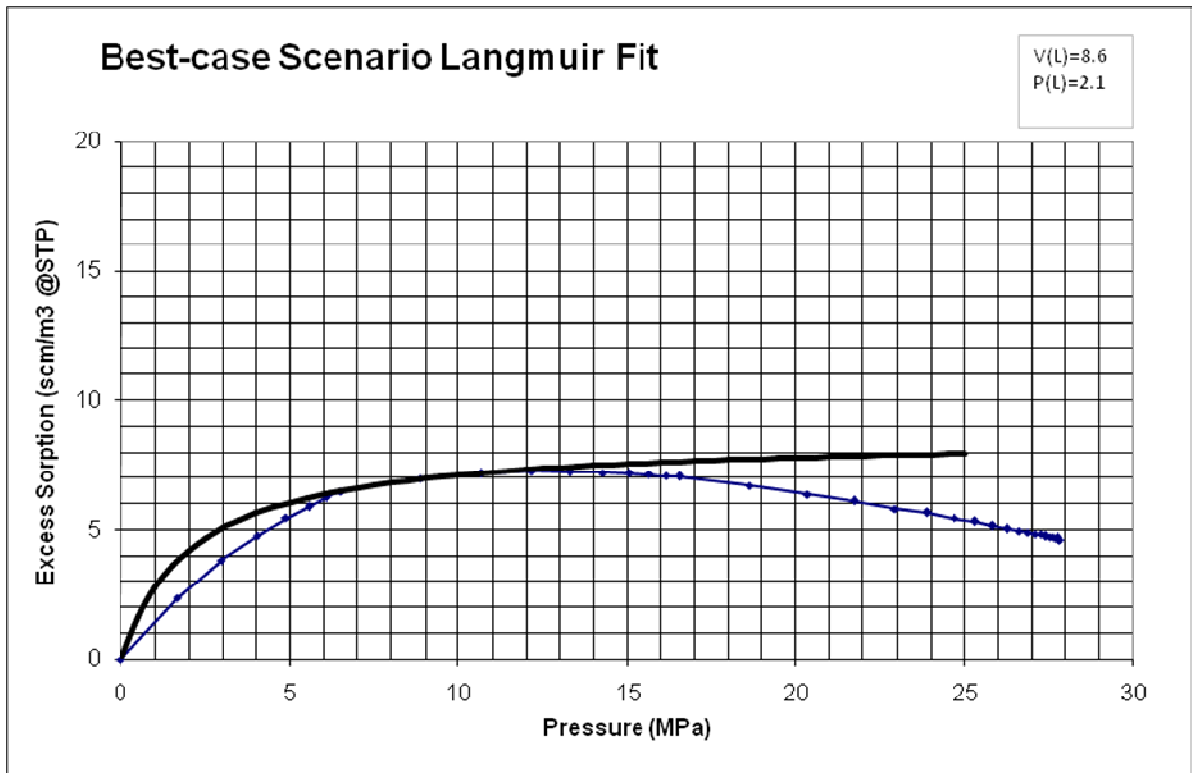
Appendix D: Bulk Mineralogy

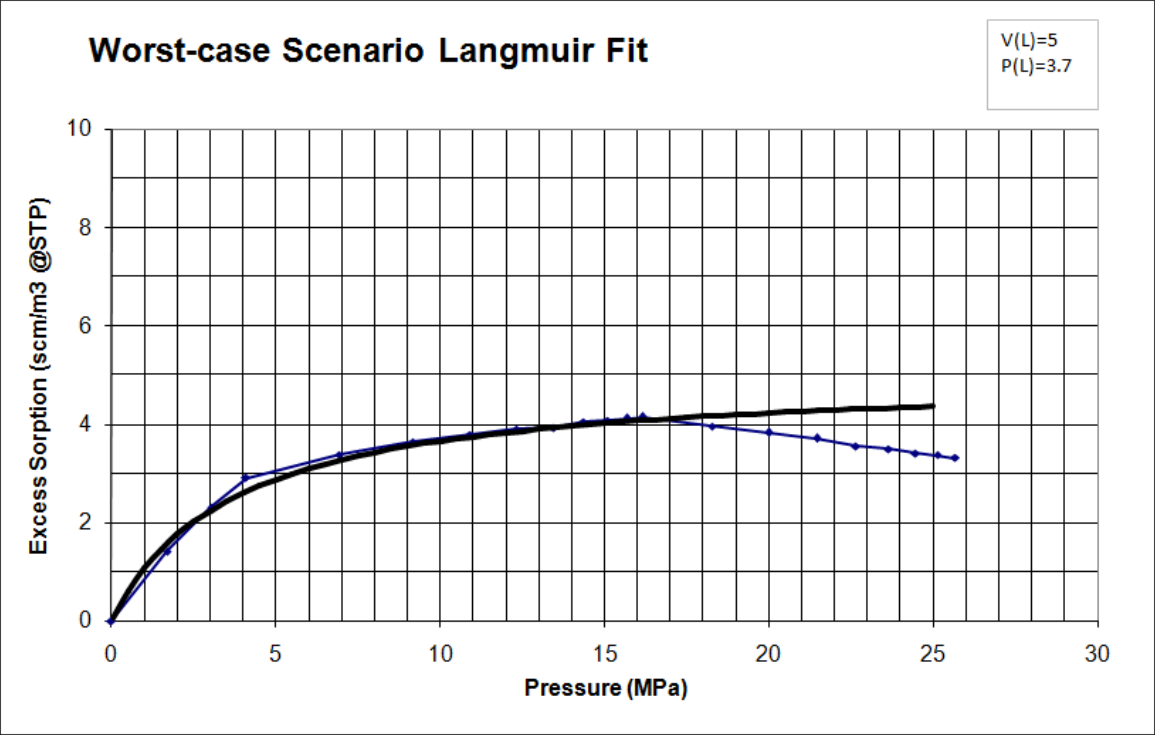
Sample	Well Name	Fm	Sample Depth (MD)	Quartz	Chlorite	Bitite/Phlogopite	K-Feldspar	Plagioclase Feldspar (undiff)	Muscovite	Glauconite	Smeectite	Kaolinite	Pyrite	Dolomite	Calcite	CaFeCO ₃ /Ankerite	Siderite	Heavy Minerals	Ca-SO ₄ /Anhydrite/Gypsum	Berite	Others/Contaminants
#1	ANDEL-02	ATAL	1687.0	18.12	5.92	0.11	1.78	2.55	42.81	0.22	2.23	21.24	0.18	0.53	1.42	0.62	0.20	1.53	0.04	0.00	0.49
#2	ANDEL-02	ATAL	1688.3	2.25	1.45	0.02	0.21	0.14	3.15	2.76	0.10	9.72	0.22	0.02	0.04	4.24	70.30	4.73	0.00	0.00	0.65
#3	ASTEN-01	ATAL	1608.0	1.12	8.11	0.02	0.01	0.03	1.43	4.63	0.21	33.95	0.27	0.01	0.08	7.32	34.28	7.79	0.00	0.00	0.73
#4	ASTEN-01	ATAL	1609.0	14.72	4.49	0.33	1.23	3.59	47.84	0.70	9.28	14.54	0.11	0.13	1.04	0.13	0.01	1.82	0.00	0.00	0.03
#5	BLESKENGRAAF-02	ATAL	1570.0	9.15	6.06	0.06	0.62	1.51	49.17	0.14	0.82	26.98	0.52	0.30	2.87	0.32	0.09	1.29	0.03	0.00	0.07
#6	BLESKENGRAAF-02	ATAL	1571.5	15.14	3.11	0.08	1.58	1.51	46.78	0.28	1.78	18.34	0.54	1.10	5.89	1.60	0.35	1.74	0.02	0.00	0.16
#7	BLESKENGRAAF-02	ATAL	1573.0	12.10	3.61	0.06	1.08	1.68	47.05	0.11	0.85	25.67	0.73	0.73	4.24	0.53	0.13	1.27	0.08	0.00	0.10
#8	BLESKENGRAAF-02	ATAL	1574.5	4.59	11.24	0.05	0.27	0.78	11.24	1.67	1.05	26.45	0.26	0.22	20.87	5.29	6.16	7.75	0.02	0.25	1.86
#9	BLESKENGRAAF-02	ATAL	1576.0	8.96	4.18	0.06	0.75	1.31	50.59	0.10	0.94	25.65	0.93	0.36	4.12	0.32	0.12	1.31	0.11	0.00	0.18
#10	BERKEL-02	ATAL	3107.3	33.25	1.33	0.03	0.14	5.34	6.39	0.04	0.48	7.00	0.34	0.59	39.61	3.26	0.05	1.76	0.05	0.00	0.33
#11	BERKEL-02	ATAL	3108.5	23.38	3.84	0.26	0.82	3.76	43.93	0.22	2.91	16.16	0.58	0.19	1.65	0.37	0.01	1.86	0.00	0.00	0.05
#12	BERKEL-02	ATAL	3110.0	18.17	3.46	0.19	0.71	2.80	50.19	0.17	3.37	17.06	0.70	0.26	1.07	0.33	0.01	1.43	0.02	0.00	0.07
#13	BERKEL-02	ATAL	3111.5	18.47	9.43	0.40	0.29	2.13	26.18	1.86	7.21	19.73	0.39	0.15	0.80	1.40	2.32	8.31	0.01	0.00	0.94
#14	BERKEL-02	ATAL	3113.0	30.09	6.45	0.33	0.87	5.80	30.91	0.31	2.33	16.82	0.52	0.31	1.97	0.97	0.03	2.05	0.04	0.00	0.18
#15	BERKEL-02	ATAL	3114.5	31.18	6.63	0.32	0.84	6.15	30.89	0.32	2.53	15.61	0.51	0.22	1.75	0.74	0.04	2.04	0.04	0.00	0.18
#16	BERKEL-02	ATAL	3116.0	37.67	2.82	0.14	0.50	7.62	21.28	0.23	3.09	18.58	0.41	0.21	3.20	1.24	0.05	2.73	0.01	0.00	0.20
#17	DONGEN-01	ATAL	1523.0	17.08	1.65	0.01	1.82	1.24	38.63	0.13	1.80	16.64	1.23	1.95	12.81	2.11	0.23	2.08	0.17	0.00	0.43
#18	DONGEN-01	ATAL	1524.0	15.73	1.27	0.01	1.13	1.93	41.49	0.09	0.94	18.34	1.52	2.35	10.88	1.72	0.11	1.94	0.01	0.00	0.55
#19	DONGEN-01	ATAL	1525.5	16.16	1.36	0.01	1.11	2.12	43.10	0.12	1.31	15.66	0.36	1.04	12.43	1.52	0.06	2.82	0.01	0.00	0.80
#20	DONGEN-01	ATAL	1527.0	14.79	1.53	0.02	1.84	0.90	44.51	0.26	1.49	14.50	0.57	1.53	12.39	2.05	0.35	2.50	0.08	0.00	0.68
#21	DONGEN-01	ATAL	1533.0	19.65	1.44	0.01	1.00	1.21	36.93	0.14	1.90	20.14	0.71	1.80	10.38	1.34	0.04	2.54	0.20	0.00	0.57
#22	DONGEN-01	ATAL	1534.5	17.20	1.54	0.01	1.20	1.19	39.15	0.14	1.00	17.62	0.73	3.11	11.21	2.01	0.08	2.74	0.03	0.28	0.76
#23	DONGEN-01	ATAL	1536.0	18.26	1.04	0.02	2.16	0.77	42.34	0.27	1.49	14.07	0.85	2.51	10.75	2.18	0.23	2.60	0.00	0.00	0.46
#24	DEN HAAG-02	ATAL	2452.5	21.96	1.58	0.14	1.68	1.98	38.51	0.30	4.51	11.33	0.91	1.64	11.36	1.43	0.07	2.41	0.03	0.00	0.15
#25	DEN HAAG-02	ATAL	2453.5	24.52	0.82	0.15	1.79	2.01	35.18	0.35	5.68	9.88	1.66	1.61	12.30	1.45	0.05	2.38	0.01	0.00	0.15
#26	DEN HAAG-02	ATAL	2454.5	23.97	0.90	0.16	1.86	2.04	34.81	0.33	5.38	9.60	0.88	1.74	13.94	1.65	0.07	2.51	0.01	0.00	0.15
#27	DEN HAAG-02	ATAL	2455.5	23.37	1.43	0.13	1.83	2.03	38.26	0.34	4.94	10.24	0.79	1.59	10.97	1.35	0.05	2.52	0.03	0.00	0.14
#28	DEN HAAG-02	ATAL	2456.5	22.29	0.94	0.15	1.56	1.86	34.87	0.34	5.29	9.67	1.72	1.35	16.24	1.18	0.10	2.19	0.05	0.00	0.19
#29	DEN HAAG-02	ATAL	2457.5	25.11	0.98	0.18	1.71	1.96	38.08	0.46	5.93	10.62	0.75	1.13	9.78	0.90	0.06	2.17	0.02	0.00	0.16
#30	DEN HAAG-02	ATAL	2458.5	25.91	1.31	0.21	1.79	1.98	40.61	0.49	5.73	11.07	0.67	1.01	6.20	0.72	0.05	2.10	0.01	0.00	0.14
#31	DEN HAAG-02	ATAL	2609.0	20.17	0.64	0.03	0.71	2.10	32.58	0.06	2.77	12.78	2.13	0.64	22.62	0.82	0.01	1.27	0.43	0.00	0.24
#32	DEN HAAG-02	ATAL	2610.0	25.35	0.31	0.01	0.29	2.61	28.51	0.03	3.29	14.11	1.17	0.55	21.71	0.56	0.00	1.11	0.22	0.00	0.15
#33	HAARLEMMERMEER	ATAL	1118.5	20.69	0.41	0.03	0.90	1.92	35.95	0.08	3.26	12.62	1.63	0.71	19.10	0.94	0.01	1.48	0.08	0.00	0.20
#34	HAARLEMMERMEER	ATAL	1121.5	16.07	2.09	0.19	0.86	1.25	51.24	0.50	12.19	13.72	0.14	0.08	0.20	0.11	0.01	1.33	0.00	0.00	0.03
#35	HAASTRECHT-01	ATAL	2087.5	18.03	0.25	0.03	1.68	3.58	29.96	0.03	0.68	3.97	1.72	2.23	34.80	1.37	0.00	1.43	0.13	0.00	0.13
#36	LOON OP ZAND-01	ATAL	2505.0	28.66	0.33	0.04	1.27	1.21	27.31	0.12	4.05	15.10	5.85	1.46	11.39	0.33	0.00	1.13	1.54	0.01	0.19
#37	LOON OP ZAND-01	ATAL	2506.5	17.84	0.65	0.06	1.42	1.56	40.66	0.18	5.64	19.11	1.55	1.05	6.37	0.38	0.00	1.31	2.02	0.00	0.21
#38	LOON OP ZAND-01	ATAL	2508.0	13.25	0.99	0.07	1.38	1.43	50.68	0.15	4.46	17.51	1.39	0.68	5.65	0.40	0.00	1.06	0.78	0.00	0.12
#39	LOON OP ZAND-01	ATAL	2509.5	9.26	4.71	0.15	0.59	1.54	30.40	0.13	4.30	11.22	1.41	0.17	24.80	4.43	0.24	4.90	0.04	0.00	0.70
#40	LOON OP ZAND-01	ATAL	2511.0	6.12	0.02	0.00	0.01	0.29	0.17	0.00	0.01	0.41	11.45	0.65	77.79	1.11	0.00	0.82	0.53	0.00	0.62
#41	LOON OP ZAND-01	ATAL	2512.5	18.05	3.44	0.30	1.66	2.35	42.13	0.83	12.06	14.49	1.24	0.12	0.67	4.49	0.02	2.06	0.01	0.00	0.07
#42	LOON OP ZAND-01	ATAL	2514.0	18.52	1.25	0.16	1.28	2.30	48.00	0.27	8.18	17.40	0.47	0.10	0.95	0.15	0.00	0.96	0.00	0.00	0.02
#43	LOON OP ZAND-01	ATAL	2515.5	21.87	4.20	0.24	1.64	3.04	40.78	0.46	6.04	17.43	0.44	0.21	1.33	0.26	0.18	1.83	0.00	0.00	0.07
#44	LOON OP ZAND-01	ATAL	2517.0	18.08	4.32	0.27	1.46	2.43	40.48	0.74	12.97	15.10	0.08	0.14	0.87	0.79	0.08	2.11	0.00	0.00	0.09
#45	LOON OP ZAND-01	ATAL	2518.5	16.37	3.70	0.23	1.37	2.26	47.46	0.41	8.67	16.91	0.02	0.12	0.58	0.31	0.02	1.52	0.00	0.00	0.05
#46	LOON OP ZAND-01	ATAL	2520.0	13.89	3.70	0.26	0.90	2.08	43.41	0.34	8.70	23.15	0.05	0.11	0.83	0.48	0.02	2.02	0.00	0.00	0.05
#47	LOON OP ZAND-01	ATAL	2522.5	18.05	1.44	0.26	1.35	2.52	46.01	0.38	7.92	17.61	0.60	0.15	1.97	0.40	0.01	1.20	0.07	0.00	0.04
#48	LOON OP ZAND-01	ATAL	2524.0	20.04	4.32	0.17	0.90	3.09	37.99	0.15	4.01	22.20	0.43	0.20	4.52	0.43	0.02	1.37	0.05	0.00	0.10
#49	LOON OP ZAND-01	ATAL	2525.5	16.76	5.07	0.13	0.82	2.39	38.11	0.17	4.48	22.79	5.75	0.18	1.41	0.23	0.09	1.34	0.22	0.00	0.06
#50	LOON OP ZAND-01	ATAL	2530.5	21.95	3.65	0.40	1.81	3.88	40.60	0.48	4.54	16.70	2.85	0.09	0.88	0.21	0.03	1.61	0.24	0.00	0.08
#51	LOON OP ZAND-01	ATAL	2580.0	21.45	0.86	0.09	1.53	3.55	46.56	0.11	3.98	11.25	0.07	0.34	5.37	3.14	0.27	1.16	0.00	0.00	0.28
#52	MOERKAPELLE-04	ATAL	1720.0	11.35	1.67	0.21	1.41	2.89	51.30	0.59	14.73	13.36	0.39	0.03	0.63	0.05	0.08	1.28	0.00	0.00	0.03
#53	MOERKAPELLE-04	ATAL	1721.5	13.38	3.07	0.22	1.07	2.63	46.01	0.54	11.65	16.30	1.03	0.09	2.20	0.12	0.02	1.61	0.04	0.00	0.04
#54	MOERKAPELLE-04	ATAL	1723.0	15.19	2.56	0.17	1.14	2.97	45.07	0.29	9.42	17.63	1.14	0.07	2.78	0.07	0.01	1.43	0.04	0.00	0.04
#55	MOERKAPELLE-04	ATAL	1724.5	11.30	3.09	0.16	0.94	2.23	44.39	0.61	9.66	15.64	0.82	0.05	8.81	0.28	0.41	1.50	0.06	0.00	0.05
#56	RUSWIJK-01	ATAL	2107.0	18.67	0.35	0.06	2.31	1.19	41.13	0.24	6.12	21.38	1.25	1.22	4.17	0.18	0.00	1.08	0.41	0.00	0.21
#57	RUSWIJK-01	ATAL	2109.0	5.11	0.03	0.00	0.06	0.41	1.96	0.00	0.04	1.09	1.02	71.83	16.55	0.95	0.00	0.72	0.03	0.00	0.19
#58	RUSWIJK-01	ATAL	2115.0	17.95	3.52	0.29	1.59	2.29	43.75	0.55	8.95	15.64	0.75	0.38	1.70	0.57	0.01	1.99	0.00	0.00	0.07
#59	RUSWIJK-01	ATAL	2116.5	18.00	2.30	0.34	1.72	2.22	42.85	0.90	11.57	14.61	0.								

Appendix D (cont'd): Heavy Minerals

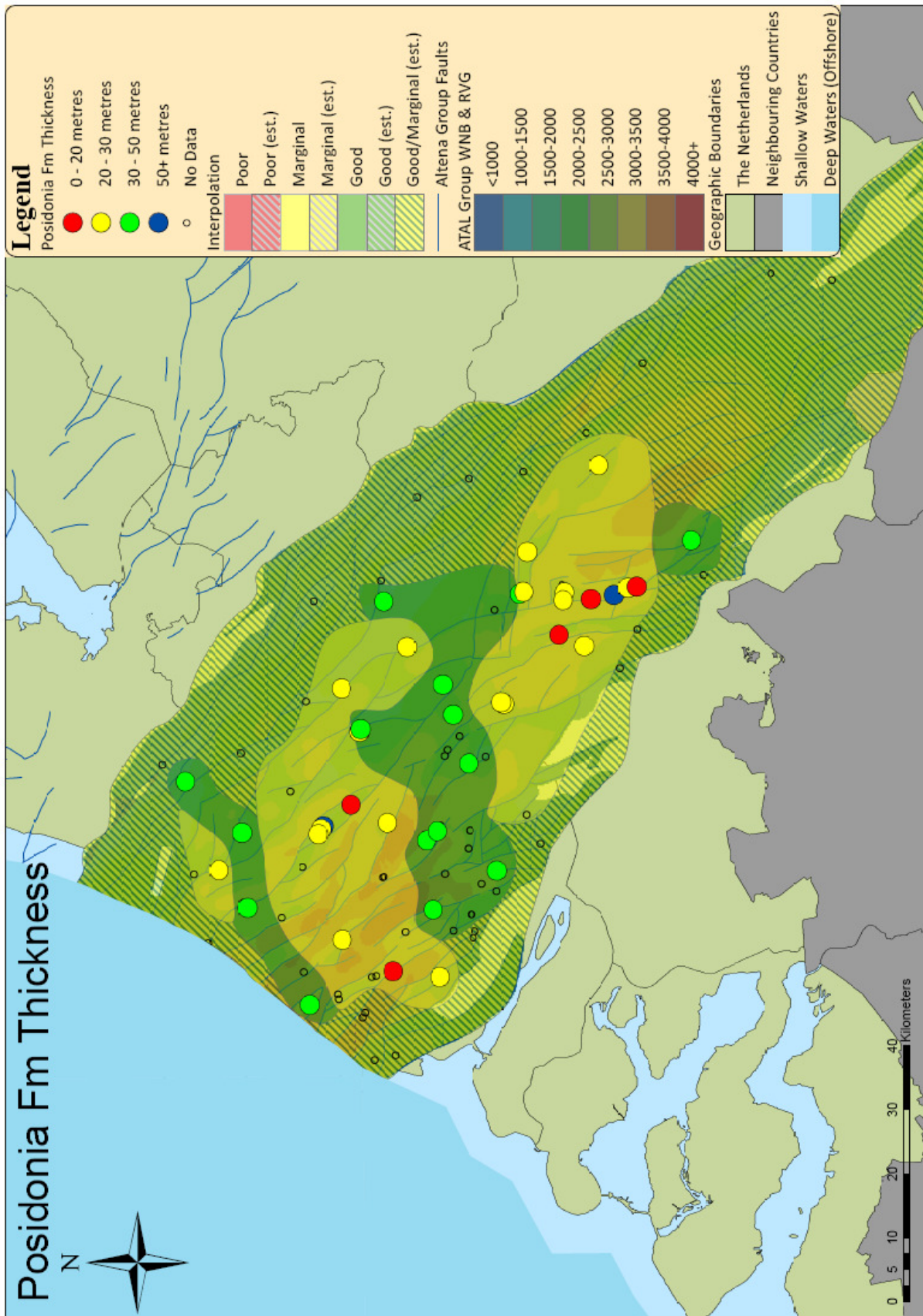
Sample	Well Name	Fn	Sample Depth (MD)	Olivine	Tourmaline	Sphene	Hornblende	Tremolite-Actinolite	Epidote	Pyroxene	Garnet	Apatite	Rutile/Anatase	Goethite	Hematite	Ilmenite	Spinel	Chromite	Leucosene	Zircon	Wollastonite
#1	ANDEL-02	ATAL	1687.0	0.005	0.051	0.000	0.395	0.031	0.000	0.227	0.114	0.011	0.673	0.001	0.000	0.021	0.000	0.000	0.000	0.003	0.000
#2	ANDEL-02	ATAL	1688.3	0.352	0.001	0.000	0.629	0.109	0.000	0.255	0.208	1.344	0.103	1.243	0.000	0.468	0.000	0.002	0.009	0.003	0.000
#3	ASTEN-01	ATAL	1608.0	0.082	0.003	0.000	1.997	0.898	0.000	1.190	2.223	0.033	0.064	0.001	0.000	1.295	0.000	0.000	0.000	0.000	0.000
#4	ASTEN-01	ATAL	1609.0	0.000	0.051	0.000	0.290	0.024	0.000	0.392	0.300	0.068	0.681	0.000	0.000	0.007	0.000	0.000	0.000	0.002	0.000
#5	BLESKENGRAAF-02	ATAL	1570.0	0.003	0.026	0.002	0.337	0.022	0.000	0.064	0.332	0.002	0.488	0.000	0.000	0.011	0.000	0.000	0.000	0.001	0.000
#6	BLESKENGRAAF-02	ATAL	1571.5	0.007	0.027	0.002	0.607	0.035	0.005	0.124	0.194	0.008	0.703	0.000	0.000	0.017	0.000	0.000	0.002	0.006	0.000
#7	BLESKENGRAAF-02	ATAL	1573.0	0.003	0.043	0.001	0.241	0.023	0.001	0.062	0.196	0.004	0.677	0.000	0.000	0.021	0.000	0.000	0.001	0.003	0.000
#8	BLESKENGRAAF-02	ATAL	1574.5	0.033	0.005	0.003	4.029	0.203	0.002	0.351	2.420	0.099	0.238	0.001	0.000	0.361	0.000	0.000	0.002	0.000	0.000
#9	BLESKENGRAAF-02	ATAL	1576.0	0.004	0.055	0.000	0.169	0.018	0.001	0.046	0.290	0.004	0.638	0.003	0.000	0.082	0.000	0.000	0.000	0.002	0.000
#10	BERKEL-02	ATAL	3107.3	0.001	0.018	0.028	0.386	0.032	0.002	0.339	0.409	0.040	0.459	0.000	0.000	0.004	0.000	0.005	0.001	0.038	0.000
#11	BERKEL-02	ATAL	3108.5	0.000	0.010	0.001	0.110	0.012	0.002	0.240	0.495	0.013	0.875	0.000	0.000	0.006	0.000	0.000	0.000	0.009	0.000
#12	BERKEL-02	ATAL	3110.0	0.000	0.073	0.000	0.130	0.017	0.000	0.169	0.217	0.008	0.803	0.000	0.000	0.007	0.000	0.000	0.000	0.007	0.000
#13	BERKEL-02	ATAL	3111.5	0.081	0.047	0.001	3.700	0.167	0.001	1.100	2.284	0.073	0.598	0.009	0.000	0.239	0.000	0.001	0.001	0.007	0.000
#14	BERKEL-02	ATAL	3113.0	0.000	0.084	0.002	0.238	0.019	0.000	0.477	0.286	0.025	0.895	0.000	0.000	0.010	0.000	0.002	0.000	0.014	0.000
#15	BERKEL-02	ATAL	3114.5	0.001	0.090	0.001	0.162	0.014	0.000	0.444	0.386	0.028	0.878	0.001	0.000	0.011	0.000	0.003	0.000	0.020	0.000
#16	BERKEL-02	ATAL	3116.0	0.000	0.083	0.005	0.509	0.042	0.001	0.637	0.564	0.021	0.847	0.000	0.000	0.008	0.000	0.002	0.000	0.013	0.000
#17	DONGEN-01	ATAL	1523.0	0.002	0.000	0.002	1.289	0.045	0.004	0.105	0.141	0.008	0.470	0.000	0.000	0.009	0.000	0.000	0.000	0.002	0.000
#18	DONGEN-01	ATAL	1524.0	0.002	0.001	0.001	1.154	0.060	0.002	0.109	0.156	0.004	0.420	0.000	0.000	0.024	0.000	0.000	0.000	0.001	0.000
#19	DONGEN-01	ATAL	1525.5	0.002	0.000	0.000	2.116	0.074	0.000	0.110	0.194	0.005	0.312	0.000	0.000	0.005	0.000	0.000	0.000	0.001	0.000
#20	DONGEN-01	ATAL	1527.0	0.005	0.000	0.001	1.674	0.076	0.002	0.132	0.173	0.005	0.424	0.000	0.000	0.010	0.000	0.000	0.000	0.002	0.000
#21	DONGEN-01	ATAL	1533.0	0.002	0.001	0.003	1.771	0.104	0.000	0.160	0.153	0.006	0.331	0.000	0.000	0.007	0.000	0.000	0.000	0.002	0.000
#22	DONGEN-01	ATAL	1534.5	0.004	0.001	0.003	1.834	0.112	0.001	0.215	0.136	0.009	0.407	0.000	0.000	0.016	0.000	0.000	0.000	0.001	0.000
#23	DONGEN-01	ATAL	1536.0	0.009	0.003	0.003	1.736	0.101	0.003	0.178	0.105	0.006	0.446	0.001	0.000	0.010	0.000	0.000	0.000	0.005	0.000
#24	DEN HAAG-02	ATAL	2452.5	0.001	0.015	0.005	1.095	0.087	0.003	0.191	0.183	0.035	0.771	0.001	0.000	0.010	0.000	0.001	0.000	0.011	0.000
#25	DEN HAAG-02	ATAL	2453.5	0.001	0.021	0.006	1.002	0.090	0.006	0.187	0.242	0.038	0.765	0.001	0.000	0.013	0.000	0.001	0.000	0.012	0.000
#26	DEN HAAG-02	ATAL	2454.5	0.001	0.019	0.006	1.163	0.100	0.004	0.207	0.209	0.036	0.742	0.001	0.000	0.012	0.000	0.000	0.000	0.013	0.000
#27	DEN HAAG-02	ATAL	2455.5	0.000	0.015	0.005	1.109	0.087	0.003	0.211	0.232	0.036	0.799	0.000	0.000	0.012	0.000	0.001	0.000	0.012	0.000
#28	DEN HAAG-02	ATAL	2456.5	0.001	0.023	0.007	0.889	0.079	0.006	0.173	0.214	0.054	0.703	0.000	0.000	0.029	0.000	0.000	0.000	0.014	0.000
#29	DEN HAAG-02	ATAL	2457.5	0.001	0.028	0.004	0.725	0.071	0.002	0.187	0.274	0.035	0.807	0.000	0.000	0.022	0.000	0.002	0.000	0.013	0.000
#30	DEN HAAG-02	ATAL	2458.5	0.001	0.025	0.003	0.620	0.061	0.002	0.192	0.273	0.034	0.860	0.000	0.000	0.018	0.000	0.001	0.000	0.015	0.000
#31	DEN HAAG-02	ATAL	2609.0	0.000	0.003	0.004	0.440	0.022	0.005	0.041	0.265	0.092	0.398	0.000	0.000	0.002	0.000	0.000	0.000	0.003	0.000
#32	DEN HAAG-02	ATAL	2610.0	0.000	0.003	0.003	0.442	0.025	0.002	0.039	0.215	0.103	0.271	0.000	0.000	0.001	0.000	0.000	0.000	0.002	0.000
#33	HAARLEMMERMEER-01	ATAL	1118.5	0.000	0.003	0.002	0.619	0.024	0.004	0.048	0.195	0.190	0.386	0.000	0.000	0.002	0.000	0.000	0.000	0.002	0.000
#34	HAARLEMMERMEER-01	ATAL	1121.5	0.000	0.042	0.000	0.184	0.009	0.000	0.096	0.341	0.005	0.636	0.000	0.000	0.008	0.000	0.001	0.000	0.010	0.000
#35	HAASTRECHT-01	ATAL	2087.5	0.000	0.004	0.006	0.998	0.048	0.003	0.114	0.123	0.085	0.442	0.000	0.000	0.001	0.000	0.000	0.000	0.003	0.000
#36	LOON OP ZAND-01	ATAL	2505.0	0.000	0.005	0.002	0.450	0.025	0.000	0.064	0.047	0.176	0.360	0.000	0.000	0.004	0.000	0.000	0.000	0.002	0.000
#37	LOON OP ZAND-01	ATAL	2506.5	0.000	0.007	0.001	0.555	0.043	0.001	0.049	0.061	0.249	0.339	0.000	0.000	0.001	0.000	0.000	0.000	0.002	0.000
#38	LOON OP ZAND-01	ATAL	2508.0	0.000	0.012	0.001	0.469	0.045	0.001	0.042	0.081	0.057	0.345	0.000	0.000	0.003	0.000	0.000	0.000	0.002	0.000
#39	LOON OP ZAND-01	ATAL	2509.5	0.005	0.010	0.001	1.948	0.031	0.012	0.304	1.043	1.296	0.227	0.000	0.000	0.019	0.000	0.000	0.000	0.002	0.000
#40	LOON OP ZAND-01	ATAL	2511.0	0.000	0.000	0.021	0.016	0.000	0.001	0.012	0.180	0.479	0.102	0.000	0.000	0.003	0.000	0.000	0.000	0.000	0.000
#41	LOON OP ZAND-01	ATAL	2512.5	0.000	0.067	0.000	0.701	0.036	0.002	0.246	0.297	0.044	0.652	0.000	0.000	0.008	0.000	0.000	0.000	0.007	0.000
#42	LOON OP ZAND-01	ATAL	2514.0	0.000	0.058	0.000	0.129	0.012	0.001	0.111	0.046	0.007	0.588	0.000	0.000	0.003	0.000	0.000	0.000	0.003	0.000
#43	LOON OP ZAND-01	ATAL	2515.5	0.001	0.093	0.001	0.235	0.022	0.001	0.338	0.344	0.014	0.764	0.000	0.000	0.010	0.000	0.002	0.000	0.008	0.000
#44	LOON OP ZAND-01	ATAL	2517.0	0.001	0.070	0.000	0.774	0.046	0.003	0.269	0.262	0.029	0.635	0.000	0.000	0.011	0.000	0.001	0.000	0.004	0.000
#45	LOON OP ZAND-01	ATAL	2518.5	0.001	0.081	0.000	0.260	0.018	0.002	0.207	0.256	0.018	0.668	0.000	0.000	0.004	0.000	0.001	0.000	0.004	0.000
#46	LOON OP ZAND-01	ATAL	2520.0	0.000	0.141	0.000	0.434	0.034	0.001	0.280	0.540	0.010	0.574	0.000	0.000	0.006	0.000	0.000	0.000	0.003	0.000
#47	LOON OP ZAND-01	ATAL	2522.5	0.001	0.069	0.000	0.190	0.021	0.002	0.160	0.112	0.008	0.620	0.000	0.000	0.006	0.000	0.001	0.000	0.008	0.000
#48	LOON OP ZAND-01	ATAL	2524.0	0.000	0.103	0.001	0.140	0.014	0.001	0.147	0.197	0.016	0.741	0.000	0.000	0.005	0.000	0.000	0.000	0.008	0.000
#49	LOON OP ZAND-01	ATAL	2525.5	0.001	0.091	0.000	0.111	0.012	0.002	0.135	0.265	0.010	0.696	0.000	0.000	0.012	0.000	0.000	0.001	0.006	0.000
#50	LOON OP ZAND-01	ATAL	2530.5	0.001	0.099	0.000	0.101	0.008	0.001	0.215	0.365	0.021	0.772	0.000	0.000	0.014	0.000	0.002	0.000	0.009	0.000
#51	LOON OP ZAND-01	ATAL	2580.0	0.001	0.021	0.005	0.251	0.026	0.001	0.276	0.057	0.040	0.474	0.001	0.000	0.002	0.000	0.000	0.000	0.001	0.000
#52	MOERKAPELLE-04	ATAL	1720.0	0.000	0.049	0.000	0.159	0.010	0.000	0.111	0.368	0.053	0.520	0.000	0.000	0.006	0.000	0.000	0.000	0.001	0.000
#53	MOERKAPELLE-04	ATAL	1721.5	0.000	0.061	0.000	0.358	0.026	0.002	0.149	0.336	0.029	0.635	0.000	0.000	0.012	0.000	0.000	0.000	0.001	0.000
#54	MOERKAPELLE-04	ATAL	1723.0	0.002	0.065	0.001	0.132	0.013	0.002	0.122	0.304	0.080	0.703	0.000	0.000	0.005	0.000	0.000	0.000	0.005	0.000
#55	MOERKAPELLE-04	ATAL	1724.5	0.001	0.024	0.001	0.419	0.014	0.002	0.114	0.352	0.103	0.457	0.000	0.000	0.010					

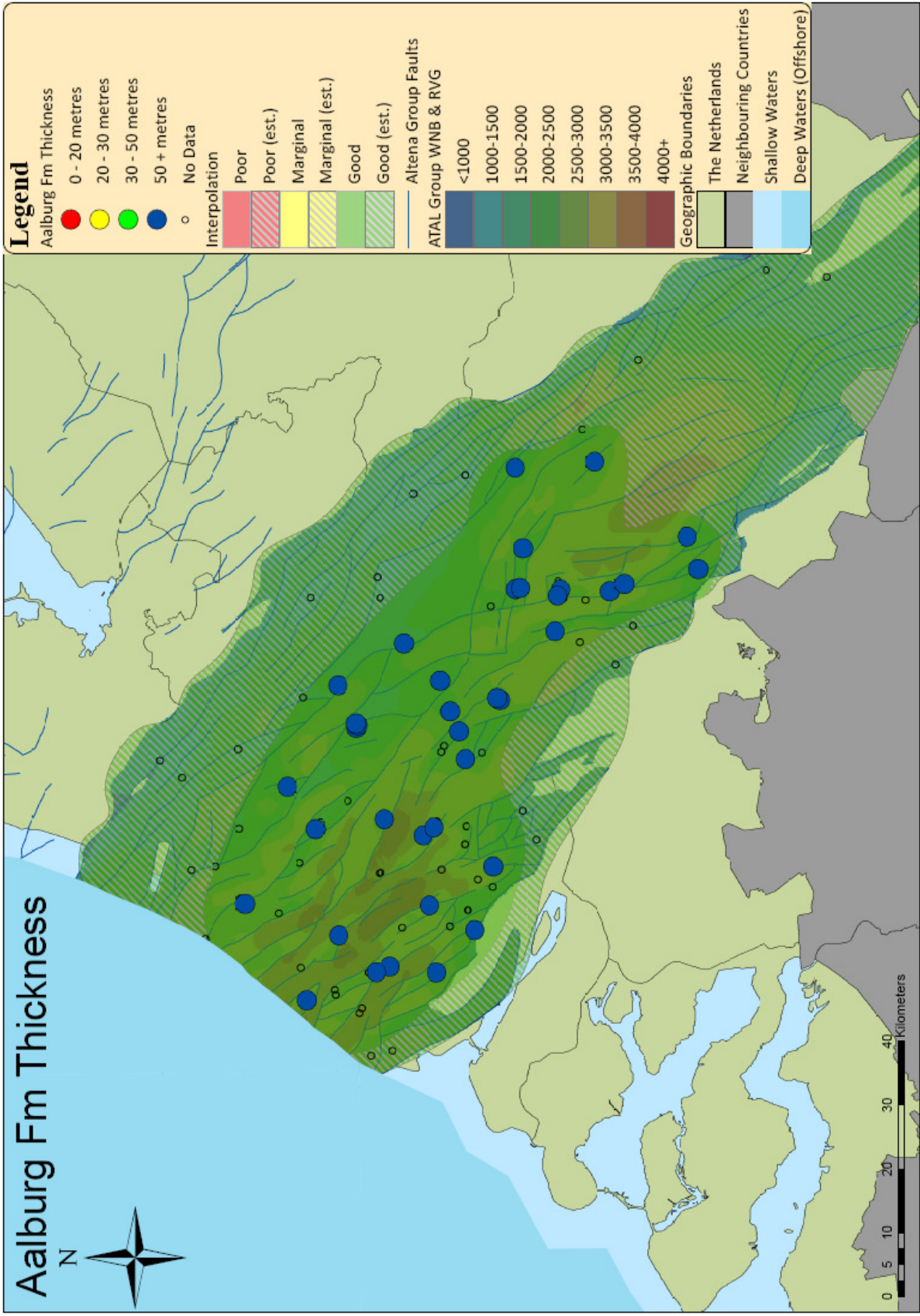
Appendix E: Sorption Measurements and Langmuir Fit

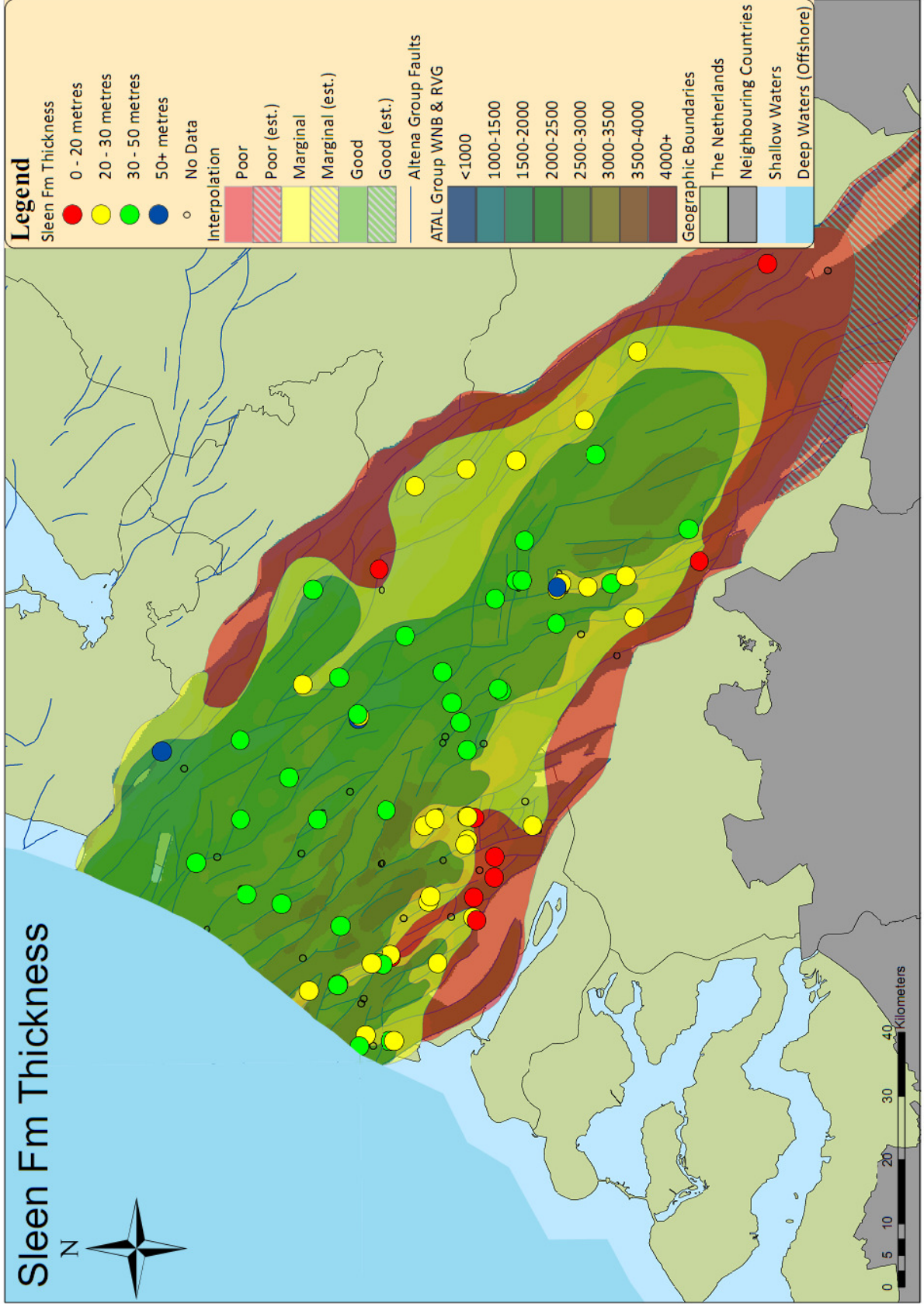




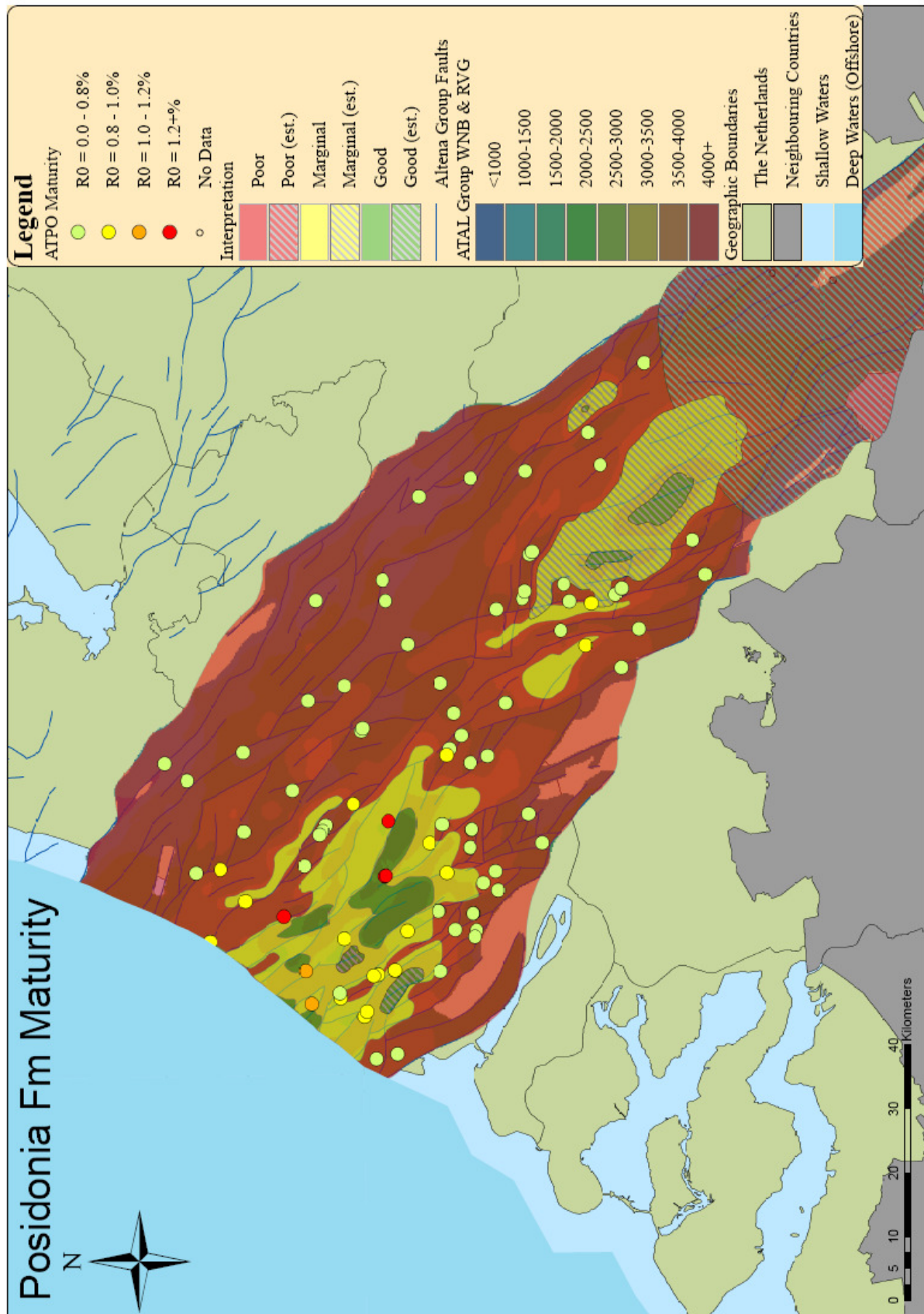
Appendix F1: Interpreted Thickness Maps

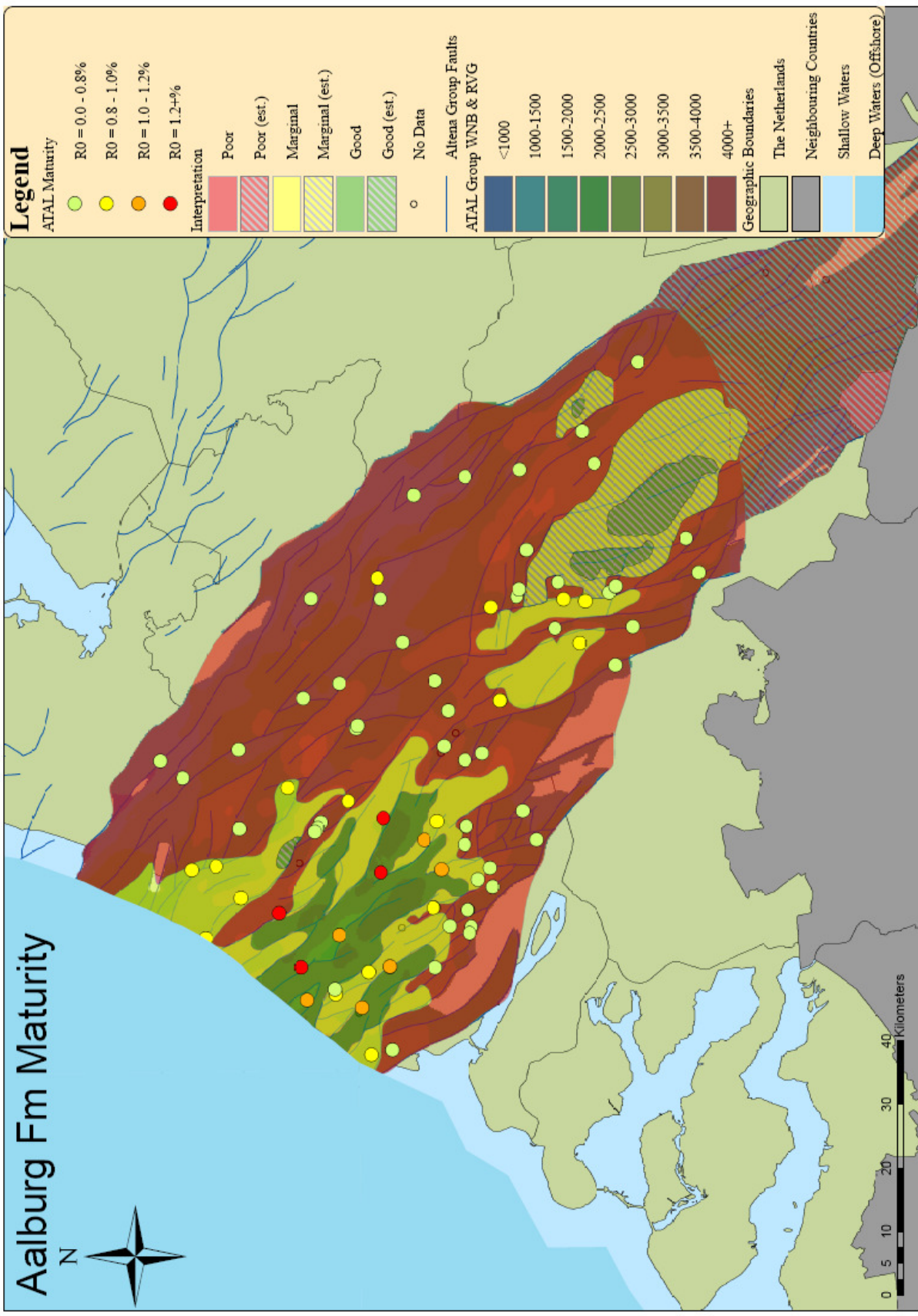


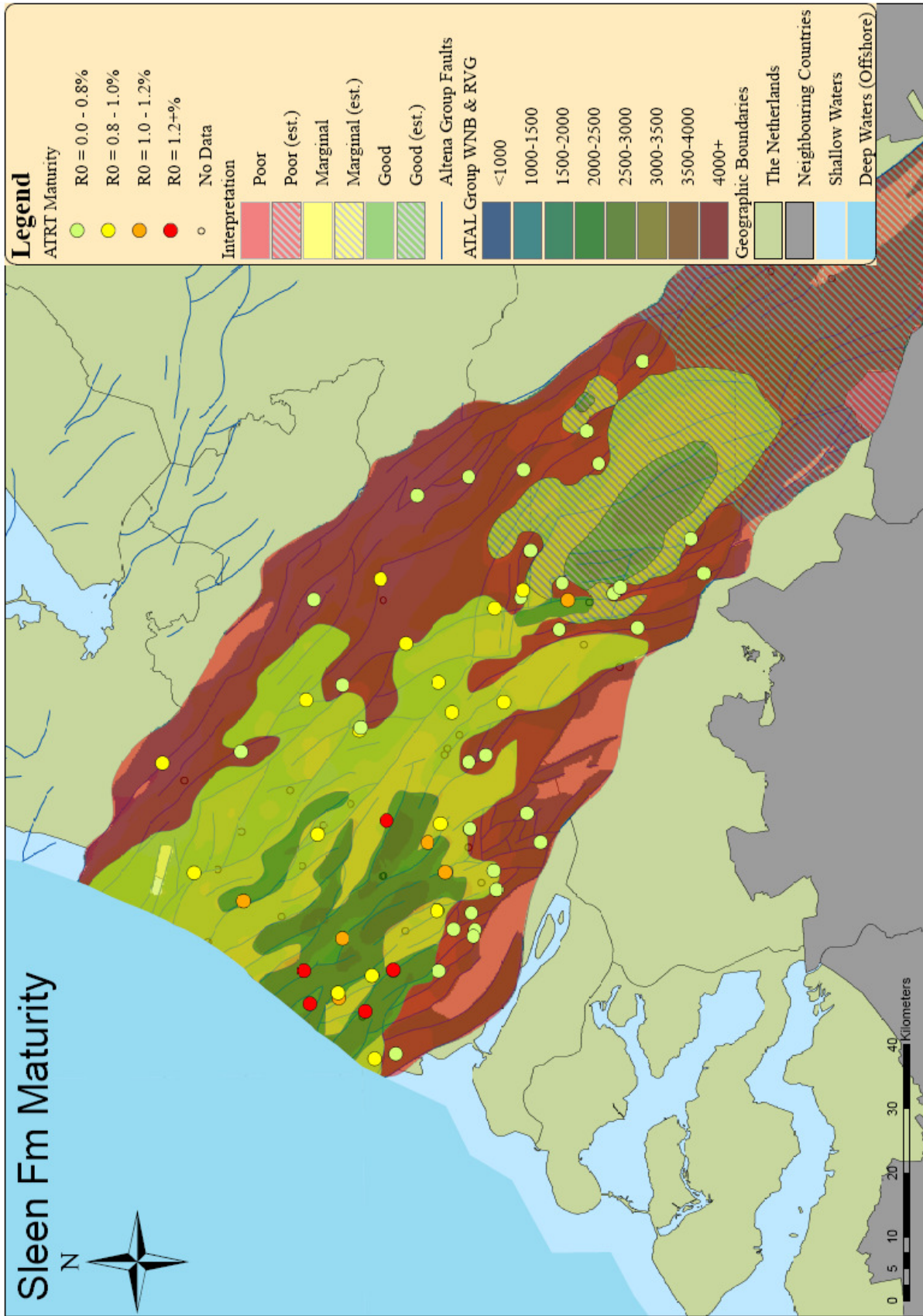




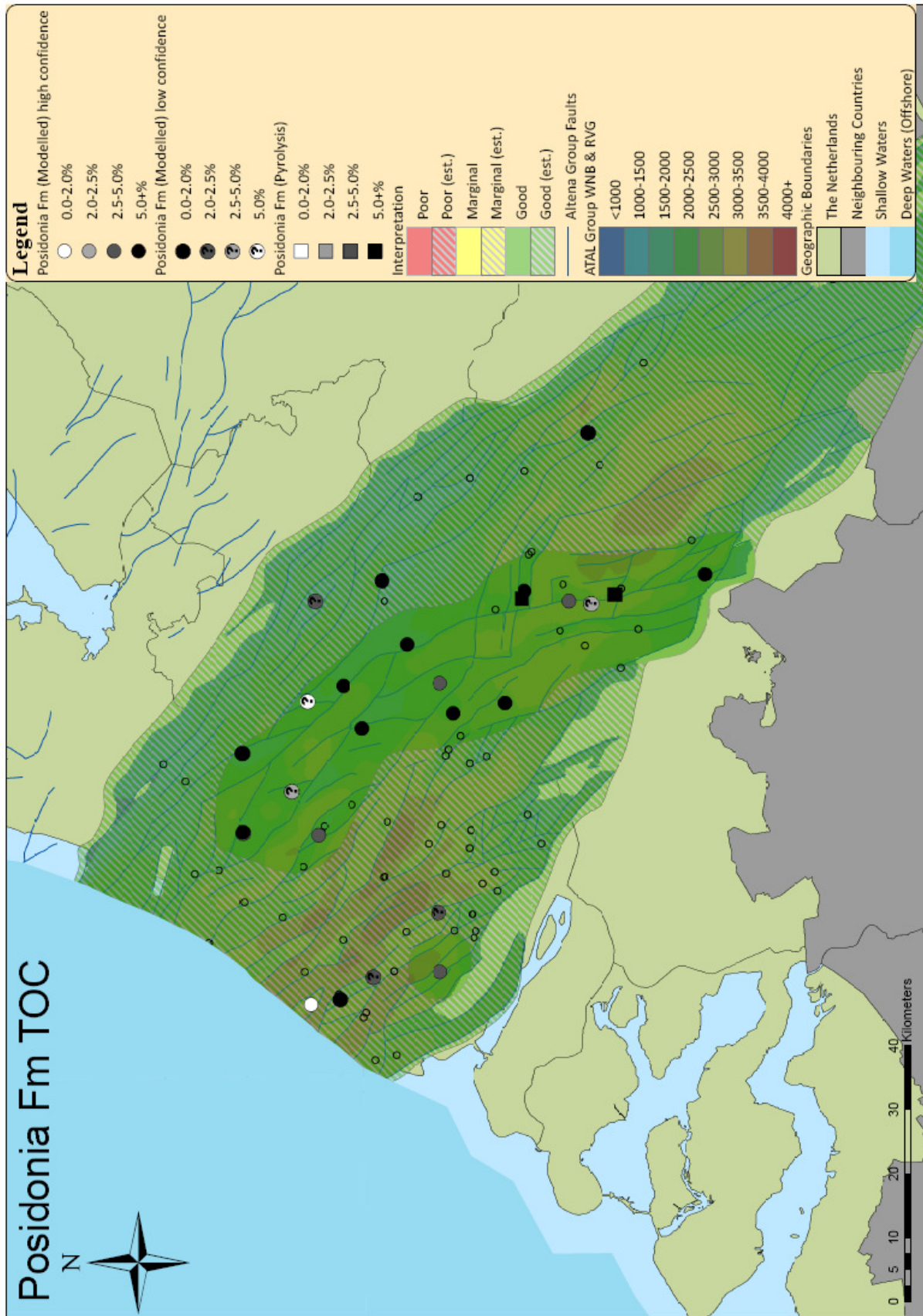
Appendix F2: Interpreted Maturity Maps

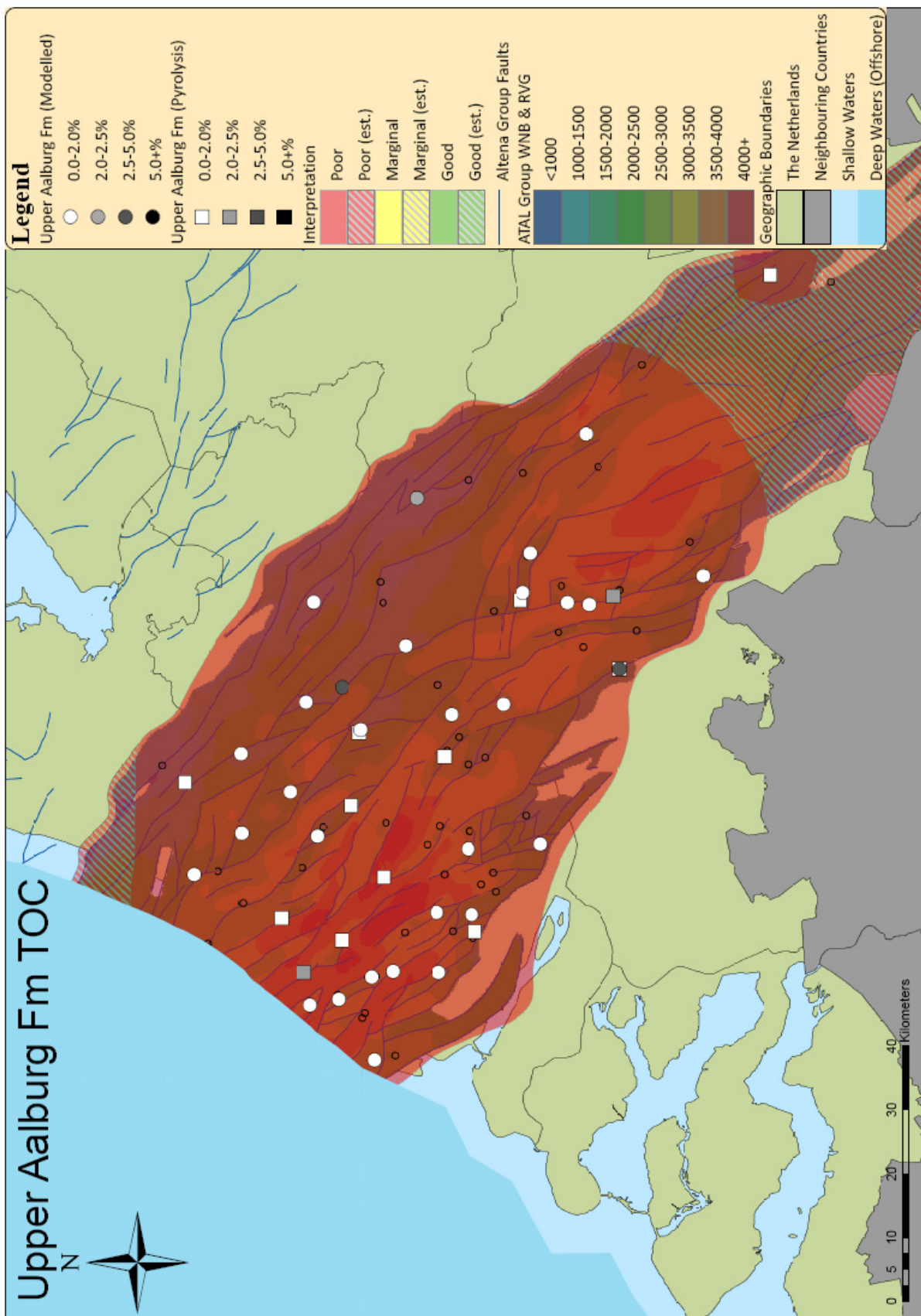


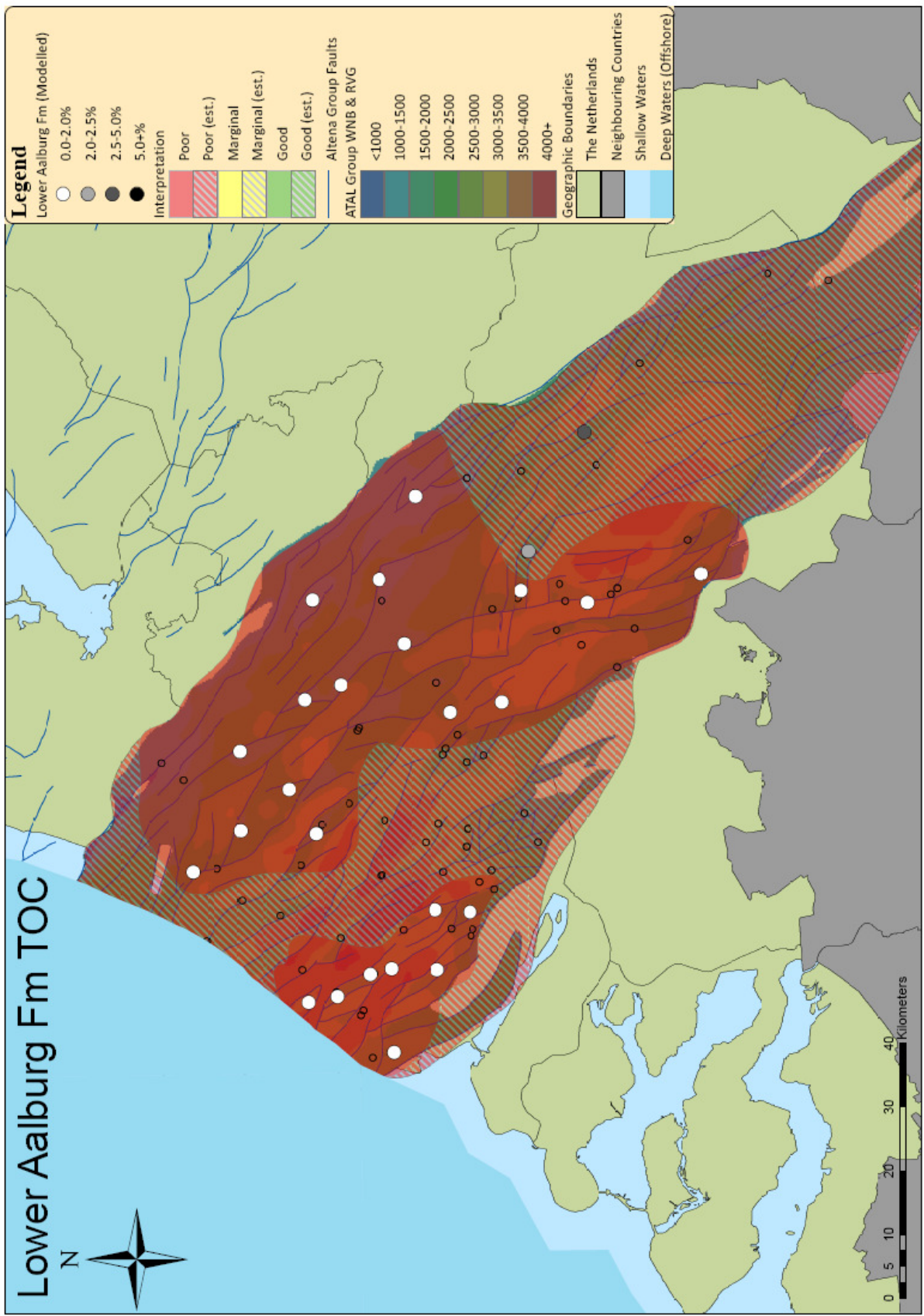


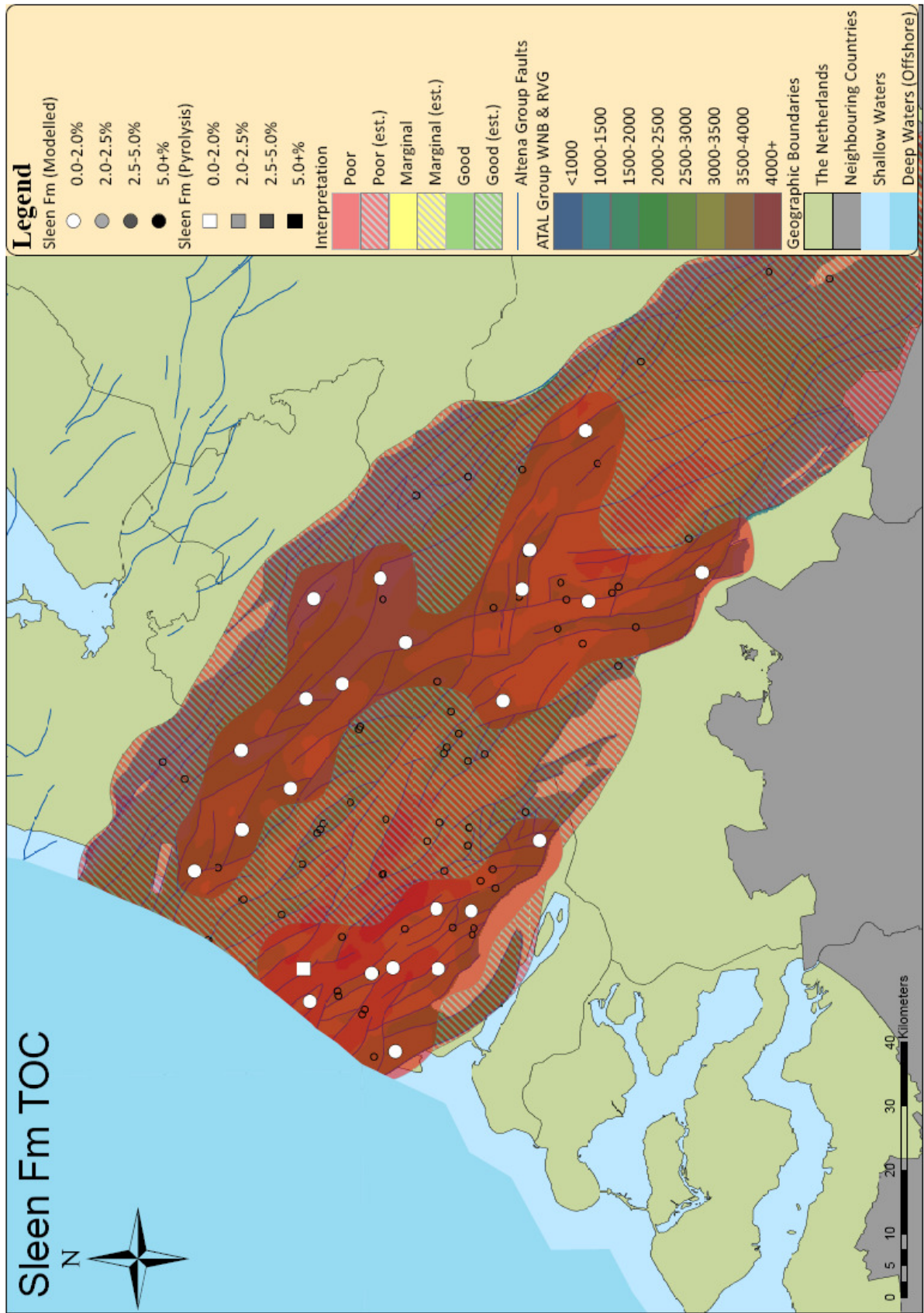


Appendix F3: Interpreted TOC Maps

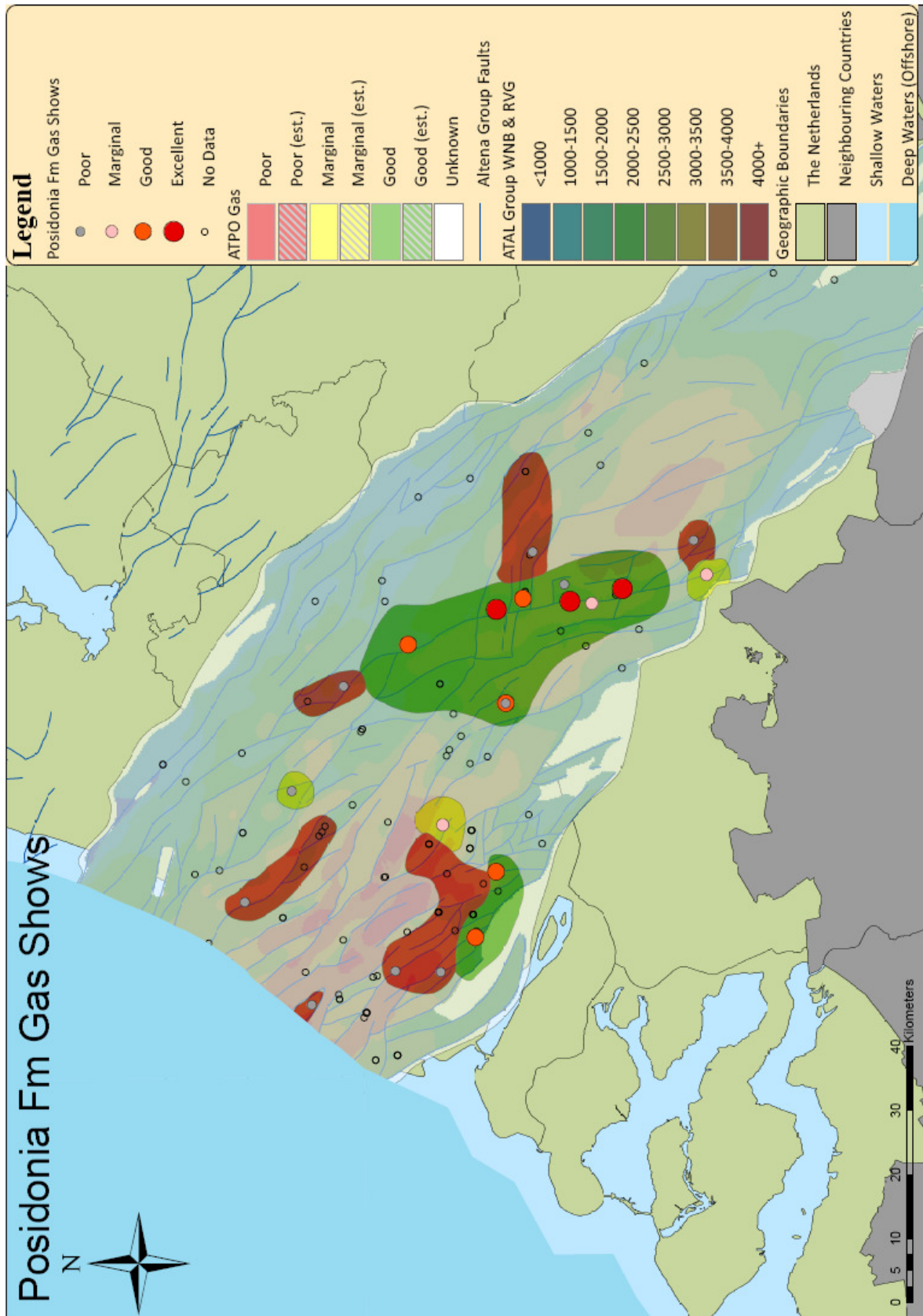


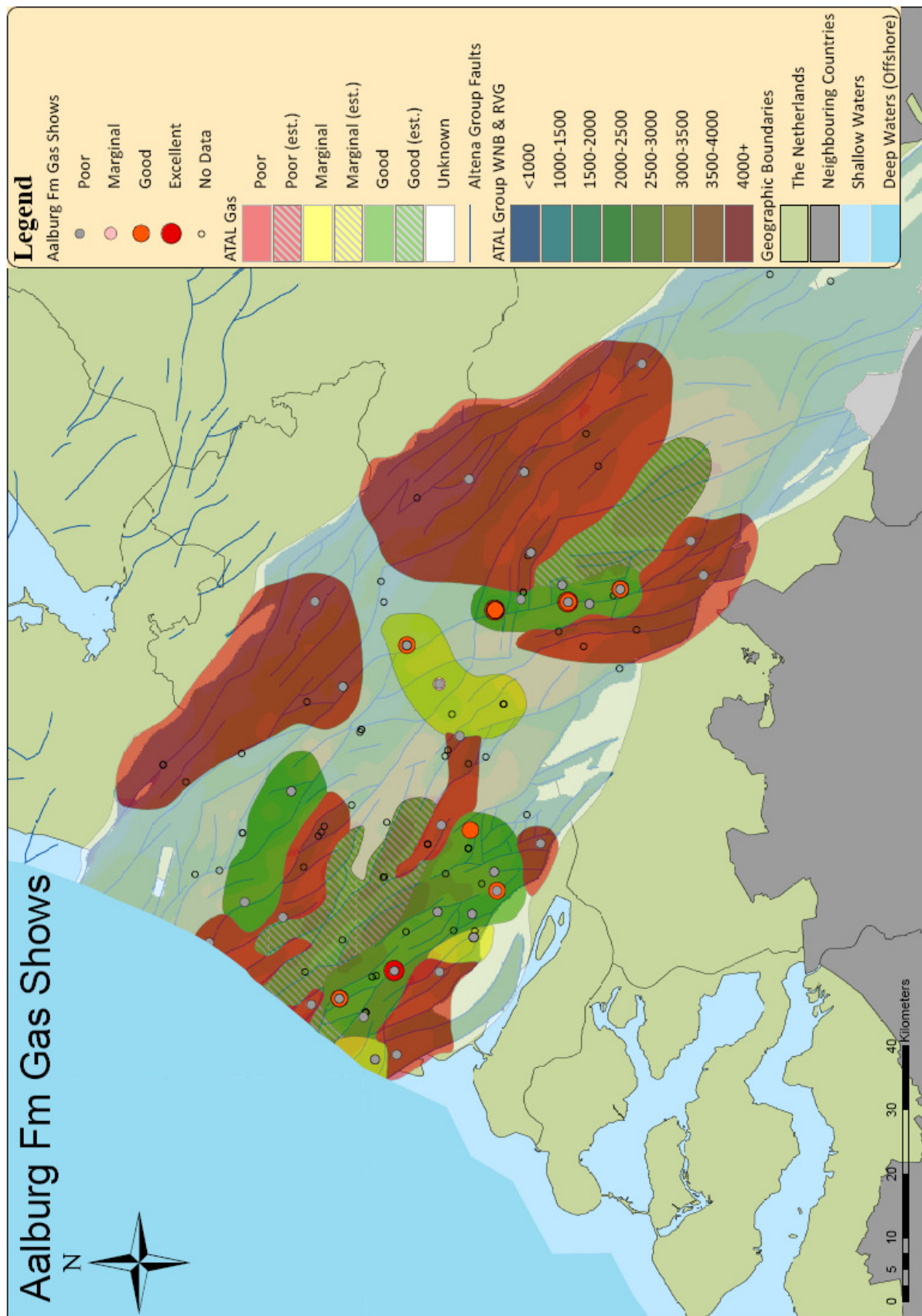


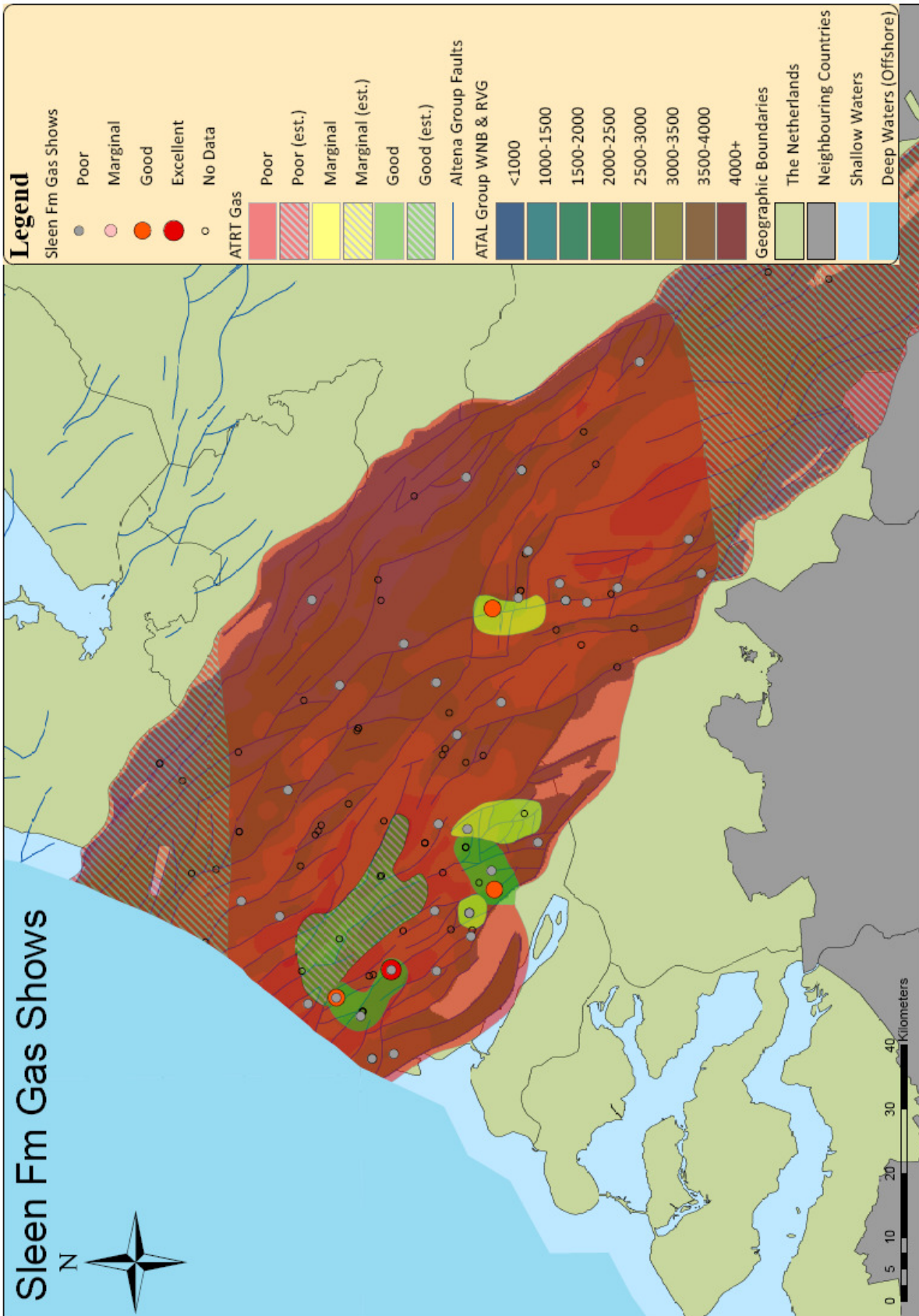




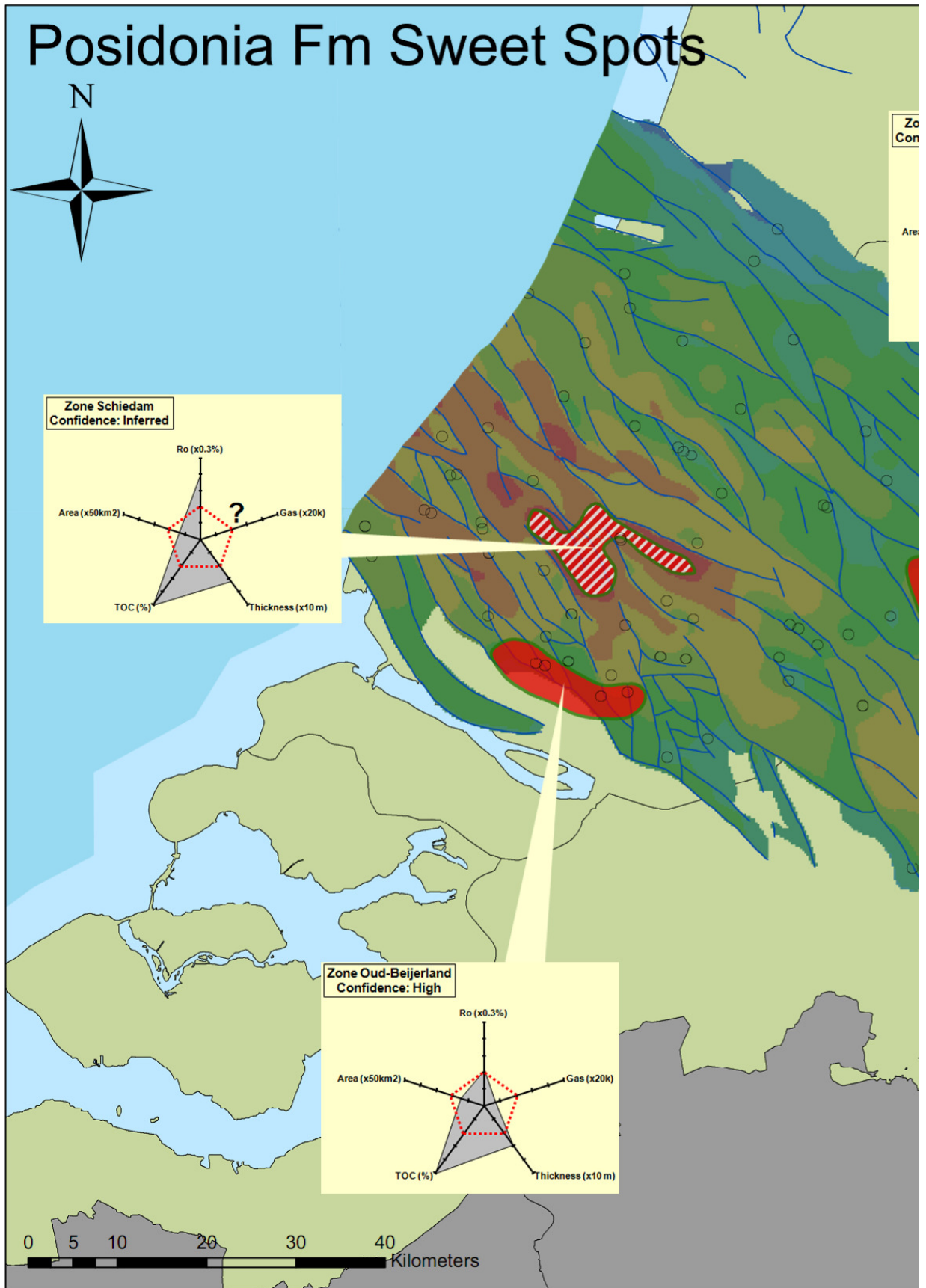
Appendix F4: Interpreted Gas Show Maps

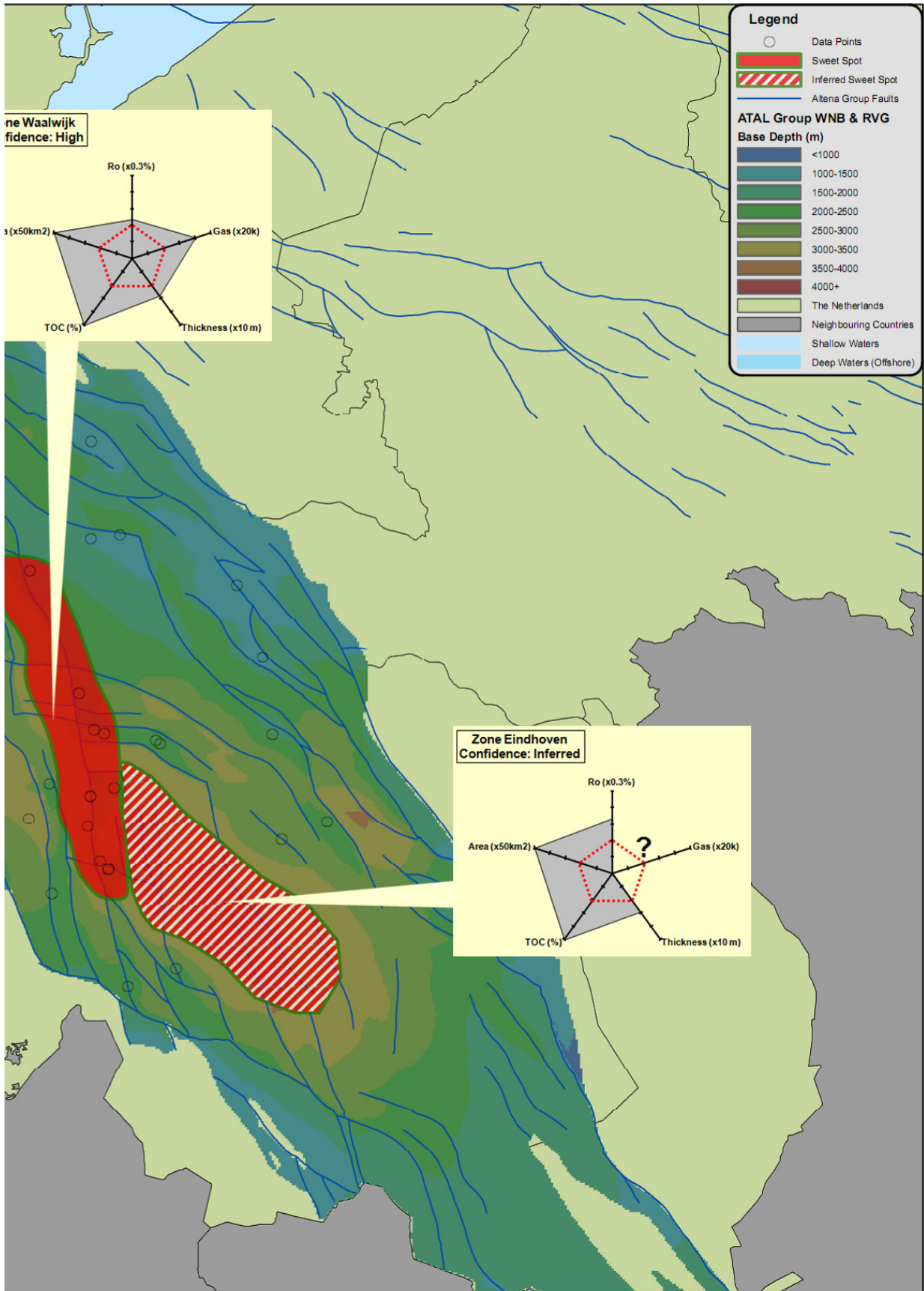


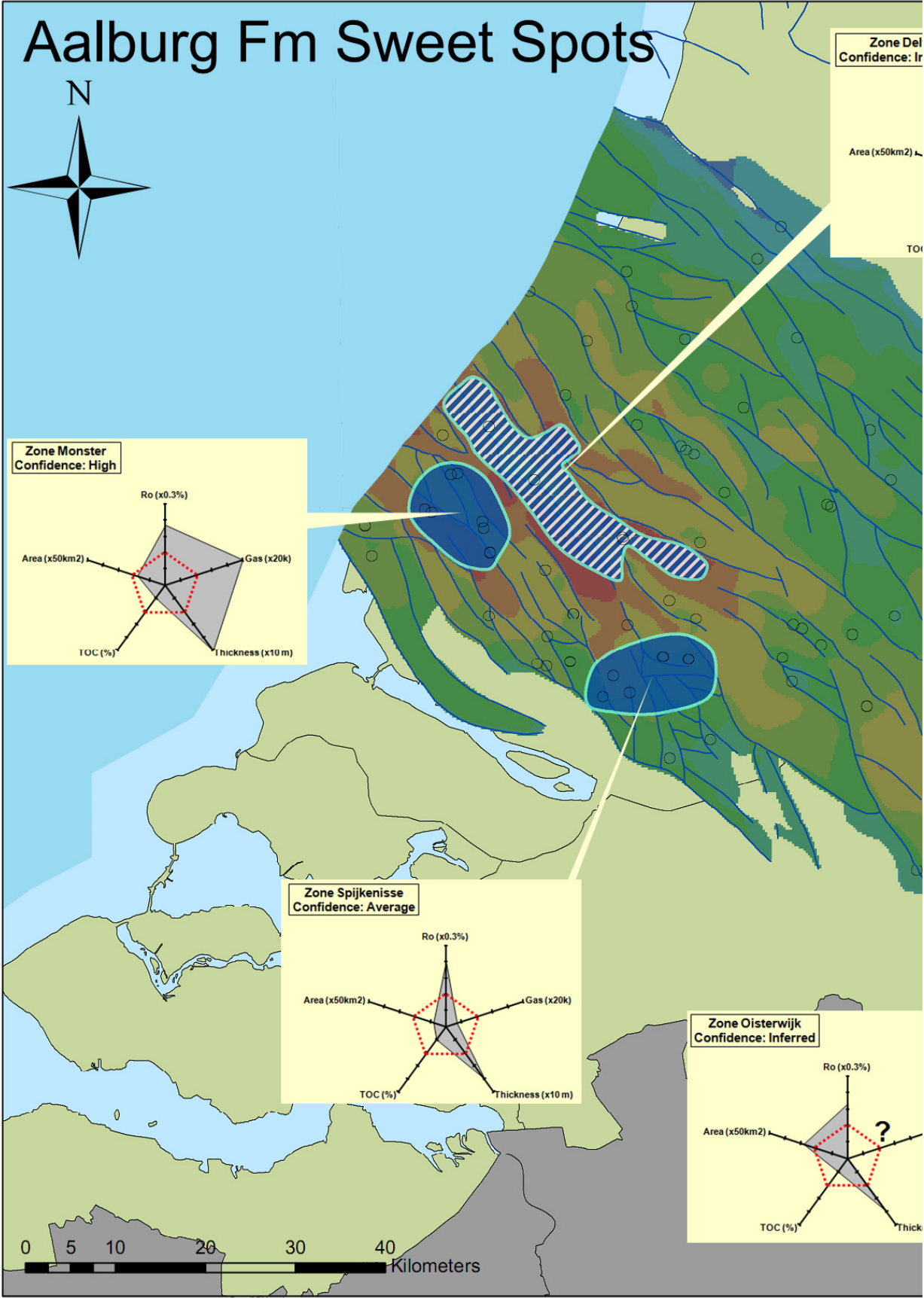


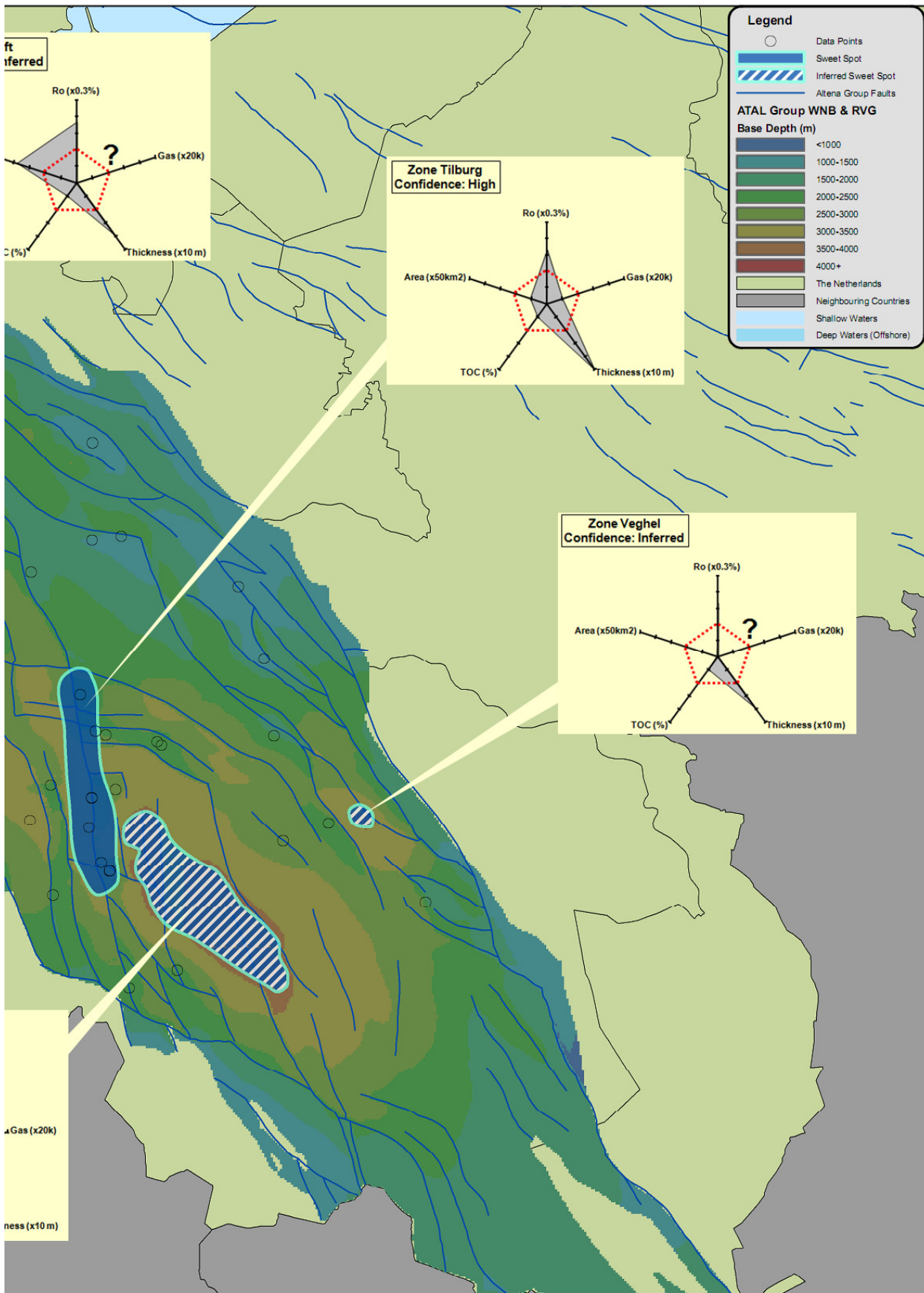


Appendix G:









Sleen Fm Sweet Spots

